VOL. 686 NO. 1 25 NOVEMBER 1994

JOURNAL OF CHROMATOGRAPHY A

INCLUDING ELECTROPHORESIS AND OTHER SEPARATION METHODS

ELSEVIER

JOURNAL OF CHROMATOGRAPHY A

INCLUDING ELECTROPHORESIS AND OTHER SEPARATION METHODS

Scope. The *Journal of Chromatography A* publishes papers on all aspects of **chromatography, electrophoresis** and related methods. Contributions consist mainly of research papers dealing with chromatographic theory, instrumental developments and their applications. In the *Symposium volumes*, which are under separate editorship, proceedings of symposia on chromatography, electrophoresis and related methods are published. *Journal of Chromatography B: Biomedical Applications* —This journal, which is under separate editorship, deals with the following aspects: developments in and applications of chromatographic and electrophoretic techniques related to clinical diagnosis or alterations during medical treatment; screening and profiling of body fluids or tissues related to the analysis of active substances and to metabolic disorders; drug level monitoring and pharmacokinetic studies; clinical toxicology; forensic medicine; veterinary medicine; occupational medicine; results from basic medical research with direct consequences in clinical practice.

Submission of Papers. The preferred medium of submission is on disk with accompanying manuscript (see *Electronic manuscripts* in the Instructions to Authors, which can be obtained from the publisher, Elsevier Science B.V., P.O. Box 330, 1000 AH Amsterdam, Netherlands). Manuscripts (in English; *four* copies are required) should be submitted to: Editorial Office of *Journal of Chromatography A*, P.O. Box 681, 1000 AR Amsterdam, Netherlands, Telefax (+31-20) 485 2304, or to: The Editor of *Journal of Chromatography B: Biomedical Applications*, P.O. Box 681, 1000 AR Amsterdam, Netherlands. Review articles are invited or proposed in writing to the Editors who welcome suggestions for subjects. An outline of the proposed review should first be forwarded to the Editors for preliminary discussion prior to preparation. Submission of an article is understood to imply that the article is original and unpublished and is not being considered for publication elsewhere. For copyright regulations, see below.

Publication information. *Journal of Chromatography A* (ISSN 0021-9673): for 1995 Vols. 683–714 are scheduled for publication. *Journal of Chromatography B: Biomedical Applications* (ISSN 0378-4347): for 1995 Vols. 663–674 are scheduled for publication. Subscription prices for *Journal of Chromatography A*, *Journal of Chromatography B: Biomedical Applications* or a combined subscription are available upon request from the publisher. Subscriptions are accepted on a prepaid basis only and are entered on a calendar year basis. Issues are sent by surface mail except to the following countries where air delivery via SAL is ensured: Argentina, Australia, Brazil, Canada, China, Hong Kong, India, Israel, Japan, Malaysia, Mexico, New Zealand, Pakistan, Singapore, South Africa, South Korea, Taiwan, Thailand, USA. For all other countries airmail rates are available upon request. Claims for missing issues must be made within six months of our publication (mailing) date. Please address all your requests regarding orders and subscription queries to: Elsevier Science B.V., Journal Department, P.O. Box 211, 1000 AE Amsterdam, Netherlands. Tel.: (+31-20) 485 3642; Fax: (+31-20) 485 3598. Customers in the USA and Canada wishing information on this and other Elsevier journals, please contact Journal Information Center, Elsevier Science Inc., 655 Avenue of the Americas, New York, NY 10010, USA, Tel. (+1-212) 633 3750, Telefax (+1-212) 633 3764.

Abstracts/Contents Lists published in Analytical Abstracts, Biochemical Abstracts, Biological Abstracts, Chemical Abstracts, Chemical Titles, Chromatography Abstracts, Current Awareness in Biological Sciences (CABS), Current Contents/Life Sciences, Current Contents/Physical, Chemical & Earth Sciences, Deep-Sea Research/Part B: Oceanographic Literature Review, Excerpta Medica, Index Medicus, Mass Spectrometry Bulletin, PASCAL-CNRS, Referativnyi Zhurnal, Research Alert and Science Citation Index.

US Mailing Notice. *Journal of Chromatography A* (ISSN 0021-9673) is published weekly (total 52 issues) by Elsevier Science B.V., (Sara Burgerhartstraat 25, P.O. Box 211, 1000 AE Amsterdam, Netherlands). Annual subscription price in the USA US$ 5389.00 (US$ price valid in North, Central and South America only) including air speed delivery. Second class postage paid at Jamaica, NY 11431. **USA POSTMASTERS**: Send address changes to *Journal of Chromatography A*, Publications Expediting, Inc., 200 Meacham Avenue, Elmont, NY 11003. Airfreight and mailing in the USA by Publications Expediting.

See inside back cover for Publication Schedule, Information for Authors and information on Advertisements.

0021-9673/94/$07.00

Printed in the Netherlands

VOL. 686, NO. 1 JOURNAL OF CHROMATOGRAPHY A 25 NOVEMBER 1994

CONTENTS

(Abstracts/Contents Lists published in Analytical Abstracts, Biochemical Abstracts, Biological Abstracts, Chemical Abstracts, Chemical Titles, Chromatography Abstracts, Current Awareness in Biological Sciences (CABS), Current Contents/Life Sciences, Current Contents/Physical, Chemical & Earth Sciences, Deep-Sea Research/Part B: Oceanographic Literature Review, Excerpta Medica, Index Medicus, Mass Spectrometry Bulletin, PASCAL-CNRS, Referativnyi Zhurnal, Research Alert and Science Citation Index)

REGULAR PAPERS

Column Liquid Chromatography

Gas Chromatography

Electrophoresis

(Continued overleaf)

Contents (continued)

SHORT COMMUNICATIONS

Gas Chromatography

Planar Chromatography

Electrophoresis

JOURNAL OF CHROMATOGRAPHY A

VOL. 686 (1994)

JOURNAL OF CHROMATOGRAPHY A

INCLUDING ELECTROPHORESIS AND OTHER SEPARATION METHODS

ELSEVIER

Amsterdam – Lausanne – New York – Oxford – Shannon – Tokyo

0021-9673/94/$07.00

ELSEVIER

Journal of Chromatography A, 686 (1994) 1–10

JOURNAL OF CHROMATOGRAPHY A

Effect of integration parameters on high-performance liquid chromatographic method development and validation

Yves-L. Grize[a,*], Heinz Schmidli[a], Jens Born[b]

[a]*Mathematical Applications Department, Ciba-Geigy Ltd., CH-4002 Basle, Switzerland*

[b]*Research Services Central Analytical Department, Ciba-Geigy Ltd., CH-4002 Basle, Switzerland*

First received 15 April 1994; revised manuscript received 27 July 1994

Abstract

An HPLC method is defined as a specific setting of the physical, chemical and data processing parameters which control the chromatographic analysis. During the development or validation of a method no special attention is usually given to the data processing parameters. However, it turns out that HPLC methods for complex samples can be very sensitive to minor changes in certain numerical integration parameters such as the threshold. A series of statistically designed chromatographic runs for a dyestuff with a very large number of peaks is presented where the interpretation of the data depends crucially on which threshold parameter value is chosen. It is therefore recommended that for development or validation of an HPLC method, especially in the context of quality control of complex substances, greater attention should be paid to the integration parameters.

1. Introduction

High-performance liquid chromatography (HPLC) is a widely used technique in the chemical industries. It has even been claimed that 50–70% of all analytical applications involve HPLC measurements [1].

The setting of the parameters (often called the separation conditions) that control the run of a chromatographic analysis is called a chromatographic method. A great deal of attention has been focused on method development, optimization and more recently method validation. The aim of HPLC method development and optimization is to find the best separation conditions for the reliable measurement of the amounts of individual components in the mixture. One goal of the validation of a given HPLC method is to check its insensitivity to small variations in the separation conditions. Clearly, optimization and validation are linked, as robustness is also a feature that an HPLC method should somehow satisfy to be really optimum.

An important type of application is the quality control and quality assurance of complex chemical substances involving a large number of components, e.g., reactive textile dyestuffs. In these applications, the chromatogram of a manufactured dyestuff is compared with that of a standard (reference) to ensure that the two samples do not differ appreciably. A typical example of the chromatogram of a reactive textile dyestuff is shown in Fig. 1, where two scales are used to show better the complexity of the chromatogram. One of the difficulties in this type of application is the importance that even small

* Corresponding author.

0021-9673/94/$07.00
SSDI 0021-9673(94)00711-X

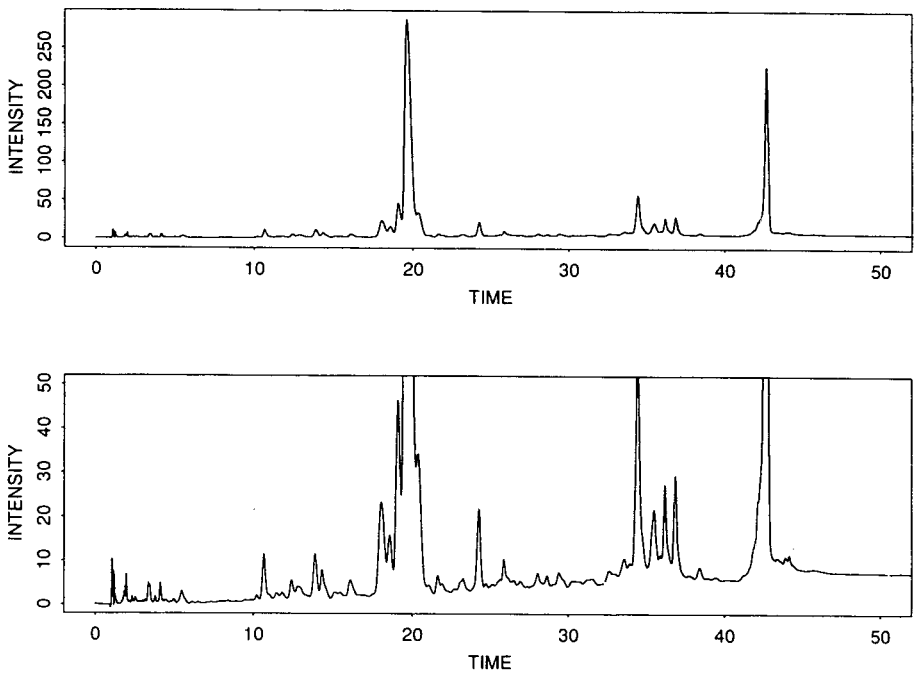

Fig. 1. Typical chromatogram of a reactive textile dyestuff.

unidentified peaks may have on the quality or toxicity of the product. In this specific context, the development of an HPLC method must aim not only at allowing a precise separation and quantification of the main components, but also, and perhaps even more important, at a systematic detection of minor components, sometimes under varying laboratory conditions.

Although the most usual strategy for developing HPLC methods in practice is still by trial and error combined with empirical knowledge and pragmatic rules, the advantages of the use of statistically designed experiments and response surfaces techniques have been recognized and are now used more frequently (e.g., [2–4]). Validation of chromatographic methods, in the past often reduced to tests of repeatability and linearity related to the areas of the most interesting peaks, are now including robustness (or ruggedness) tests. These tests, which must show that a method is insensitive to small changes in the method parameters, are also increasingly based on statistically designed experiments (e.g., [5–7]).

Chromatographic separation depends clearly on a large number of factors, including physical and chemical properties of the sample mixture and of the mobile and stationary phases and data processing parameters. Typically in the development and validation of HPLC methods the physical and chemical parameters are varied while the data processing parameters remain fixed. These data processing parameters can be separated into two groups: hardware parameters and software parameters. The hardware parameters are, e.g., flow control, temperature control, lamp current, photodiode-array detection (DAD)-specific and electronic parameters which influence the detected signals that are stored. The software parameters, on the other hand, are used to interpret and report the results from the stored data. The software parameters are often also called integration and calibration parameters. Usually no or only little attention is paid to the integration parameters. Further, manufacturers usually do not provide any indications on how to choose the settings of these parameters, and in practice a value in the middle of the

permitted range is arbitrarily chosen and kept fixed.

However, during our investigations on the validation of an HPLC method for a quality control application, we found instead that slight modifications of the values of certain integration parameters have surprising effects on the robustness of a method measured by the number of detected peaks. Why the number of detected peaks was chosen as the robustness criterion will be explained in Section 2.1. More specifically, when comparing a series of chromatograms obtained under different separation conditions (which is exactly what one does when using statistically designed experiments), the choice of integration parameter values may change the result of this comparison considerably: a method that first appears to be robust (number of detected peaks stable) may, after changing the integration parameters, lose its robustness (number of detected peaks unstable). In other words, the relative importance of the effects of the separation parameters may change when the integration parameters change. In practice, this means that two experimenters, after having performed exactly the same experiments, but having analysed their results under only slightly different settings of the integration parameters, may come to completely different conclusions in deciding which separation condition is better. This finding provided the main motivation for this paper, where our aim is to warn HPLC method developers about the possible sensitivity of the interpretation of their results to apparently innocuous integration parameter settings. In fact, we believe that data processing parameters must also be considered during HPLC method development and validation. We hope that the developers of HPLC methods will in future give more attention to these influences and provide advice to practitioners on how to adjust the integration parameters.

The paper is organized as follows: in Section 2 we describe the experimental background, explain why we chose the number of peaks as our robustness criterion and describe the different integration parameters; in Section 3 the effect of one integration parameter, the threshold, on the robustness analysis of an HPLC method used for the quality control of a dyestuff is described; and in Section 4 conclusions are drawn.

2. Experimental background

2.1. Robustness criterion

The usual optimization criterion for HPLC method development is the maximization of the minimum separation (or resolution) between adjacent peaks under the hypothesis that the number of components to be detected in the sample is known. However, in many industrial applications, e.g., in reactive textile dyestuffs production, this number of components is usually large and unknown. Of course, a chromatogram with a high resolution and a small number of peaks may be obtained, but this may be due to co-elution of many components. Also, in quality control or quality improvement applications, i.e., those of interest to us, it is a priori possible that certain small peaks will affect the quality of the product. For example, a very small amount of red in a yellow dyestuff has catastrophic consequences. For a typical chromatogram, see again Fig. 1. As it is not known in advance which component will affect quality, the total number of detected components is an important criterion for method selection.

One might at first think that it is enough simply to set the instrument threshold at its highest sensitivity, i.e., the one which corresponds to the chosen signal-to-noise ratio (e.g., 6σ), and then proceed with the experimentation. However, at this value peak detection is no longer reliable and far too many peaks are detected (in our case almost 200; see Table 1). There is therefore an unknown reasonable range of possible threshold values above the detection limit which still allows the detection of many potentially relevant small peaks and nevertheless gives a good resolution. In practice, one chooses an arbitrary value on the sensitive side of the threshold scale and keeps it fixed. The HPLC method is then developed at this threshold. During method development the number of

detected peaks is one response of interest among others such as minimum resolution and retention time. Multi-criteria optimization techniques (see, e.g., [8]) can be used at this stage. Finally, for validation purposes, the number of detected peaks is a very simple summary measure to check the robustness at detecting many small peaks. Of course, other measures could also be used, e.g., which monitor the area percentage of the major peaks. However, these other criteria are much more complex and more error-prone than the number of detected peaks. Especially in the context of validation of a method for complex substances with many small peaks, the number of peaks appears simple and yet sufficiently informative.

There are situations other than the quality control of complex substances where the total number of detected peaks can be used as a robustness criterion. For example, in the analysis of environmental samples, an a priori unknown number of components with very low concentrations need to be detected. Here again one is primarily concerned with maximizing the number of detectable components. Clearly, after this has been achieved, the HPLC method must be further improved by optimizing other criteria such as resolution of peaks known to be important or retention time. Finally, an important validation criterion is the stability of the number of detected peaks under changes in certain parameters.

2.2. Experimental conditions

The sample mixture was a commercially available reactive dye, Cibacron Red C-2G (500 mg dissolved in water). The chromatographic method to be tested was a gradient method. The end-points of the mobile phases were (1) a mixture of 10% acetonitrile and water and (2) 10% water and acetonitrile. Methanol was used as additional organic modifier. As ion-pairing agent tetrabutylammonium perchlorate was used and sodium citrate was used as a buffer. The columns were 125 mm × 4 mm I.D. and filled with 5-μm Hypersil ODS.

The chromatographic system was a Hewlett-Packard Model 1090M with three low-pressure pumps, autoinjector and column oven and DAD was applied. One of eight possible channels was used to acquire chromatograms at 254 nm. The spectral resolution chosen was 4 nm and the time resolution for the chromatograms was 0.003–0.004 min. The spectra and the chromatograms were stored on completion of the chromatographic run. Data editing and calculations such as determination and integration of peaks were executed afterwards using the stored data.

The background noise σ was measured using a blank chromatogram and a signal-to-noise ratio of 6 was taken throughout to ensure that no artifactual peaks would occur. This means that only peaks greater than 6σ were ultimately reported even if the chosen threshold value was smaller.

2.3. Integration parameters

The evaluation of the acquired raw data is done by mathematical integration. The integration algorithms identify peaks which are characterized by position on the time scale, height, area, width at half-height, symmetry, etc. The integration sensitivity can be adjusted by three integration parameters: threshold, area reject and peak width [9]. These three parameters are briefly described.

Threshold

The threshold is a value which expresses the minimum peak height detected by the integrator. This value lies on a scale from −12 to 25. On that scale, −12 is the most sensitive threshold and 25 the least sensitive threshold. The correspondence between this scale and the DAD milli-absorption units (mAU) scale is given by $\mathrm{mAU} = 2^{(th+2)}$, where *th* is the threshold value. Because the HP 1090M system used a 16-bit A/D converter, only sixteen different threshold values can be used.

Area reject

The decision on whether or not to store a peak is made at the end of the peak. The area reject

sets the area of the smallest expected peak. Thus the integrator ignores any peak which is smaller than this value. The smallest possible area reject value is zero.

Minimum peak width

The minimum peak width sets the value of the narrowest peak to be detected. Thus the integrator ignores any peak whose width is smaller than this value. The unit of peak width is time measured in minutes. The narrowest possible peak is 0.001 min.

A separate study not described here has shown that the threshold is the most influential of these three parameters on the number of detected peaks. Therefore, subsequently we only study the effect of this parameter.

3. Effect of threshold on the robustness analysis of an HPLC method

3.1. Experimental design

Before a newly developed HPLC method is used on a routine basis, e.g., for the control of product quality in different laboratories of a company, its robustness to small changes in the factor levels should be checked. If no significant effect is found then the method is robust and can be used routinely. Otherwise, either the influential factors have to be controlled more precisely, or a new, more robust method has to be developed. Statistically designed experiments can be used to test the robustness of a method by systematically varying the most important factors, for example, according to a fractional factorial experiment. Designed experiments are very helpful as the information needed can be obtained with a minimum number of experiments, which is especially important if there are many factors. Further, such experiments where the factors are varied simultaneously allow the estimation of possible interactions between the factors (synergisms). Recently, a number of such statistically designed experiments for robustness studies of HPLC have been reported (see, e.g., [7]).

For a newly developed method for determining the reactive dye Cibacron Red C-2G, previous experiments had identified four factors that were likely to affect the robustness of the method if deviations from their nominal values would occur. The four factors and their minimum and maximum deviations are as follows: I, the amount of ion pair agent, 0.4–0.6 g/l (nominal 0.5 g/l); M, amount of methanol, 28–32% (v/v) [nominal 30% (v/v)]; P, pH value, 6.2–6.6 (nominal 6.4); and C, the producer of columns, 0 = HP (Hewlett-Packard) or +1 = ST (Stagroma).

The factor C summarizes the properties of the columns of the different distributors, such as number of theoretical plates, filling procedures and ageing characteristics. It was included because different laboratories of the company may well use different column types if not otherwise specified.

In order to study the effects of such deviations, the factors were systematically varied according to a full factorial design, hence giving $2^4 = 16$ experiments. In addition, four of these experiments were repeated to provide information on the repeatability of the measurements. For each setting of the factors a chromatographic run was obtained. Then this chromatogram was analysed for each threshold value between −12 and 4 and the reported number of detected peaks was stored. The design and the number of peaks obtained for each factor combination and each different threshold value are given in Table 1.

3.2. Effect of threshold on the number of detected peaks and on repeatability

First the general effect of threshold on the number of detected peaks is examined. Fig. 2 shows this effect for the four different separation conditions that were run twice. We see that in each instance the number of peaks decreases monotonically as the value of the threshold parameter increases. This is, of course, what one would expect from the definition of this parameter. On the left side of the scale the curves are roughly constant. Clearly in that area the thres-

Table 1
Experimental design and results, showing the design (columns C, I, M, P) and for each of the 20 experiments the number of detected peaks obtained for each threshold value varying from −12 to 4

Run no.	C	I	M	P	Threshold																
					−12	−11	−10	−9	−8	−7	−6	−5	−4	−3	−2	−1	0	1	2	3	4
1	1	0.4	28	6.2	180	179	179	175	167	147	133	119	100	76	53	34	21	8	4	1	1
2	1	0.4	28	6.6	191	190	189	183	165	155	140	117	99	75	54	33	18	7	4	1	1
3	1	0.4	32	6.2	165	164	162	162	156	148	132	118	96	71	52	34	18	9	4	2	1
4	1	0.4	32	6.2	148	148	148	147	141	133	124	108	91	69	50	31	14	6	4	2	1
5	1	0.4	32	6.6	179	178	178	172	165	153	134	118	100	71	54	32	18	8	4	1	1
6	1	0.4	32	6.6	162	160	161	156	149	141	129	110	93	71	52	30	15	7	4	1	1
7	1	0.6	28	6.2	165	165	163	161	155	145	135	114	95	69	46	26	18	9	4	2	2
8	1	0.6	28	6.6	172	171	171	165	150	128	123	104	85	69	44	26	17	9	4	2	2
9	1	0.6	32	6.2	155	153	153	152	143	128	115	101	80	65	38	26	16	7	4	2	2
10	1	0.6	32	6.6	179	178	178	172	155	136	131	110	83	67	43	25	16	9	4	2	2
11	0	0.4	28	6.2	193	191	190	182	169	153	142	132	121	89	59	45	22	8	4	3	1
12	0	0.4	28	6.6	179	179	178	184	171	150	139	128	109	88	60	43	21	9	5	3	1
13	0	0.4	32	6.2	193	192	192	187	169	143	135	121	104	82	62	40	21	9	5	3	1
14	0	0.4	32	6.6	167	167	168	166	146	141	134	121	112	93	66	43	26	12	5	3	1
15	0	0.6	28	6.2	180	180	177	175	166	152	141	126	110	85	60	33	20	9	6	2	2
16	0	0.6	28	6.6	195	192	193	186	177	159	142	129	112	84	57	36	19	9	5	2	2
17	0	0.6	32	6.2	183	183	182	181	168	155	143	123	99	82	56	32	23	10	4	2	2
18	0	0.6	32	6.2	180	180	179	176	165	154	144	121	101	80	52	33	22	10	5	3	2
19	0	0.6	32	6.6	197	196	195	188	176	165	148	133	104	82	54	30	19	10	5	3	2
20	0	0.6	32	6.6	187	186	186	184	172	158	138	124	101	83	55	30	18	11	5	4	3

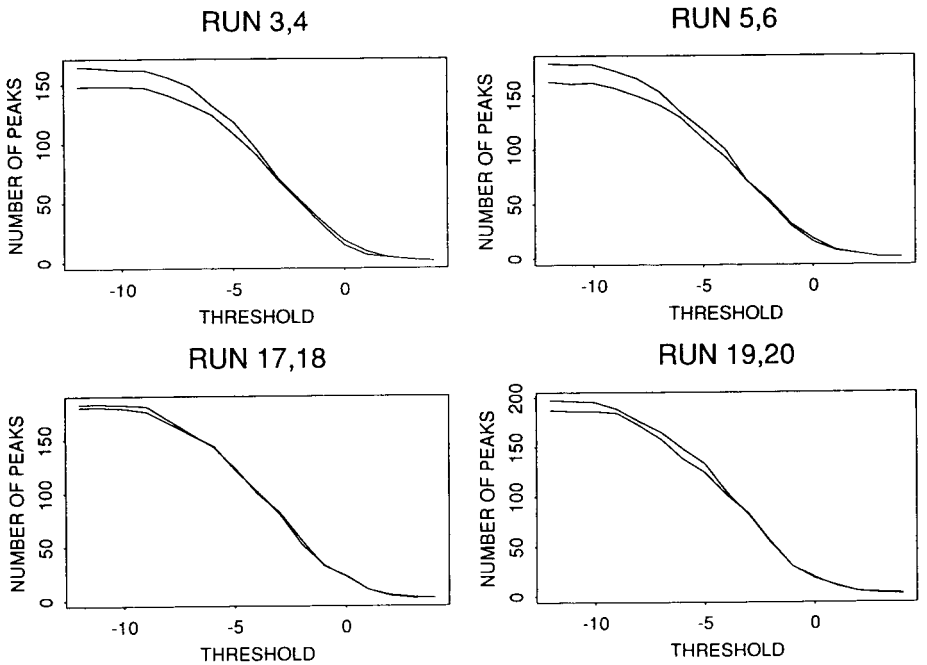

Fig. 2. Repeatability of measurements. The chromatograms corresponding to four different separation conditions (the run numbers correspond to Table 1) were obtained twice and analysed with different values of the threshold parameter. The graphs show how the number of detected peaks changes with the threshold.

hold was below the 6σ detection limit. As can be seen from Table 1, this was the case for all 20 chromatographic runs.

For the dyestuff under consideration the routine threshold value used in the laboratory before our study was undertaken was -2. It is interesting to observe that it is exactly around this value, say in the range from -5 to 0, that the number of peaks varies most. Fig. 2 shows also that in the four repeated cases the size of the threshold effect is clearly distinct from the repeatability error.

That the setting of the threshold parameter affects the number of peaks is, of course, obvious. What is interesting here is the strong non-linearity of this effect and therefore the high sensitivity to threshold values. This fact is, in our opinion, not sufficiently emphasized by the manufacturers of HPLC instruments. However, the full impact of this sensitivity will be shown below, when the number of detected peaks in different chromatograms is used to infer which are the most crucial parameters affecting the quality of the chromatographic run.

Note: when other data handling systems are used (e.g., Spectra-Physics and PE Nelson systems), the aspect of the curves of Fig. 2 may change, but they remain strongly non-linear.

The repeatability between two similar HPLC runs is summarized in Fig. 3, which shows how the relative standard deviation (R.S.D.) changes with the threshold value. For a given threshold, the R.S.D. was calculated as $(S^2/N)^{1/2}$, where S^2 is the average of the sample variance over the four runs which were repeated once (here simply the average squared differences in the number of peaks) and N is the average number of peaks. In the range from -12 to 0, the R.S.D. remains roughly constant at 5%. This is a desirable feature and allows one to compare directly results obtained for different values of the threshold. For positive values the R.S.D. is no longer meaningful because the average number of peaks is almost zero.

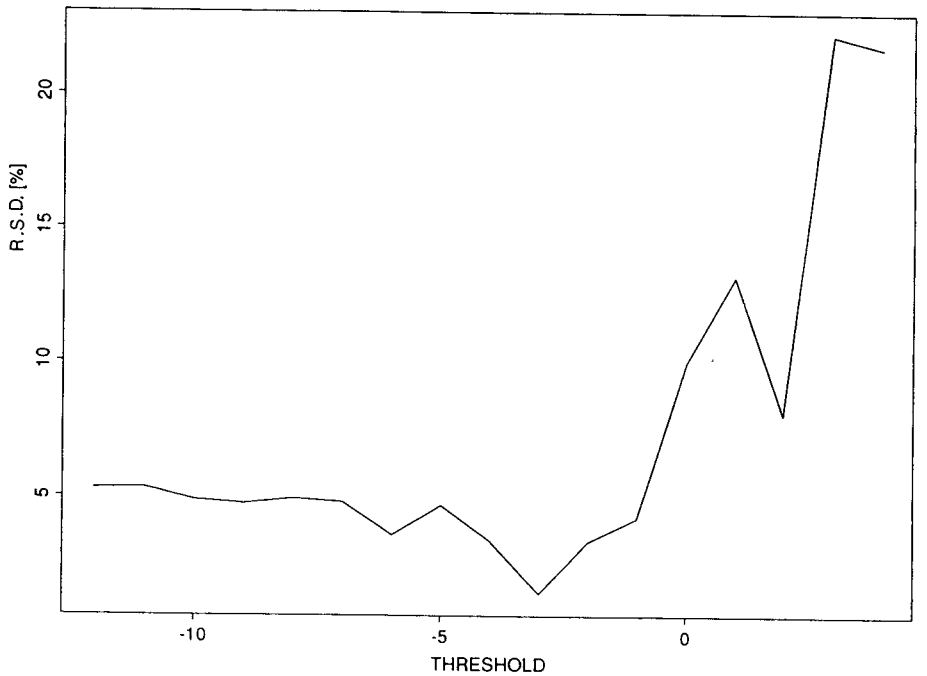

Fig. 3. The relative standard deviation is essentially constant for threshold values in the range −12 to 0.

3.3. *Effect of threshold on the analysis*

A full factorial design allows the estimation of all main effects of the four factors *C*, *P*, *I* and *M* and their eleven interactions *CP*, *CI*, . . . , *CPI*, . . . , *CPIM*. Hence, for a fixed value of the threshold, the 20 experiments can be analysed jointly by multiple regression. Such an analysis gives the effect (model coefficient) of the fifteen model variables *C*, *P*, . . . , *CPIM* on the number of peaks together with their *t*-values. The *t*-value of an effect is the ratio of the model coefficient and its estimated standard deviation. Absolute *t*-values larger than, say, 2 correspond roughly to a significance level below 5% and thus suggest that the effect of the corresponding variable should not be neglected, i.e., that the corresponding variable poses a robustness problem.

To visualize the results, the *t*-values for a range of threshold values are displayed in Fig. 4. This type of graph is called a λ-plot (see [10]) and conveniently summarizes the entire experiments and analyses by showing which are the likely relevant factors for each threshold value. Each connected line corresponds to the *t*-values of one of the fifteen model variables. Those lines that stand out have been labelled by the name of their corresponding model variable. For example, one sees that for a threshold of −5, only the factor *C* has an effect, whereas for the only slightly different threshold of −3 the three factors *C*, *I* and *M* are important and also the interaction between *M* and *P* (and perhaps even other interactions). Hence, by considering only the data corresponding to a threshold of −5, one would think that no robustness problem due to changes in *I*, *P* or *M* could occur. Therefore, it seems sufficient to specify the column type (here HP since this type tends to increase the number of peaks, as can be seen from Fig. 4) to ensure stability in the number of detected peaks. This is not, of course, what would have been deduced if only the data corresponding to a threshold of −3 had been considered.

Further, the graph shows also that the effect of column type (*C*) is consistently present (and always negative) almost throughout the range of threshold values. On the other hand the factor

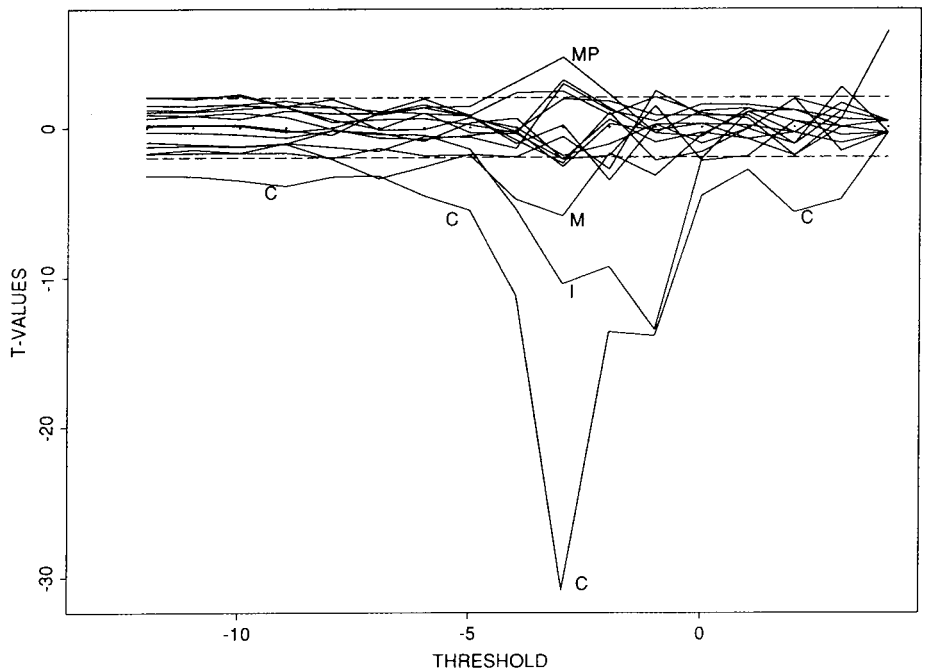

Fig. 4. λ-Plot of the 15 model variables. The plot illustrates how the t-values of each model variable varies with the threshold. Variables whose t-values exceed 2 in absolute value (horizontal dashed lines at 2 and −2) are likely to influence the number of detected peaks.

amount of methanol (M) is only significant for threshold values between −4 and −3. Finally, one also sees that it is for a threshold value of −3 that the greatest number of significant model variables occurs. This shows the variety of information that can be read from a λ-plot.

However, the main conclusion of the analysis is that the effects of column type, amount of ion-pairing agent and amount of methanol depend critically on the value of the threshold parameter. In other words, there is an interaction between threshold and the factors C, I and M. At this stage the experimenter faces the following difficult choice: either a specific threshold value can be chosen once and for all as adequate, perhaps based on some other aspects of the chromatogram, past experience or a priori knowledge of the expected number of peaks, or the HPLC method must be modified, so as to be less sensitive to small modifications of the threshold. Which road to pursue may be situation dependent. In any case, the experimenter has been warned that the threshold value is crucial in analysing the results of this series of experiments.

After having found this unsuspected effect of the threshold, we re-analysed other robustness experiments, not reported here, carried out with the same dyestuff. Our results were similar in that again we found that the analysis of factorial experiments was different depending on the threshold value.

4. Conclusions

In those situations where the number of detected peaks is at least one of the main concerns such as for substances with many important small components, this investigation illustrates a number of issues:

(1) The non-linearity of the number of detected peaks with respect to the value of the

threshold has shown that great care should be taken when setting the value of this parameter.

(2) The value of the threshold should be incorporated in any analysis involving the comparison of chromatograms such as obtained after performing a series of experiments like a factorial design. The analysis may differ greatly with the threshold.

(3) Any method validation study should consider the influence of the threshold. In fact if it does not seem to be possible to specify which threshold is adequate, the method should be robust for a reasonable range of threshold values. This means that the threshold and perhaps further data processing parameters should be incorporated in the experimental design together with the other separation parameters.

(4) During method development the situation is even more difficult. Different settings of the threshold could affect the optimization strategy and lead to very different optimum settings of the factors.

Although the points discussed above were made only in relation to the threshold parameter, similar conclusions could probably be drawn for other data processing parameters. Observe also that these points are not hardware dependent, but are a consequence of the necessary processing of the data.

In our opinion, the issues in this paper illustrate well a general feature of modern scientific measurements in that the complexity of modern laboratory instrumentation often discourages some from trying to understand how their system works. The neglect of apparently innocuous parameters may have dramatic consequences.

Acknowledgement

We thank S. Lahely for her great help with the laboratory work and one of the Editors for his critical but encouraging remarks which helped us to better formulate and justify our approach.

References

[1] F. Erni, presented at the *17th International Symposium on Column Liquid Chromatography, Hamburg, 9–14 May 1993*, Abstract No. O-111.
[2] B. Bourguignon, F. Marcenac, H.R. Keller, P.F. de Aguiar and D.L. Massart, *J. Chromatogr.*, 628 (1993) 171–189.
[3] P. Billot and B. Pitard, *J. Chromatogr.*, 623 (1992) 305–313.
[4] Q.S. Wang, R.Y. Gao, B.W. Wang and D.P. Fan, *Chromatographia*, 38 (1994) 187–190.
[5] M. Mulholland and J. Waterhouse, *J. Chromatogr.*, 395 (1987) 539–551.
[6] M. Mulholland, *Trends Anal. Chem.*, 7 (1988) 383–389.
[7] J.A. Van Leeuwen, L.M.C. Buydens, Vandeginste, G. Kateman, P.J. Schoenmakers and M. Mulholland, *Chemometr. Intell. Lab. Syst.*, 10 (1991) 337–347; and references cited therein.
[8] H.R. Keller, D.L. Massart and J.P. Brabs, *Chemom. Intell. Lab. Syst.*, 11 (1991) 175–189.
[9] Hewlett Packard Analytical Division, *HPLC ChemStation Fact File*, (1987) 3-27–3-47.
[10] G.E.P. Box, *Technometrics*, 30 (1988) 1–17.

ELSEVIER

Journal of Chromatography A, 686 (1994) 11–20

JOURNAL OF CHROMATOGRAPHY A

Measurement of narrow-distribution polydispersity using multi-angle light scattering

David W. Shortt

Wyatt Technology Corporation, 802 E. Cota Street, Santa Barbara, CA 93103, USA

First received 17 May 1994; revised manuscript received 25 July 1994

Abstract

Molecular radius information obtained with multi-angle laser light scattering combined with gel permeation chromatography was used to obtain an upper limit for the polydispersity $\bar{M}_w/\bar{M}_n$ of a narrow-distribution polystyrene standard dissolved in toluene. The radius obtained by light scattering is independent of any other detector and so is not affected by interdetector delay volumes or interdetector broadening. The value obtained for $\bar{M}_w/\bar{M}_n$ was 1.00096 ± 0.00004, much closer to unity than previously reported. Column broadening was found to be responsible for nearly all the observed peak width.

1. Introduction

The molecular mass distribution (MMD) of samples prepared by termination-free chain addition polymerization is theoretically close to a Poisson distribution, in which the molecular mass polydispersity $\bar{M}_w/\bar{M}_n$ (where $\bar{M}_w$ is the weight-average molecular mass and $\bar{M}_n$ is the number-average molecular mass) is predicted to be very close to unity [1–3]. In practice, the methods available to measure whole-polymer $\bar{M}_w$ and $\bar{M}_n$ directly (for example, light scattering and osmometry, respectively) are only accurate to 1–2%, making determination of polydispersities smaller than about 1.03 impossible. Gel permeation chromatography (GPC) allows samples to be separated by molecular size and then detected, typically by a differential refractive index (DRI) detector. In traditional GPC one injects a series of narrow-distribution polymer standards of known molecular masses M to create a calibration curve [4] of log M vs. elution volume V. The DRI chromatogram for an unknown sample is then used along with the calibration curve to determine the molecular mass averages and MMD for the unknown [5]. A number of factors affect the accuracy of this determination, among them conformation differences between the calibration standards and the unknown, and band broadening in the chromatographic system. When studying narrow-MMD samples, band broadening is a particularly important issue and has been discussed by many researchers [6–8]. The presence of broadening makes calculating the polydispersity of very narrow distribution samples difficult. In this paper we shall use the term "column broadening" to refer to any broadening prior to the first detector in the system, and "interdetector broadening" to refer to subsequent broadening occurring in various detectors' flow cells and/or connecting tubing. Interdetector broadening is

0021-9673/94/$07.00
SSDI 0021-9673(94)00708-X

particularly important when signals from various instruments are compared.

With the use of molecular mass-sensitive techniques such as light scattering (LS) combined with GPC it is possible to determine molecular masses directly [9]. Since the LS signal is proportional to the product of molecular mass and concentration, one can determine the molecular mass by taking the ratio of the LS and DRI signals. This technique allows accurate molecular mass and radius determination for each slice across a sample peak without column calibration. When using GPC–LS, the effect of broadening is to make the calculated molecular mass values more constant than they should be, decreasing the calculated polydispersity of the sample. In addition, interdetector broadening which occurs between the LS and DRI detectors causes the calculated molecular mass values to be incorrect because one signal is broadened more than the other. The presence of interdetector broadening makes determination of polydispersities less than 1.01 very difficult, even when corrections are applied. However, by using thermal field flow fractionation to correct for interdetector broadening, Giddings [10] showed that a polystyrene sample with a nominal polydispersity of 1.06 actually had a value closer to 1.003.

Furthermore, in order to combine properly the signals from multiple instruments, it is important to determine the interdetector delay volume accurately. The effect of changes in assumed delay volume on molecular mass determinations with LS has been discussed in detail by Wyatt and Papazian [11]. The effect is relatively small; it does not affect the calculation of $\bar{M}_w$ at all, and it changes $\bar{M}_n$ by only a few percent. Unfortunately, when we are attempting to calculate accurately the polydispersity of a narrow-MMD peak, an effect of even a few percent makes molecular mass measurements unsuitable for this purpose.

Multi-angle laser-light scattering (MALLS) provides not only the molecular mass but also the mean square molecular radius. At the low concentrations typical of GPC separations, the calculated molecular radius values are independent of the DRI detector, so they depend neither on the interdetector delay volume nor on interdetector broadening. Thus molecular radius is an excellent way to study the polydispersity of narrow-MMD samples. This paper describes a new technique which uses the molecular radius values obtained by GPC–MALLS to calculate the polydispersity of a narrow-MMD polystyrene standard, taking proper account of column broadening effects. First a model of a simple chromatographic system with Gaussian peaks and Gaussian broadening is presented. Effects of interdetector delay volume and broadening on the calculation of molecular mass and radius are discussed. Data from narrow-MMD polystyrene standards are presented, and the radius information is used to place a new upper limit on the polydispersity of one of these narrow standards.

2. Theory

2.1. Model of a simple chromatographic system

Let us consider a simple chromatographic system. We shall assume a single Gaussian peak. This means the normalized concentration signal is given by

$$h(V) = 2\left(\frac{\ln 2}{\pi}\right)^{1/2} \cdot \frac{m_0}{w_0} \cdot \exp\left[-4 \ln 2(V - V_0)^2 / w_0^2\right] \quad (1)$$

where m_0 is the mass of solute in the peak, V_0 is the peak elution volume and w_0 is the full width at half maximum (FWHM) of the true, unbroadened peak. We further assume that the column separation is log–linear according to molecular mass as

$$M(V) = 10^{A + BV} \quad (2)$$

where A and B are constants and $M(V)$ is the molecular mass at elution volume V. Likewise, if the separated molecules have a conformation (random coil, rigid rod, sphere, etc.) which is independent of molecular mass, then the column separation in root mean square (rms) radius $\langle r^2 \rangle^{1/2}$ follows a similar relation:

$$\langle r^2\rangle^{1/2}(V) = 10^{C+DV} \tag{3}$$

where $\langle r^2\rangle^{1/2}(V)$ is the rms radius of the molecules at elution volume V.

The molecular mass polydispersity is equal to the ratio $\bar{M}_w/\bar{M}_n$, where $\bar{M}_n$ and $\bar{M}_w$ are given by [12]

$$\bar{M}_n = \frac{\int h(V)\,dV}{\int h(V)/M(V)\,dV}$$

$$\bar{M}_w = \frac{\int M(V)h(V)\,dV}{\int h(V)\,dV} \tag{4}$$

The limits of integration are taken to be $-\infty$ to $+\infty$. Integrating these relations using Eqs. 1 and 2 gives

$$\bar{M}_w/\bar{M}_n = \exp[(\ln 10)^2 B^2 w_0^2/8 \ln 2] \tag{5}$$

For a suitably narrow-distribution sample, $Bw_0 \ll 1$, and we have the following approximation:

$$\bar{M}_w/\bar{M}_n \cong 1 + (\ln 10)^2 B^2 w_0^2/8 \ln 2 \cong 1 + 0.96 B^2 w_0^2 \tag{6}$$

Thus the polydispersity depends only on the product Bw_0. Even though real chromatographic peaks differ somewhat from Gaussian, peaks from narrow-distribution samples can be fit quite successfully by a Gaussian line shape, and so this relation provides a reasonable estimate of the polydispersity.

2.2. Light scattering

The following equation [13] describes the Rayleigh–Gans–Debye (see [14]) approximation for the Rayleigh ratio $R(\theta)$ of light scattered at an angle θ by macromolecules having a weight-average molecular mass $\bar{M}_w$, in the limit of small concentrations c:

$$\frac{R(\theta)}{K^* c} = \bar{M}_w P(\theta) - 2A_2 \bar{M}_w^2 P^2(\theta) c \tag{7}$$

Here K^* is an optical constant given by

$$K^* = 4\pi^2 (dn/dc)^2 n_0^2 / N_A \lambda_0^4 \tag{8}$$

for vertically polarized incident light, where n_0 is the solvent refractive index, N_A is Avogadro's number, λ_0 is the vacuum wavelength of the incident light, and dn/dc is the refractive index increment. The scattering function $P(\theta)$ describes the angular dependence of the scattered light and will be discussed in more detail below. Here it suffices to remark that $P(\theta \to 0) = 1$ for any molecular conformation or size satisfying the Rayleigh–Gans–Debye approximation. The quantity A_2 is the second virial coefficient which describes solvent–solute interactions and can usually be ignored for the low concentrations common in GPC. Furthermore, in chromatography we assume a separated sample so that at each elution volume V only one molecular mass species is present, implying $\bar{M}_w = M$. Thus for GPC we have the following useful expression:

$$R(\theta) = K^* c M P(\theta) \tag{9}$$

In the low-angle limit $R(\theta \to 0) = K^* cM$. We shall explore the implications of imperfect chromatographic separation in Section 2.4 below.

We define $LS(V)$ to be the measured light-scattering signal [proportional to $R(\theta)$] in the limit $\theta \to 0$. Thus $LS(V)$ is proportional to the product of the molecular mass $M(V)$ and the concentration signal $h(V)$:

$$LS(V) \propto M(V)h(V) \propto \exp[\ln 10\,(A + BV) - 4 \ln 2\,(V - V_0)^2/w_0^2] \tag{10}$$

which can be rewritten as

$$LS(V) \propto \exp\left[-4 \ln 2 \left(V - V_0 - \frac{\ln 10}{8 \ln 2} B w_0^2\right)^2 \Big/ w_0^2\right] \tag{11}$$

ignoring constant additive terms in the exponential. This implies that the LS signal is itself a Gaussian with the same FWHM but shifted with respect to $h(V)$ by a volume $(\ln 10)Bw_0^2/8 \ln 2$. Since B, the slope of the molecular mass calibration curve, is typically negative in GPC, the shift is to smaller elution volumes. When analyzing data, we measure $LS(V)$ from the light-scattering instrument, $h(V)$ from the DRI detec-

tor, and we take the ratio $LS(V)/h(V)$ to recover $M(V)$.

2.3. Size information from multi-angle light scattering

Multi-angle light scattering allows determination of the molecular size as well as the molecular mass. The angular dependence of the scattered light is described by the scattering function $P(\theta)$, where θ is the scattering angle. For molecules smaller than about $\lambda/20$, where λ is the wavelength of the scattered light in solution, $P(\theta)$ can be well approximated by

$$P(\theta) = 1 - \frac{16\pi^2}{3\lambda^2} \cdot \langle r^2 \rangle \sin^2(\theta/2) \quad (12)$$

where $\langle r^2 \rangle$ is the mean square radius of the molecules. For larger molecules, more terms containing higher powers of $\sin^2(\theta/2)$ are required. Alternatively, one can use a specific model for $P(\theta)$ which assumes a certain molecular conformation such as random coil, rigid rod, or sphere. For example, ideal random coils [15] scatter according to

$$P(\theta) = 2(e^{-x} - 1 + x)/x^2 \quad (13)$$

where

$$x = (4\pi/\lambda)^2 \langle r^2 \rangle \sin^2(\theta/2) \quad (14)$$

In any case, the mean square radius $\langle r^2 \rangle$ is proportional to the low-angle derivative of $P(\theta)$ with respect to $\sin^2(\theta/2)$. For any given slice, $R(\theta) \propto P(\theta)$ as long as c is small enough that the A_2 term in Eq. 7 can be neglected. Therefore, to calculate $\langle r^2 \rangle$ for a particular slice one fits the angular LS data $R(\theta)$ to one of the above models. For example, using Eqs. 9 and 12 gives the complete model

$$R(\theta) = a\left[1 - \frac{16\pi^2}{3\lambda^2} \cdot \langle r^2 \rangle \sin^2(\theta/2)\right] \quad (15)$$

where a is equal to K^*cM. Since λ is known, Eq. 15 is a model having two parameters, a and $\langle r^2 \rangle$. Note that a serves as a scaling factor; if we arbitrarily double all the $R(\theta)$ values, a doubles but $\langle r^2 \rangle$ remains unchanged. Thus the value of $\langle r^2 \rangle$ determined from the model is independent of the value of a, and therefore of c, and hence independent of the concentration detector and interdetector delay volume. Even if we had no concentration signal, we would still obtain $\langle r^2 \rangle$ correctly (of course, in this case we would obtain a meaningless value of M). The independence of $\langle r^2 \rangle$ from c is extremely important, for it will allow us to make meaningful statements about the polydispersity of narrow-distribution standards without the errors associated with delay volume inaccuracy or interdetector broadening.

2.4. Effect of peak broadening on molecular masses and radii calculated from light-scattering data

We shall assume Gaussian broadening [4] characterized by a FWHM of w_G. Then the normalized (i.e., unit area) broadening kernel is

$$G(V) = \left(\frac{\ln 2}{\pi}\right)^{1/2} \cdot \frac{2}{w_G} \cdot \exp(-4 \ln 2 V^2/w_G^2) \quad (16)$$

If we have a concentration chromatogram $h(V)$, the broadened chromatogram $F(V)$ is then given by Tung's convolution integral [16]

$$F(V) = \int h(y)G(V-y)\,dy \quad (17)$$

where the limits of integration are taken to be $-\infty$ to $+\infty$. It is not difficult to show that the convolution of two Gaussian peaks is itself Gaussian and that the peak widths add in quadrature. For example, the observed FWHM of $F(V)$ is given by

$$w_{obs}^2 = w_0^2 + w_G^2 \quad (18)$$

The LS signal is also broadened, and we must account for the fact that when multiple molecular mass species are present, the amount of light scattered is proportional to the weight average of those species. The observed molecular mass as measured by the LS detector is the ratio of the broadened LS signal to the broadened concentration signal:

$$M_{obs}(V) = \frac{\int M(y)h(y)G(V-y)\,dy}{\int h(y)G(V-y)\,dy} \quad (19)$$

Integration of Eq. 19 is tedious but straightforward; the result is that $M_{obs}(V)$, like $M(V)$, is log–linear but with a slope B_{obs} given by the simple expression

$$B_{obs} = Bw_0^2/w_{obs}^2 \quad (20)$$

Details of the derivation of Eq. 20 are given in the Appendix. Thus the effect of broadening on the combination of DRI and LS detectors is to reduce the magnitude of the apparent slope of the calibration curve, making the peak appear to have a smaller polydispersity. For a broad distribution peak $w_{obs} \approx w_0$ and $B_{obs} \approx B$. For a very-narrow-distribution peak, however, $w_{obs} >> w_0$ and B_{obs} approaches zero. Therefore any estimate of the polydispersity of a narrow-distribution peak must include the effects of broadening.

A similar analysis may be performed to obtain the observed rms radius $\langle r^2\rangle_{obs}^{1/2}(V)$. In this case, however, it is the so-called z-average mean square radius, not the weight average, to which the LS detector responds [17]. The result for the observed rms radius is

$$\langle r^2\rangle_{obs}^{1/2}(V) = \left[\frac{\int \langle r^2\rangle(y)M(y)h(y)G(V-y)\,dy}{\int M(y)h(y)G(V-y)\,dy}\right]^{1/2} \quad (21)$$

which is again log–linear with a slope D_{obs} given by an expression directly analogous to Eq. 20:

$$D_{obs} = Dw_0^2/w_{obs}^2 \quad (22)$$

Details of this derivation are given in the Appendix. This relation allows us to recover the unbroadened width w_0 if we know the observed width w_{obs}, the observed rms radius calibration slope D_{obs}, and the true calibration slope D. The quantity w_{obs} is easy to obtain from a sample's chromatogram, and D_{obs} can be obtained by measuring the rms radius at each slice across the sample peak. The true calibration slope D can be obtained by injecting a series of narrow standards and constructing the rms radius calibration curve. Once w_0 has been determined, it can be used in Eq. 6 to obtain the polydispersity. This is the procedure we shall use below.

In calculating the effect of broadening on molecular mass we have assumed that the peak undergoes no additional broadening in passing from one instrument to the other. If some interdetector broadening occurs, the ratio of LS to DRI gives calculated molecular masses which do not lie on a log–linear curve, and the results depend on which detector is connected first in line. Typically the LS detector is first, followed by the DRI detector. In this case the DRI signal is broadened more than the LS signal, and the calculated molecular masses are too large at the peak center and too small on either side [18]. This effect, like the delay volume effect discussed by Wyatt and Papazian [11], is small but is more pronounced for narrow peaks. Interdetector broadening depends heavily on the particular flow design of the various instruments and may be far from Gaussian. The calculated radius is not affected by interdetector broadening since the DRI signal is not used. This is another reason why radius measurements, if available, are superior to molecular mass measurements when studying the polydispersity of narrow-distribution samples.

3. Experimental

Data were collected from a chromatograph made up of an LDC Analytical Model 396-57 pump, two columns (300 mm × 8 mm; MZ Analysentechnik, Mainz, Germany; styrene–divinylbenzene; 5 μm particle diameter; 10^6 and 10^4 Å pore diameter; ambient temperature), a Wyatt Technology Model DAWN DSP-F laser photometer and a Waters Model 410 differential refractometer. The mobile phase was toluene and the flow-rate was 1.0 ml/min. The delay volume between the LS instrument and the DRI detector was measured to be 184 μl, meaning that the DRI detector's cell was 184 μl down-

stream of the LS detector's cell. Stainless-steel tubing with I.D. 0.25 mm was used for all connections. A series of Pressure Chemical polystyrene standards of nominal molecular masses 30, 65, 130, 200, 400 and 950 kg/mol was injected. The injection volume for all samples was 100 μl. Column loading ranged from 0.6 mg for the 30 kg/mol sample to 0.03 mg for the 950 kg/mol sample. Data points were collected every 1.0 s. Molecular masses and rms radii were calculated independently for each sample using Wyatt Technology's ASTRA chromatography software version 1.1.5 for Macintosh.

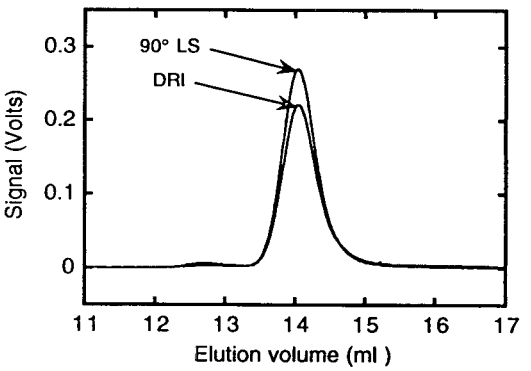

Fig. 1. 90° LS and DRI signals for nominal 400 kg/mol polystyrene in toluene.

4. Analysis and results

First, all the data were analyzed to verify that reasonable values are obtained for both molecular mass and radius for the samples of interest. Table 1 shows the results for the samples used in this study. Molecular mass and radius values in Table 1 were calculated for slices near the tops of the respective peaks. Since the polydispersity calculations will depend on precise radius measurements, it is important to use data with a high signal-to-noise ratio. The nominal 400 and 950 kg/mol samples gave the highest relative precision for the rms radius. Although column calibration is not necessary to determine molecular masses or sizes from LS data, in order to calculate the polydispersity of narrow standards it will prove necessary to measure the slope of log $\langle r^2 \rangle^{1/2}$ vs. V and log M vs. V to obtain the coefficients B and D in Eqs. 2 and 3. We expect these coefficients to be functions of V since the calibration curves are not exactly log–linear. Thus it is important to measure B and D at the elution volume of interest. For these reasons, the 400 kg/mol sample was chosen for polydispersity analysis, with the 200 and 950 kg/mol samples providing additional data used to determine B and D.

Fig. 1 shows the 90° LS and DRI signals for the 400 kg/mol sample as a function of elution volume. The FWHM w_{obs} of the peaks is 0.54 ± 0.01 ml. There is no statistically significant difference in the FWHM for the two peaks, although a small amount of additional tailing can be seen in the DRI signal on close examination. Peaks for the other samples were of similar quality. The slopes of the molecular mass and radius calibration curves were determined by fitting the data in Table 1 for the 200, 400 and 950 kg/mol samples. The best-fit slope of log M vs. V, which

Table 1
Peak molecular mass and rms radius results for six polystyrene standards in toluene

Nominal molecular mass (kg/mol)	Peak elution volume (ml)	M (kg/mol)	$\langle r^2 \rangle^{1/2}$ (nm)
30	18.92	29.9 ± 0.8	6 ± 1
65	17.51	65 ± 1	9.7 ± 0.4
130	16.46	133.0 ± 0.4	14.2 ± 0.3
200	15.48	206.0 ± 0.4	18.0 ± 0.3
400	14.04	406 ± 1	26.8 ± 0.2
950	12.30	954 ± 2	45.1 ± 0.2

The nominal values are supplied by the manufacturer. Values for M and $\langle r^2 \rangle^{1/2}$ are the values for slices at the center of the peaks.

is B in Eq. 2, is -0.209 ± 0.002 ml^{-1}. The best-fit slope of log $\langle r^2 \rangle^{1/2}$ vs. V, or D in Eq. 3, is -0.128 ± 0.002 ml^{-1}.

If no broadening were present in the chromatograms of Fig. 1, then the observed peak width w_{obs} would be due only to differences in molecular mass across the peak, and $w_{obs} = w_0$. We could then use w_0 along with the calibration slope B to calculate $\bar{M}_w/\bar{M}_n$ via Eq. 6. The above values for w_0 and B give $\bar{M}_w/\bar{M}_n = 1.0122 \pm 0.0005$. According to Eq. 18 the presence of broadening makes the observed peak wider than with no broadening. Because the true width is always smaller than the observed width, this simple calculation therefore puts a rough upper bound on the sample's polydispersity.

Fig. 2 shows the rms radius as a function of elution volume across the peak of nominal 400 kg/mol polystyrene. The 90° LS signal is superimposed. At the edges of the peak where the signal-to-noise ratio is low, the rms radius is uncertain. But across the center FWHM of the peak, the rms radius exhibits little variation. Since the radius calculation is independent of the DRI signal, delay volume and interdetector broadening are not factors. This makes the molecular radius an excellent parameter to observe effects of column broadening. The observed flatness in Fig. 2 could have two causes: (i) the sample is extremely monodisperse, and the observed width of the peak is due entirely to column broadening; (ii) the sample has significant polydispersity but has been broadened so much by the columns (in accordance with Eq. 22) that the observed slope is near zero. To calculate the true polydispersity it is thus necessary to determine the amount of column broadening present.

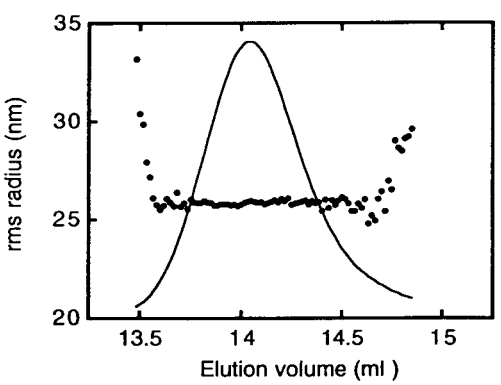

Fig. 2. Calculated rms radius as a function of elution volume for the sample of Fig. 1. The 90° LS signal is overlaid.

The unbroadened width w_0 for a narrow-distribution sample can be calculated from Eq. 22 if we determine both D and D_{obs} as well as w_{obs}. The value of D was shown above to be -0.128 ± 0.002 ml^{-1}. As determined above, $w_{obs} = 0.54 \pm 0.01$ ml. The value of D_{obs} can be obtained by fitting the radius data from Fig. 2 and finding the slope. The typical uncertainty in the radius measurements for each slice is about 0.3 nm, obtained from statistically analyzing the fluctuation in the LS data for the slices within the FWHM of Fig. 2. These uncertainties, combined with the radius data within the FWHM, yield $D_{obs} = 0.004 \pm 0.005$ ml^{-1}. Analysis of a second injection of the same sample gives $D_{obs} = 0.0008 \pm 0.003$ ml^{-1}. In other words, D_{obs} is zero to within its uncertainty, a result consistent with visual inspection of the FWHM region of Fig. 2. To be conservative, let us take two standard deviations of the slope with the larger uncertainty, or 0.01 ml^{-1}, as an upper bound on the magnitude of D_{obs}. Mathematically, this means $|D_{obs}| < 0.01$ ml^{-1}. Using two standard deviations gives a 95% confidence interval in the results. We then find from Eq. 22 that $w_0 < 0.151 \pm 0.003$ ml. Note that the unbroadened width is smaller than w_{obs} by at least a factor of 3.6. Thus almost all the observed width of 0.54 ml is due to broadening. The limit on $|D_{obs}|$ is an upper bound, with 95% confidence, and so the value of w_0 is also an upper bound.

Finally, having determined we can apply Eq. 6 to calculate the polydispersity. The result is $\bar{M}_w/\bar{M}_n < 1.00096 \pm 0.00004$. This is a surprisingly small polydispersity. To gain an understanding of why the result is so small, note that Eq. 6 implies that $\bar{M}_w/\bar{M}_n - 1$ is proportional to w_0^2. Earlier in this section we saw that assuming $w_0 = w_{obs}$ implies a polydispersity of about 1.012. In fact w_0 is smaller than w_{obs} by at least a factor of 3.6 due to column broadening, and $\bar{M}_w/\bar{M}_n - 1$ is therefore smaller by the square of this factor, or

about 13. Thus the true polydispersity must be at least 13 times closer to unity than 1.012, or roughly 1.001. The theoretical lower limit for the polydispersity of the Poisson distribution is $1 + x^{-1}$, where x is the degree of polymerization [3]. For a 400 000 g/mol polymer with a repeat unit mass of about 100 g/mol, x is about 4000. The theoretical lower limit is then 1.00025, about four times closer to unity than measured. Thus the polydispersity measured here, even though it is small, is consistent with the polymerization mechanism.

The values for $\bar{M}_w/\bar{M}_n$ calculated from Eq. 6 depend on the assumption of a Gaussian peak shape, but not strongly. Deviations from Gaussian peaks, for example extra peak tailing, show up as a somewhat different coefficient of $B^2w_0^2$ in Eq. 6. A large change in this coefficient, even a factor of two, does not significantly alter the conclusions of this paper. The expression in Eq. 22 for the change in apparent slope D depends on the peak and the broadening being Gaussian. Again, the dependence is not a strong one; as long as the peaks and broadening are approximately Gaussian, the conclusions presented are valid.

In the case of Gaussian broadening, Hamielec and Ray [19] derived correction factors for the various molecular mass moments, assuming refractometer chromatograms are used. These expressions assume a linear calibration curve but do not assume a Gaussian peak shape. Their results show that the necessary polydispersity correction factor is $\exp[-(\ln 10)^2B^2w_G^2/8 \ln 2]$, or 0.9890 ± 0.0004. Applying this factor to the value 1.0122 obtained from the calibration curve and the DRI signal gives a corrected polydispersity of 1.0011 ± 0.0006, a value consistent with the results presented in this paper. This approach requires high precision in the knowledge of B and w_G in order to determine the polydispersity of a narrow standard. In contrast, the method presented in this paper requires placing an upper bound on the radius calibration slope from which small polydispersities may be calculated with relatively high precision.

To check whether the broadening was due to the columns or to the LS flow cell, observed peak widths were compared for two configurations: (i) the standard configuration used for the experiments described above, and (ii) the same configuration with an additional LS flow cell inserted in line between the columns and the LS instrument. The observed peak width w_{obs} increased by only about 5% in the second configuration, indicating that the great majority of the broadening occurred in the columns and not in the LS instrument.

5. Conclusions

A new technique was demonstrated using molecular radius values obtained by GPC–MALLS across a peak to calculate the polydispersity of narrow-distribution standards. The sensitivity of the technique can approach the theoretical limit of the Poisson distribution. The upper limit obtained for a narrow polystyrene in toluene is much closer to unity than previously measured but still consistent with the polymerization mechanism.

Appendix

In this appendix we derive Eqs. 20 and 22. We begin with the expression for $M_{obs}(V)$ in Eq. 19:

$$M_{obs}(V) = \frac{\int M(y)h(y)G(V-y)\,dy}{\int h(y)G(V-y)\,dy} \tag{A1}$$

Substituting the expressions for $h(y)$, $M(y)$, and $G(V-y)$ from Eqs. 1, 2 and 16, respectively, we obtain

$$M_{obs}(V) = \frac{\int 10^{A+By} \exp[-4 \ln 2\,(y-V_0)^2/w_0^2] \exp[-4 \ln 2\,(V-y)^2/w_G^2]\,dy}{\int \exp[-4 \ln 2\,(y-V_0)^2/w_0^2] \exp[-4 \ln 2\,(V-y)^2/w_G^2]\,dy} \tag{A2}$$

Noting that $10^x = \exp(x \ln 10)$ and combining the exponentials gives

$$M_{obs}(V) = \frac{\int \exp\{\ln 10\,(A + By) - 4 \ln 2\,[(y - V_0)^2/w_0^2 + (y - V)^2/w_G^2]\}\,dy}{\int \exp\{-4 \ln 2\,[(y - V_0)^2/w_0^2 + (y - V)^2/w_G^2]\}\,dy} \quad \text{(A3)}$$

The exponentials in the integrals are quadratic polynomials in y, so we can use the standard expression

$$\int_{-\infty}^{+\infty} \exp(-ay^2 + by + c)\,dy = \sqrt{\frac{\pi}{a}} \exp(b^2/4a + c) \quad \text{(A4)}$$

with proper choices of a, b and c for the numerator (num) and denominator (den). These quantities are:

$$a_{den} = a_{num} = a = 4 \ln 2 \cdot \left(\frac{1}{w_G^2} + \frac{1}{w_0^2}\right)$$

$$b_{den} = 8 \ln 2 \cdot \left(\frac{V}{w_G^2} + \frac{V_0}{w_0^2}\right)$$

$$b_{num} = b_{den} + B \ln 10$$

$$c_{den} = -4 \ln 2 \cdot \left(\frac{V^2}{w_G^2} + \frac{V_0^2}{w_0^2}\right)$$

$$c_{num} = c_{den} + A \ln 10 \quad \text{(A5)}$$

Our goal is to form the ratio

$$M_{obs}(V) = \frac{\sqrt{\frac{\pi}{a}} \cdot \exp(b_{num}^2/4a + c_{num})}{\sqrt{\frac{\pi}{a}} \cdot \exp(b_{den}^2/4a + c_{den})} = \exp\left(\frac{b_{num}^2 - b_{den}^2}{4a} + c_{num} - c_{den}\right) \quad \text{(A6)}$$

Substituting values from Eq. A5 and cancelling yields

$$M_{obs}(V) = \exp\left[\frac{(Vw_0^2 + V_0 w_G^2 + Bw_0^2 w_G^2 \ln 10/16 \ln 2)B \ln 10}{w_0^2 + w_G^2} + A \ln 10\right] \quad \text{(A7)}$$

which can be rewritten as

$$\log[M_{obs}(V)] = \frac{(Vw_0^2 + V_0 w_G^2 + Bw_0^2 w_G^2 \ln 10/16 \ln 2)B}{w_0^2 + w_G^2} + A \quad \text{(A8)}$$

This expression is clearly linear in V with a slope B_{obs} given by

$$B_{obs} = Bw_0^2/(w_0^2 + w_G^2) = Bw_0^2/w_{obs}^2 \quad \text{(A9)}$$

which is the required expression.

For the mean square radius $\langle r^2 \rangle_{obs}(V)$, the derivation is analogous, and we obtain

$$\langle r^2 \rangle_{obs}(V) = \exp\left(\frac{b_{num}^2 - b_{den}^2}{4a} + c_{num} - c_{den}\right) \quad \text{(A10)}$$

The quantities a, b_{den} and c_{den} are the same as in Eq. A5. The quantities b_{num} and c_{num} are given by

$$b_{num} = b_{den} + B \ln 10 + 2D \ln 10$$

$$c_{num} = c_{den} + A \ln 10 + 2D \ln 10 \quad \text{(A11)}$$

Substituting yields

$$\log[\langle r^2 \rangle_{obs}(V)] = \frac{2[Vw_0^2 + V_0 w_G^2 + (B + D)w_0^2 w_G^2 \ln 10/8 \ln 2]D}{w_0^2 + w_G^2} + A + 2C \quad \text{(A12)}$$

which is linear in V with a slope given by $2Dw_0^2/(w_0^2 + w_G^2)$. Note that this is the slope for the mean square radius; the slope for the rms radius is one-half this value, or

$$D_{obs} = Dw_0^2/(w_0^2 + w_G^2) = Dw_0^2/w_{obs}^2 \quad \text{(A13)}$$

which is the required result.

References

[1] P.J. Flory, *J. Am. Chem. Soc.*, 62 (1940) 1561.
[2] P.J. Flory, *Principles of Polymer Chemistry*, Cornell Univ. Press, Ithaca, NY, 1953.

[3] M. Morton, *Anionic Polymerization: Principles and Practice*, Academic Press, London, 1983.
[4] W.W. Yau, J.J. Kirkland and D.D. Bly, *Modern Size-Exclusion Liquid Chromatography*, Wiley-Interscience, New York, 1979.
[5] N.C. Billingham, *Molar Mass Methods in Polymer Science*, Halsted Press, New York, 1977.
[6] W.W. Yau, H.J. Stoklosa and D.D. Bly, *J. Appl. Polym. Sci.*, 21 (1977) 1911.
[7] A.E. Hamielec, in J. Janca (Editor), *Steric Exclusion Liquid Chromatography of Polymers* (*Chromatographic Science Series*, Vol. 25), Marcel Dekker, New York, 1984, Ch. 3.
[8] G.R. Meira, in H.G. Barth and J.W. Mays (Editors), *Modern Methods of Polymer Characterization*, Wiley, New York, 1991, Ch. 2.
[9] P.J. Wyatt, *Anal. Chim. Acta*, 272 (1993) 1.
[10] J.C. Giddings, *J. Appl. Polym. Sci.*, 33 (1987) 117.
[11] P.J. Wyatt and L.A. Papazian, *LC·GC*, 11 (1993) 862.
[12] D.W. Shortt, *J. Liq. Chromatogr.*, 16 (1993) 3371.
[13] B.H. Zimm, *J. Chem. Phys.*, 16 (1948) 1093.
[14] H.C. van de Hulst, *Light Scattering by Small Particles*, Dover, New York, 1981.
[15] P. Debye, *J. Phys. Coll. Chem.*, 51 (1947) 18.
[16] L.H. Tung, *J. Appl. Polym. Sci.*, 10 (1966) 375.
[17] P. Kratochvíl, in M.B. Huglin, *Light Scattering from Polymer Solutions*, Academic Press, London, 1972, p. 344.
[18] P.J. Wyatt, *J. Chromatogr.*, 648 (1993) 27.
[19] A.E. Hamielec and W.H. Ray, *J. Appl. Polym. Sci.*, 13 (1969) 1319.

ELSEVIER

Journal of Chromatography A, 686 (1994) 21–29

JOURNAL OF CHROMATOGRAPHY A

Equilibrium and kinetic parameters of the adsorption of α-chymotrypsinogen A onto hydrophobic porous adsorbent particles

A. Tongta[a], A.I. Liapis[a,*], D.J. Siehr[b]

[a]*Department of Chemical Engineering and Biochemical Processing Institute, University of Missouri–Rolla, Rolla, MO 65401-0249, USA*

[b]*Department of Chemistry and Biochemical Processing Institute, University of Missouri–Rolla, Rolla, MO 65401-0249, USA*

First received 5 November 1993; revised manuscript received 14 July 1994

Abstract

Adsorption equilibria and rate kinetics for the binding of α-chymotrypsinogen A onto hydrophobic porous adsorbent particles, have been investigated for three different temperatures. The results show that the amount of protein adsorbed increases as the temperature increases.

The values of the parameters that characterize the mechanisms of pore diffusion and adsorption were determined. The values of the pore diffusion coefficient and the values of the time constants for the mass transfer steps of pore diffusion and adsorption suggest that the pore diffusion mechanism in the porous structure of the adsorbent particles is rate limiting. An analysis of the results of the adsorption of α-chymotrypsinogen A suggests that the heat of adsorption is positive, and this would indicate that the adsorption of α-chymotrypsinogen A onto the hydrophobic adsorbent particles used in this work is entropically driven.

1. Introduction

The design, optimization, scale-up and control of affinity adsorption systems require that the mass transfer and adsorption mechanisms are quantified. The most commonly used mode of operation in affinity adsorption separations is the fixed bed mode with axial flow [1]. Batch (finite bath) adsorption systems could be appropriate where the fluid to be processed was of high viscosity or contains particulate material. It has been shown [1–7] that, for a given affinity adsorption system, the parameters that characterize the intraparticle mass transfer mechanisms in purely diffusive adsorbent particles (for affinity adsorption systems with perfusive particles, Refs. 8–14 should be consulted) as well as the adsorption mechanisms should be independent of the operational mode (e.g., batch, fixed bed, fluidized bed), and therefore, if these parameters are estimated by utilizing information obtained from finite bath experiments (batch experiments are easier to perform and analyze [1–7,15,16] than column experiments), then their values could characterize the mechanisms (intraparticle mass transfer and adsorption mechanisms) in other operational modes.

In this work, the dynamic and equilibrium

* Corresponding author.

0021-9673/94/$07.00
SSDI 0021-9673(94)00663-6

behavior of the adsorption of α-chymotrypsinogen A onto the surface of the pores of SynChroprep Propyl HIC porous adsorbent particles is studied by performing finite bath experiments. Then the experimental dynamic and equilibrium adsorption data are used together with the predictions calculated from a mathematical model to obtain the values of the parameters that characterize the mechanisms of pore diffusion and adsorption in the adsorbent particles for α-chymotrypsinogen A.

2. Mathematical model

In this work, single-component adsorption is considered to occur in purely diffusive adsorbent particles (in purely diffusive adsorbent particles the intraparticle convective velocity [9] is taken to be equal to zero) suspended in the liquid of a finite bath, and the mass transfer and interaction steps are as follows: (i) the transport of adsorbate from the bulk fluid to the external surface of the adsorbent particle (film mass transfer); (ii) the transport of adsorbate within the porous adsorbent particle (intraparticle pore diffusion); (iii) the interaction between the adsorbate molecules and the active sites on the surface of the pores of the adsorbent particle (adsorption step). The porous adsorbent particles are suspended in the liquid of the finite bath by agitation so that the liquid has free access, and the bulk concentration of the adsorbate is taken to be uniform throughout the bath except in a thin film (film mass transfer resistance) of liquid surrounding each particle.

A differential mass balance for the adsorbate in the fluid phase of the finite bath gives

$$\frac{dC_d}{dt} = \left(\frac{1-\epsilon}{\epsilon}\right) \cdot \left(\frac{\alpha+1}{r_0}\right) \cdot K_f[C_p(t,r_0) - C_d] \quad (1)$$

Eq. 1 can be used for particles having geometry of slab, cylinder or sphere by putting $\alpha = 0$, 1 or 2, respectively. The initial condition of Eq. 1 is given by

$$C_d = C_{d0} \text{ at } t = 0 \quad (2)$$

The transport of the adsorbate in the adsorbent particle is considered to be governed by the diffusion [2,7] of the species in the pore fluid (pore diffusion) of the particle. The intraparticle (pore diffusion) transport mechanism is taken to be one-dimensional and in particles that have an axis of symmetry. It is understood that in the case of the slab and the cylinder, the particles are of infinite extent or alternatively one must artificially assume that the ends of a finite cylinder or edges of a finite slab are sealed in order to keep the problem one-dimensional. A differential material balance for the adsorbate in the adsorbent particle is given by

$$\frac{\partial(\epsilon_p C_p)}{\partial t} + \frac{\partial C_s}{\partial t} = \frac{1}{r^\alpha} \cdot \frac{\partial}{\partial r} \cdot \left(r^\alpha \epsilon_p D_p \cdot \frac{\partial C_p}{\partial r}\right) \quad (3)$$

The initial and boundary conditions for Eq. 3 are

$$C_p = 0 \text{ at } t = 0,\ 0 \leq r \leq r_0 \quad (4)$$

$$C_s = 0 \text{ at } t = 0,\ 0 \leq r \leq r_0 \quad (5)$$

$$\epsilon_p D_p \cdot \left.\frac{\partial C_p}{\partial r}\right|_{r=r_0} = K_f[C_d - C_p(t,r_0)], \quad t > 0 \quad (6)$$

$$\left.\frac{\partial C_p}{\partial r}\right|_{r=0} = 0, \quad t > 0 \quad (7)$$

If restricted [1,5,7,13] pore diffusion occurs, then ϵ_p and D_p could vary with the loading of the adsorbate in the adsorbed phase, as shown by the restricted pore diffusion mathematical model of Petropoulos et al. [7]. If the effect of restricted pore diffusion on the mass flux of the adsorbate is not significant, then the values of ϵ_p and D_p may be considered to be constant [1,2,5,7].

It is apparent that Eq. 3 can be solved only if an appropriate expression for the term $\partial C_s/\partial t$ is available. This term represents the accumulation of the adsorbed species on the internal surface of the porous adsorbent particle, and it can be quantified if a mathematical expression could be constructed that would describe the mechanism of the adsorption of the adsorbate onto the active site on the surface of the pore. In this work, the interaction between unbound adsor-

bate A in the pore fluid and vacant active site S on the surface of the pore is considered to be of the form [1–3]

$$A + S \underset{k_2}{\overset{k_1}{\rightleftarrows}} AS \tag{8}$$

where AS represents the adsorbate–active site complex. Then assuming elementary interactions, the rate of the adsorption step may be described by the following second-order reversible interaction:

$$\frac{\partial C_s}{\partial t} = k_1 C_p (C_T - C_s) - k_2 C_s \tag{9}$$

The accumulation term, $\partial C_s/\partial t$, in Eq. 9 becomes equal to zero when adsorption equilibrium is established, and the following expression for the equilibrium isotherm is then obtained:

$$C_s = \frac{C_T K C_p}{1 + K C_p} \tag{10}$$

Eq. 10 represents the Langmuir equilibrium adsorption model where

$$K = K_0 \cdot \exp(-\Delta H/RT) \tag{11}$$

Eq. 11 is the Van 't Hoff equation and represents the temperature dependence of the equilibrium association constant, K ($K = k_1/k_2$); the parameter ΔH in Eq. 11 represents the heat of adsorption. It is worth mentioning that at equilibrium the value of C_p in Eq. 10 should be equal to the value of C_d.

It should be noted at this point that the adsorption mechanism presented in Eq. 8 and whose dynamic and equilibrium quantitative expressions are given by Eqs. 9 and 10, respectively, represents the simplest non-linear adsorption mechanism. Complex non-linear adsorption mechanisms that could account for other phenomena in biomolecule adsorption such as steric effects, conformational changes, multipoint adsorption, and lateral interactions have been presented by Liapis and co-workers [1,2,4,7], Norde [17], Lundstrom et al. [18], Yon [19], Mark et al. [20] and Myers [21]; the determination of the parameters that characterize the adsorption steps of complex non-linear adsorption mechanisms requires data from different complex experiments that are not yet well established and which are beyond the scope of the present work. In this work, the goal is to obtain values for the phenomenological parameters that characterize (a) pore diffusion of the adsorbate in the pore fluid and (b) adsorption of the adsorbate on the surface of the pores of the adsorbent particles, from simple, inexpensive, and easy-to-perform batch experiments and non-linear adsorption models which could provide appropriate approximate representations for the mechanisms of pore diffusion and adsorption and whose numerical solution could be obtained efficiently with a small amount of computational effort and without using a super-computer. The values of the phenomenological parameters of pore diffusion and adsorption obtained from the combination of simple batch adsorption experiments and non-linear adsorption models described in this work, could then be used to simulate, examine, and study the adsorption of the adsorbate in fixed bed, fluidized bed, periodic counter-current bed, and continuous counter-current bed chromatographic columns. This simulation approach could (a) reduce significantly the experimental effort, (b) provide useful information about the relative importance of the film mass transfer, pore diffusion, and adsorption mechanisms, (c) provide useful quantitative results for the rates of the mass transfer and adsorption mechanisms, and (d) could provide reasonable quantitative information about the adsorption efficiency of different modes of operation, and this would be useful in selecting the system and mode of operation that could be used in the scale-up process.

The initial condition of Eq. 9 is given by Eq. 5. Eqs. 1, 3 and 9 could now be solved simultaneously (assuming that the values of C_{d0}, ϵ, ϵ_p, r_0, K_f, k_1, k_2, C_T and D_p are known) in order to obtain the dynamic behavior of C_d, C_p and C_s. In this work, the values of C_{d0}, ϵ, ϵ_p and r_0 are known. The value of the film mass transfer coefficient, K_f, of the adsorbate in Eqs. 1 and 6, is calculated from the following expression [22]:

$$K_f = \frac{2D_{mf}}{d_p} + 0.31 \cdot \left[\frac{(\Delta\rho)\mu g}{\rho^2}\right]^{1/3} \cdot \left(\frac{\mu}{\rho D_{mf}}\right)^{-2/3} \quad (12)$$

The values of C_T and K ($=k_1/k_2$) are obtained from the experimental equilibrium adsorption data; and the values of k_1 and D_p (the parameter k_2 in Eq. 9 is replaced by k_1/K) are obtained by matching the dynamic predictions of the theoretical model with the experimental data (the variation of C_d with time, t) obtained from the batch experiments. Then the value of k_2 is obtained from the values of k_1 and K since $k_2 = k_1/K$. The parameters D_p, k_1 and k_2 characterize the mechanisms of pore diffusion and adsorption, and their values should be independent [1–7] of the operational mode (e.g., batch, fixed bed, periodic counter-current bed, fluidized bed).

Eqs. 1, 3 and 9 were solved by using the numerical method described in Refs. 2, 4 and 13.

3. Experimental

3.1. Materials

The adsorbent particles are SynChroprep Propyl HIC Lot No. 1853, and were purchased from SynChrom, Lafayette, IN, USA. These adsorbent particles are spherical, and are formed from macroporous silica to which a polyamide layer containing a propyl hydrophobic ligand is covalently bonded. The diameter of the adsorbent particles is 15 μm and their density is 0.5 g/ml, as reported by SynChrom. The void fraction (porosity), ϵ_p, of the adsorbent particles is 0.55 [23,24], while the mean pore diameter of the pores of the particle (porous silica) before the polyamide layer is put on, is between 279 and 299 Å [24]. It is important to note at this point that the mean pore diameter of the adsorbent particles should be lower because when the polyamide layer is put on the diameter of the pores should become smaller; furthermore, the pore connectivity [7] of the pores of the porous particles could be changed when the polyamide layer is put on the surface of the pores of the porous particles. The pore-size distribution, mean pore diameter, and pore connectivity of the pores of the porous adsorbent particles were requested [24] but could not be provided by SynChrom.

The protein α-chymotrypsinogen A was purchased from Sigma, St. Louis, MO, USA. The molecular mass and the isoelectric point of α-chymotrypsinogen A are 25 000 daltons and 9.1, respectively [25].

The filters used were Durapore (polyvinylidine difluoride) membrane filters with a pore size of 5.0 μm. The filter holders were Swinnex, 13 mm disk filter holders, and the filters were trimmed in order to fit in the filter holders. The filters and the filter holders were purchased from Millipore, Bedford, MA, USA.

3.2. Methods

α-Chymotrypsinogen A was dissolved in 0.1 M phosphate buffer containing 1.8 M ammonium sulfate. To a 100-ml beaker, 50 ml of buffer containing protein was added, a stirring bar was placed in the beaker, the beaker was covered with Parafilm, and set on top of a submersible magnetic stirrer in a constant-temperature water bath. The solution was stirred at 1200 rpm for 0.5 h while the solution reached thermal equilibrium.

In the batch experiments with α-chymotrypsinogen A, 0.1 g of adsorbent particles were added. Samples of 0.8 ml were removed from the continuously stirred suspension at various time intervals. The concentration of α-chymotrypsinogen A was measured at 5, 10 and 20 min and every 20 min thereafter until there was no further change in protein concentration in two consecutive samples.

Since adsorbent particles were suspended in the removed sample, the sample was filtered through a Millipore filter into a cuvette with a volume of 0.9 ml and a light path of 1 cm before being read at 280 nm in an Hitachi U-2000 spectrophotometer; the duration of this filtration is less than 10 s. After the reading was made, the solution was returned to the finite bath (the

beaker with the protein solution and the adsorbent particles).

Protein solutions with initial concentrations of about 0.1, 0.2, 0.3, 0.4, 0.5 and 0.6 mg/ml were used at three different buffered pH values (5.0, 7.0 and 9.0) and three different temperatures (15, 25 and 35°C). Forty-five different solutions in duplicate were run [26]. Both dynamic (unsteady-state) and equilibrium adsorption data were measured [26].

4. Results and discussion

In Fig. 1 the equilibrium experimental and theoretical results of the adsorption of α-chymotrypsinogen A onto SynChroprep Propyl HIC porous adsorbent particles are presented for pH 5.0 and three different temperatures (15, 25 and 35°C); the theoretical results were obtained by using Eq. 10. The error in the values of C_s in Fig. 1 is ± 0.5 kg/m^3 particle, and this is a relatively small error if one considers the magnitude of the values of C_s in Fig. 1. The correlation coefficient between the experimental and theoretical data in Fig. 1 is about 0.9978, and this indicates that the correlation is good. In Table 1, the values of the parameters C_T and K of Eq. 10 that provided the best fit between the experimental and theoretical equilibrium data shown in Fig. 1, are presented. Experimental and theoretical equilibrium data for pH values of 7.0 and 9.0 are reported in Ref. [26].

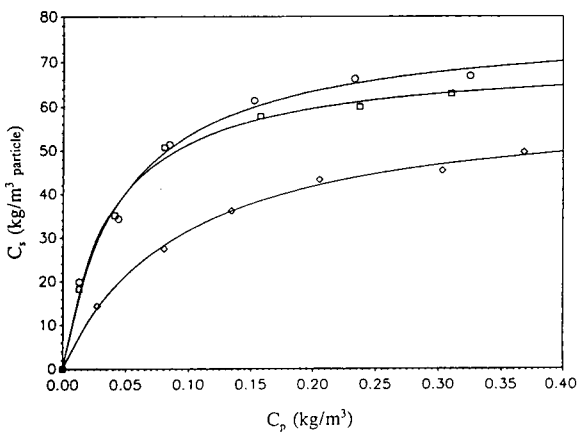

Fig. 1. Equilibrium adsorption isotherms for α-chymotrypsinogen A; pH 5.0. ◇ = Experimental results at 15°C; □ = experimental results at 25°C; ○ = experimental results at 35°C; lines = theoretical results.

Table 1
Values of the parameters C_T and K of Eq. 10 for α-chymotrypsinogen A; pH 5.0

Temperature (°C)	C_T (kg/m^3 particle)	K (m^3/kg)
15	60.95	10.82
25	70.71	26.77
35	78.22	21.52

While there is no clear trend in the values of the equilibrium association constant, K, presented in Table 1, the value of the apparent maximum capacity C_T increases as the temperature is increased from 15 to 35°C. This increase in the value of C_T with temperature could be caused by swelling of the polyamide layer containing the propyl hydrophobic ligand, making more binding sites available in the interior of the porous adsorbent particles; it should be mentioned at this point that we were told [24] that it is possible for the polyamide layer (containing the propyl hydrophobic ligand) to swell. The increase in the value of C_T could also be due to deviations from the Langmuir-type equilibrium behavior in which every binding site is equivalent. However, the experimental data in Fig. 1 are, for practical purposes, quantitatively described satisfactorily by Eq. 10. It is worth mentioning at this point that the overall free energy change ΔG ($\Delta G = \Delta H - T\Delta S$) associated with the adsorption of α-chymotrypsinogen A, could have a rather complex temperature dependence since hydrophobic interactions are largely entropic [27,28] in nature, while electrostatic interactions contribute to the enthalpy. The results in Fig. 1 show that the amount of protein adsorbed at equilibrium increases as the temperature increases.

Once the values of the equilibrium parameters K and C_T have been determined, then the values of the kinetic parameters D_p, k_1 and k_2 that characterize the mechanisms of pore diffusion

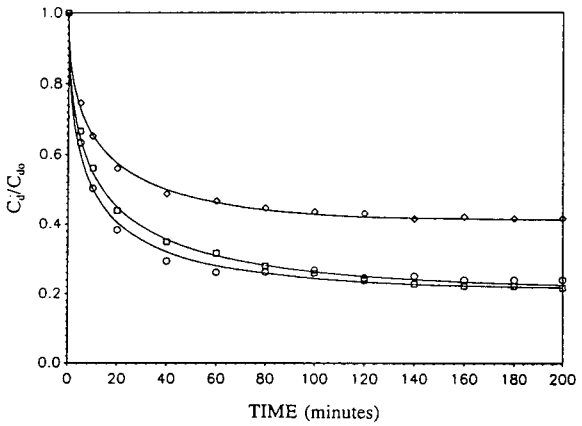

Fig. 2. Dynamic finite bath adsorption of α-chymotrypsinogen A; pH 5.0. ◇ = Experimental results at 15°C and C_{d0} = 0.19 kg/m^3; □ = experimental results at 25°C and C_{d0} = 0.19 kg/m^3; ○ = experimental results at 35°C and C_{d0} = 0.18 kg/m^3; lines = theoretical results.

and adsorption could be determined. The kinetic parameter k_2 in Eq. 9 is replaced by the term k_1/K, and thus, Eq. 9 takes the following form:

$$\frac{\partial C_s}{\partial t} = k_1 C_p (C_T - C_s) - (k_1/K) C_s \qquad (13)$$

The values of the kinetic parameters D_p and k_1 are determined by matching the dynamic experimental adsorption data obtained from batch experiments with the theoretical predictions obtained from the solution of the mathematical model presented in Eqs. 1–7 and 13. The value of the kinetic parameter k_2 is then calculated from the expression $k_2 = k_1/K$. The value of the film mass transfer coefficient K_f in Eqs. 1 and 6 is calculated from the expression in Eq. 12. In this work, the values of the parameters ϵ_p, r_0 and ϵ are as follows: $\epsilon_p = 0.55$ [23,24]; $r_0 = 7.5 \cdot 10^{-6}$ m; $\epsilon = 0.996$. The values of the temperature, T, and the initial concentration, C_{d0}, of the adsorbate in the finite bath are reported in the caption of Fig. 2.

In Fig. 2 the dynamic (batch) experimental and theoretical results of the adsorption of α-chymotrypsinogen A onto SynChroprep Propyl HIC porous adsorbent particles are presented for pH 5.0 and three different temperatures (15, 25 and 35°C). The experimental error in determining the ratio C_d/C_{d0} in Fig. 2 is ± 0.01. The correlation coefficient between the experimental and theoretical results in Fig. 2 is about 0.9989, and this indicates that the correlation is good. Experimental and theoretical dynamic adsorption data for pH values of 7.0 and 9.0 are reported in Ref. [26]. In Table 2, the values of the kinetic parameters D_p and k_1 that provided the best fit between the batch experimental and theoretical adsorption data shown in Fig. 2, are presented. Also in Table 2, the value of K_f, in Eqs. 1 and 6 of the mathematical model, calculated from Eq. 12 is presented, as well as the value of k_2 calculated from the expression $k_2 = k_1/K$. The values of the free molecular diffusion coefficient, D_{mf}, calculated from Eq. 8 in Ref. [29], are also presented in Table 2, so that their values can be compared with the values of the pore diffusion coefficient, D_p. Furthermore, in Table 2 the time constants for (a) pore diffusion, $(r_0)^2/D_p$, (b) interaction (adsorption) between adsorbate molecules and active sites, $1/(k_1 C_{d0})$,

Table 2
Values of the kinetic parameters for α-chymotrypsinogen A; pH 5.0

Temperature (°C)	K_f (m/s)	D_{mf} (m^2/s)	D_p (m^2/s)	D_p/D_{mf}	k_1 (m^3/kg·s)	k_2 (s^{-1})	r_0^2/D_p (s)	d_p^2/D_p (s)	$1/k_1 C_{d0}$ (s)	$1/k_2$ (s)
15	$5.48 \cdot 10^{-5}$	$7.22 \cdot 10^{-11}$	$8.70 \cdot 10^{-13}$	$1.20 \cdot 10^{-2}$	13.38	1.24	64.516	258.065	0.387	0.806
25	$6.12 \cdot 10^{-5}$	$8.93 \cdot 10^{-11}$	$9.77 \cdot 10^{-13}$	$1.09 \cdot 10^{-2}$	9.07	0.34	57.471	229.885	0.583	2.941
35	$7.18 \cdot 10^{-5}$	$1.22 \cdot 10^{-10}$	$1.29 \cdot 10^{-12}$	$1.06 \cdot 10^{-2}$	1.70	0.08	43.668	174.672	3.214	12.50

and (c) desorption of adsorbed adsorbate molecules, $1/k_2$, are presented. Some researchers might recommend that the time constant for pore diffusion might be estimated [30] from the approximate expression $(1/30)(d_p^2/D_p)$. However, the work of Knox and Scott [30] from which the approximate expression $(1/30)(d_p^2/D_p)$ might be inferred, is based on the linear Van Deemter theory for liquid chromatography which concerns itself with linear adsorption isotherms. But in the work presented in this paper, the mathematical model and the adsorption isotherm are nonlinear, and thus, the expression $(1/30)(d_p^2/D_p)$ would not be applicable. Some researchers consider the term d_p^2/D_p to represent the time constant for pore diffusion, and for this reason the values of the term d_p^2/D_p have been included in Table 2; it should be noted at this point that the majority of investigators consider the term r_0^2/D_p to represent the time constant of pore diffusion in purely diffusive adsorbent particles (the adsorbent particles of this work are considered to be purely diffusive because the intraparticle fluid velocity is considered to be equal to zero).

The dynamic experimental data in Fig. 2 are, for practical purposes, described satisfactorily by the dynamic theoretical results obtained from the solution of the batch adsorption model represented by Eqns. 1–7 and 13. The dynamic data in Fig. 2 indicate that the amount of adsorbed adsorbate increases as the temperature increases.

The data in Table 2 show that the values of the pore diffusion coefficient are about two orders of magnitude smaller than the values of the free molecular diffusion coefficient. Also, by comparing the values of the time constants r_0^2/D_p, $1/(k_1 C_{d0})$, and $1/k_2$ in Table 2, it can be observed that the time constant for pore diffusion is many times larger than the time constants of the adsorption and desorption steps. Furthermore, the time constant for desorption is larger than the time constant for adsorption. The results in Table 2 suggest that the adsorption step occurs significantly faster than the desorption step, while the slowest mechanism of the overall adsorption process is the mass transfer step of the adsorbate in the pores of the porous adsorbent particles. Thus, the rate-limiting step for the adsorption of α-chymotrypsinogen A onto the hydrophobic porous adsorbent particles employed in this work, is the pore diffusion step. This finding and the values of the ratio D_p/D_{mf} in Table 2 suggest that when the polyamide layer containing the propyl hydrophobic ligand is put on the surface of the pores of the porous silica, it has an important effect on the pore-size distribution, mean pore radius, and pore connectivity [1,7] of the resulting porous structure of the adsorbent particles. Furthermore, the adsorption of α-chymotrypsinogen A on the surface of the pores of the adsorbent particles could alter [1,7] the pore-size distribution, mean pore radius, and pore connectivity of the porous structure of the adsorbent particles as the adsorption process is proceeding and the loading of adsorbed adsorbate is increasing.

The values of the parameters k_1 and k_2 for α-chymotrypsinogen A in Table 2 decrease as the temperature is increased; furthermore, the value of k_1 is about an order of magnitude larger than the value of k_2. If the forward and reverse interaction rate constants k_1 and k_2 for the adsorption of α-chymotrypsinogen A are described by an Arrhenius expression,

$$k_1 = k_{10} \cdot \exp(-E_1/RT) \tag{14}$$

$$k_2 = k_{20} \cdot \exp(-E_2/RT) \tag{15}$$

then, by using the values of k_1 and k_2 in Table 2, one obtains the following values for the pre-exponential factors k_{10} and k_{20}, and the activation energies E_1 and E_2: $k_{10} = 3.09 \cdot 10^{-13}$ m^3/kg·s, $k_{20} = 5.72 \cdot 10^{-19}$ s^{-1}, $E_1 = -18.09$ kcal/mol and $E_2 = -24.18$ kcal/mol (1 cal = 4.184 J). From these data the parameters $K_0 = k_{10}/k_{20}$ and $\Delta H = E_1 - E_2$ in Eq. 11 can be calculated, and their values are as follows: $K_0 = 5.40 \cdot 10^5$ m^3/kg and $\Delta H = 6.09$ kcal/mol. Thus, the adsorption of α-chymotrypsinogen A onto the adsorbent particles used in this work appears to be endothermic, since $\Delta H > 0$. Furthermore, the fact that $\Delta H > 0$, whereas the adsorption proceeds spontaneously ($\Delta G < 0$; $\Delta G = \Delta H -$

$T\Delta S$), indicates that an increase of entropy must be the driving force behind the adsorption of α-chymotrypsinogen A onto the adsorbent particles considered in this work.

5. Conclusions and remarks

The equilibrium and rate kinetics of the adsorption of α-chymotrypsinogen A onto hydrophobic porous adsorbent particles was studied experimentally and theoretically for three different temperatures. The results show that the amount of adsorbed protein increases as the temperature increases.

The calculated values for the pore diffusion coefficient and for the time constants of the mass transfer steps of pore diffusion, adsorption, and desorption, suggest that the rate-limiting step for the adsorption of α-chymotrypsinogen A onto the hydrophobic porous adsorbent particles employed in this work, is the pore diffusion step. The heat of adsorption for the α-chymotrypsinogen A system was found to be positive, and this would indicate that the adsorption of α-chymotrypsinogen A onto the hydrophobic adsorbent particles used in this work, is entropically driven.

The values of the parameters that characterize the mechanisms of pore diffusion and adsorption, determined in this work from information obtained from finite bath adsorption experiments and the mathematical model, could be used to characterize the same mechanisms when adsorption of α-chymotrypsinogen A occurs in a fixed bed, in a periodic counter-current bed, in a continuous counter-current bed, or in a fluidized bed.

Symbols

A molecule of adsorbate
AS adsorbate-active site complex
C_d concentration of adsorbate in the bulk fluid phase of finite bath, kg/m^3
C_{d0} initial concentration of adsorbate in bulk fluid phase of finite bath, kg/m^3
C_p concentration of adsorbate in pore fluid, kg/m^3
C_s concentration of adsorbate in adsorbed phase, kg/m^3 particle
C_T apparent maximum concentration of adsorbate in adsorbed phase, kg/m^3 particle
D_{mf} free molecular diffusion coefficient of adsorbate, m^2/s
D_p pore diffusion coefficient of adsorbate (in adsorbent particle), m^2/s
d_p mean diameter of the adsorbent particles ($d_p = 2r_0$), m
E_1 activation energy, kcal/mol
E_2 activation energy, kcal/mol
g standard acceleration of free fall, 9.80665 m/s^2
K equilibrium association constant ($K = k_1/k_2$), m^3/kg
K_f film mass transfer coefficient of adsorbate, m/s
K_0 pre-exponential factor in the Van 't Hoff equation, m^3/kg
k_1 forward interaction rate constant in reaction 8, $m^3/kg \cdot s$
k_{10} pre-exponential factor in Eq. 14, $m^3/kg \cdot s$
k_2 reverse interaction rate constant in reaction 8, s^{-1}
k_{20} pre-exponential factor in Eq. 15, s^{-1}
r radial distance in adsorbent particle, m
r_0 radius of adsorbent particle
R universal gas constant
S vacant active site
t time, s
T temperature, K

Greek letters

α form factor; 0, 1 and 2 for slab, cylinder and sphere, respectively
ΔG Gibbs free energy
ΔH heat of adsorption, kcal/mol of adsorbate
ΔS entropy
$\Delta\rho$ density difference between the particulate and continuous phases, kg/m^3
ϵ void fraction in finite bath
ϵ_p void fraction in porous adsorbent particle
μ viscosity of liquid solution, $kg/m \cdot s$
ρ density of liquid solution, kg/m^3

Acknowledgement

A.T. gratefully acknowledges the financial support of his graduate studies by the Royal Thai Government.

References

[1] A.I. Liapis, *Sep. Purif. Methods*, 19 (1990) 133.
[2] B.H. Arve and A.I. Liapis, *AIChE J.*, 33 (1987) 179.
[3] B.J. Horstmann and H.A. Chase, *Chem. Eng. Res. Des.*, 67 (1989) 243.
[4] M.A. McCoy and A.I. Liapis, *J. Chromatogr.*, 548 (1991) 25.
[5] A. Johnston and M.T.W. Hearn, *J. Chromatogr.*, 512 (1990) 101.
[6] A.I. Liapis, *J. Biotechnol.*, 11 (1989) 143.
[7] J.H. Petropoulos, A.I. Liapis, N.P. Kolliopoulos, J.K. Petrou and N.K. Kanellopoulos, *Bioseparation*, 1 (1990) 69.
[8] N.B. Afeyan, N.F. Gordon, I. Mazsaroff, L. Varady, S.P. Fulton, Y.B. Yang and F.E. Regnier, *J. Chromatogr.*, 519 (1990) 1.
[9] A.I. Liapis and M.A. McCoy, *J. Chromatogr.*, 599 (1992) 87.
[10] M.A. McCoy, A.I. Liapis and K.K. Unger, *J. Chromatogr.*, 644 (1993) 1.
[11] N.B. Afeyan, S.P. Fulton and F.E. Regnier, *J. Chromatogr.*, 544 (1991) 267.
[12] A.I. Liapis and M.A. McCoy, *J. Chromatogr. A*, 660 (1994) 85.
[13] M.A. McCoy, *Ph.D. Dissertation*, Department of Chemical Engineering, University of Missouri–Rolla, Rolla, MO, 1992.
[14] A.I. Liapis, *Math. Modelling Sci. Computing*, 1 (1993) 397.
[15] E.N. Lightfoot, M.C.M. Cockrem, S.J. Gibbs and A.M. Athalye, in N.N. Li and H. Strathmann (Editors), *Separation Technology*, Engineering Foundation, New York, 1988, pp. 122–154.
[16] A.I. Liapis, in N.N. Li and H. Strathmann (Editors), *Separation Technology*, Engineering Foundation, New York, 1988, pp. 420–487.
[17] W. Norde, *Adv. Colloid Interface Sci.*, 25 (1986) 267.
[18] I. Lundstrom, B. Ivarsson, U. Jonsson and H. Elwing, in W.J. Feast and H.S. Munro (Editors), *Polymer Surfaces and Interfaces*, Wiley, New York, 1987, p. 201.
[19] R.J. Yon, *J. Chromatogr.*, 457 (1988) 13.
[20] A.E. Mark, P.D. Jeffrey and L.W. Nichol, *J. Theor. Biol.*, 131 (1988) 137.
[21] A.L. Myers, in A.I. Liapis (Editor), *Fundamentals of Adsorption*, Engineering Foundation, New York, 1987, p. 3.
[22] C.J. Geankoplis, *Transport Processes and Unit Operations*, Prentice Hall, Englewood Cliffs, NJ, 1993.
[23] T. Dawson, personal communication, 1992.
[24] H. Freiser, personal communication, 1994.
[25] *Worthington Enzyme Manual*, Worthington Biochemical Corp., Freehold, NJ, 1972, pp. 58 and 129.
[26] A. Tongta, *M.S. Thesis*, Department of Chemical Engineering, University of Missouri–Rolla, Rolla, MO, 1994.
[27] F.H. Arnold and H.W. Blanch, *J. Chromatogr.*, 355 (1986) 13.
[28] M.A. McCoy, B.J. Hearn and A.I. Liapis, *Chem. Eng. Commun.*, 108 (1991) 225.
[29] M.E. Young, P.A. Carroad and R.L. Bell, *Biotechnol. Bioeng.*, 22 (1980) 947.
[30] J.H. Knox and H.P. Scott, *J. Chromatogr.*, 282 (1983) 297.

ELSEVIER

Journal of Chromatography A, 686 (1994) 31–43

JOURNAL OF CHROMATOGRAPHY A

Temperature as a variable in reversed-phase high-performance liquid chromatographic separations of peptide and protein samples
I. Optimizing the separation of a growth hormone tryptic digest

W.S. Hancock[a,1], Rosanne C. Chloupek[a], J.J. Kirkland[b], L.R. Snyder[c,*]

[a]*Genentech, Inc., 460 Point San Bruno Boulevard, South San Francisco, CA 94080, USA*
[b]*Rockland Technologies Inc., 538 First State Boulevard, Newport, DE 19804, USA*
[c]*LC Resources Inc., 26 Silverwood Court, Orinda, CA 94563, USA*

First received 31 December 1993; revised manuscript received 2 August 1994

Abstract

Peptide and protein samples are often complex mixtures that contain a number of individual compounds. The initial HPLC separation of such samples typically results in the poor resolution of one or more band pairs. Various means have been suggested for varying separation selectivity so as to minimize this problem. In this study of a tryptic digest of recombinant human growth hormone, the simultaneous variation of temperature and gradient steepness was found to be a convenient and effective means of varying selectivity and optimizing the separation. The use of computer simulation greatly facilitated this investigation.

1. Introduction

Peptide and protein samples often contain 20 or more individual components. The complete separation of such samples poses a real challenge, because statistical considerations suggest that one or more peak-pairs will usually be poorly resolved [1]. One way out of this dilemma is a systematic variation of separation selectivity. This approach is widely used for the separation of typical small-molecule samples [2]. In the case of peptide and protein samples, however, the control of selectivity has received less attention. When a change in selectivity is desired, the usual approach is a change of the column or mobile phase [3].

The use of elevated temperatures for the reversed-phase HPLC separation of samples containing peptides or proteins has been advocated [4], primarily as a means of increasing column efficiency or shortening run time. For samples of this type, a few studies [5,6] have shown that a change in column temperature can also affect separation selectivity. The most popu-

* Corresponding author.
[1] Present address: Hewlett-Packard Laboratories, 3500 Deer Creek Road 26U, Palo Alto, CA 94304, USA.

0021-9673/94/$07.00
SSDI 0021-9673(94)00779-9

lar conditions for the reversed-phase separation of peptide or protein samples involve acetonitrile–water gradients with the addition of 0.1% trifluoroacetic acid (TFA) to maintain a low pH in the mobile phase. However, the combination of low pH (≈ 1.9) and higher temperature operation can result in a very short life for commonly used alkyl-silica columns [7], which in turn limits the application of temperature optimization. This problem has been overcome recently by the development [8] and commercialization of so-called "sterically protected" reversed-phase packings that are extremely stable at low pH (pH < 2) and high temperature (> 90°C).

For the reversed-phase separation of peptide and protein samples, it has been shown that a change in gradient steepness can be quite effective in changing peak spacing and resolution [9–13]. Because a change in temperature or gradient steepness is more convenient than a change of column or mobile phase, this suggests the *combined* use of temperature and gradient steepness as a means of optimizing the separation of peptide or protein samples. This possibility is explored in the present paper, using a tryptic digest of recombinant human growth hormone (rhGH) as example. In the following paper [14], we examine other samples and consider whether the combined use of changes in temperature and gradient steepness is likely to be generally useful for the separation of peptide or protein mixtures.

2. Theory

2.1. Gradient steepness

The theory of gradient elution is now well established and a good understanding exists concerning the effects of gradient steepness on separation [15–17]. Retention times in gradient elution can be related to sample retention under isocratic conditions, which for reversed-phase separation can be approximated as

$$\log k = \log k_w - S\varphi \quad (1)$$

Here k is the retention factor of the solute, and φ is the volume fraction of organic (acetonitrile) in the mobile phase. Values of k_w and S are characteristic of each solute in the sample. Many examples of the applicability of Eq. 1 for peptide or protein samples have been reported [17–20]. Values of S and k_w for each solute can be obtained from two experimental gradient separations of the sample, and retention times in gradient elution can then be predicted as a function of gradient conditions [17]. Two compounds that elute adjacent to each other in the chromatogram will often show significant changes in band spacing when isocratic solvent strength or gradient steepness is varied [12,21]. The resolution of such band-pairs can usually be accomplished when values of S for the two compounds differ by 5% or more [21].

2.2. Temperature

Small-molecule separations

Much is known concerning the effects of column temperature on reversed-phase separation, primarily from experimental studies of small-molecule samples ($M_r < 1000$). In most cases isocratic retention k can be related to absolute temperature T as

$$\log k = A + B/T \quad (2)$$

A is a function of the phase ratio and entropy of retention, ΔS; B is proportional to the enthalpy of retention (ΔH). Values of ΔH are usually negative, so that retention decreases at higher temperatures. For small-molecule samples, several studies [22–27] have shown that values of $-\Delta H$ and B are usually larger for later bands in the chromatogram. Melander et al. [22] have expressed this relationship quantitatively by noting (for solute molecules of similar structure) that there is often a linear relationship between the enthalpy and entropy of retention. This concept leads to an equation of the form

$$\log k_T = C\Delta H + D \quad (3)$$

Here, k_T refers to k values for different solutes at some temperature T; C and D are

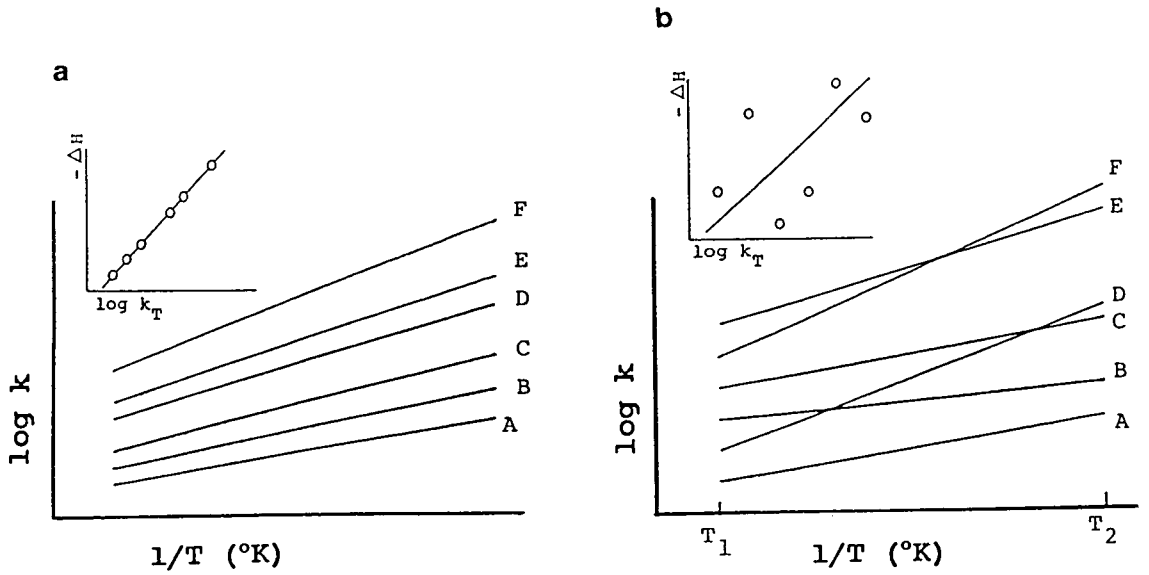

Fig. 1. Hypothetical representation of temperature selectivity for (a) a separation obeying Eq. 3 and (b) a separation deviating from Eq. 3.

constants for separations with the same experimental conditions (including temperature). Fig. 1a illustrates the form of log k vs. $1/T$ plots (different solutes) for a system where Eq. 3 is obeyed.

If Eq. 3 is obeyed exactly for different solutes in a given reversed-phase system, no major changes in selectivity can be expected when the temperature is varied. That is, the sequence of bands in the chromatogram cannot change as a function of temperature, and any bands that are unresolved at one temperature ($\alpha = 1$) will be unresolved at all temperatures. This relationship implies that a change in temperature will be of little value in improving band spacing, which is often the case for the separation of neutral molecules. Fig. 1a illustrates this situation; the retention order of bands A–E (A < B < C < D < E < F) is the same, regardless of the temperature of separation.

While previous workers have generally regarded temperature as a less useful means of controlling selectivity for increased resolution (e.g., [23,25]), a number of small-molecule studies have shown significant changes in band spacing as temperature is varied [27–32]. This failure of Eq. 3 is commonly associated with the existence of more than one separation process or "mechanism", as well as certain related effects: (1) retention of the solute on more than one stationary phase site (e.g., cationic samples retained on alkyl groups vs. silanols); (2) acid–base reactions of the sample molecule with the formation of different species (e.g., AH and A^-, BH^+ and B); (3) other secondary equilibria such as ion pairing. In addition, differences in molecular shape for different solute molecules can lead to a failure of Eq. 3 [33].

Fig. 1b illustrates the consequences when a reversed-phase separation deviates markedly from Eq. 3. The separation order observed at temperature T_2 (A < B < C < D < E < F) is quite different than that observed at temperature T_1 (A < D < B < C < F < E). Band-pairs B/D and E/F are unresolved ($\alpha = 1.0$) at intermediate temperatures, but are well separated at higher and lower temperatures.

A similar pattern is observed for a change in either temperature or φ; if φ replaces $1/T$ in Fig. 1, plots of the same form are obtained. As a result, in isocratic separation run time and *average* resolution decrease for an increase in either

T or φ. However, maximum resolution for the worst-separated band-pair often occurs for intermediate values of T or φ, because of changes in selectivity. For gradient elution, similar changes in selectivity can be effected by (a) a change in gradient steepness (equivalent to a change in isocratic φ) or (b) a change in temperature.

An increase in gradient steepness results in a compression of the chromatogram with narrower bands and a shortening of the run time. A change in temperature for a gradient separation does not result in a compressed chromatogram, due to the elution of each band at a lower value of φ at higher T. That is, the effect of T on k *during* gradient elution is almost exactly cancelled by a corresponding change in φ at elution (this can be seen by comparing Figs. 4 and 5); see also the discussion of Ref. [17].

Separations of peptides and proteins

The above discussion of effects that are likely to lead to deviations from Eq. 3 suggests that changes in selectivity with temperature will often be significant in the separation of peptide and protein samples. These solute molecules usually contain acidic and basic groups whose ionization can vary with pH and temperature. The most common mobile phase (acetonitrile–water plus added TFA) allows ion pairing of basic groups with the TFA [34], and changes in selectivity with temperature are both expected and commonly observed in ion-pair systems. Molecular conformation (and shape) is also known to vary among different peptide and protein solutes. For these various reasons, it should not be surprising if important changes in selectivity are observed for peptide and protein samples as temperature is varied.

The combined effects of a change in temperature T and gradient steepness on the spacing of bands within the chromatogram Δt_R (difference in retention times for two adjacent bands) can be approximated as

$$\Delta t_R = \Delta\Delta t_R(T) + \Delta\Delta t_R(\text{steepness}) \quad (4)$$

where $\Delta\Delta t_R(T)$ refers to a change in Δt_R due to a change in temperature and $\Delta\Delta t_R$(steepness) refers to a change in Δt_R due to a change in gradient steepness. A practical question concerns the relative magnitudes of these temperature and gradient steepness effects and whether they are correlated or independent. If changes in retention of comparable magnitude result from practical changes in T (e.g., by 30–40°C) or gradient steepness (e.g., change in gradient time by a factor of 3–4), either temperature or gradient steepness would be useful for controlling band spacing. If changes in band spacing with temperature or gradient steepness are independent of each other (non-correlated), then the *combined* use of these two variables should be especially useful for controlling selectivity and optimizing separation. On the basis of our present knowledge, there is no obvious reason why any correlation should exist between selectivity effects caused by changes in temperature or gradient steepness.

3. Experimental

3.1. Equipment and materials

The HPLC equipment used is described in Ref. [13]. The column was a 15×0.46 cm Zorbax SB-C_8 (300 Å pore diameter, "sterically protected", 5-μm particles; Rockland Technologies). All experiments used water (A) and acetonitrile (B) gradients, with 0.1% trifluoroacetic acid (TFA) added to each solvent. Other conditions are indicated in the text, tables or figures. Solvents were preheated to the temperature of the column by using a precolumn coil of capillary tubing maintained at column temperature. The tryptic digest of rhGH was prepared as described in Ref. [13].

3.2. Computer simulations

Experimental data were used as a basis for predicting separation as a function of gradient conditions and thereby arriving at general conclusions for the present sample. These predictions were based on computer simulations using DryLab/Windows software (LC Resources, Wal-

nut Creek, CA, USA). The use of this software for similar separations of rhGH tryptic peptides is described in Ref. [13].

4. Results and discussion

4.1. Computer simulation

Experiments were carried out to allow the separation of the rhGH digest to be predicted as a function of gradient steepness and temperature. Three runs each were made at 20, 40 and 60°C (gradient times of 30, 60 and 120 min). The 30- and 120-min runs were used for computer simulation; the 60-min run served as a check on peak tracking and the accuracy of computer simulation. These chromatograms are moderately complex, as seen in Fig. 2 for separation at 60°C with a 120-min gradient. The numbering in Fig. 2 and elsewhere in the present study is the same as was used in Ref. [13]. The numbered peaks represent major peptides, but several smaller peaks are also evident in the chromatogram of Fig. 2. Peak 20 of Fig. 2 is small and often obscured by other minor peaks eluting in this region; for this reason, we ignore peak 20 in further discussions. Our object here is not the optimized separation of this particular sample, but rather the use of these separations to illustrate certain general conclusions.

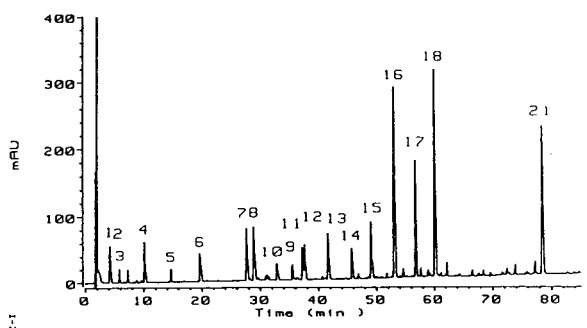

Fig. 2. Separation of 100 μg of rhGH tryptic digest using a 120-min linear gradient at 60°C. Peak numbering as in Ref. [13]. Conditions: column, 15 × 0.46 cm, 300 Å, Zorbax SB-C_8; 0–60% B gradient in 120 min; flow-rate, 1.0 ml/min. Other conditions as in the Experimental section.

The reliability and accuracy of computer simulation was first tested by predicting retention times for the 60-min gradient runs at the three temperatures. These values were compared with experimental retention times as summarized in Table 1. The average error in predicted retention times was ± 0.06 min or 0.3%. Similarly, the average error in predicted retention time differences (proportional to resolution) was only ± 1.1%. These checks assure that predictions based on computer simulation will be sufficiently accurate for our present purpose.

The value of N for these separations was obtained using the present computer simulation software. Either resolution R_s or bandwidth W can be predicted for various values of N. The value of N which gave the best overall agreement between calculated and predicted values of R_s and W was assumed to be correct. Resolution measurements for overlapped peak-pairs gave values of N which ranged from 4800 to 6100, as temperature was varied from 20 to 60° C.

4.2. Effect of changes in gradient steepness and temperature

The DryLab simulation software can summarize resolution as a function of gradient time (steepness) in the form of a resolution map. Examples for the rhGH sample and three different temperatures are shown in Fig. 3, where R_s

Table 1
Verification of computer simulation for the separation of rhGH tryptic digest sample

Temperature (°C)	Average error (min/%)[a]	
	Retention time t_R	Difference in t_R [b]
20	±0.05 min/±0.2%	±0.02 min/±0.9%
40	±0.06 min/±0.3%	±0.02 min/1.0%
60	±0.08 min/≡0.4%	±0.03 min/1.3%

Predicted and experimental retention times are compared for the 60-min gradient runs, based on experimental data for 30- and 120-min runs and computer simulation.

[a] Error expressed as either min or %.

[b] Error in retention differences for adjacent bands, proportional to error in predicted resolution.

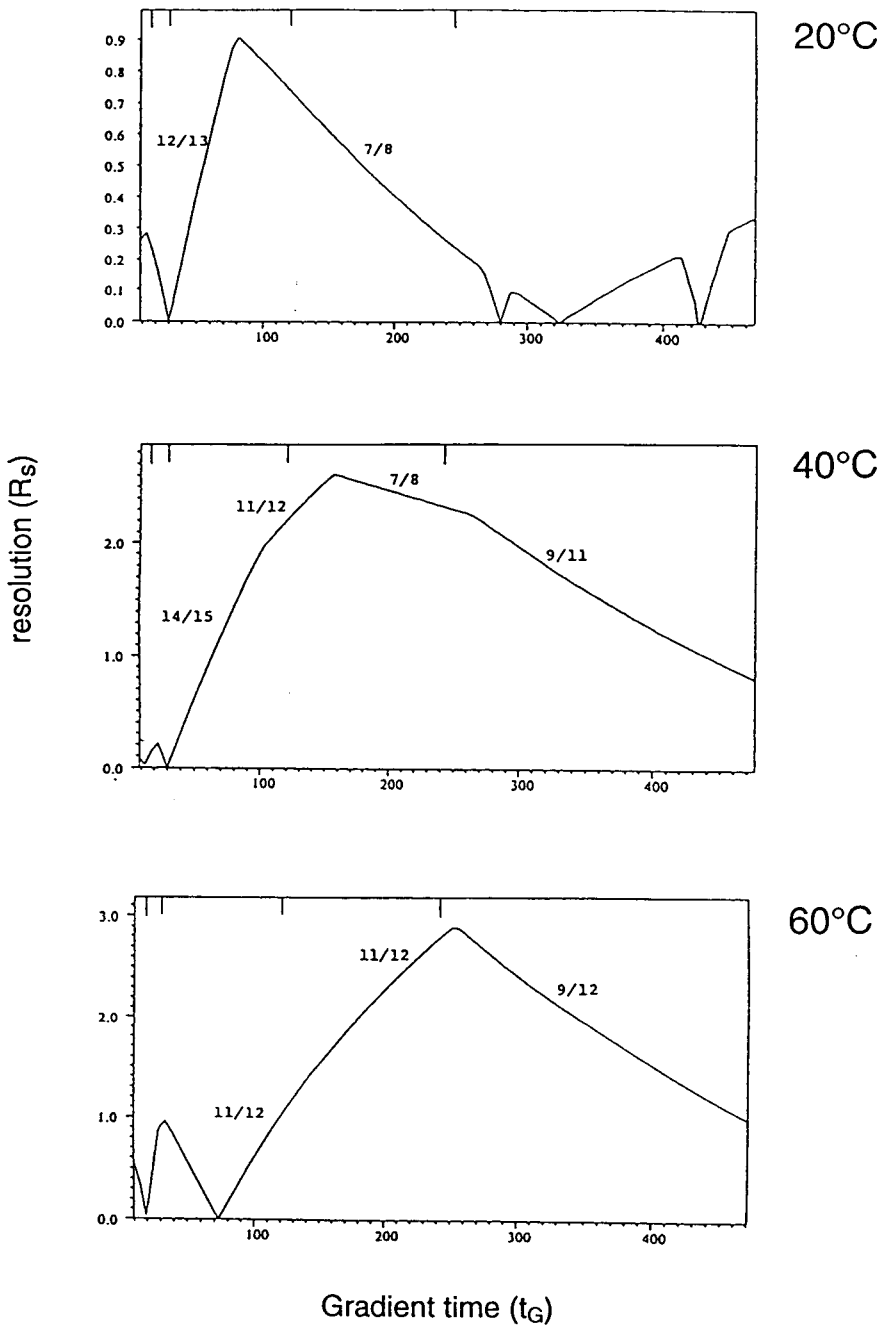

Fig. 3. Resolution maps of rhGH tryptic digest as a function of gradient time and temperature (20, 40 and 60°C). Other conditions as in Fig. 1. Numbers refer to critical (least resolved) band-pairs.

for the critical (least resolved) band-pair is plotted vs. gradient time. If temperature were unimportant as a determinant of selectivity and peak spacing, these three maps would look generally similar, with little change in the maximum attainable resolution. As seen in Fig. 3, this is not the case. Each resolution map has a quite different appearance; the optimum gradient time varies from 70 min for separation at 20° to 250 min at 60°, and the maximum attainable resolution varies from $R_s = 0.9$ (20°C, poor) to $R_s = 2.8$ (60°C, excellent). The critical peak-pairs (numbers shown within Fig. 3) also change with temperature (see discussion below).

The above observations concerning Fig. 3 suggest that temperature is a potentially important variable for controlling band spacing and resolution in the case of peptide mixtures. Thus the combined variation of temperature and gradient steepness as in Fig. 3 allows a much greater sample resolution than can be attained via changes in gradient time alone. This is also evident in the change in critical band pairs as temperature is varied. Peak-pairs 7/8 and 12/13 are least resolved at 20°C, peak-pairs 7/8, 9/11, 11/12 and 14/15 are critical at 40°C, and peak-pairs 9/12 and 11/12 limit resolution at 60°C.

The effect of gradient steepness on controlling peak spacing and resolution is illustrated in Fig. 4, where the critical peaks 7–15 are shown for three different gradient times (30, 60 and 120 min) and a temperature of 40°C. Peak-pair 7/8 is little affected by change in gradient time, whereas peak-pairs 9/10, 11/12 and 14/15 become better resolved as gradient time increases. A similar comparison of the effect of temperature on the separation of these bands is shown in Fig. 5. Here peak-pair 7/8 becomes better separated as temperature increases, peak-pair 11/12 is best separated at an intermediate temperature (40°C), and peak-pair 14/15 reverses between 20 and 60°C. The advantage of a good choice of gradient steepness and temperature is apparent in the examples of Figs. 4 and 5. The best of these separations (Figs. 4 and 5) is seen for a temperature of 40°C and a gradient time of 120 min; see also the resolution maps of Fig. 3.

4.3. Prediction of separation as a function of temperature and gradient steepness: solute retention parameters S and k_w for each peptide

Computer simulation for the prediction of the reversed-phase gradient separation of peptide or protein samples has been described [10–13]. Two initial experimental separations are used to derive values of the isocratic parameters S and k_w for each sample component (Eq. 1). Table 2 summarizes values of S (software derived) for the various peptides of the rhGH digest. Data for S as a function of temperature have been reported for several small-molecule samples (see review of Ref. [35]). Generally, there is no change or a slight decrease in S with increasing temperature. This trend was also observed for the rhGH digest as shown in Fig. 6. Here, values of S at 20°C are plotted vs. values at 60°C. The solid line for $y = x$ in Fig. 6 confirms that S is relatively independent of temperature for this peptide sample, considering likely errors in the derived values of S. Consequently, the effects of a change in gradient steepness on peak spacing should be similar at different temperatures.

Values of the solute parameter $\log k_w$ also vary with temperature, as summarized in Table 3. The quantity k_w is defined as the value of k for an isocratic separation with 0% B (no organic). Values of $\log k_w$ generally decrease with temperature, as expected for a retention process that releases heat when the solute molecule is sorbed onto the column packing. If values of S and k_w are interpolated from the data of Tables 2 and 3 as a function of temperature, retention times and resolution can be predicted for any temperature and gradient conditions. This approach would allow the generation of resolution maps as in Fig. 3 for other temperatures, so as to define the best possible values of gradient time and temperature for this sample. Further work is required to confirm that this simple approach will be applicable (a reviewer has suggested that the scatter of data in Fig. 6 could represent a possible complication).

The selection of "best" values of temperature and gradient steepness for an HPLC separation

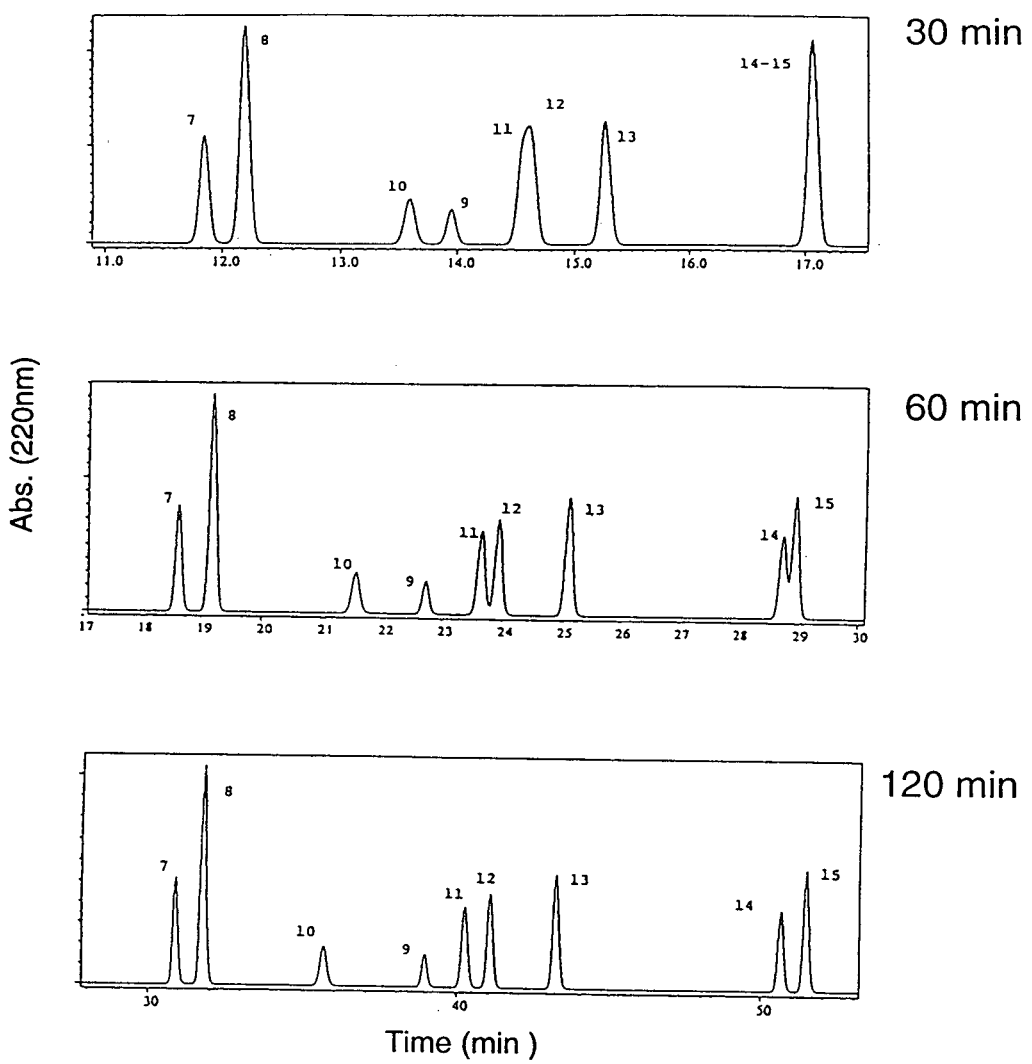

Fig. 4. Separation of rhGH tryptic peptides 7–15 as a function of gradient time (steepness). Conditions as in Fig. 1, 40°C.

requires consideration of the relative importance of both resolution and run time. It is convenient to choose an adequate resolution (e.g., baseline separation or $R_s > 1.5$) and then select the shortest possible run time. From the data of Fig. 2, $R_s > 1.5$ can be achieved with an 85-min gradient at 40°C or a 150-min gradient at 60°C, but not at all at 20°C. Thus, in this case, a temperature of 40°C is better than either 20 or 60°C.

4.4. Non-correlation of selectivity effects due to changes in temperature or gradient steepness

Figs. 3–5 for the rhGH digest suggest that selectivity effects due to a change in temperature are different from effects due to a change in gradient steepness. That is, the simultaneous variation of temperature and gradient steepness should be especially useful in optimizing sepa-

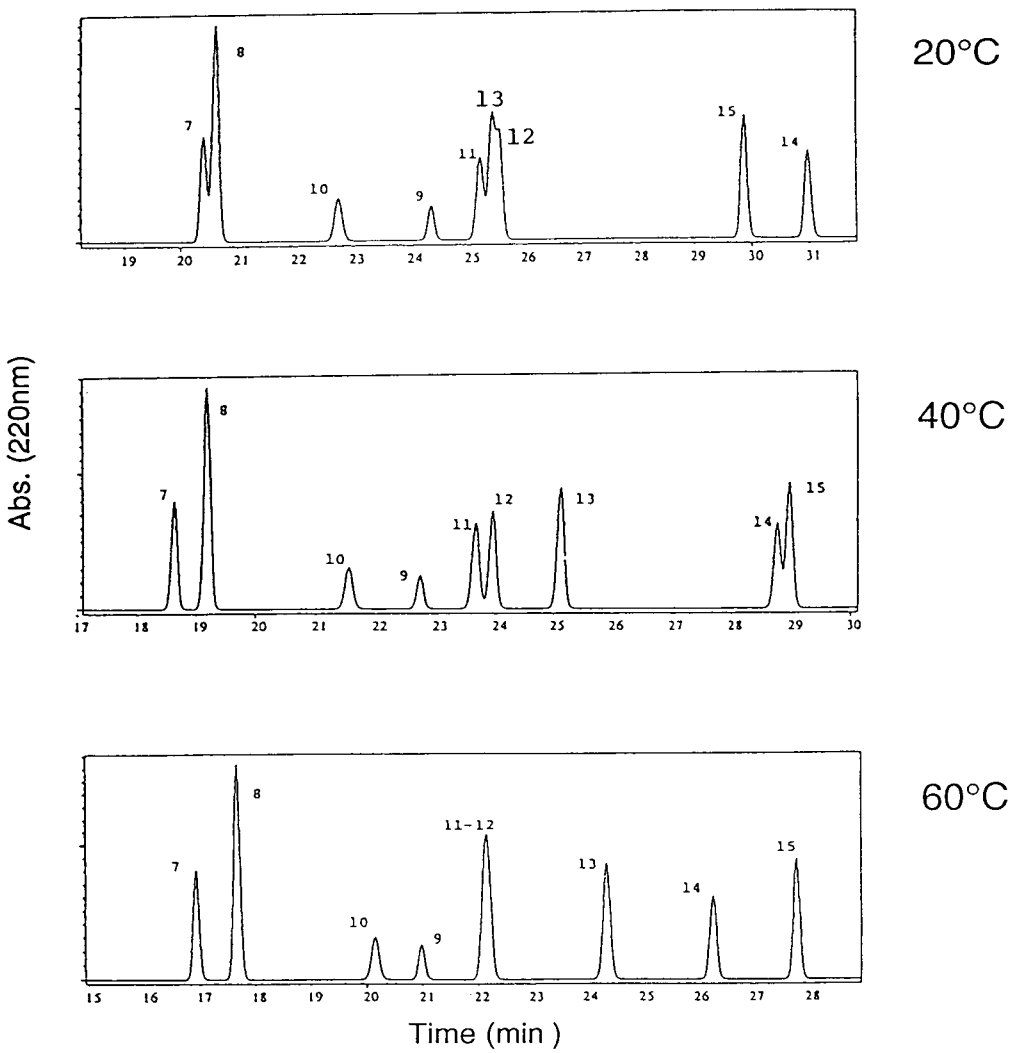

Fig. 5. Separation of rhGH peptides 7–15 as a function of temperature. Conditions as in Fig. 1, 60-min gradients.

ration. A more objective statement of this conclusion can be reached as follows. Table 4 summarizes values of $\Delta t_R(T)$ for a change in temperature from 60 to 20°C, corrected for differences in gradient time. Average values of $\Delta t_R(T)$ are reported for each peptide. Differences in $\Delta t_R(T)$ for each pair of adjacent peptides [equal to $\Delta\Delta t_R(T)$] are also reported. The quantity $\Delta\Delta t_R(T)$ is a direct measure of a change in selectivity due to temperature; values of $\Delta\Delta t_R > 0.5$ min are indicative of band-pairs whose resolution can be affected significantly by a change in temperature. The spacing of band-pairs 7/8 ($\Delta\Delta t_R = -0.6$), 9/10 (-0.7), 13/14 (3.0) and 14/15 (-2.2) should be responsive to a change in temperature, and this is illustrated in the examples of Fig. 5.

The temperature-selectivity data of Table 4

Table 2
Values of the gradient-steepness parameter S for the rhGH peptides

Peak	S at each temperature				Difference in S for adjacent bands (ΔS)
	20°C	40°C	60°C	Average	
2	24.3	31.1	22.0	(26)[a]	
3	15.7	18.5	23.6	(19)[a]	
4	23.7	26.6	28.5	(26)[a]	
5	12.5	13.6	14.1	13.4	1.5
6	14.2	15.1	15.5	14.9	9.0
7	22.8	24.2	24.8	23.9	−2.0
8	21.3	22.1	22.3	21.9	0.6
9	22.3	22.6	22.5	22.5	−5.9
10	16.8	16.7	16.4	16.6	2.4
11	17.4	18.7	21.0	19.0	0.9
12	21.7	20.3	17.7	19.9	−0.9
13	19.8	19.0	18.1	19.0	1.1
14	20.7	19.8	19.9	20.1	2.5
15	22.7	22.9	22.2	22.6	1.4
16	27.6	28.3	28.1	28.0	−3.1
17	24.9	25.0	24.4	24.9	8.9
18	32.7	34.7	34.0	33.8	−2.6
19	30.7	31.9	31.1	31.2	−12.9
21	18.5	18.5	17.9	18.3	

Determined from data for 30- and 120-min gradient times.
[a] Less reliable values due to early elution of bands.

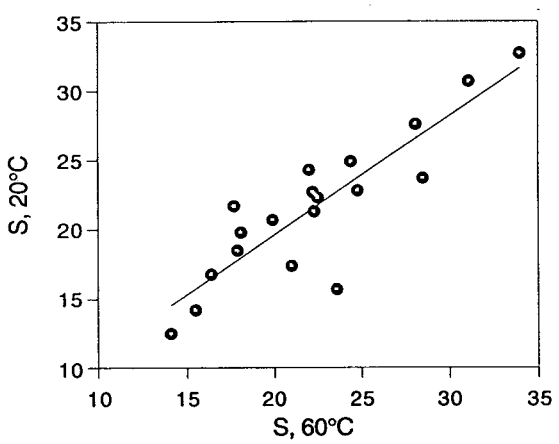

Fig. 6. rhGH tryptic peptide values for S at 20°C vs. 60°C (software derived, see Table 2).

plus S values from Table 2 allow a test of whether simultaneous changes in temperature and gradient steepness are worthwhile for the present sample. If values of $\Delta t_R(T)$ do *not* correlate with values of S, then it can be concluded that the effects of temperature and gradient steepness operate independently, and it will be profitable to change temperature and gradient selectivity simultaneously. If, on the other hand, a strong correlation exists between $\Delta t_R(T)$ and S, the use of either temperature or gradient steepness should result in similar selectivity effects; i.e., the simultaneous use of these two variables would be less useful.

Fig. 7 compares changes in band spacing as a result of changes in temperature and gradient steepness. Values of Δt_R for a change in temperature from 60 to 20°C (average values from Table 4), are plotted vs. average values of S (Table 2) for peptides 5–21 in the rhGH sample. The

Table 3
Values of the gradient-steepness parameter k_w for the rhGH peptides

Peak	Log k_w at each temperature		
	20°C	40°C	60°C
2	0.90	0.59	0.24
3	1.07	0.79	0.52
4	1.74	1.49	1.18
5	1.62	1.50	1.32
6	2.11	1.99	1.77
7	3.87	3.64	3.31
8	3.71	3.50	3.20
9	3.40	3.19	2.91
10	4.68	4.36	3.96
11	3.92	3.89	3.97
12	4.43	4.23	3.46
13	4.83	4.22	3.92
14	6.01	5.10	4.02
15	5.75	5.85	5.43
16	7.85	7.67	7.22
17	7.36	7.24	6.81
18	10.00	10.33	9.78
19	9.66	9.84	9.33
21	7.46	7.50	7.18

Determined from data for 30- and 120-min gradient times.

marked scatter of the resulting plot ($r^2 = 0.00$) indicates no correlation of these two quantities, confirming the value of simultaneous variation of temperature and gradient steepness for the purposes of controlling band spacing.

4.5. Column stability

The use of temperatures >50°C for the low-pH reversed-phase separation of peptide or protein samples has been avoided in the past because of the instability of available bonded-phase columns. The use of low-pH mobile phases (e.g., 0.1% TFA in acetonitrile–water) can lead to a rapid loss of bonded phase, even at temperatures near ambient [36–39]. This loss in bonded phase causes continuous changes in retention time and a loss in column plate number. Such changes complicate peak identity assignments, make quantitation more difficult, and require more frequent (and expensive) column replacement.

Recent improvements in the bonded phases available for reversed-phase HPLC have resulted in commercially available columns that are much more stable toward low-pH, high-temperature operation [8,40,41]. These new columns (StableBond, Rockland Technologies) are based on "sterically protected" silanes, in which the methyl groups of the usual alkyldimethylsilane bonded phase are replaced with bulkier groups such as isopropyl or isobutyl. The use of these monomeric sterically protected phases ensures repeatable separations and excellent column performance during the life of the column, even for aggressive separation conditions. This in turn makes possible the effective use of temperature optimization as illustrated in the present study.

5. Conclusions

Narrow- and wide-pore "sterically protected" reversed-phase column packings are now commercially available for use under low-pH, high-temperature conditions. These silica-based packings allow temperatures as high as 90°C (without loss of bonded phase) for the efficient separation of peptide or protein samples. This in turn makes possible the use of temperature as a means of varying separation selectivity. In the present study of the separation of a tryptic digest of rhGH, it was found that peak spacing changed significantly when column temperature was varied from 20 to 60°C. It was further observed that the combined use of temperature and gradient steepness provided an efficient procedure for the control of peak spacing and optimization of separation for this sample. At the same time, this approach to selectivity control is more convenient than alternatives such as a change of column or mobile phase, because temperature and gradient steepness can be varied via the system controller. The following paper [14] provides further examples of this kind, which suggests that this approach to the optimized separation of peptide and protein samples is generally applicable.

Table 4
Changes in retention time t_R for a change in temperature from 60 to 20°C as a function of gradient time t_G

Band	Change in t_R (min) for different t_G [a]				Inter-band change ($\Delta\Delta t_R$)[b]
	30 min	60 min	120 min	Average	
2	3.9	3.6	2.2	3.0	0.6
3	4.4	3.6	2.7	3.6	−0.7
4	3.2	2.9	2.6	2.9	0.1
5	3.2	2.8	2.5	2.8	0.2
6	3.2	3.0	2.8	3.0	0.5
7	3.6	3.4	3.4	3.5	−0.6
8	3.0	2.9	2.8	2.9	0.4
9	3.4	3.3	3.3	3.3	−0.7
10	2.5	2.6	2.6	2.6	0.5
11	3.4	3.0	2.8	3.1	0.1
12	3.0	3.2	3.4	3.2	−0.2
13	0.9	1.2	1.5	1.2	3.4
14	4.6	4.7	(3.3)	4.6	−2.5
15	2.0	2.0	2.1	2.1	0.7
16	2.8	2.7	2.8	2.8	−1.1
17	1.6	1.7	1.7	1.7	0.0
18	1.8	1.7	1.7	1.7	−0.3
19	1.4	1.3	1.4	1.4	−1.1
21	0.3	0.4	0.3	0.3	

[a] Values for 30- and 120-min runs are corrected for the effect of gradient time; data for 30-min runs have been multiplied by 2 and the data for the 120-min runs have been multiplied by 1/2.
[b] E.g., for bands 6/7, it is the average change for band 7 minus the change for band 6; i.e., $\Delta\Delta t_R = 3.5 - 3.0 = 0.5$.

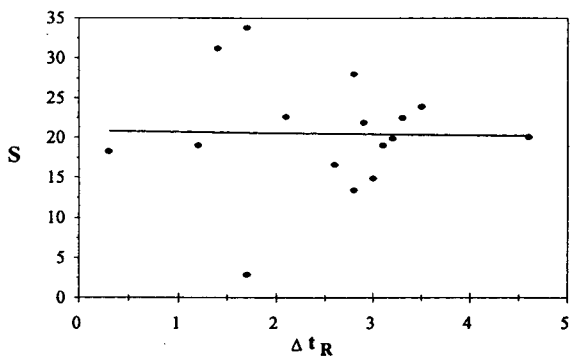

Fig. 7. Non-correlation of temperature and gradient-steepness selectivity effects for the rhGH sample. The change in peptide retention time (Δt_R, min) for a change in temperature from 60 to 20°C (average values of Table 4) is plotted vs. the average value of S (Table 2) for bands 5–21. $\Delta t_R = 20.8 - 0.13S$; $r^2 = 0.0003$; error y (S) estimate = 7.5.

Acknowledgement

One of us (L.R.S.) was supported in part by a Small Business Innovation Research (SBIR) grant from the National Institutes of Health (US Department of Health and Human Services).

References

[1] J.M. Davis and J.C. Giddings, *Anal. Chem.*, 53 (1983) 418.
[2] L.R. Snyder, J.L. Glajch and J.J. Kirkland, *Practical HPLC Method Development*, Wiley-Interscience, New York, 1988.
[3] C.T. Mant and R.S. Hodges (Editors), *High-Performance Chromatography of Peptides and Proteins: Separation, Analysis and Conformation*, CRC Press, Boca Raton, FL, 1991.
[4] F.D. Antia and Cs. Horváth, *J. Chromatogr.*, 435 (1988) 1.
[5] M. Herold and L. Winzer, *BioTec (Wuerzberg, Ger)*, 4 (1992) 47.

[6] N.M. McKern and H.K. Edskes, *Biomed. Chromatogr.*, 7 (1993) 15.
[7] K.D. Nugent, W.G. Burton, T.K. Slattery, B.F. Johnson and L.R. Snyder, *J. Chromatogr.*, 443 (1988) 381.
[8] J.J. Kirkland, C.H. Dilkes, Jr. and J.E. Henderson, *LC·GC*, 11 (1993) 290.
[9] J.L. Glajch, M.A. Quarry, J.F. Vasta and L.R. Snyder, *Anal. Chem.*, 58 (1986) 280.
[10] B.F.D. Ghrist, L.R. Snyder and B.S. Silverman, in K.M. Gooding and F.E. Regnier (Editors), *HPLC of Biological Macromolecules*, Marcel Dekker, New York, 1990, p. 403.
[11] B.F.D. Ghrist and L.R. Snyder, *J. Chromatogr.*, 459 (1988) 25, 43.
[12] J.W. Dolan, D.C. Lommen and L.R. Snyder, *J. Chromatogr.*, 485 (1989) 91.
[13] R.C. Chloupek, W.S. Hancock and L.R. Snyder, *J. Chromatogr.*, 594 (1992) 65.
[14] R.C. Chloupek, W.S. Hancock, B.A. Marchylo, J.J. Kirkland, B.E. Boyes and L.R. Snyder, *J. Chromatogr. A*, 686 (1994) 45.
[15] L.R. Snyder, in Cs. Horváth (Editor), *High-Performance Liquid Chromatography —Advances and Perspectives*, Vol. 1, Academic Press, New York, 1980, p. 207.
[16] P. Jandera and J. Churacek, *Gradient Elution in Column Liquid Chromatography*, Elsevier, Amsterdam, 1985.
[17] L.R. Snyder and M.A. Stadalius, in Cs. Horváth (Editor), *High-Performance Liquid Chromatography —Advances and Perspectives*, Vol. 4, Academic Press, New York, 1986, p. 195.
[18] S. Terabe, H. Nishi and T. Ando, *J. Chromatogr.*, 212 (1981) 295.
[19] M.A. Stadalius, H.S. Gold and L.R. Snyder, *J. Chromatogr.*, 296 (1984) 31.
[20] K.K. Unger, G. Jilge, J.N. Kinkel and M.T.W. Hearn, *J. Chromator.*, 359 (1986) 61.
[21] J.W. Dolan, L.R. Snyder and M.A. Quarry, *Chromatographia*, 24 (1987) 261.
[22] W. Melander, D.E. Campbell and Cs. Horváth, *J. Chromatogr.*, 158 (1978) 215.
[23] H. Colin, J.C. Diez-Masa, G. Guiochon, T. Czajkowska and I. Miedziak, *J. Chromatogr.*, 167 (1978) 41.
[24] A. Robbat, Jr. and T.-Y. Liu, *J. Chromatogr.*, 513 (1990) 117.
[25] E.J. Kikta and E. Grushka, *Anal. Chem.*, 48 (1976) 1098.
[26] Gy. Vigh and Z. Varga-Puchony, *J. Chromatogr.*, 196 (1980) 1.
[27] J. Chmielowiec and H. Sawatzky, *J. Chromatogr. Sci.*, 17 (1979) 245.
[28] C.P. Terweij-Groen and J.C. Kraak, *J. Chromatogr.*, 138 (1977) 245.
[29] S.M. Kim, *J. Chromatogr.*, 247 (1982) 103.
[30] K. Jinno, M. Yamagami and M. Kuwajima, *Chromatographia*, 25 (1988) 974.
[31] R.H. Ingraham, S.Y.M. Lau, A.K. Taneja and R.S. Hodges, *J. Chromatogr.*, 327 (1985) 77.
[32] Z.-S Li, J. Attias and B. Marin, *C.R. Acad. Sci., Serie 3*, 315 (1992) 127.
[33] L.R. Snyder, *J. Chromatogr.*, 179 (1979) 167.
[34] D. Guo, C.T. Mant and R.S. Hodges, *J. Chromatogr.*, 386 (1987) 205.
[35] K. Valkó, L. R. Snyder and J.L. Glajch, *J. Chromatogr. A*, 656 (1993) 501.
[36] J.L. Glajch, J.C. Gluckman, J.G. Charikovsky, J.M. Minor and J.J. Kirkland, *J. Chromatogr.*, 318 (1985) 23.
[37] J.L. Glajch, J.J. Kirkland and J. Kohler, *J. Chromatogr.*, 384 (1987) 81.
[38] U. Anthoni, C. Larsen, P.H. Nielsen and C. Christophersen, *Anal. Chem.*, 59 (1987) 2435.
[39] N. Saglialno, Jr., T.R. Floyd, R.A. Hartwick, J.M. DiBussolo and N.T. Miller, *J. Chromatogr.*, 443 (1988) 155.
[40] J.J. Kirkland, J.L. Glajch and R.D. Farlee, *Anal. Chem.*, 61 (1989) 2.
[41] J.L. Glajch and J.J. Kirkland, *LC·GC*, 8 (1990) 140.

ELSEVIER

Journal of Chromatography A, 686 (1994) 45–59

JOURNAL OF CHROMATOGRAPHY A

Temperature as a variable in reversed-phase high-performance liquid chromatographic separations of peptide and protein samples
II. Selectivity effects observed in the separation of several peptide and protein mixtures

Rosanne C. Chloupek[a], William S. Hancock[a,1], Brian A. Marchylo[b], Joseph J. Kirkland[c], Barry E. Boyes[c], Lloyd R. Snyder[d,*]

[a]*Genentech, Inc., 460 Point San Bruno Boulevard, South San Francisco, CA 94080, USA*
[b]*Canadian Grain Commission, Grain Research Laboratory, Winnipeg, Manitoba, Canada*
[c]*Rockland Technologies Inc., 538 First State Boulevard, Newport, DE 19804, USA*
[d]*LC Resources Inc., 2930 Camino Diablo, Suite 110, Walnut Creek, CA 94596, USA*

First received 31 December 1993; revised manuscript received 2 August 1994

Abstract

Changes in band spacing as a function of temperature and/or gradient steepness were investigated for four peptide or protein samples. Reversed-phase HPLC in a gradient mode was used to separate tryptic digests of tissue plasminogen activator and calmodulin. Additionally, a synthetic peptide mixture and a storage protein sample from wheat were studied. Simultaneous changes in gradient steepness and temperature were found to provide considerable control over band spacing and sample resolution.

The effects of temperature and gradient steepness on selectivity in these systems appear to be complementary. Simultaneous optimization of both temperature and gradient steepness thus represents a powerful and convenient means of controlling band spacing and separation. Because of the complexity of these sample chromatograms, computer simulation proved to be a useful tool in both interpreting these experiments and in optimizing final separations.

1. Introduction

The preceding paper [1] noted possible problems in achieving the separation of complex peptide or protein samples. One approach is to change conditions so as to optimize selectivity or peak spacing within the chromatogram. Several established means of altering separation selectivity have been reported [2]: column source or type (e.g., C_4 vs. cyano), change in the organic solvent (acetonitrile, propanol, etc.), the use of ion-pairing conditions, variation of pH or ionic strength. Nevertheless, most reversed-phase separations of peptide and protein samples em-

* Corresponding author.
[1] Present address: Hewlett-Packard Laboratories, 3500 Deer Creek Road 26U, Palo Alto, CA 94304, USA.

0021-9673/94/$07.00
SSDI 0021-9673(94)00778-O

ploy a "standard" set of preferred conditions: a short-chain alkyl-silica column (e.g., C_3 or C_4) and gradient elution with an acetonitrile–water mobile phase containing ca. 0.1% trifluoroacetic acid (TFA). While the use of these conditions has several practical advantages, one consequence is that practical workers make only limited use of changes in conditions in order to control peak spacing and separation.

The preceding paper [1] suggests that the advantages of low-pH acetonitrile gradients can be retained while selectivity is varied by means of simultaneous changes in temperature and gradient steepness. In this paper we examine whether this approach for optimizing the separation of peptide and protein samples is likely to prove widely applicable.

2. Experimental

2.1. Equipment, materials and procedures

The equipment used to collect the experimental data reported here is described in Refs. 3–7. The columns were 15 × 0.46 cm Zorbax, 300 Å pore diameter, 5-μm SB-C_8 for recombinant tissue plasminogen activator (rt-PA) and the cereal storage protein sample. The calmodulin and synthetic peptide separations used a 15 × 0.46 cm Zorbax, 80 Å pore, 3.5-μm SB-C_{18} column. Each of these columns (Rockland Technologies) has a "sterically protected" bonded phase that is stable at low pH and high temperature.

The materials and samples used in the present study are described in Refs. 3 (cereal proteins), 5 (calmodulin digest) and 7 [reduced and S-carboxymethylated (RCM) rt-PA digest].

All gradients used water (A) and acetonitrile (B) with 0.1% added TFA.

Computer simulations were carried out as described in the preceding paper [1], using DryLab/windows software (LC Resources).

2.2. Tryptic mapping (LC–MS)

A 100-μl aliquot containing 100 μg of the RCM rt-PA tryptic digest was loaded onto a 15 × 0.46 cm Zorbax SB-C_8 column at a flow-rate of 0.5 ml/min using a Hewlett-Packard 1090M HPLC system. The sample was separated with 0–60% B gradients in 30 and 120 min. Column temperature was 40°C. The effluent was split 1:20 with a Valco tee, to give a flow-rate of 25 μl/min into the ionspray nebulizer (Sciex). The balance of the column effluent was diverted to the HPLC system (monitored at 220 nm).

MS analysis was carried out in quadrupole —one of a Sciex API III triple-quadrupole mass spectrometer. The quadrupole was scanned from 300 to 2000 u in 4.3 s, using a step size of 0.5 u and a 1.2-ms dwell time per step. The intensity of the plot was adjusted manually to minimize interference due to background.

3. Results and discussion

3.1. RCM rt-PA tryptic digest

Computer simulation

Initial runs at 30, 60 and 120 min for temperatures of 20, 40 and 60°C were carried out as in the case of the recombinant human growth hormone (rhGH) digest [1]. As expected for a digest with 54 theoretical peptide fragments, the resulting chromatograms were much more complex and poorly resolved (Fig. 1a). In addition to the major peptides (labeled in Figs. 2–5; see Ref. [7] for structures), there are a large number of minor peaks. Because of the complexity of these chromatograms, peak tracking was quite difficult. The use of area measurements for this purpose was complicated by the frequent overlap of minor peaks with peptides of interest and changes in relative peak position as a function of temperature and gradient steepness. This difficulty was largely overcome by two expedients. First, chromatograms measured at 280 nm were used in selected cases, since these chromatograms were less complicated and somewhat easier to interpret. Additionally, area ratios for 280 nm vs. 220 nm detection provided a further check on peak matching. Second, on-line MS measurements were carried out on the 30- and 120-min runs at 40°C, which aided both matching and identification of the major peptide peaks in these runs.

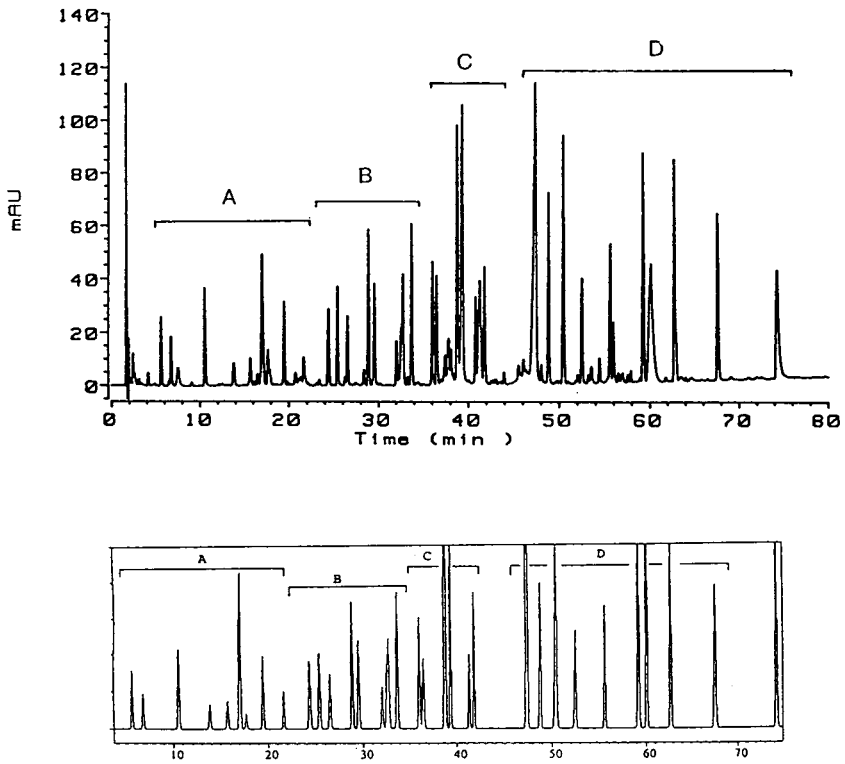

Fig. 1. Separation of rt-PA tryptic digest at 40°C with a 0–60% B 120-min gradient. Other conditions as in Fig. 2 of Ref. [1]. (Top) Experimental chromatogram; (bottom) Computer simulation for major peptides only. Letters A–D designate groups of peptides discussed in text.

Data for the 60- and 120-min runs at a given temperature were used as input to computer simulation, with comparison of experimental and predicted retention times for the 30-min run. The results were similar to those reported in Ref. [1] for the rhGH sample; peak matching and subsequent computer simulations appeared to be accurate and reliable. The use of input runs (60- and 120-min gradients) that differed in gradient time by only a factor of 2 was expected to decrease the accuracy of measured gradient steepness (S) values. However, very crowded chromatograms made direct use of the 30-min gradient data for computer simulation inconvenient and potentially less reliable. Experimental values of the column plate number N for these various separations were determined from resolution measurements as described in Ref. [1]: $N = 4400$ (20°C), 5600 (40°C) and 7000 (60°C).

Effect of changes in gradient steepness and temperature

While rt-PA digest data were obtained for three different temperatures, only the 40 and 60°C data were used for computer simulation. The lower value of N for the 20°C runs combined with the large number of bands to make it almost impossible to untangle the major peptide bands for peak tracking and data entry. Another complication was the complete overlap of certain band-pairs for all values of gradient steepness at 20, 40 or 60°C. This made the use of total-sample resolution maps (as in Fig. 3 of Ref. [1]) unfeasible, because at each temperature one or more critical band pairs had $R_s = 0$ for all values of gradient time t_G. Resulting maps would therefore be completely uniformative. For these and other reasons, we divided the chromatogram into four separate groups of bands (A–D) as shown

in Fig. 1 (lower panel). We will illustrate the effects of temperature and gradient steepness for these individual groups (as in Ref. [1] for the rhGH sample).

Fig. 2 shows chromatograms of group A at 40 and 60°C for both 60- and 120-min gradients. Peaks X1-A, -B and -C comprise peptides T9, T36 and T44, but it was not possible to determine which band corresponds to a specific peptide using only the 40°C MS identification. An increase in temperature improves the separation of the group of peptides labeled "X1" and "T39"; these compounds are optimally resolved at 60°C with a 60-min gradient.

Fig. 3 shows chromatograms of group B as a function of temperature and gradient steepness. This group of compounds exhibits striking changes in relative band position as both temperature and gradient steepness are varied. Group B would be adequately separated ($R_s >$ 1.0) with a temperature of 40°C and a gradient time of 90 min (not shown).

Fig. 4 shows chromatograms of group C as a function of temperature and gradient steepness.

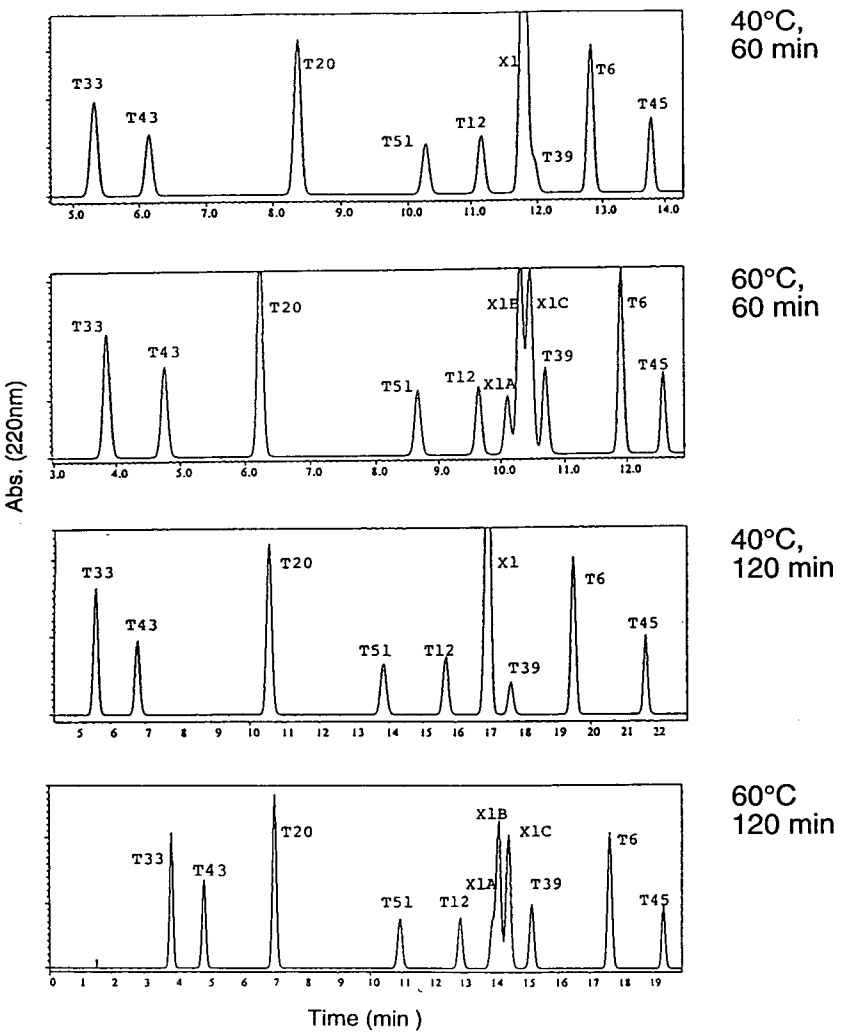

Fig. 2. Effect of changes in temperature and gradient steepness on the separation of group A of the rt-PA digest (see Fig. 1). Temperature and gradient times indicated next to each panel. Computer simulations for N = experimental value.

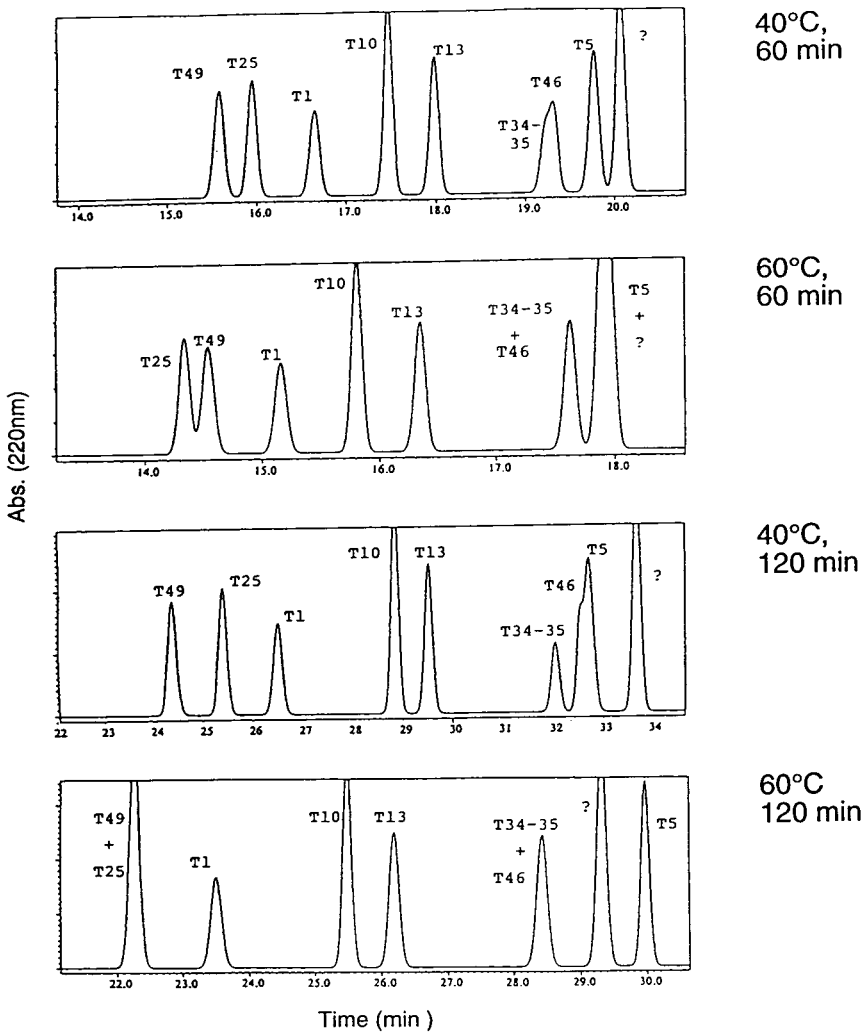

Fig. 3. Effect of changes in temperature and gradient steepness on the separation of group B of the rt-PA digest (see Fig. 1). Temperature and gradient times indicated next to each panel. Computer simulations for N = experimental value.

Again, large changes in relative band position occur as a function of varying temperature or gradient steepness. Complete separation of this group is predicted for a 120-min gradient and a temperature of about 50°C (not shown).

Fig. 5 shows chromatograms of group D as a function of temperature and gradient steepness. Early bands X3-A, -B and -C (comprising T15, T24 and an unidentified peptide) are only separated at 60°C and a gradient time of 120 min. A good separation of this group should result for a gradient time of 120 min and a temperature of about 50°C (not shown).

The examples of Figs. 2–5 further confirm that a variation of temperature is often a powerful means for changing the band spacing of a peptide sample. Not only can major changes in band position be effected by a change in temperature, but these effects appear to be independent of concomitant changes that result from changes in gradient steepness. This is further shown in Fig. 6, where the change in retention with tempera-

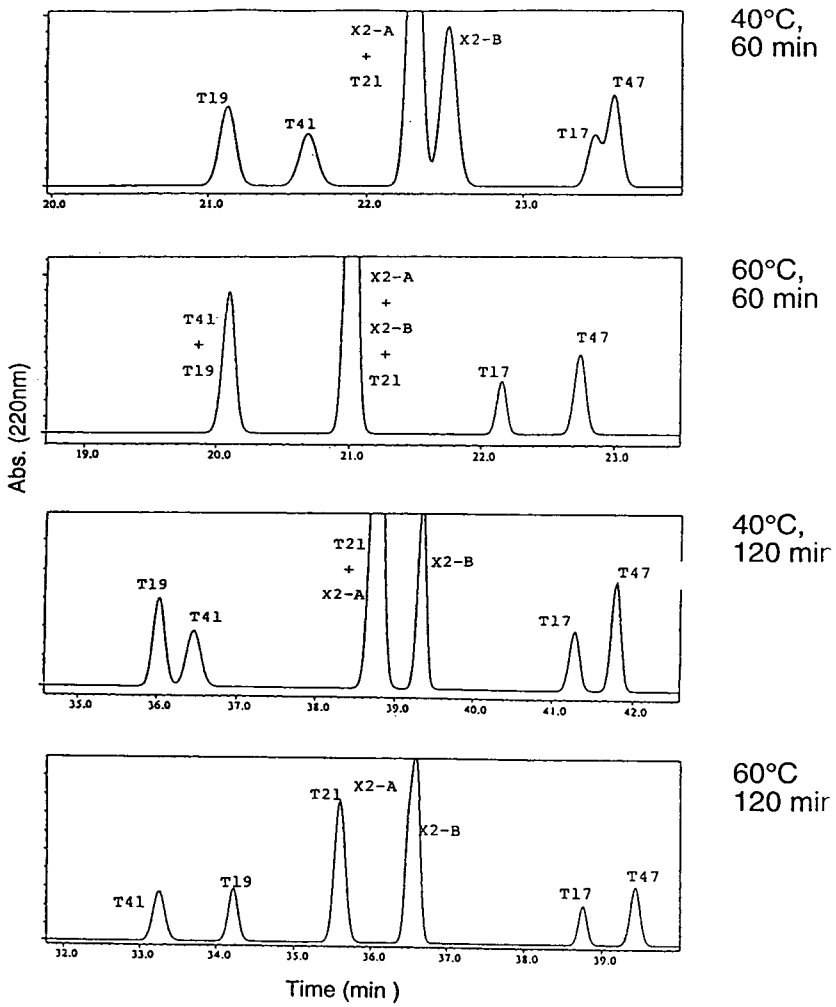

Fig. 4. Effect of changes in temperature and gradient steepness on the separation of group C of the rt-PA digest (see Fig. 1). Temperature and gradient times indicated next to each panel. Computer simulations for N = experimental value.

ture (Δt_R) is plotted vs. S for the various peak-pairs of the rt-PA digest; cf. discussion of Fig. 7 of Ref. [1]; the correlation ($r^2 = 0.10$) is quite low.

As in the case of the rhGH sample [1], values of S do not change much with temperature. This is illustrated in Fig. 7, where values of S for 40°C are plotted vs. values for 60°C.

3.2. Calmodulin tryptic digest

This sample was separated at two different temperatures (35 and 85°C) as shown in Fig. 8. The resulting chromatograms are much simpler than seen previously, with only a dozen or so major peaks being separated. The 85°C separation exhibits narrower bands (as expected), but apart from this difference the two chromatograms look quite similar. This suggests that little change in peak spacing has resulted as a result of this large change in temperature. Upon closer inspection, however, there are at least three significant changes in selectivity. The resolution of doublet "A" in Fig. 8 is the same at the two temperatures, despite the decrease in bandwidth at 85°C. This means that the retention time

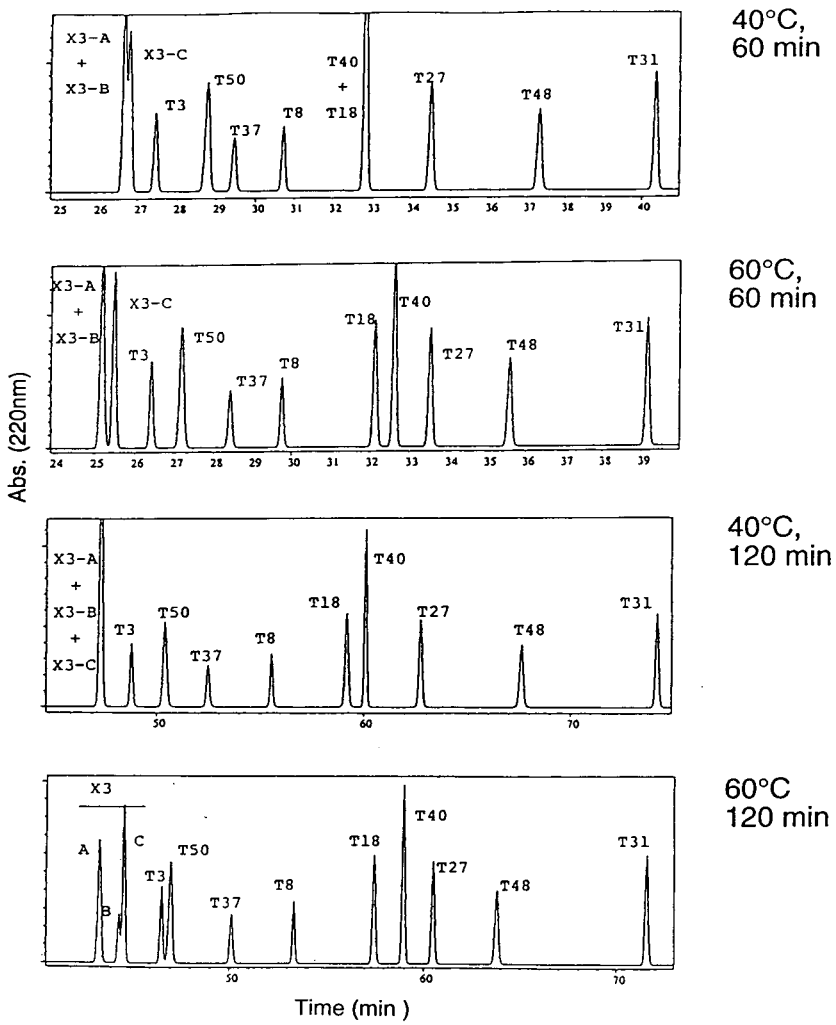

Fig. 5. Effect of changes in temperature and gradient steepness on the separation of group D of the rt-PA digest (see Fig. 1). Temperature and gradient times indicated next to each panel. Computer simulations for N = experimental value.

difference for this peak-pair is actually reduced somewhat as temperature increases. A similar (but more pronounced) decrease in retention time difference is seen for peak-pair B as temperature is increased. Finally, peak-pair C is unseparated at 35°C but is completely resolved at 85°C.

The best overall separation of the calmodulin digest probably occurs at 85°C. The effects of gradient steepness on this separation were not studied, but it is likely that a further improvement in resolution could have been effected by optimizing gradient time as well as temperature.

3.3. Cereal protein sample

The separation of this sample is shown in Fig. 9 for two different temperatures: 50 and 70°C. Chromatograms were actually obtained for 30, 50 and 70°C and for gradient times of 30, 60 and 120 min. Because of the complexity of this sample, it was not feasible to carry out computer simulations for the entire sample. Nevertheless, the data obtained so far allow us to examine the utility of temperature variation as a means of controlling band spacing and selectivity for this sample.

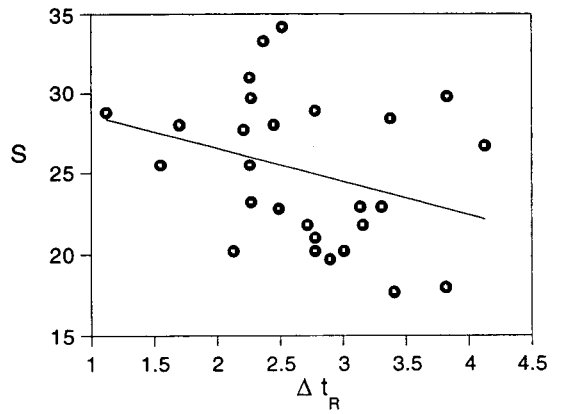

Fig. 6. Non-correlation of temperature and gradient-steepness (S) selectivity effects for the rt-PA tryptic digest sample. The change in peptide retention time (Δt_R, min) for a change in temperature from 60 to 40°C (120-min gradient) is plotted vs. the average value of S for the peak-pair. $\Delta t_R = 3.92 - 0.050S$; $r^2 = 0.105$; standard error y (Δt_R) estimate = 0.65.

Three different groups of compounds in this sample are identified in Fig. 9: peaks A–F, G–J and K–P. We were able to carry out provisional peak tracking for each of these three groups, which allowed subsequent computer simulations as for the rt-PA digest sample. A best fit of the simulated and experimental chromatograms yielded a plate number of $N = 1000$ for the 50°C separations and $N = 1500$ for the 70°C runs. The predicted values (Ref. [8]) for an average column and compounds of this molecular mass were $N = 1600$ and 2250, respectively. The lower experimental plate numbers (by about 35%) suggest a minor problem with either (a) column efficiency or (b) "non-ideal" effects which are common for protein samples [9]. As expected, the use of a higher temperature (70°C) results in a significant increase (20%) in peak capacity. However, this effect is subordinated to changes in selectivity with temperature. The chromatograms for 30°C separation were markedly less resolved than for 50 or 70°C. This is probably the result of both a lower plate number and more serious "non-ideal" effects at 30°C.

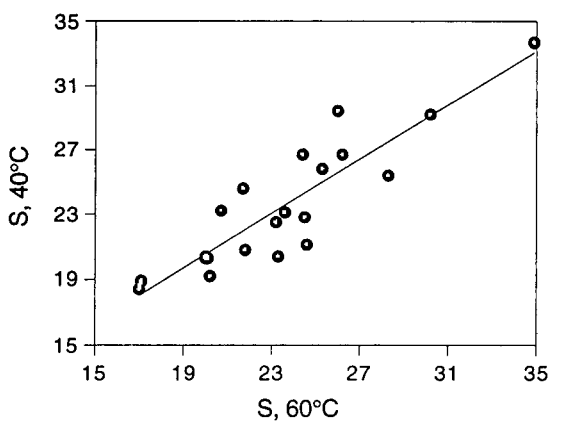

Fig. 7. rt-PA tryptic peptide values for S at 40 vs. 60°C (software derived).

Computer simulations were carried out for 50 and 70°C separations as a function of gradient time. Input values for 60- and 120-min runs allowed the prediction of retention times for the 30-min gradients, as a check on the reliability of peak tracking and computer simulation. Experimental and predicted retention times at 30°C were in agreement within $< 1\%$.

A qualitative comparison of the two separations of Fig. 9 shows several apparent changes in band spacing due to this difference in temperature. For example, the two band-clusters indicated by arrows are markedly different in appearance. At 50°C three major bands plus a large shoulder are apparent, while at 70°C only one distinct band plus two shoulders can be seen. It should also be kept in mind that the higher peak capacity at 70°C would otherwise favor the better separation of this group of proteins.

Fig. 10 shows the separation of group A–F as a function of temperature and gradient steepness. No changes in retention order were noted for the major peaks in this group, although there are obvious changes in selectivity as a function of temperature. Peaks D and E move apart as temperature is increased, while peak C moves from B toward D at the higher temperature. On balance, the best separation of this group is obtained at 50°C with a gradient time of 120 min.

Fig. 11 shows the separation of the largest peaks in group G–J. While these peaks are well resolved for all conditions, we see that peak I moves closer to band J as temperature is increased. The separation of group K–P (Fig. 12) shows that peaks L/M and O/P are only resolved at 70°C with a 120-min gradient. The best

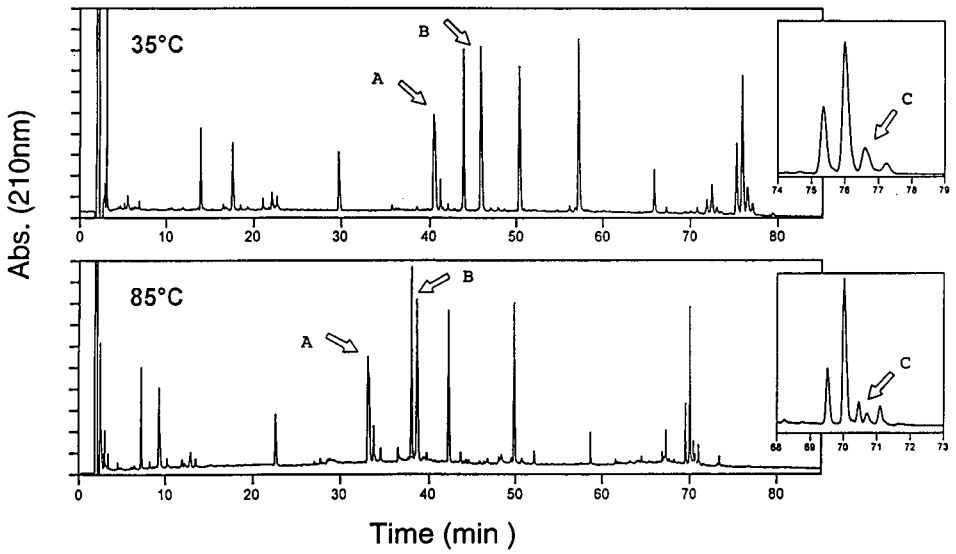

Fig. 8. Calmodulin tryptic digest. Separation at two different temperatures. Conditions: 15 × 0.46 cm Zorbax 80 SB-C_{18} column (3.5 μm); solvent A, 0.1% TFA in water; solvent B, 0.1% TFA in acetonitrile; gradient of 5–60% B in 90 min; 0.75 ml/min; detection at 210 nm. See Ref. [6] for details.

overall separation of this group of bands is obtained at 70°C with a 120-min gradient.

As for the case of the rt-PA sample, values of S for bands A–P were compared at 50 and 70°C (Fig. 13). Somewhat greater scatter was noted vs. the correlation of Fig. 7, presumably because of the greater complexity of these chromatograms and resulting errors in retention time measurements. The correlation of changes in retention time (50°C value minus 70°C value, 120-min gradients) with average values of S (Fig. 14) was somewhat better than for the rhGH and rt-PA samples: $S = 108 - 10.6\Delta t_R$, $r^2 = 0.50$. However the standard error of S (14.1) is large enough to confirm that the temperature selectivity effects observed for the cereal protein sample are both significant and relatively independent of changes in selectivity as a result of change in gradient steepness.

3.4. Synthetic peptide mixture

A sample of five synthetic peptides described by Mant and Hodges [10] was separated by reversed-phase gradient elution at three temperatures (35, 60 and 85°C), other conditions the same; see Fig. 15 and Table 1. These peptides (labeled A–E) are structurally related decapeptides which are acetylated at the amino terminus and amidated at the carboxyl terminus (except for A which is unacetylated). The only other structural difference is in the amino acids at positions 3 and 4 from the amino terminus: A and C, Ala–Gly; B, Gly–Gly; D, Val–Gly; E, Val–Val. Because of these small differences in peptide structure, smaller temperature selectivity effects were expected.

Fig. 15 (and Table 1) show that bands A and B move apart as temperature is increased. Due to the wider spacing of bands B–E, changes in their relative retention are visually less apparent. Table 1 summarizes the changes in retention time with temperature for each peptide; it is seen that the increase in retention time as temperature is decreased from 85 to 35°C decreases regularly from band A to E. Also, a reduced spacing of *all* bands in the chromatogram results as temperature decreases, which results in an increase in resolution of all bands in this sample at the higher temperature, apart from any change in column efficiency with temperature.

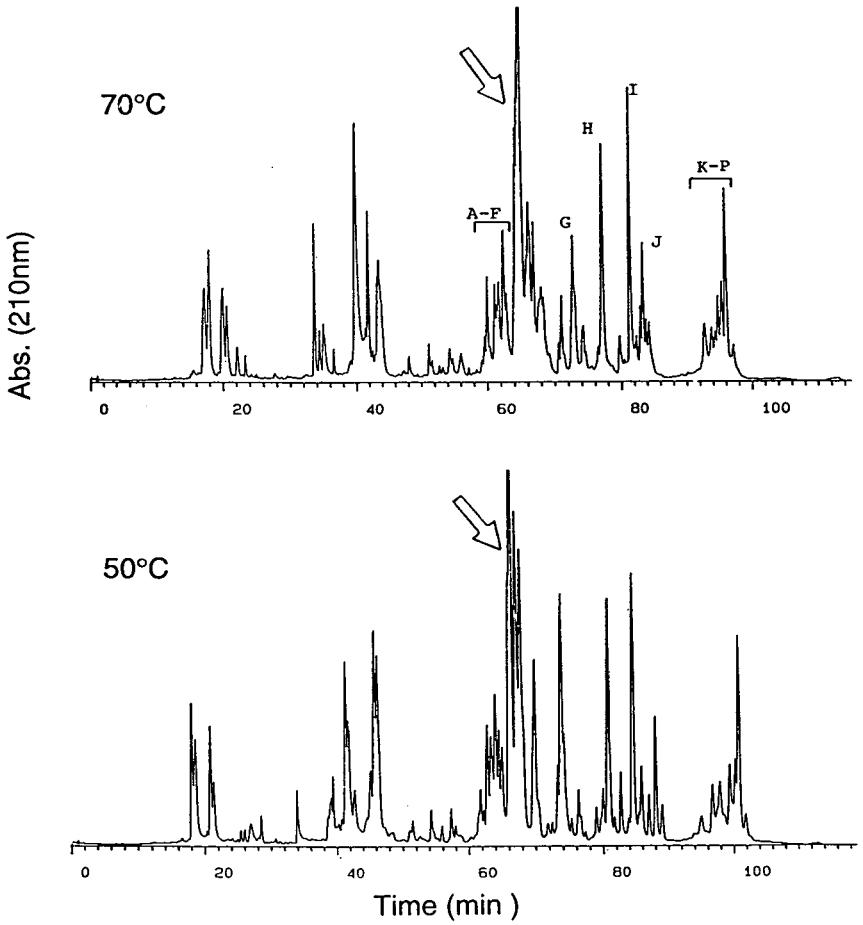

Fig. 9. Separations of cereal storage proteins as a function of temperature. Conditions: 15 × 0.46 cm Zorbax Rx-300 C_8, 23–48% B gradient (acetonitrile–water plus 0.1% TFA) in 120 min, 1 ml/min, detection at 210 nm. Temperature as noted in figure.

Finally, impurity I of Fig. 15 moves towards peak E as temperature increases, so that the separation of all six bands (A–E plus I) is optimum for a temperature between 60 and 85°C.

Curiously, bandwidth *increases* with increasing temperature in the separations of Fig. 15. This is in contrast to the other samples described here and in Ref. [1]. While the experimental bandwidths of Table 1 for a temperature of 35°C are close to values predicted for a well-packed column, the experimental values at 85°C are about 40% higher than predicted.

3.5. The practical application of temperature/gradient optimization

The foregoing examples suggest that band spacing for the reversed-phase separations of peptide or protein samples can be effectively manipulated by the simultaneous variation of gradient steepness and temperature. The application of this approach to different samples will take different forms, however, depending on sample complexity. We can differentiate arbitrarily between samples containing more or less than 25 major components (the same samples

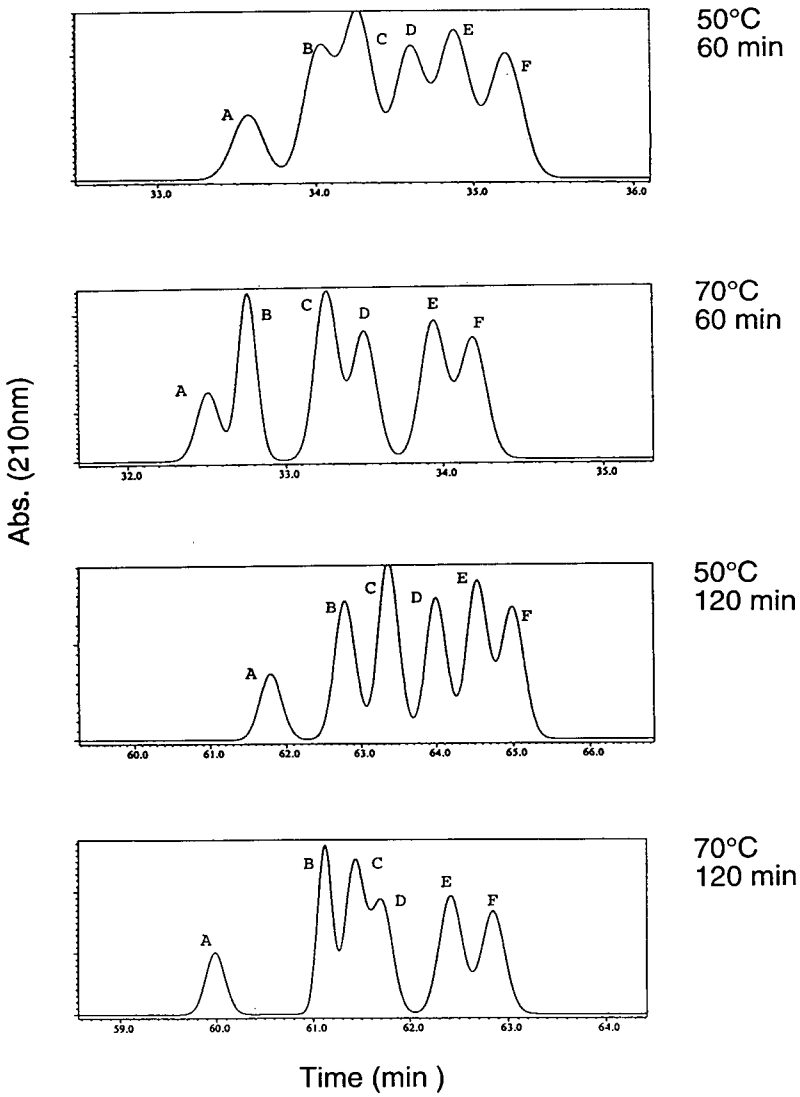

Fig. 10. Separation of cereal protein peaks A–F of Fig. 9 as a function of gradient steepness and temperature. Conditions as in Fig. 9 except as noted. Computer simulations for N = experimental value.

may be assigned to either group, depending on which components we define as "major").

Less-complex samples (< 25 major components)

The expectation is that samples of this type will be separable by some combination of gradient conditions and temperature. Initial runs should be carried out at a temperatures which will maximize column efficiency; e.g., 40–80°C. Computer simulation can then yield resolution maps for different temperatures, as in Fig. 3 of Ref. [1]. If the best choice of temperature and gradient time appears unpromising, it may be necessary to explore other means of changing

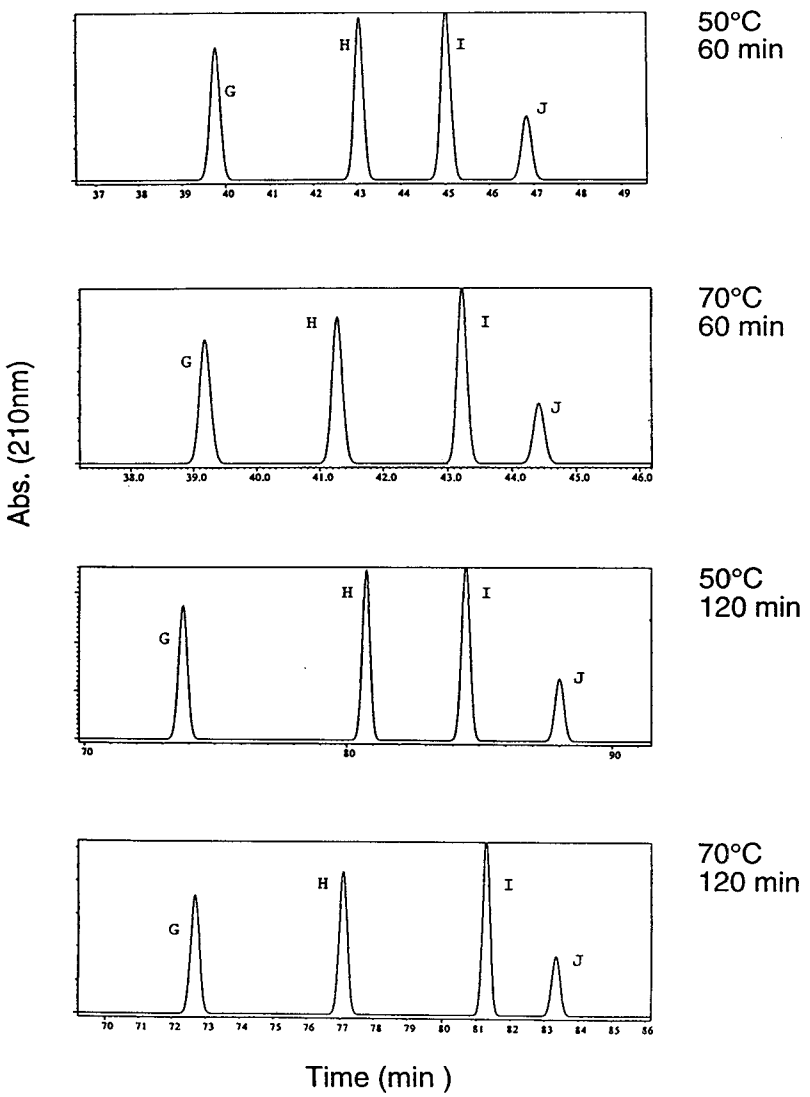

Fig. 11. Separation of cereal protein peaks G–J of Fig. 9 as a function of gradient steepness and temperature. Conditions as in Fig. 9 except as noted. Computer simulations for N = experimental value.

selectivity [2]. Alternatively, the use of a longer, smaller-particle column may prove successful.

More-complex samples (>25 major components).

As shown in the present examples of the rt-PA digest and cereal protein samples, it is unlikely that a single HPLC separation will be able to resolve all the bands in samples such as this —regardless of gradient and temperature optimization. Very complex samples usually require an initial separation into a small number of fractions by one HPLC method (e.g., ion exchange), followed by further separation of each fraction with a different HPLC method (e.g., reversed phase).

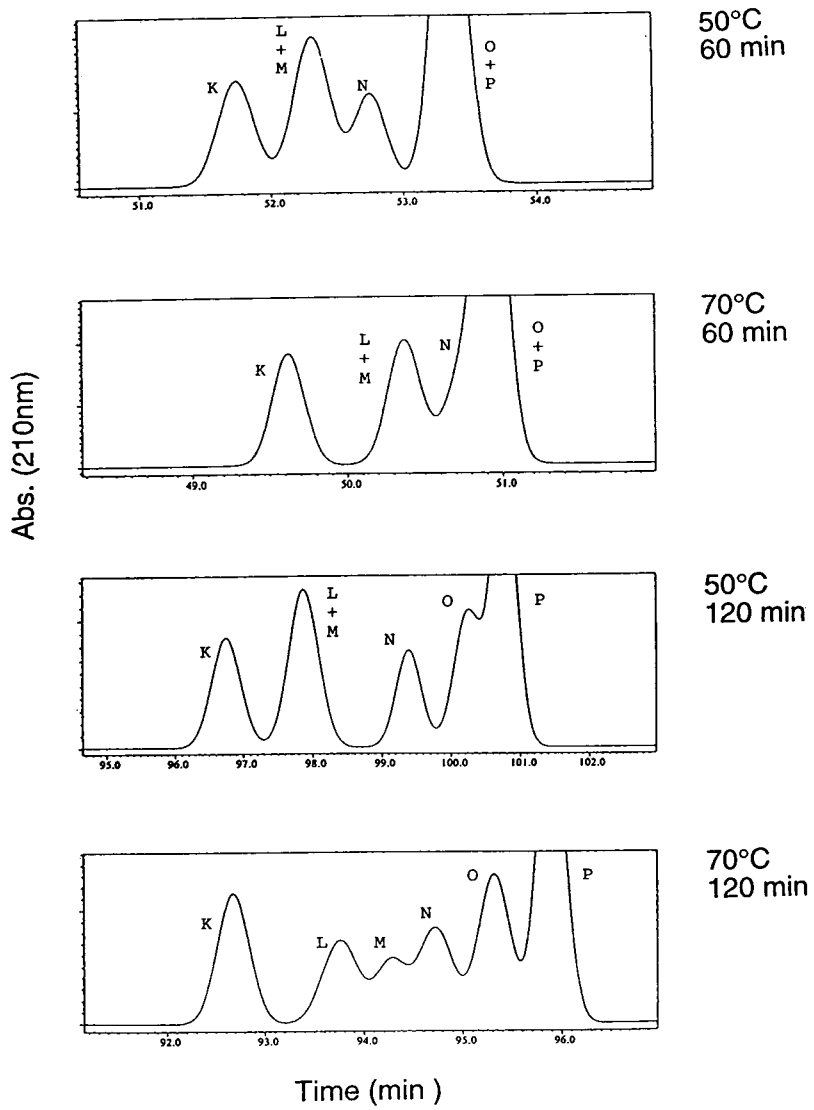

Fig. 12. Separation of cereal protein peaks K–P of Fig. 9 as a function of gradient steepness and temperature. Conditions as in Fig. 9 except as noted. Computer simulations for N = experimental value.Cereal protein sample.

An alternative is to optimize temperature and gradient steepness for the adequate separation of different sub-sets of the sample. This would have been successful in the case of the rt-PA digest, where each of the sub-groups A–D were separable by some choice of temperature and gradient time.

4. Conclusions

Separations by reversed-phase gradient elution of three peptide and one protein sample were studied as a function of temperature and/or gradient steepness. As in the case of the rhGH peptide sample of Ref. [1], it was found that

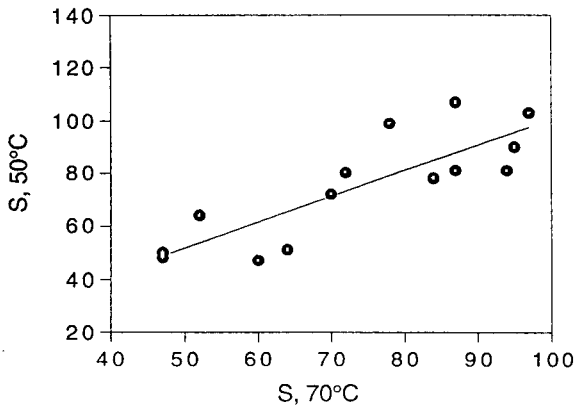

Fig. 13. Cereal storage protein values for S at 40 vs. 60°C (software derived).

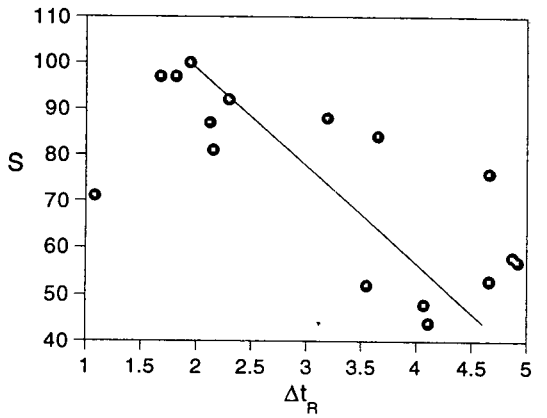

Fig. 14. Non-correlation of temperature and gradient-steepness (S) selectivity effects for the cereal storage protein sample. The change in protein retention time (Δt_R, min) for a change in temperature from 70 to 50°C (120-min gradient) is plotted vs. the average value of S for the peak-pair.

these two variables each have a considerable effect on the spacing of bands within the chromatogram. Their combined effects cannot be duplicated by varying temperature while holding gradient steepness constant nor by varying gradient steepness while holding temperature constant. There should therefore be a considerable advantage in optimizing temperature and gradient steepness simultaneously for the separation of other peptide and protein samples. The convenience of controlling separation by simple adjustments in temperature and gradient steepness represents an additional advantage of this approach. One limitation of this approach is that the use of low-pH mobile phases requires columns that are stable under these conditions; e.g., sterically protected C_8 or C_{18} columns.

For very complex mixtures which contain a large number of both major and minor components, no realistic change in selectivity will

Table 1
Summary of retention times and bandwidths for the separation of the synthetic peptide sample (Fig. 15) as a function of temperature

Peptide	Retention time (min)			
	35°C	60°C	85°C	Δt_R [a]
A	9.73	9.04	7.97	1.76
B	9.84	9.22	8.25	1.59
C	10.28	9.71	8.78	1.50
D	11.60	11.08	10.22	1.38
E	13.11	12.72	11.97	1.14
Average bandwidth[b]				
Experimental	6.3 s	6.6 s	7.1 s	
Calculated	6.7 s	5.7 s	5.0 s	

[a] Difference in retention time, 35°C minus 85°C; e.g., the difference in retention times (Δt_R) for band A is 9.73 − 7.97 = 1.76 min.
[b] Baseline bandwidth values; experimental values average for five peptides; calculated values according to Ref. [9] ($A = 0.5$).

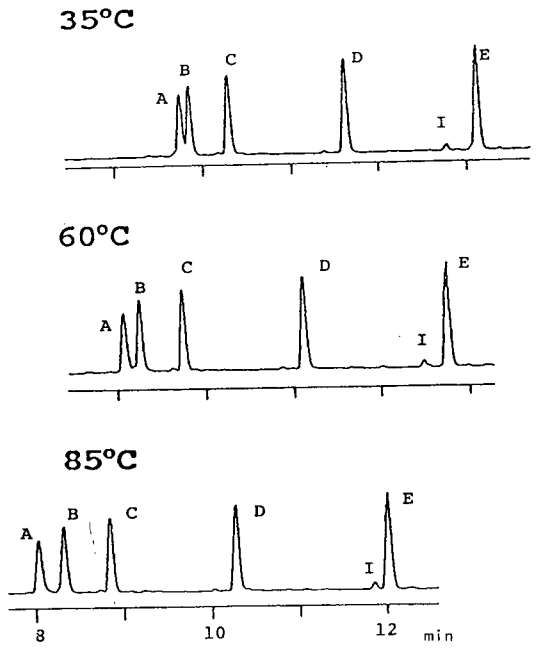

Fig. 15. Synthetic peptide sample. Separation at different temperatures. Conditions: column, 15 × 0.46 cm Zorbax SB-C_{18} (3.5 μm); 0–30% B in 15 min; solvent A, 0.05% TFA in water; solvent B, 0.045% TFA in acetonitrile; 2.0 ml/min; detection at 215 nm. Sample described in Ref. [10].

allow the separation of all compounds of interest. This was true for both the rt-PA and cereal protein samples studied by us. In these and similar cases, it may be necessary to carry out more than one separation of the sample.

References

[1] W.S. Hancock, R.C. Chloupek, J.J. Kirkland and L.R. Snyder, *J. Chromatogr. A*, 686 (1994) 31.
[2] C.T. Mant and R.S. Hodges (Editors), *High-Performance Chromatography of Peptides and Proteins: Separation, Analysis and Conformation*, CRC Press, Boca Raton, FL, 1991.
[3] B.S. Marchylo, D.W. Hatcher and J.E. Kruger, *Cereal Chem.*, 65 (1988) 28.
[4] B.S. Marchylo, D.W. Hatcher and J.E. Kruger, *J. Cereal Sci.*, 9 (1989) 113.
[5] B.S. Marchylo, D.W. Hatcher, J.E. Kruger and J.J. Kirkland, *Cereal Chem.*, 69 (1992) 371.
[6] B.E. Boyes and J.J. Kirkland, *Peptide Res.*, 6 (1993) 249.
[7] V. Ling, A.W. Guzetta, E. Canova-Davis, J.T. Stults, W.S. Hancock, T.R. Covery and B.I. Shushan, *Anal. Chem.*, 63 (1991) 2909.
[8] L.R. Snyder and M.A. Stadalius, in Cs. Horváth (Editor), *High-Performance Liquid Chromatography —Advances and Perspectives*, Vol. 4, Academic Press, New York, 1986, p. 195.
[9] K.D. Nugent, W.G. Burton, T.K. Slattery, B.F. Johnson and L.R. Snyder, *J. Chromatogr.*, 443 (1988) 381.
[10] C.T. Mant and R.S. Hodges, in C.T. Mant and R.S. Hodges (Editors), *High-Performance Chromatography of Peptides and Proteins: Separation, Analysis and Conformation*, CRC Press, Boca Raton, FL, 1991, p. 289.

ELSEVIER

Journal of Chromatography A, 686 (1994) 61–71

JOURNAL OF CHROMATOGRAPHY A

Comprehensive study on binding capacity of human immunoglobulin G to Avid AL affinity gel

Joseph Y. Shi, Randal A. Goffe*

Unisyn Technologies, Inc., Suite 106, 14272 Franklin Avenue, Tustin, CA 92680, USA

First received 11 April 1994; revised manuscript received 3 August 1994

Abstract

Avid AL is an affinity chromatographic gel based on a synthetic ligand which has been designed for the purification of immunoglobulins. The binding capacities of the gel for human IgG were investigated under different conditions; various salts; salt concentrations; different buffer systems with pH ranging from 3.8 to 10.0; and, tissue culture supernatant supplemented with 20% serum. At a similar ionic strength, the binding capacity changed according to the salting out effect of the ions used. Kinetic parameters of the affinity adsorption showed that a strong salting out effect significantly decreased the dissociation constant. Avid AL gel purified IgG from human serum with a capacity of 26.2 mg/ml gel using binding buffer containing sodium sulfate. Recombinant Protein A gel was used as a control. In this study it also exhibited enhanced binding capacity with a high salt concentration binding buffer.

1. Introduction

A synthetic ligand, Avid AL, which has been described in earlier studies from our laboratories [1–3], has been found to bind with high affinity to antibodies of many species; including species whose immunoglobulins do not bind well to Protein A or Protein G. Moreover, the advantage of Avid AL gel, with a low-molecular-mass synthetic affinity ligand, compared with Protein A or Protein G is its ability to withstand acid, base, organic solvent, proteolytic enzyme and autoclaving treatment [4]. Due to its action as a biospecific affinity chromatographic material, many protocols have been successfully developed for purification of monoclonal antibodies from serum, tissue culture supernatants, and ascites fluids [5,6]. In many cases, specialized and proprietary buffer systems must be employed in order to increase the binding capacity of the affinity chromatography gel, because the affinity adsorption between ligand and target protein is affected by the type of salt, ionic strength, components of buffer, and pH of solution.

In this report, we describe the effects of different types of salt and pH values on the binding capacity of Avid AL gel, and the results of the binding behavior of the gel using supernatants of cell culture media supplemented with 20% serum.

2. Materials and methods

Avid AL gel was produced by UniSyn Technologies (Tustin, CA, USA). A commercial

* Corresponding author.

0021-9673/94/$07.00
SSDI 0021-9673(94)00732-2

recombinant Protein A (rProtein A) gel was provided by RepliGen (Cambridge, MA, USA). Solutions of purified human IgG containing a concentration of 12.5 mg/ml were purchased from The Binding Site (San Diego, CA, USA). Human serum was obtained from Sigma (St. Louis, MO, USA). Cell culture media (RPMI-1640) and fetal bovine serum (FBS) were obtained from Mediatech (Herndon, VA, USA) and Summit Biotechnology (Greeley, CO, USA), respectively. All other chemicals were of analytical grade.

2.1. Human IgG binding to Avid AL gel

Human IgG was bound to Avid AL gel by placing 18.0 μl of purified human IgG in 972.0 μl phosphate-buffered saline (PBS; 0.02 *M* phosphate, 0.14 *M* sodium chloride, pH 7.0) with 10.0 μl of Avid AL gel taken from a bulk of 20 ml which was washed first with regeneration buffer (20% methanol and 1% acetic acid in water, pH 3.4) and then with PBS for equilibration of the gel before using to bind IgG. The binding adsorption was run in a test tube overnight at 4°C with rotating on a Fisher hematology/chemistry mixer (Fisher Scientific, Pittsburgh, PA, USA). Unbound human IgG in solution, after binding was complete, was determined by using a radial immunodiffusion (RID) assay and a spectrophotometer at 750 nm with Dc protein assay (Bio-Rad, Hercules, CA, USA). The centrifuged supernatant of 5.0 μl was applied to a radial immunodiffusion plate (The Binding Site) following standard operating protocol. The binding capacity of Avid AL gel was determined by calculation of the corresponding amount of IgG for mass balance. The same was done with a rProtein A gel as a reference under the same conditions as used to determine the binding capacity of Avid AL gel.

2.2. pH dependence of human IgG binding

In order to evaluate the effect of buffer systems with different pH values on the binding capacity of Avid AL gel, five buffers were prepared including acetate buffer solution (0.1 *M*, pH 3.8, 4.5 and 5.5), PBS (pH 7.0, 8.0 and 8.5), carbonate buffer solution (0.1 *M*, pH 8.0), borate buffer solution (0.1 *M*, pH 8.0, 9.0 and 10.0), and Tris buffer solution (0.1 *M*, pH 8.0). Pre-equilibrated Avid AL gel (10.0 μl) was added to 972.0 μl of each buffer solution with 18.0 μl of purified human IgG. The binding of IgG to Avid AL gel was performed using the adsorption-equilibrium condition described above.

2.3. Chemical dependence of human IgG binding

Seven solutions, one for each of seven inorganic salts —NaCl, Na_2SO_4, $(NH_4)_2SO_4$, $MgCl_2$, NH_4CH_3COO, NH_4Cl and KCl— dissolved in PBS were prepared. Solution concentrations of 0.25, 0.50 and 0.75 *M* in each salt were prepared by diluting a 1.0 *M* solution of each salt. Since $MgCl_2$ has a solubility of less than 1.0 *M*, concentrations of 0.25, 0.50 and 0.75 *M* were used in the experiment. All of the solutions had a pH value of 7.0. Solutions of both NaN_3, where the concentration was changed from 0.0125 to 0.20% (v/v), and phenol red (from 2.5 to 20 mg/l) were used as factors to illustrate the effect of chemicals commonly used as a preservative and indicator of pH value in the cell culture, respectively, on the binding capacity of Avid AL gel. Conditions identical to those described above have been duplicated for all of the experiments.

2.4. Column configuration

Approximate 0.5 ml of Avid AL gel was packed into a 1.0-ml column. A Rainin (Woburn, MA, USA) peristaltic pump with an 8-channel head was used for buffer delivery. The column was washed with regeneration buffer until a baseline was obtained according to the absorbance, $A_{280\,nm}$, given by an LKB UV detector. The column was then pre-equilibrated with PBS. A sample of 1.35 ml of filtered human serum dissolved in 10.35 ml of binding buffer

was pumped through the column with a flow-rate of 0.25 ml/min, and 1.0-ml fractions were collected from the start of the loading step. The amount of fed human IgG was about 22 mg. Bound IgG was eluted using neutral elution buffer provided by UniSyn Technologies with a flow-rate of 1.0 ml/min. Protein output was measured and the absorbance of each fraction at 280 nm was used to estimate the protein concentration. Between runs the column was washed with regeneration buffer and PBS with minimal to no protein elution seen. Electrophoretic analyses were performed on 8–25% polyacrylamide gradient gels by using the Phast system from Pharmacia. The amount of purified IgG in fractions was confirmed using radial immunodiffusion.

3. Results and discussion

3.1. Salting-out effect in IgG purification with Avid AL

The effect of different types of salts on the binding capacity of Avid AL gel is summarized in Fig. 1. By adjusting the salt concentration to the same ionic strength in the assay (1.28 *M*), sodium sulfate, ammonium sulfate, ammonium acetate, ammonium chloride and sodium chloride gave an increase of the binding ability up to 44, 38, 33, 30 and 13%, respectively, as compared to potassium chloride. The same ionic strength (1.28 *M*) of buffer containing $MgCl_2$ showed a decreased binding capacity corresponding to 91.2% as compared to the same

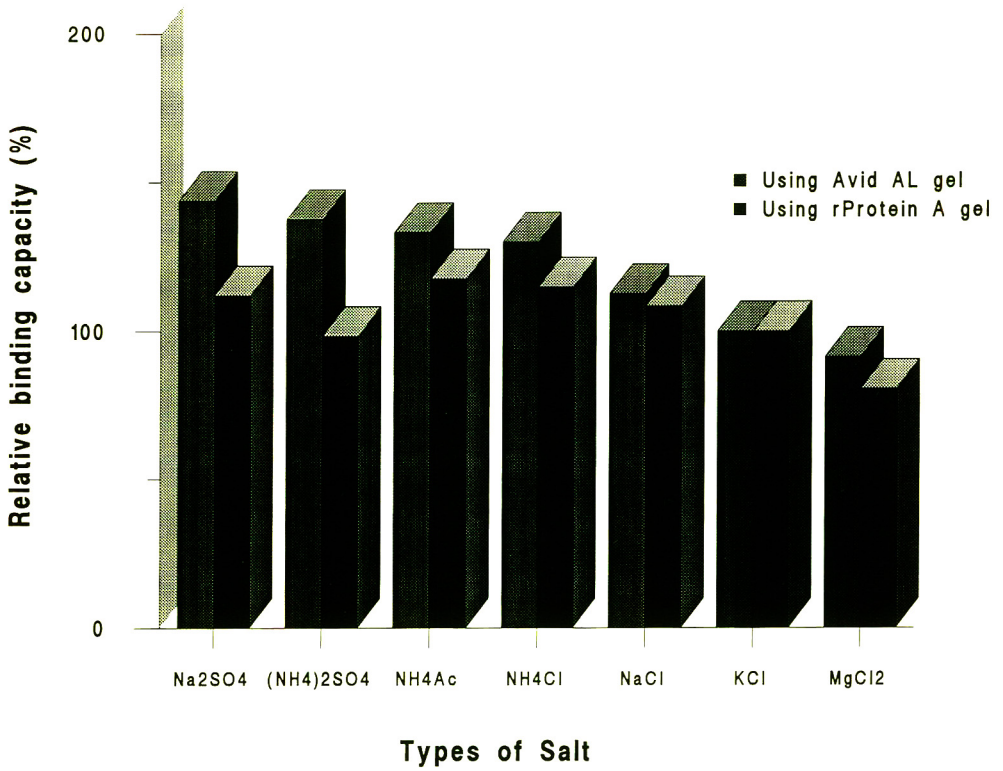

Fig. 1. Effect of various salts on purified human IgG binding to Avid AL and rProtein A gels. The binding capacity is shown as a relative value (percentage of the binding capacity obtained with KCl) and assayed at a total ionic strength of 1.28 *M* in buffer with pH of 7.0.

ionic strength of KCl. From the data, the salt effect on the binding capacity with respect to the various anions and cations can be deduced to be as follows: $SO_4^{2-} > CH_3COO^- > Cl^-$, and $NH_4^+ > Na^+ > K^+ > Mg^{2+}$. This represents the Hofmeister series of the salting out effect of ions (see [7]). For studies of the binding characteristics of Avid AL gel we used rProtein A gel as a reference. The results shown in Fig. 1 indicate that use of the salts, ammonium acetate, ammonium chloride, sodium sulfate and sodium chloride results in an increase of the binding ability to 18, 15, 12 and 8%, respectively, as compared to potassium chloride with the same ionic strength (1.28 *M*) in the buffer. However, for any given salt, no significant relationship has been observed between the binding capacity and the ionic strength for rProtein A gel.

Table 1 summarizes the effect of salt type and concentration on the partition coefficient, α, which is defined as the fraction of the total solute (purified human IgG) adsorbed at any instant because the affinity adsorption of purified human IgG to Avid AL gel represents a partitioning of solute between two phases, liquid and solid. We found that the binding capacity of Avid AL gel improves at higher ionic strengths of Na_2SO_4 and $(NH_4)_2SO_4$ with increasing α. By increasing the ionic strength from 0.75 to 3.0 *M*, a 1.8–2.2-fold increase in α was observed with Na_2SO_4 and $(NH_4)_2SO_4$. However, as expected for cations, only a weak effect on α was observed with increasing ionic strength from 0.25 to 1.0 *M* ($NH_4^+ > Na^+ > K^+ > Mg^{2+}$).

The parameters for the binding of purified human IgG to Avid AL gel, where the 9.4 to 27.5 mg IgG were added per ml gel, were determined using PBS containing different concentrations of Na_2SO_4 (from 0.25 to 1.00 *M*). The corresponding binding capacity is shown in Fig. 2. The apparent dissociation constant, K_a (mg/ml in solution), and the theoretical binding capacity of Avid AL gel, C_t (mg/ml gel), under the given experimental conditions are described by the equation:

$$1/P = C_t/(K_a P_b) - 1/K_a$$

where P is the IgG concentration in free solution at equilibrium with Avid AL gel and P_b is the IgG bound onto the Avid AL gel (mg/ml gel). Both K_a and C_t can be estimated from double reciprocal plots of the respective binding saturation curves and the values are summarized in Table 2. The dissociation constants for purified human IgG in PBS obtained under equilibrium conditions were 0.048, 0.022, 0.0058, 0.0052 and 0.0046 mg/ml, for Na_2SO_4 concentrations of 0, 0.25, 0.50, 0.75 and 1.00 *M*, respectively. It is apparent from Fig. 2 and Table 2 that the value of the dissociation constant estimated for purified human IgG binding to Avid AL gel decreased with increasing concentration of Na_2SO_4 in PBS (pH 7.0). The difference be-

Table 1
Salt effect on the partition coefficient of purified human IgG binding to Avid AL and rProtein A gels

Salt	α^a		α^b		α^c		α^d	
	Avid AL	rProtein A	Avid AL	rProtein A	Avid AL	rProtein	Avid AL	rProtein A
Na_2SO_4	0.45	0.49	0.63	0.47	0.76	1.00	0.83	0.97
$(NH_4)_2SO_4$	0.32	0.45	0.60	0.34	0.69	0.61	0.71	0.56
NH_4Ac	0.42	0.45	0.57	0.55	0.37	0.46	0.49	0.51
NH_4Cl	0.41	0.42	0.40	0.49	0.45	0.55	0.46	0.50
NaCl	0.40	0.48	0.45	0.51	0.41	0.47	0.40	0.47
KCl	0.40	0.42	0.39	0.46	0.36	0.38	0.36	0.43
$MgCl_2$	0.31	0.32	0.35	0.40	0.38	0.40	n.d.	n.d.

n.d. = Not determined.
[a–d] Tested at a salt concentration of 0.25, 0.50, 0.75 and 1.00 *M*, respectively.

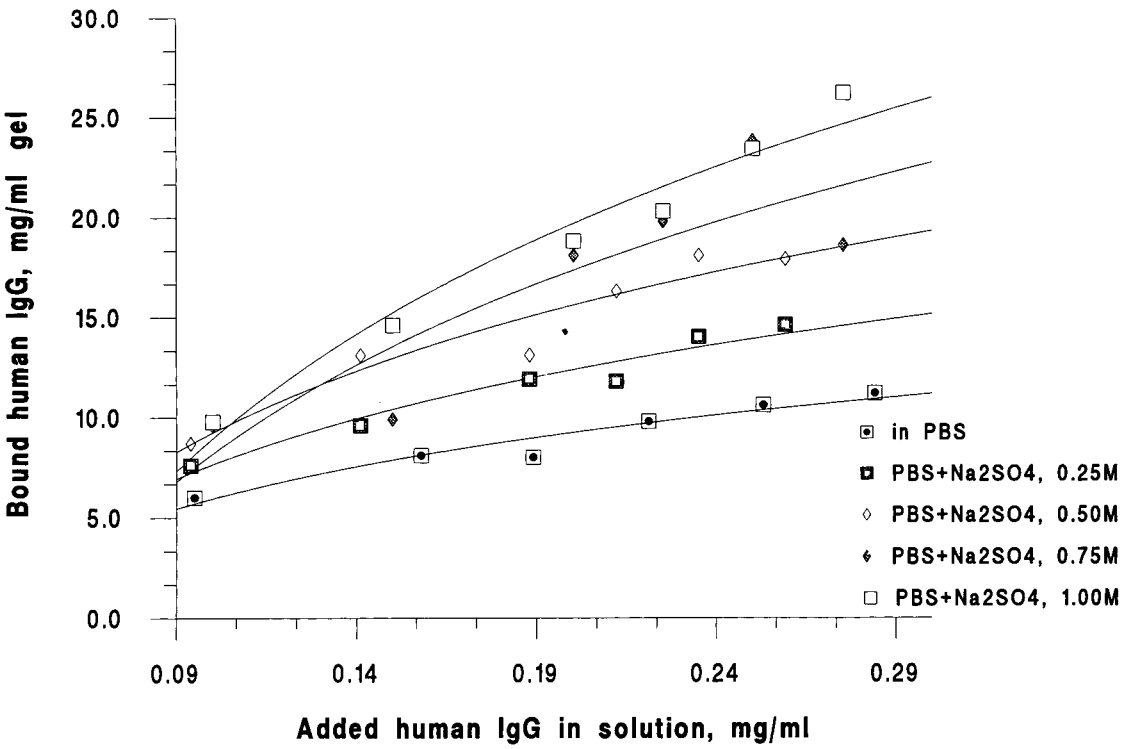

Fig. 2. Relationship between the concentration of purified human IgG and the amount of IgG bound in PBS containing different concentrations of Na_2SO_4 (the saturation curves).

tween K_a values for purified human IgG in PBS with no added Na_2SO_4 and in PBS plus 1.00 *M* of Na_2SO_4 was as much as ten-fold. The theoretical binding capacity of Avid AL gel for purified human IgG was 13.5 mg/ml gel in PBS, which is similar to the results reported by Ngo and Khatter [4], who used a packed Avid AL column (0.4 ml) and tested the binding capacity under equilibrium conditions.

The salting out effect of anions, such as sulfate, rather than the ionic strength is the major factor responsible for the observed increase in the binding capacity of Avid AL gel. It is assumed that this is made possible by a lowering of the dissociation constant for the affinity adsorption of purified human IgG onto the gel. This suggests that the high ionic strength causes aggregation by strengthening hydrophobic

Table 2
Binding parameters of Avid AL gel for purified human IgG in PBS containing different concentrations of Na_2SO_4

Na_2SO_4 concentration (*M*)	Dissociation constant K_a (mg/ml)	Binding ability C_t (mg/ml gel)
PBS	0.0480	13.5
PBS + Na_2SO_4, 0.25	0.0220	16.1
PBS + Na_2SO_4, 0.50	0.0058	22.7
PBS + Na_2SO_4, 0.75	0.0052	27.1
PBS + Na_2SO_4, 1.00	0.0046	29.9

interaction between proteins. Consequently, in the presence of sulfate the specific affinity of IgG for Avid AL may be improved by reducing the repulsion between IgG molecules. In general, the repulsion of bound IgG molecule on the gel prevents the affinity attraction of additional unbound IgG molecules to an available adjacent ligand. For rProtein A gel, the effect of salting out increases the hydrophobic attraction between rProtein A and IgG. Therefore, the opportunity for enhancing IgG binding to functional sites of rProtein A is realized.

These initial results were confirmed by performing column chromatography experiments. 0.5 ml of Avid AL gel was packed in a 1.0-ml column. The chromatograms shown in Fig. 3 are for such columns, wherein human serum was diluted by either PBS (regular binding buffer) or PBS containing 0.75 *M* of Na_2SO_4 as an improved binding buffer. The bound IgG, then, was eluted using neutral elution buffer with pH of 7.4. Between runs the column was washed with regeneration buffer and PBS with minimal to no protein elution seen. This operation yielded 8.0 mg and 14.6 mg bound IgG on the column, respectively. The binding capacity for Avid AL in the high salt buffer was calculated at 26.2 mg IgG/ml gel based on the amount of IgG eluted, which was 2.1-fold higher than those of the run using PBS as a binding buffer. A comparison of the characteristics for IgG purification using Avid AL gel has been listed in Table 3 for the two binding buffer systems. In both cases, the IgG was recovered at greater than 90% purity estimated by using the ratio of eluted IgG amount determined by RID to eluted protein amount determined by spectrophotometry at 280 nm. This result was confirmed by use of sodium dodecyl sulfate–polyacrylamide gel electrophoresis (8–25%) analysis, as shown in Fig. 4. In particular, albumin and possibly transferrin in human serum cannot be strongly adsorbed onto the Avid AL gel in presence of high salt buffer solution when the amount of IgG being isolated is more concentrated than other proteins in solution [1]. Therefore, non-specific adsorption, as a major source of contamination in IgG purification by Avid AL gel, has not been significantly observed when sodium sulfate was added to increase the ability to isolate IgG from human serum (see lane 8 in Fig. 4).

3.2. Effect of sodium azide on IgG–Avid AL binding

In contrast to the effect of salts studied on binding capacity, a significant decrease in the binding capacity of either Avid AL gel or rProtein A gel can result when sodium azide, commonly used as a bacteriostatic, is present in PBS as a binding buffer. But the proposed structure of the affinity ligand is consistent with its functioning as an electron acceptor. Therefore, it is possible that the sodium azide, as an electron donor, competes with IgG molecules for binding the affinity ligand and consequently displaces the IgG from the functional site. In this case, the relative binding capacity of Avid AL with increasing sodium azide from 0.0125 to 0.20% (v/v) showed a corresponding decrease of 97.2 to 70.8%, respectively, as compared to the binding capacity of Avid AL in PBS only (see Fig. 5). Under the same conditions, rProtein A gel exhibits a similar corresponding decrease of 94.5 to 52.0%, respectively, as compared to the binding capacity of rProtein A gel obtained in PBS.

3.3. Effect of phenol red on IgG–Avid AL binding

The same reason can be used to describe the decrease in the binding capacity of Avid AL gel when phenol red, which is usually used as a pH indicator in cell culture medium, is present in binding buffer (PBS). Fig. 6 shows the binding behavior of Avid AL gel and rProtein A gel for human IgG in PBS containing phenol red where the concentration was varied from 2.5 mg/ml to 20.0 mg/l. Defining the interaction between the ligand and IgG in PBS as 100%, a significant decline (to 50.9%) was observed for the binding capacity of Avid AL in the presence of 20.0 mg/l of phenol red in binding buffer. A similar decrease (to 78.7%) in binding capacity is observed

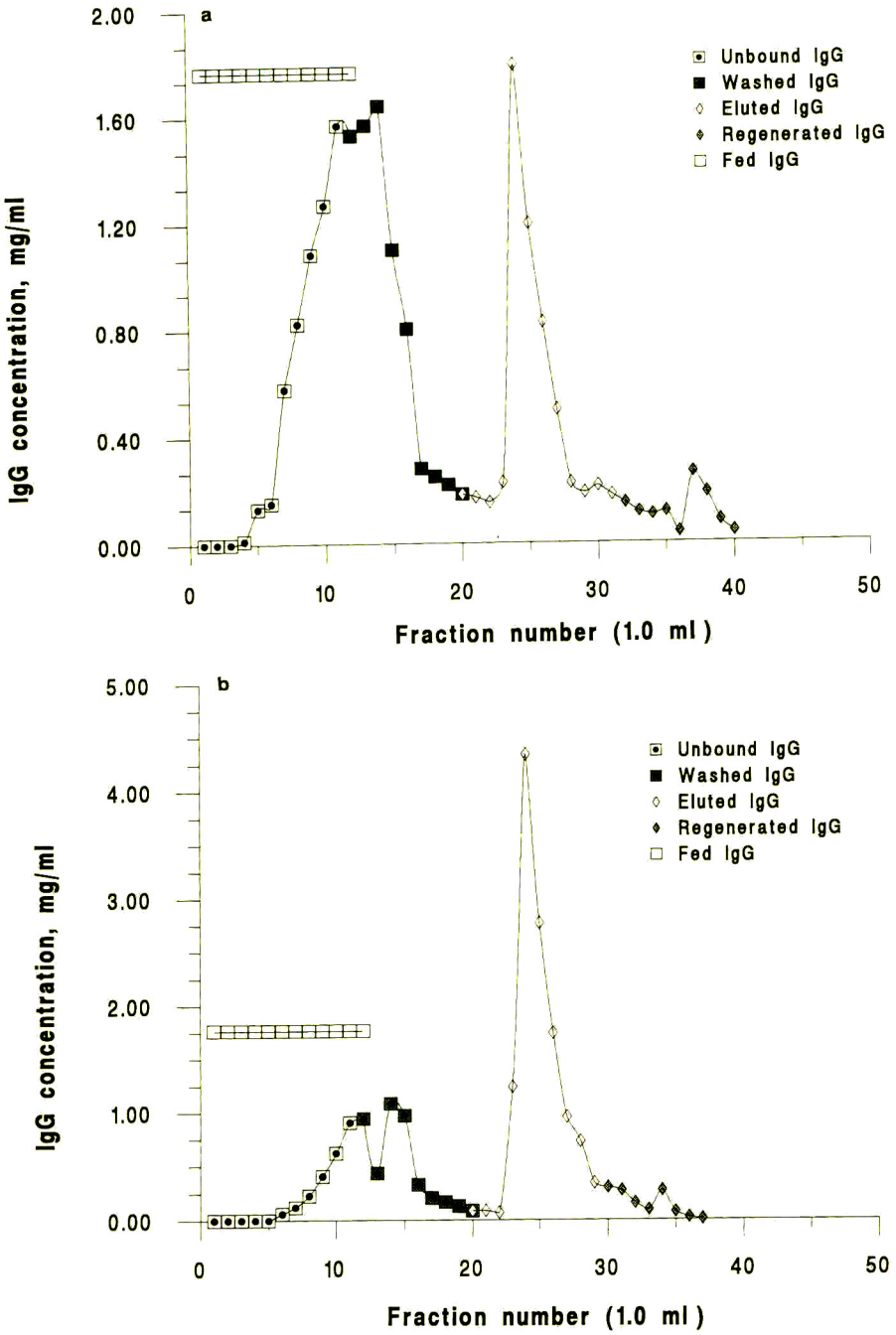

Fig. 3. (a) Isolation of IgG from human serum by Avid AL gel with PBS loading and washing conditions. (b) Isolation of IgG from human serum by Avid AL gel with PBS–0.75 *M* of sodium sulfate loading and washing conditions. For both of experiments, gel volume was 0.5 ml. Human serum was diluted 8.9-fold with binding buffer to make a IgG concentration of about 2 mg/ml in solution and applied at the flow-rate of 0.25 ml/min at room temperature. Fractions of 1.0 ml were collected. Elution was carried out with neutral elution buffer, pH 7.4.

Table 3
Comparison of properties of purifying IgG from human serum using Avid AL gel in two different binding buffer systems

Item	Experiment	
	1	2
Volume of column (ml)	0.5	0.5
Binding buffer	PBS	PBS + 0.75 *M* Na_2SO_4
Fed IgG (mg)	21.2	21.2
Bound IgG (mg)	8.0	14.6
Eluted IgG (mg)	6.2	13.1
Regenerated IgG (mg)	1.0	0.9
Recovery yield (%): IgG bound/IgG eluted	77.5	89.7
Binding capacity (mg/ml gel): IgG eluted/volume of column	12.4	26.2

Each IgG amount shown was calculated based on the data determined by RID.

for the rProtein A gel in the presence of 20.0 mg/l of phenol red in PBS.

Addition of FBS to the binding buffer results in an even more pronounced decrease in the binding capacity of Avid AL for human IgG. With respect to the affinity adsorption in PBS at pH 7.0, the use of PBS containing 20% FBS resulted in a decrease of the binding capacity of Avid AL to 42.5%. The determined binding capacities of Avid AL gel and rProtein A gel have been listed in Table 4. Use of the cell-culture medium, RPMI, in place of PBS appears to result in little or no significant change in the IgG binding capacity of Avid AL gel or rProtein A gel. At a concentration of 20% FBS in either PBS or RPMI, the binding capacity of Avid AL decreased to 42.5 and 46.2%, respectively (see Table 4). However, no significant influence on the binding capacity of rProtein A gel was observed under the same conditions. On the other hand, as can be seen in Table 4, increasing the concentration of Na_2SO_4 in this system decreases the amount of affinity adsorption on Avid AL gel. In contrast, rProtein A gel showed an increase in IgG binding capacity with the increase in Na_2SO_4 concentration. In order to avoid disturbance by undesired proteins during purification of the target protein, dilution of undesired proteins, such as those in FBS, in solution may be necessary before using this affinity gel. It is commonly understood that high concentration of undesired proteins can lower the affinity adsorption between target protein and affinity ligand.

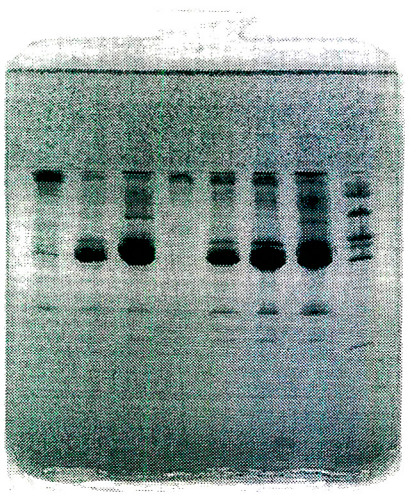

Fig. 4. Sodium dodecyl sulfate gradient (8–25%)–polyacrylamide gel electrophoresis in non-reducing conditions of fractions obtained from human serum in Fig. 3. Lanes: 1 = Molecular mass marker reference proteins; 2 = unfractionated human serum; 3, 6 = unbound, flow-through fractions; 4, 7 = unbound, after column wash; 5, 8 = fractions eluted with neutral elution buffer, pH 7.4. Lanes 3–5 are corresponding to Fig. 3a, lanes 6–8 to Fig. 3b.

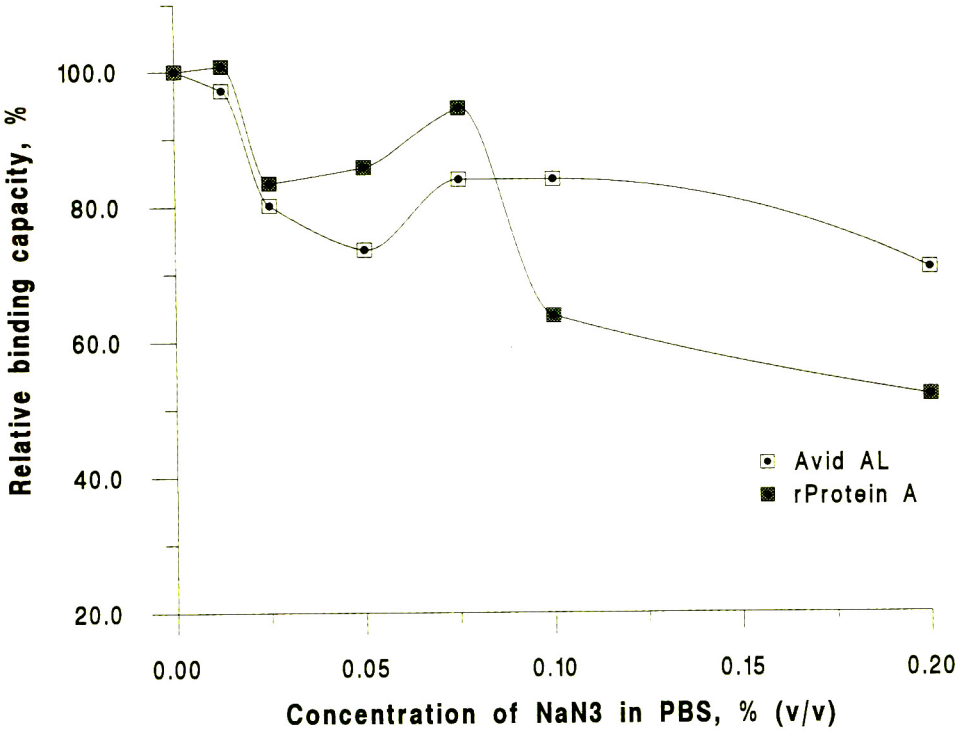

Fig. 5. Effect of NaN_3 in PBS on the binding capacity of Avid AL and rProtein A gels. The binding capacity is shown as a relative value corresponding to that obtained in PBS without NaN_3.

3.4. Effect of pH on IgG–Avid AL binding

Previous studies indicated that Avid AL was chemically stable to acid and base treatments. For further characterization of Avid AL, a wide range of buffers with different pH values has been used to evaluate the binding capacity. Five buffers ranging in pH from 3.8 to 10.0 were tested to determine the effect of pH on IgG binding to this gel. Fig. 7 shows the binding capacity of each gel at each pH relative to the binding capacity in PBS at pH 7.0. Obviously, Avid AL continues to work well for binding IgG, when pH of the binding buffer has an acidic value. Using other buffers with pH higher than 7.0, less binding of purified human IgG to Avid AL relative to rProtein A gel was observed. Unfortunately, at pH 3.8, neither Avid AL nor rProtein A gels can adsorb any measurable quantity of IgG. From the data shown in Fig. 7, it has been realized that in the range of pH 7.0–8.5, the Avid AL gel has similar binding ability in PBS, carbonate or borate buffers. However, use of primary amine buffering system, such as Tris buffer, allows the primary amine to compete with the IgG for binding to either Avid AL or rProtein A gel. Therefore, decreased binding capacities of both gels have been obtained.

4. Conclusions

In general, the affinity chromatographic gel Avid AL displays a significant increase in binding capacity for human immunoglobulin with increasing concentration of Na_2SO_4. Approximately 13.1 mg of human IgG has been recovered from a column with packed 0.5 ml of Avid AL gel. This binding capacity of 26.2 mg/

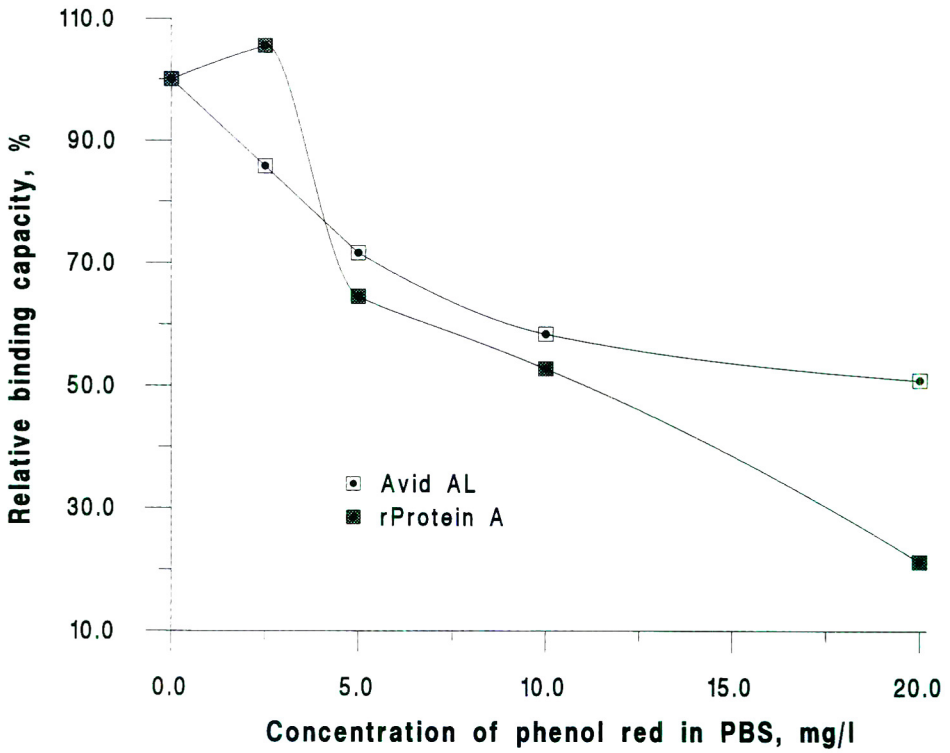

Fig. 6. Effect of phenol red in PBS on the binding capacity of Avid AL and rProtein A gels. The binding capacity is shown as a relative value corresponding to that obtained in PBS without phenol red.

Table 4
Effect of cell culture medium supplemented 20% FBS with and without Na_2SO_4 on the binding capacities of both Avid AL and rProtein A gels in batch assay at pH of 7.0

Binding buffer	Avid AL[a] (%)	rProtein A[a] (%)
PBS	100	100
RPMI	97.2	90.6
PBS + 20% FBS	42.5	90.6
RPMI + 20% FBS	46.2	86.6
RPMI + 20% FBS + 0.25 *M* Na_2SO_4	49.1	70.9
RPMI + 20% FBS + 0.50 *M* Na_2SO_4	45.3	89.8
RPMI + 20% FBS + 0.75 *M* Na_2SO_4	41.5	93.7
RPMI + 20% FBS + 1.00 *M* Na_2SO_4	36.8	131.5

[a] The binding capacity is shown as a relative value (percentage of the binding capacity obtained in PBS).

ml gel is far superior to the binding capacities reported previously [3]. It is important to note that binding buffer containing sodium azide will harshly decrease the affinity adsorption of IgG to Avid AL. In addition, diluting the tissue culture supernatants supplemented 20% FBS is necessary to reduce either the concentration of other mixed proteins or the percentage of phenol red presented for successful IgG purification using Avid AL affinity adsorption chromatography. Considering the above results in the presence of 20% FBS supplemented in tissue culture supernatants, rProtein A gel appears to be the most suitable material for human IgG purification without significant decrease in binding capacity. As a synthetic ligand, Avid AL maintains functional activity in acidic conditions in which rProtein A gel can lose its affinity binding capacities, even through with elevating pH over 7.0 rProtein A gel appears to be preferable in binding capaci-

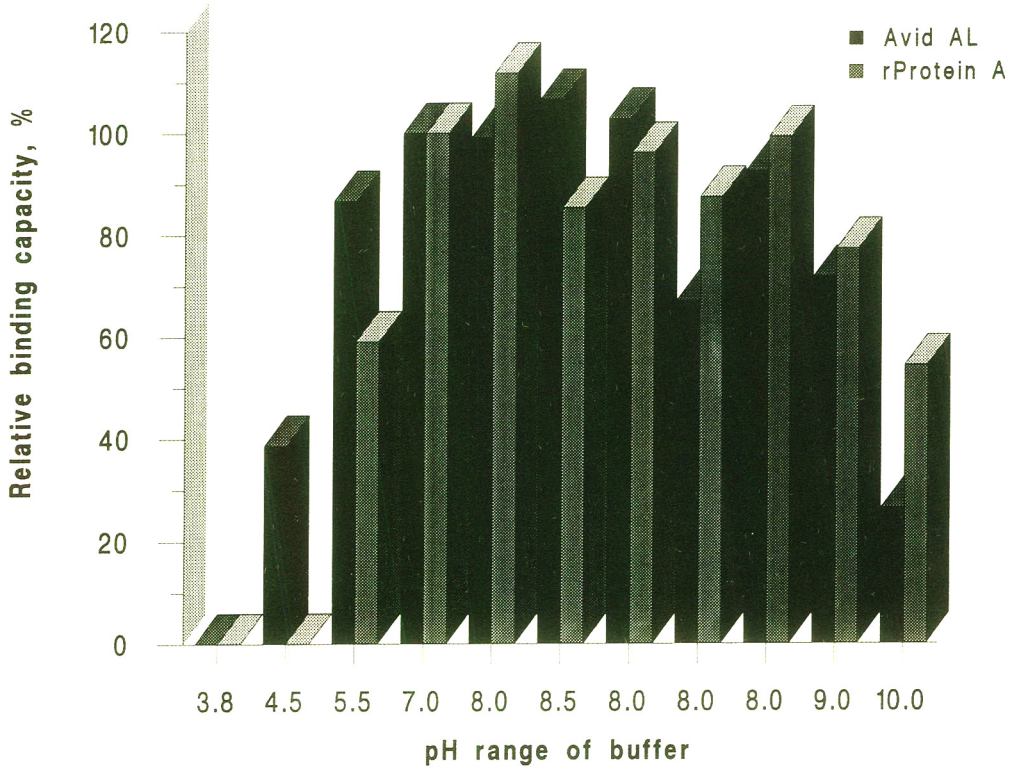

Fig. 7. Effect of pH on binding capacity of Avid AL and rProtein A gels. The relative binding capacity is shown corresponding to that obtained in PBS, pH 7.0. pH 3.8 = sodium acetate; pH 4.5 = sodium acetate; pH 5.5 = sodium acetate; pH 7.0 = PBS; pH 8.0 = PBS; pH 8.5 = PBS; pH 8.0 = sodium carbonate, Tris and sodium borate (from left to right); pH 9.0 = sodium borate; pH 10.0 = sodium borate.

ty relative to that observed with Avid AL gel. This unique ability to efficiently bind immunoglobulins at low pH may be exploited in GMP purification protocols. Therefore, the combination between virus inactivation and the column loading step, to reduce overall processing time, will be investigated in future studies.

Acknowledgements

We thank Drs. David Lowrey, Gerry Wuenschell and Chinh Tran for their valuable help and advice. We also are indebted to Anna Nguyen for her technical assistance.

References

[1] T.T. Ngo and N. Khatter, *J. Chromatogr.*, 510 (1990) 281–291.
[2] D. Narinesingh, A. Pope, N. Khatter and T.T. Ngo, *Anal. Lett.*, 24 (1991) 2005–2015.
[3] N. Khatter, R.S. Matson and T.T. Ngo, *Am. Lab.*, 23(8) (1991) 32LL–RR.
[4] T.T. Ngo and N. Khatter, *J. Chromatogr.*, 597 (1992) 101–109.
[5] T.T. Ngo and N. Khatter, *Appl. Biochem. Biotechnol.*, 30 (1991) 111–119.
[6] J. Rosenberg, R.V. Sluis and T.T. Ngo, *Am. Biotech. Lab.*, May (1993) 82.
[7] R. Scopes, in C.R. Cantor (Editor), *Protein Purification, Principles and Practice*, Springer, New York, 1984, pp. 47–50.

ELSEVIER

Journal of Chromatography A, 686 (1994) 73–83

JOURNAL OF CHROMATOGRAPHY A

Purification of synthetic peptides with the aid of reversible chromatographic probes☆

H.L. Ball, G. Bertolini, S. Levi, P. Mascagni*

Italfarmaco Research Centre, Via dei Lavoratori 54, 20092 Cinisello Balsamo, Milan, Italy

First received 2 March 1994; revised manuscript received 20 July 1994

Abstract

The application of reversible chromatographic probes for the purification of synthetic peptides by reversed-phase (RP) and affinity chromatography is described. In previous work the concept of a one-step purification procedure based on the acid-stable fluorenylmethoxycarbonyl (Fmoc) group was considered. Similar probes were used to purify peptides from 17 to 104 residues in length, using ion-exchange and RP media. The RP probes described here represent simplified versions of those reported previously. Further, the application of a new probe containing biotin, for affinity chromatography, is demonstrated. Stepwise solid-phase peptide synthesis was performed using both Boc and Fmoc chemistries and N-(2-chlorobenzyloxycarbonyloxy)succinimide as a capping reagent. The chromatographic probes were incorporated on to the "target" peptide as active succinimidyl carbonate derivatives. After cleavage using either hydrogen fluoride or trifluoroacetic acid, purification was performed on either RP media or immobilized avidin. Treatment with organic base yielded the free purified product. The efficiency of the new probe molecules and the capping procedure was demonstrated by the purification of two polypeptides, 46 and 101 residues in length.

1. Introduction

Stepwise solid-phase peptide synthesis (SPPS), first introduced by Merrifield [1], suffers inherently from the accumulation of impurities at each step in chain assembly, due to the premature termination of the peptide chain (truncated sequences) and incomplete acylation of the free amino groups, which can then react with the next or subsequent residues [2]. The latter generates a family of deletion peptides that lack one or more amino acids.

In general, conventional chromatographic techniques have sufficient resolving power, when used singularly or in combination, to separate the target peptide (up to 40 residues in length) from contaminating deletion and truncated impurities. However, as the length of peptide sequence increases, the chromatographic differences between the desired product and its closely related impurities become less resolvable. Hence, in order to obtain a homogeneous product, several purification steps are required using techniques that separate material on the basis of diverse physical properties (e.g., lipophilicity, charge or molecular mass). The disadvantage,

* Corresponding author.

☆ Presented at the *13th International Symposium on HPLC of Proteins, Peptides and Polynucleotides, San Francisco, CA, 30 November–3 December, 1993.*

0021-9673/94/$07.00
SSDI 0021-9673(94)00709-8

apart from the expertise required in the use of different techniques, is the consequent loss of material at each purification step and the additional time involved.

We have developed a reversible purification system that is based on the capping of unreacted amino groups and the addition of a chromatographic probe molecule, bearing either lipophilic or charged groups, to the N-terminus of the target peptide [3–5]. The derivatized peptides, up to 104 residues in length, had all been synthesized using the Boc strategy and were readily separated from underivatized impurities.

Derivatization of the target peptide with a group with specific and predefined chromatographic properties has been investigated previously. Several methods have been suggested that involve the reversible chemical modification of peptides in an attempt to facilitate purification; however, their application to polypeptide chains has not been described [6]. More recently, several other molecules have been described for the purification of peptides up to 85 residues in length [7], including a biotinylated probe [8]. The latter was used to purify a 67-residue peptide that had been synthesized with acetic anhydride as capping agent. It has been suggested that repeated exposure to acetic anhydride is detrimental to the growing peptide chain, causing side-reactions [9]. This observation becomes particularly important as the length of the peptide increases.

In previous publications we demonstrated the concept of reversible chromatographic probes for reversed-phase (RP) and ion-exchange purification [3–5]. In this work, new RP probes, {4-[(4-cyclohexylbutyryl)aminomethyl]fluoren-9-yl}methyl (**1**) and [4-(dodecylaminocarbonyl) fluoren-9-yl]methyl (**2**) succinimidyl carbonates, that were simpler to prepare, were used. Further, the purification method has been extended to a new class of molecules containing biotin, i.e., {4-[(biotinylglycylglycyl)aminomethyl]fluoren-9-yl}methyl succinimidyl carbonate (**3**) for affinity chromatography, as illustrated in Fig. 1. In addition we also show the validity of the method for the purification of peptides that were synthesized using fluorenylmethoxycarbonyl (Fmoc) chemistry. Two polypeptides, 46 and 101 residues in length, were chemically synthesized using Fmoc and Boc strategies, respectively.

2. Experimental

2.1. Chemicals and reagents

All Boc and Fmoc amino acid derivatives, together with the capping reagent N-(2-chlorobenzyloxycarbonyloxy)succinimide, were supplied by Novabiochem. Solvents for peptide synthesis were obtained from Applied Biosystems. Deprotection and cleavage of Boc-synthesized peptides was performed using anhydrous hydrogen fluoride (HF) from Matheson and an all-Kel-F apparatus (Peptide Institute, Osaka, Japan) Deionized water was prepared with a Milli-Q purification system (Millipore–Waters) and acetonitrile (HPLC grade) was obtained from Merck.

2.2. Peptide synthesis

Boc-synthesized peptides

The peptides were synthesized on PAM–copoly(styrene–divinylbenzene) resin [PAM = 4-(carboxyamidomethyl)benzyl ester], prederivatized with the first amino acid, using an automated Applied Biosystems Model 430A peptide synthesizer and optimized chemical protocols [10] on a 0.5-mmol scale. Dicyclohexylcarbodiimide (DCC) or DCC–hydroxybenzotriazole (HOBt) in the case of Asn, Gln and Arg amino acids were used as activating reagents. When the synthesis was performed without the additional capping step, double coupling cycles were performed, whereas for capped peptides single coupling was used. One millimole of the capping agent, N-(2-chlorobenzyloxycarbonyloxy)succinimide, was loaded into cartridges. The ABI software was modified so that, when required, the capping reagent would be dissolved automatically in N-methylpyrrolidone (NMP)–dichloromethane (DCM) (3:1), together with 1

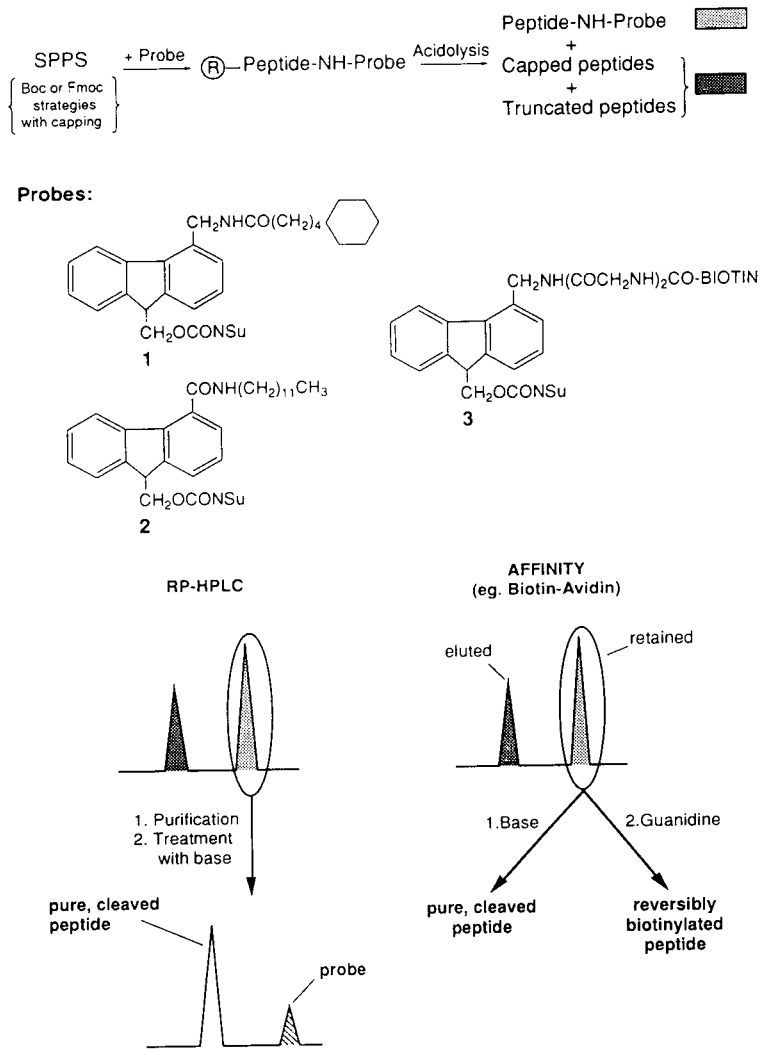

Fig. 1. General scheme showing application of chromatographic probes **1**, **2** and **3**.

ml of 2 *M* diisopropylethylamine (DIEA) in NMP, transferred to the reaction vessel via the concentrator and then vortex mixed for 5 min. The capping agent was then washed from the peptidyl-resin with DCM. At the end of the synthesis the N-terminal protecting group was removed using trifluoroacetic acid (TFA)–DCM (50:50) for 30 min. After neutralization with 5% DIEA in DCM, the chromatographic probes were introduced as described below.

Deprotection of the peptide and its cleavage from the resin were achieved using a low trifluoromethylsulphonic acid (TFMSA)–high HF procedure [10]. The dried peptidyl-resin was first treated with TFMSA–1,4-butanedithiol–*p*-cresol–dimethyl sulphide–TFA (5:1:4:15:25) at 0°C for 2 h, followed by the high-HF procedure, HF–1,4-butanedithiol–*p*-cresol (20:1:1). The crude peptide was precipitated with cold dry diethyl ether and then dissolved in 20% acetic acid solution. The peptide solution was then lyophilized to yield the crude dry peptide.

Fmoc-synthesized peptides

A 0.25-mmol amount of Fmoc–Ser(tBu)–Sasrin resin (substitution value 0.69 mmol/g) was used. Single coupling cycles were performed with capping, as described for the Boc-synthesized peptides, except that 2-(1*H*-benzotriazol-1-yl)-1,1,3,3-tetramethyluronium hexafluorophosphate (HBTU) was used as activating agent. Incorporation of the chromatographic probes in the N-terminally deprotected peptidyl-resin were performed as described below.

Removal of the side-chain protecting groups and cleavage of the peptide from the resin were achieved with 95% TFA containing ethanedithiol–thioanisole (1:2) for 90 min at room temperature. The crude cleavage mixture was filtered and then precipitated with cold diethyl ether. The precipitate was isolated by centrifugation (1132 *g* for 3 min), washed with further diethyl ether, then dissolved in 20% acetic acid solution before being lyophilized to give the crude dry product.

Synthesis of chromatographic probes

The lipophilic (**1** and **2**) and biotinylated (**3**) probes were synthesized from the central 9-(hydroxymethyl)fluorene-4-carboxylic acid molecule, using essentially the same method as described earlier [5]. The results of the improved synthesis will be described elsewhere.

Attachment of chromatographic probes

The freshly deprotected peptidyl-resin was allowed to swell in DCM, then 2 equiv. of the chromatographic probe were dissolved in sufficient trifluoroethanol (TFE)–DCM (1:3) to give a concentration of approximately 0.2 *M* and subsequently transferred to the peptidyl-resin. The mixture was vortex mixed in a micro-reaction vessel for 90 min. The coupling efficiency was determined using quantitative ninhydrin analysis [11]. If the reaction had not gone to completion, the reaction was continued for a further 90 min. The peptidyl-resin was then washed with DCM and dried under vacuum in preparation for cleavage.

2.3. Purification

Preparative isoelectric focusing

Purification of synthetic protein was performed in a Rotofor (Bio-Rad) preparative isoelectric focusing cell under denaturing conditions (i.e., 8 *M* urea). The Rotofor cell was loaded with 30 ml of 8 *M* urea containing 2% ampholytes (p*I* range 3–9). Separation was performed at 15°C until each component had focused at its appropriate pH (usually 2–3 h). The contents of each of the twenty cells were harvested and analysed both for protein content, as determined by analytical RP-HPLC, and pH. Cells containing material with similar retention times were then combined and re-fractionated using a narrower pH range. Following analysis, the cells containing the most homogeneous material were combined. A final purification step, which also desalted the protein, was then performed on RP media.

High-performance liquid chromatography

Analytical and semi-preparative RP-HPLC was achieved using a Shimadzu LC10 system, equipped with a dual-wavelength detector. Peptides were analysed on Vydac C_4 and C_{18} columns (150 × 4.6 mm I.D.). Separations were achieved using linear gradients from 0 to 100% B in 30 min at a flow-rate of 1 ml/min. Solvent A was water–0.045% TFA and solvent B was acetonitrile–0.036% TFA. Detection was effected at 220 and 301 nm (to measure the absorbance due to the fluorene ring). Semi-preparative separations were conducted on either Vydac C_4 or C_{18} columns (250 × 10 mm I.D.) at a flow-rate of 3 ml/min.

Affinity chromatography

Immobilized avidin (Pierce) was loaded into a 5-ml disposable polypropylene column and equilibrated with sodium acetate buffer (pH 4). The crude HF cleavage product was dissolved in 10% acetic acid, filtered and the pH was adjusted to 4 using 0.1 *M* NaOH. The peptide solution was then incubated with the immobilized avidin for 30 min with occasional mixing. A portion of supernatant was removed and ana-

lysed by RP-HPLC to determine whether all the biotinylated protein had been bound. If derivatized material was still present in the solution, the incubation was continued for a further 30 min. The resin was washed with sodium acetate buffer and then water. A 5% aqueous solution of triethylamine (TEA) was then added and left for 15 min, which removed the peptide from the biotinylated probe–avidin complex. The solution was collected and neutralized with 10% acetic acid and the purified free protein was desalted on a Brown–Lee C_4 RP column (30 × 4.6 mm I.D.) and finally lyophilized.

Size-exclusion chromatography

Size-exclusion chromatography was performed on an FPLC (Pharmacia) instrument using a Sephadex 75 column (300 × 10 mm I.D.). The eluting buffer was Dulbecco's phosphate-buffered saline (PBS) containing Ca/Mg ions at pH 7.2. The flow-rate was 0.5 ml/min and the eluting proteins were detected at 220 nm.

2.4. Analysis

The purified Fmoc-derivatized and free peptides were analysed by amino acid analysis and electrospray mass spectrometry (ESI-MS). A Beckman System Gold system was used to determine the amino acid content of the samples. Peptidic material was hydrolysed in 1 ml of hydrochloric acid–propionic acid (1:1) at 110°C for 21 h. The hydrolysed samples were reduced under vacuum and then dissolved in buffer containing β-alanine as internal standard.

ESI-MS was performed on a Finnigan MAT (San Jose, CA) Model 700 instrument.

3. Results and discussion

3.1. Synthesis of the 46-residue cytoplasmic domain (β2-subunit) of CD18 using Fmoc chemistry

As the peptides chosen to demonstrate the application of the probe molecules had been synthesized using the Boc chemical procedure [3–5], it was now necessary to investigate the procedure for the purification of Fmoc-synthesized peptides. Further, the introduction of an efficient capping procedure that did not cause side-reactions was required in order to optimize the purification method. The peptide chosen was a 46-residue sequence from the cytoplasmic domain of CD18 (hereafter referred to as β2-subunit) [12], which was synthesized using single coupling cycles, with HBTU–HOBt as activating agents. For the capping procedure it was decided to use N-(2-chlorobenzyloxycarbonyloxy)succinimide for two reasons: (i) it is a solid that can be dissolved immediately prior to use, thus avoiding problems associated with instability, and (ii) the by-products are not as potentially harmful as those generated by acetic anhydride (i.e., acetic acid). To perform the capping procedure in an automated fashion on the ABI 430A, two cartridges were prepared for each residue in the sequence, one containing the amino acid and the other 1 mmol of the capping agent, N-(2-chlorobenzyloxycarbonyloxy)succinimide. While the activated amino acid was being coupled to the peptidyl-resin, the second cartridge containing the capping agent was dissolved in NMP–DCM with 1 ml of 2 *M* DIEA in NMP. On completion of the coupling cycle, the capping agent was transferred to the reaction vessel via the instrument concentrator column to terminate any free amino groups. A 5-min reaction was found to be sufficient for an effective capping procedure. A more detailed description of the capping procedure will be discussed elsewhere. At the end of the synthesis the peptidyl-resin was deprotected with 20% piperidine in NMP in preparation for the introduction of the chromatographic probes.

3.2. RP-HPLC purification of the 46-residue β2-subunit of CD18

Two different lipophilic probes, **1** and **2**, were attached, as the active carbonate derivatives, to the 46-residue peptidyl-resin. A 2-equiv. amount of the activated probes was dissolved in DCM–TFE (3:1) and added to the freshly deprotected peptidyl-resin. The incorporation of the probe was monitored by quantitative ninhydrin analysis

[11] and was found to be complete after 90 min. The derivatized peptide was then cleaved from the resin support using 95% TFA. The effectiveness of the combination of this capping procedure and the separation achieved between underivatized and derivatized peptides was then examined.

The crude cleavage products for the peptides derivatized with probes **1** and **2** gave the chromatograms shown in Fig. 2A and C, respectively. The profiles of the two chromatograms were essentially identical in that two main groups of peaks were obtained, an earlier eluting group of low-intensity peaks (labelled 1) and a later eluting material (labelled 2) representing the major component of the crude product. The latter peak was collected for both probes, lyophilized and analysed for amino acid content (data not shown) and by ESI-MS [β2-subunit adduct + probe **1** (expected, 5887; found, 5887) and β2-subunit adduct + probe **2** (expected, 5917; found, 5917)]. The results indicated that the correct products had been isolated. A slight shoulder on the right of peak 2 (Fig. 2A and C) was isolated and shown, by ESI-MS, to be 57 u higher than the molecular ion, which would correspond to the partial deprotection of a butyl group.

To obtain the free peptide, it was then necessary to treat the Fmoc-derivatized material with 5% aqueous TEA for 15 min. Interestingly, the type of Fmoc probe used had a significant effect on the rate of β-elimination. Where the substituent at position 4 on the fluorene ring was

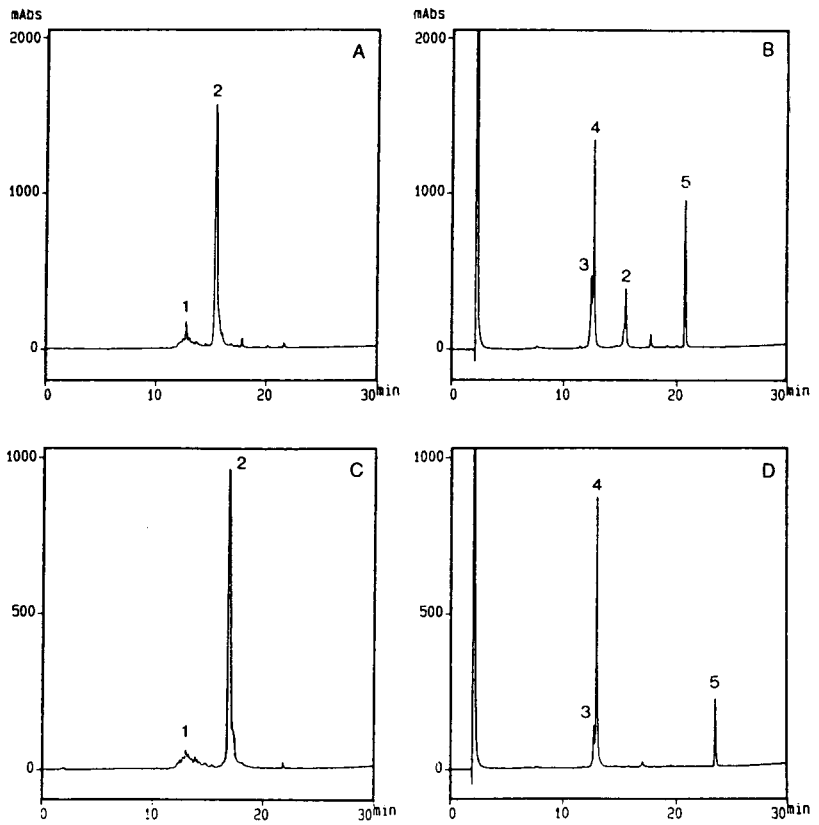

Fig. 2. Analytical RP-HPLC on a Vydac C_4 column (150 × 4.6 mm I.D.) connected to a Shimadzu LC10 LC system. Solvent A, water–0.045% TFA; solvent B, acetonitrile–0.036% TFA; gradient, 0–100% B in 30 min; flow-rate, 1 ml/min; detection, 220 nm. (A) Crude β2-subunit adduct + **1**; (B) purified β2-subunit adduct + **1**; (C) crude β2-subunit adduct + **2**; (D) purified β2-subunit adduct + **2**.

alkyl, as in probe **1**, a large proportion of derivatized peptide still remained after 15 min (labelled 2, Fig. 2B). A further 30 min were required for complete cleavage of the probe. However, in the case of handle **2**, where the fluorene ring is substituted with an electron-withdrawing moiety (i.e. carboxyl group) at position 4, the urethane group was more sensitive to base and quantitative cleavage of the handle from the peptide was achieved in 15 min. RP-HPLC analysis of the cleaved peptides (labelled 4, Fig. 2B and D) showed the β2-subunit (labelled 4) to be highly homogeneous, which, following isolation, was confirmed by amino acid analysis (data not shown) and ESI-MS (expected, 5483; found, 5483). The earlier eluting peak labelled 3 (Fig. 2B and D) was also collected and found to be the correct sequence with Met in its oxidized form (ESI-MS: found, 5499). The peak labelled 5, which had strong absorbance at 301 nm, due to the presence of the fluorene ring, was the cleaved by-product of the chromatographic probe. The overall yield of the β2-subunit following RP purification and desalting was 33% using probe **1** and 36% for lipophilic probe **2**.

3.3. *Synthesis of 101-residue heat shock protein from* Rattus norvegicus

Previously, the derivatization of the 104-residue HIV-1 p24gag fragment 270–373 with a lipophilic probe resulted in a separation of 7 min, on RP media, between underivatized and derivatized polypeptides [5]. As the chemical synthesis did not involve a capping step, the chromatographic probe was attached to both the target peptide and deletion sequences. Therefore, based on the success of the capping agent, N-(2-chlorobenzyloxycarbonyloxy)succinimide, when applied to the Fmoc strategy, its application to Boc chemistry was investigated. The 2-chlorobenzyloxycarbonyloxy group is stable to treatment with TFA and therefore remains attached to the truncated peptides, even after cleavage of the peptide from the resin, in the case of Fmoc-synthesized peptides. However, as the difference in hydrophobicity between capped and uncapped material is reduced, the ability to cleave the terminating group during HF treatment further benefits its application in peptides synthesized by the Boc strategy, particularly in the case of large peptides.

The M_r 10 000 heat shock protein from *R. norvegicus* (hereafter referred to as rat Hsp10) [13] was synthesized in 3 days, using the single delivery of activated amino acid, followed by the transfer of a freshly prepared solution of capping reagent, as described above. At the end of the synthesis the peptidyl-resin was N-terminally deprotected and a portion was treated with the hydrophobic probe **2**. Cleavage of the resins was achieved using the low TFMSA–high HF protocol.

3.4. *RP-HPLC purification of 101-residue rat Hsp10*

The crude underivatized (Fig. 3A) and derivatized (Fig. 3B) polypeptides were injected on to an analytical RP column. In the latter chromatogram two main products eluted. The early-eluting peak (labelled 1, Fig. 3B) was collected and shown by ESI-MS to be a large terminated peptide caused by the incomplete coupling (greater than 50%) of Gln^{60} to Pro^{61} (found, 4574). As Gln^{60} was coupled to Pro, a secondary amine, the problem was not detected by quantitative ninhydrin analysis [11], which was used to follow the amino acid coupling efficiency, thus further enhancing the relevance of the strategy for the synthesis of the protein. The later eluting peak (labelled 2, Fig. 3B) absorbed strongly at 301 nm, which suggested it to be the polypeptide derivatized with **2**. Further, the disappearance of peak 2 (Fig. 3A) also supported the conclusion that the later eluting peak was derivatized rat Hsp10. The latter was collected, re-injected on RP media (Fig. 3C) and then treated with 5% aqueous TEA to release the free polypeptide. After desalting on an RP column to remove the base and the cleaved chromatographic probe, the purified rat Hsp10 polypeptide (labelled 1, Fig. 3D) was analysed by ESI-MS (Fig. 4A), which showed that the correct material had been obtained (expected, 10 770; found, 10 772). The overall yield for the one-step purification pro-

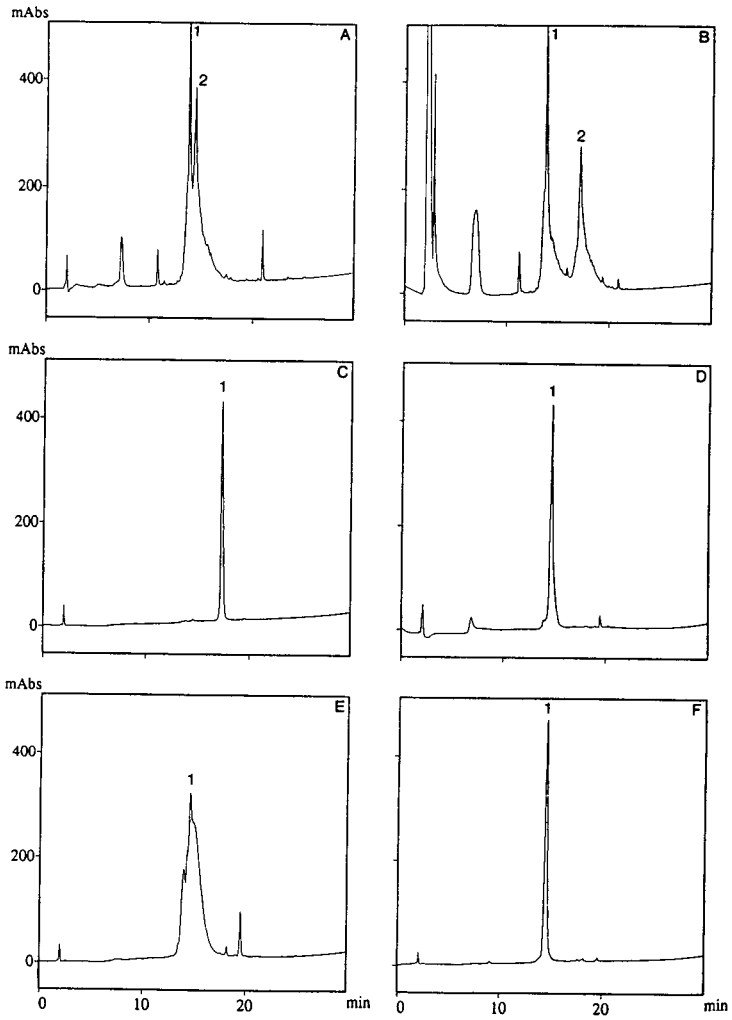

Fig. 3. Analytical RP-HPLC on a Vydac C_4 column (150 × 4.6 mm I.D.) connected to a Shimadzu LC10 LC system. Solvent A, water–0.045% TFA; solvent B, acetonitrile–0.036% TFA; gradient, 0–100% B in 30 min; flow-rate, 1 ml/min; detection, 220 nm. (A) Crude rat Hsp 10 without probe **2** attached; (B) crude rat Hsp10 derivatized with probe **2**; (C) purified rat Hsp10 derivatized with probe **2**; (D) C after treatment with 5% aqueous TEA; (E) crude uncapped rat Hsp10; (F) rat Hsp10 (uncapped) after purification by Rotofor and RP-HPLC.

cedure was 8%, a relatively low value owing to the high proportion of truncated peptide. ESI-MS (Fig. 4A) also showed the presence of some low-intensity peaks with molecular masses of 10 644 and 10 654. These corresponded to deletion peptides lacking Gln and Asp residues, respectively, indicating that although the capping procedure is efficient, further refinement is required for full protection against incomplete couplings.

The importance and efficiency of the capping procedure were demonstrated when a second synthesis of rat Hsp10 was performed using double coupling cycles and no capping [14]. The crude polypeptide obtained as described above gave the RP profile shown in Fig. 3E. A three-

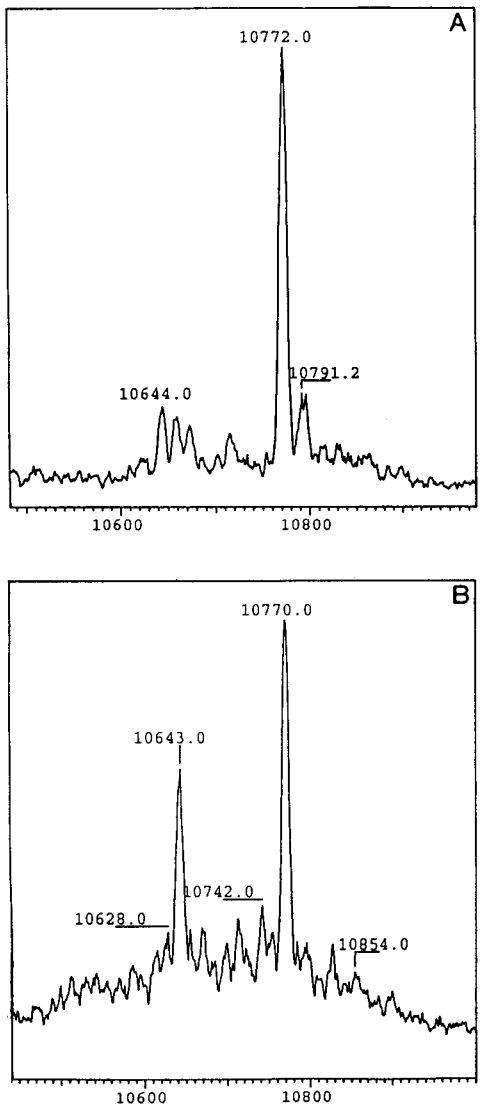

Fig. 4. ESI-MS analysis. (A) Purified free rat Hsp10 after one-step RP-HPLC purification; (B) rat Hsp10 (uncapped) after purification by Rotofor and RP-HPLC. Values represent mass units.

step purification procedure was conducted involving isoelectric focusing in a Rotofor cell (ampholyte pH range 3–10) under denaturing conditions, followed by re-fractionation with a narrower pH range. The cells containing similar material were combined and passed through a semi-preparative RP column both to desalt the sample and to provide a purification step on the basis of hydrophobicity. The purified material (overall yield 4.2%) was injected on to an analytical RP-HPLC column (Fig. 3F) and gave a sharp peak. Unfortunately, ESI-MS analysis (Fig. 4B) of the product clearly showed the presence of the same deletion peptide lacking Gln^{60} (expected, 10 642; found, 10 643), the point at which difficulties were encountered during the first synthesis. Thus, even after a three-step purification procedure a large proportion of impurity still remained as the chromatographic properties of the target sequence and the deletion peptide with Gln missing were so similar.

The homogeneity of the purified material can be critical to the biological function of the synthetic peptide. Rat Hsp10 in its biologically active form, as a co-chaperone, adopts a folded form consisting of seven monomers [15]. The folded structure binds to an M_r 60 000 chaperone in the presence of ATP and it is the complex which then helps other proteins fold correctly [15].

The ability of purified rat Hsp10 from the one-step RP purification with Fmoc probe **2** and that from the three-step purification procedure (uncapped) to fold correctly in a spontaneous manner was investigated. Solutions of 1 mg/ml of each were prepared in PBS buffer at pH 7.2 containing calcium and magnesium ions, heated to 70°C for 5 min then left at room temperature for 45 min [14]. The material thus treated was loaded on to a size-exclusion column, resulting in the appearance of two main folded forms, corresponding to heptameric and trimeric or tetrameric structures, for each of the rat Hsp10 samples [14]. In the case of the capped protein the ratio of heptamer to incorrectly folded species (i.e., tetramer) was 3:1. However, in the uncapped product that had undergone purification in a Rotofor cell and RP-HPLC, the ratio was reduced to 1:3 (heptamer-to-trimer) (data not shown). Hence, from these results, it appeared that if correct folding was dependent on the homogeneity of the monomeric material, then the protein that was synthesized with capping and then purified using a lipophilic chro-

matographic probe yielded a product with greater purity.

3.5. Affinity purification of the 46-residue β2-subunit of CD18

One of the most efficient purification techniques available is affinity chromatography. One of the most widely used interactions for the purposes of purification is the use of avidin, which exhibits an extremely high association constant for biotin. Although the covalent attachment of biotin directly to the peptidyl-resin has been described [16], the application of reversible biotinylated groups has been limited [8].

The effectiveness of biotin when attached to the Fmoc-based group was then examined. The probe synthesized possessed two Gly residues between the fluorene ring and biotin to ensure that the interaction with the immobilized avidin was not restricted by the bulkiness of the former. The probe was activated as the carbonate (**3**) and then used to derivatize an aliquot of the freshly deprotected β2-subunit peptidyl-resin. Quantitative ninhydrin analysis showed that after a 90-min reaction time, only 85% incorporation had been achieved. An additional 90 min resulted in the same amount of coupling, so the reaction was stopped and the derivatized peptidyl-resin cleaved using TFA. RP-HPLC of the crude cleavage material (Fig. 5A) showed two main products, labelled 1 and 2. The later eluting peak labelled 2 was thought to be the biotinylated product, as it exhibited strong absorbance at 301 nm and due to the lipophilicity of the fluorene ring eluted later with respect to the underivatized peptide. This was confirmed by its isolation and ESI-MS analysis (expected, 6075; found, 6075).

To determine if the immobilized avidin recognized the biotinylated material, 10 mg of crude peptide were dissolved in sodium acetate buffer (pH 4), filtered and incubated with the resin-bound avidin for 30 min with occasional mixing. An aliquot of the supernatant was removed and injected on to RP media, which indicated a decrease in the proportion of peak 2 (data not shown). The larger than expected amount of peak 1 suggested that incomplete derivatization with Fmoc probe **3** had occurred, as indicated by the ninhydrin analysis described previously. Therefore, a longer reaction time would be required to optimize the amount of affinity label on the peptidyl-resin. The resin was then washed with buffer to remove any unbound material, equilibrated in water and treated for 15 min with

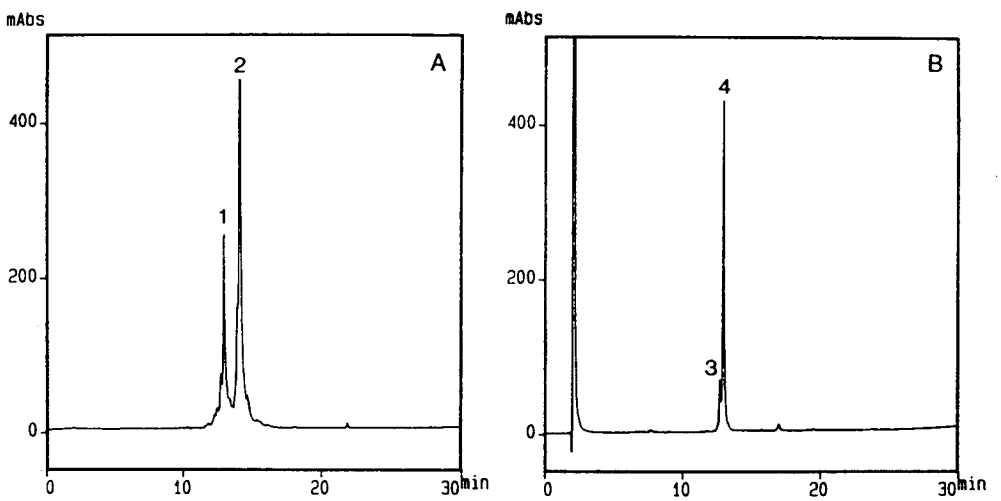

Fig. 5. Analytical RP-HPLC on a Vydac C_4 column (150 × 4.6 mm I.D.) connected to a Shimadzu LC10 LC system. Solvent A, water–0.045% TFA; solvent B, acetonitrile–0.036% TFA; gradient, 0–100% B in 30 min; flow-rate, 1 ml/min; detection, 20 nm. (A) Crude β2-subunit adduct + 3; (B) purified β2-subunit after elution from immobilized avidin with base.

5% aqueous TEA to cleave the urethane group linking the target peptide to the resin support through the biotinylated probe **3**. The supernatant containing the free purified peptide was collected and acidified with 20% acetic acid and an aliquot was analysed by RP-HPLC (labelled 4, Fig. 5B). The resulting profile showed the product to be homogeneous and it was almost identical with that obtained following purification with lipophilic probe **2** (Fig. 2D). The remaining material was desalted by RP-HPLC, yielding 3 mg (33%) of purified β2-subunit after lyophilization and shown by ESI-MS to have the correct molecular mass (expected, 5483; found, 5483). The peak labelled 3 (Fig. 5B) was found to be the β2-subunit with Met in its oxidized form, consistent with the results obtained previously (ESI-MS: found, 5499).

4. Conclusions

New simplified Fmoc-based probes containing either extremely hydrophobic groups or biotin have been synthesized. The probes were then incorporated on the peptidyl-resin as active carbonates to permit separation by either RP-HPLC or biotin–avidin affinity chromatography. The chromatographic probes were used successfully to purify two synthetic polypeptides, 46 and 101 residues in length. The former represents the first example of the application of these probes to a peptide synthesized using the Fmoc protocol. To convert possible deletion peptides into truncated sequences and thereby prevent their derivatization with the probes, a new capping procedure was applied that overcame the instability of acetic anhydride solutions and the harmful reactivity of its by-products. The procedure involved the use of N-(2-chlorobenzyloxycarbonyloxy)succinimide, which was freshly dissolved and transferred automatically by the peptide synthesizer at the end of each coupling reaction. The combined application of capping procedure and chromatographic probes **1**, **2** or **3**, when used to purify the 46- and 101-residue polypeptides, clearly demonstrated that highly homogeneous material could be obtained after a one-step purification procedure.

Acknowledgements

We thank Dr. P. Lucietto, Dr. G. Fossati and Dr. P. Giuliani for the synthesis of rat Hsp10 (uncapped) and Dr. P. James, Protein Chemistry Laboratories, ETH, Zurich, Switzerland, for ESI-MS analyses.

References

[1] R.B. Merrifield, *J. Am. Chem. Soc.*, 85 (1963) 2149.
[2] S.B.H. Kent and I. Clark-Lewis, in K. Alitalo, D. Partanen and A. Vaheri (Editors), *Synthetic Peptides in Biology and Medicine*, Elsevier, Amsterdam, 1985, pp. 29–57.
[3] H.L. Ball, C. Grecian, S.B.H. Kent and P. Mascagni, in J.E. Rivier and G.R. Marshall (Editors), *Proceedings of the 11th American Peptide Symposium*, Escom, Leiden, 1989, pp. 435–436.
[4] H.L. Ball, S.B.H. Kent and P. Mascagni, in E. Giralt and D. Andreu (Editors), *Proceedings of the 21st European Peptide Symposium*, Escom, Leiden, 1990, pp. 323–325.
[5] H.L. Ball and P. Mascagni, *Int. J. Pept. Protein Res.*, 40 (1992) 370.
[6] R.B. Merrifield and A.E. Bach, *J. Org. Chem.*, 43 (1978) 4808.
[7] A.R. Brown, S.L. Irving and R. Ramage, *Tetrahedron Lett.*, 34 (1993) 7129.
[8] S. Funakoshi, H. Fukuda and N. Fujii, *J. Chromatogr.*, 638 (1993) 21.
[9] S.B.H. Kent, personal communication.
[10] S.B.H. Kent, *Annu. Rev. Biochem.*, 57 (1988) 957.
[11] V.K. Sarin, S.B.H. Kent, J.P. Tam and R.B. Merrifield, *Anal. Biochem.*, 117 (1981) 147.
[12] T.K. Kishimoto, K. O'Connor, A. Lee, T.M. Roberts and T.A. Springer, *Cell*, 48 (1987) 681.
[13] D.J. Hartman, N.J. Hoogenraad, R. Condron and P.B. Hoj, *Biochim. Biophys. Acta*, 1164 (1993) 219.
[14] H.L. Ball, P. Giuliani, P. Lucietto and P. Mascagni, *Biomedical Peptides, Proteins and Nucleic Acids*, in press.
[15] D.J. Hartman, N.J. Hoogenraad, R. Condron and P.B. Hoj, *Proc. Natl. Acad. Sci. U.S.A.*, (1992) 3394.
[16] T.J. Lobl, M.R. Diebel and A.W. Yen, *Anal. Biochem.*, 170 (1988) 502.

ELSEVIER

Journal of Chromatography A, 686 (1994) 85–91

JOURNAL OF CHROMATOGRAPHY A

High-performance liquid chromatography of some alkaloids on unmodified silica gel with aqueous–organic solvent mixtures

W. Gołkiewicz*, J. Kuczyński, W. Markowski, L. Jusiak

Department of Inorganic and Analytical Chemistry, Medical Academy, Staszica 6, 20-081 Lublin, Poland

First received 14 December 1993; revised manuscript received 29 July 1994

Abstract

The application of eluents composed of methanol–aqueous phosphoric buffer was investigated for the high-performance liquid chromatographic separation of alkaloids on a silica stationary phase. These eluents were shown to be very useful for preliminary analytical chromatography and allow the conditions for the preconcentration of some alkaloids from crude extracts to be established. The effects of different eluent pH values and methanol concentrations were examined.

1. Introduction

In most instances, the micropreparative isolation of alkaloids from plant material is carried out by liquid–liquid extraction. The content of alkaloids in plants is very low, so large volumes of organic solvents, usually chloroform, are necessary.

Preconcentration of alkaloids from aqueous extracts on columns filled with Ameberlite XAD or chemically bonded organic stationary phases is very expensive, because continued injection of plant extracts, with strongly retained solutes, degrades the column performance.

During the last decade, unmodified silica gel with aqueous solvent mixtures has been successfully applied to separate a large number of organic base mixtures on both analytical [1–6] and preparative scales [7–9].

The utility of silica gel with aqueous–organic buffered eluents in chromatographic systems for the separation of basic organic compounds has been demonstrated for basic pharmaceuticals [1,2], nucleosides [10], amino acids [11], biogenic amines [11,12], dipeptides [13], alkaloids [5,6,14,15], anaesthetics [3] and tricyclic antidepressants [3,6]. The main difference between the chromatographic systems used in these investigations [1–7,9–15] lies in the mobile phase composition; some eluents consisted of aqueous buffer and an organic solvent [1–4,6,7,10,14,15] and some also contain small amount of long-chain quaternary ammonium compounds [5,11,16,17] (e.g., cetyltrimethylammonium bromide).

The retention mechanism on unmodified silica gel with buffered aqueous–organic solvent

* Corresponding author.

0021-9673/94/$07.00
SSDI 0021-9673(94)00717-9

eluents is complex. Organic amines at pH < 8 are at least partially protonated and are separated predominantly by ion-exchange interactions [1–3]. Bidlingmeyer and co-workers [3,4] pointed out that hydrophobic interactions must also be effective and that silica seems to be behaving in a reversed-phase mode. Cox and Stout [18] have also confirmed that the retention mechanism is a combination of ion exchange for compounds ionized under the conditions of elution and hydrophobic interaction for non-ionized materials. It was also confirmed [18] that the retention of organic bases is a complex function of the organic modifier, buffer concentration and pH.

Alkaloids usually occur in plants as salts of organic and inorganic acids with complex mixtures of water-soluble compounds, such as proteins, tannins or lipids [19]. It is often a great problem to remove these compounds from extracts during the isolation and purification of alkaloids.

It follows from TLC and HPLC investigations [14,15,24] that the retention of ternary and quaternary alkaloids in a system of silica gel with buffer–methanol increases with increasing water (buffer) content in the mobile phase. It should be stressed that quaternary alkaloids are more strongly retained than ternary alkaloids. Such differences in retention create the chance to preconcentrate quaternary alkaloids by frontal analysis of an alkaloid mixture contained in an extract or to separate the quaternary and ternary alkaloids contained in a crude extract into two groups, by using a very simple and cheap chromatographic system.

As mentioned, the retention of basis organic compounds depends on the composition and pH of the mobile phase, so it was necessary to check in detail how these parameters influence the retention of alkaloids. In this investigation, the retention behaviour of some alkaloids (mainly from *Chelidonium maius* L.) was studied as a function of the pH and concentration of the mobile phase. The results obtained will be of help in finding the optimum conditions for the micropreparative isolation of alkaloids from plant material.

2. Experimental

2.1. Apparatus

The experiments were carried out using a Type 302 liquid chromatograph (Institute of Physical Chemistry of the Polish Academy of Sciences, Warsaw, Poland), which consisted of syringe pump, a UV detector (fixed wavelength, 254 nm) and a four-port injection valve. A 100 × 4 mm I.D. stainless-steed column (ZOCh, Lublin, Poland) packed with 10-μm LiChrosorb Si 60 (Merck, Darmstadt, Germany) was used for measurements of capacity factors. The dead volume of the column was calculated after injection of a methanolic solution of benzene.

2.2. Chemicals

LiChrosorb Si 60, methanol and protopine were obtained from Merck, orthophosphoric acid and sodium hydroxide were supplied by the Polish Reagents Factor (Gliwice, Poland). The other compounds used came from various commercial sources or were obtained as gifts; they were used as received. Stock solutions of alkaloids were prepared in methanol at a concentration of 1 mg/ml. All solvents were filtered and degassed in vacuum before chromatography. The buffers were prepared from orthophosphoric acid by titration to the required pH with 5 *M* sodium hydroxide solution, followed by dilution to the final concentration of 0.2 *M*. Mobile phases of a given volume fraction were prepared by a mixing constant amount (volume) of phosphate buffer and various volumes of methanol and doubly distilled water. The pH of each portion of the mobile phase was checked with a calibrated pH meter; the stated pH of the solutions, measured after addition of modifier, refers to the organic–aqueous mobile phases.

Micropreparative preconcentration of alkaloids was carried out using a disposable, laboratory-made column (10 × 1 cm I.D.) packed with 40–60-μm Kieselgel 60 (Merck). A large volume (about 1 l) of dilute acidic (pH 6) aqueous plant extract was flushed through this

column and then the adsorbed alkaloids were eluted with 35 ml of methanol which contained 10% of 0.1 *M* HCl.

3. Results and discussion

3.1. Effect of co-solvent and pH of the mobile phase

It has been shown that the selectivity in ion-exchange chromatography on silica gel or alumina can be substantially improved by the addition of organic solvents to the aqueous mobile phase [5,6,14,15,21,22]; usually methanol or acetonitrile is used as the modifier. An explanation of this phenomenon can be formulated on the basis of changes in solvation of the competing cations and in solute ionization. In this work, improved selectivity is caused by changes in the methanol concentration in the mobile phase.

The capacity factors (k') of alkaloids were determined as a function of the methanol concentration of the mobile phase, keeping the buffer concentration and pH constant (Figs. 1 and 2). In all instances the capacity factor first decreases more or less sharply with increasing methanol content, passes through a minimum at ca. 50% of methanol in the mobile phase at lower pH and at ca. 70% at higher pH (7.4–8.5) and then increases moderately at higher methanol contents. The exact position of the minimum of the $k' = f(\varphi_{MeOH})$ depends on the degree of protonation of alkaloids and the polarity of the solute [5,21]. As the content of water increases, the retention of the alkaloids increases and for eluents rich in water, k' sometimes cannot be measured. The appearance of a retention minimum suggests that there are at least two contributing chromatographic mechanisms. Curves of similar shapes were reported previously for amino compounds and "pseudo-reversed-phase" conditions [5,14,18].

As can be seen from Figs. 1 and 2, the methanol content is a very valuable parameter for adjusting the retention and improving the selectivity. It should be noted that the content of

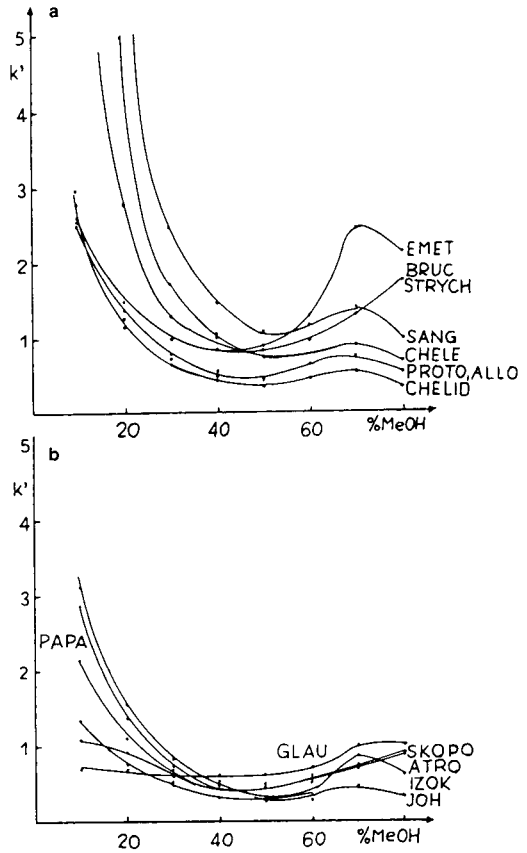

Fig. 1. Effect of the concentration of methanol on the capacity factors of alkaloids. Stationary phase: LiChrosorb Si 60, d_p = 10 μm. Mobile phase: methanol–water–phosphate buffer (pH 3.50). Constant ionic strength. Samples: BRVC = brucine; STRYCH = strychnine; EMET = emetine; SANG = snaguinarine, CHELE = chelerithrine; CHELID = chelidonine; PROTO = protopine; ALLO = allocrypropine; ATRO = atropine; GLAV = glaucine; SKOPO = scopolamine; IZOK = isocorydine; JOH = yohimbine; PAPA = papaverine.

methanol in the mobile phase also influences the column efficiency.

A final and more specific way to influence retention and selectivity is to vary the pH of the mobile phase (compare Figs. 1 and 2). For an ion-exchange mechanism to be operative, the solutes must be present in ionic form and silanol groups must be ionized. Silica gel can be used as a cation-exchange material at medium to high pH values [1,3]. The number of accessible ion-

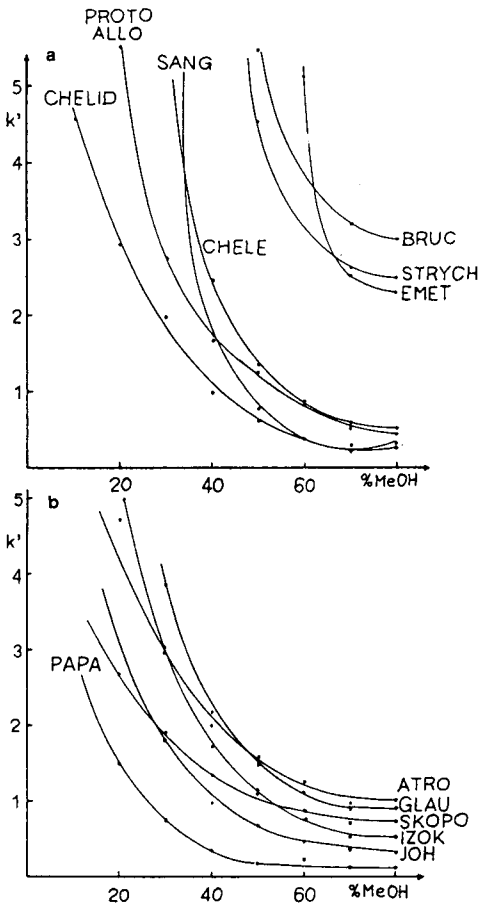

Fig. 2. Effect of the concentration of methanol on the capacity factors of alkaloids. pH of the mobile phase, 6.70. Other conditions and samples as in Fig. 1.

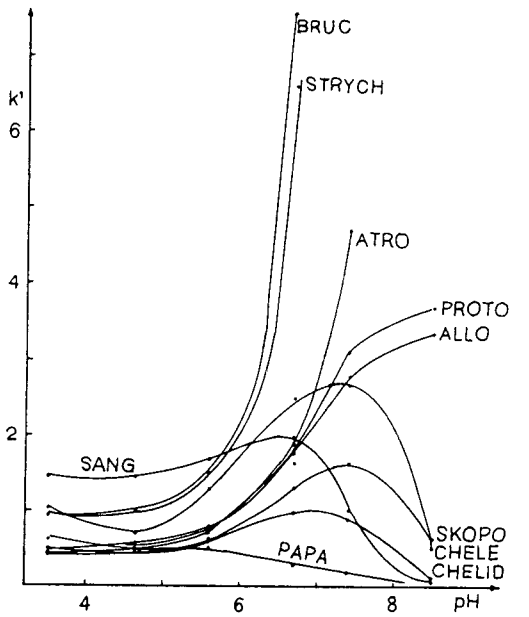

Fig. 3. Effect of pH of the mobile phase on the capacity factors of alkaloids. Constant concentration of methanol (40%, v/v). Other conditions and samples as in Fig. 1.

ized silanol groups also depends on the pH of the mobile phase and the pK_a of the silica surface. Usually below pH ca. 4 the cation-exchange capacity is very limited and increases sharply with increase in pH. Further, basic compounds are largely ionized at pH values up to $pK_a - 1$ and then rapidly become neutral at $pK_a + 1$. Consequently, the retention of non-ionized amines, when an ion-exchange mechanism is involved, decreases rapidly when the pH is increased to one unit over the pK_a. Both statements are well illustrated in Fig. 3, where the effect of pH on retention at a constant concentration of methanol is shown. For all the alkaloids investigated, as the pH is increased the retention also increases to a maximum value, after it decreases.

It is well known that the pK values of acids and bases vary with the composition of mixtures of water and organic solvents [23]. This is demonstrated in Figs. 4 and 5, where the retention behaviours of two alkaloids at various compositions of buffer–MeOH mobile phases were measured as a function of pH. It is readily seen that the maximum retention of the k vs. pH relationship, for different compositions of buffer–MeOH, is shifted from the left (higher concentration of methanol) to the right (lower concentration of methanol). It should also be stressed that the retention of glaucine or chelerithrine, at a given pH, decrease with increasing of methanol content in the mobile phase. These variations in alkaloid retention can be interpreted by a change in ionization [5,22] and solvation [5,18] of the solutes. It is seen from Fig. 3 that a maximum separation factor α is obtained at a pH value intermediate between the two pK_A values, so even a 0.3–0.4 change in pK_A (e.g., when the concentration of methanol is

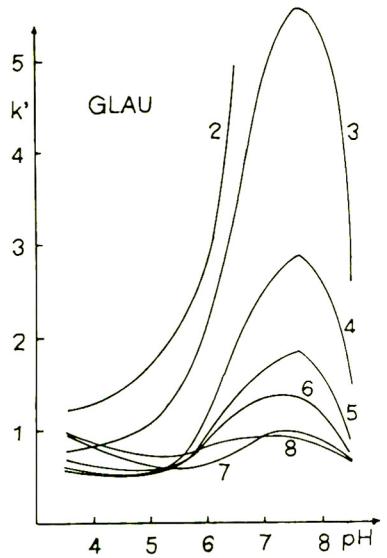

Fig. 4. Influence of pH (actual pH in mixed aqueous–organic solvent) and methanol concentration on the retention behaviour of glaucine. The concentration of the mobile phase is indicated by first digit of the methanol percentage, e.g., 1 = 10% of methanol.

changed from 20 to 40%) can result in significant changes in retention and selectivity, particularly when the pH of the aqueous–organic phase is near the pK_A [23].

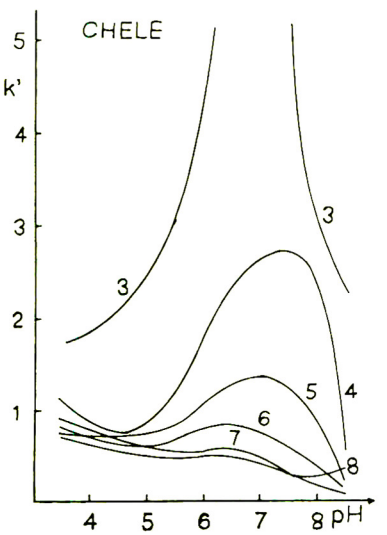

Fig. 5. Influence of pH and methanol concentration on the retention behaviour of chelerithrine. Conditions as in Fig. 4.

3.2. Three-dimensional networks

In laboratory practice, optimization of the mobile phase is restricted to changing its composition or pH, keeping the other parameter constant. Combined optimization of the pH and concentration of the mobile phase can show additional selectivity effects and the region of strongest retention of alkaloids. For basic solutes there is also a second selectivity effect from the influence of the modifier on the pK_A values of the buffer and the solutes [22].

The dependence of the capacity factor, k', on the concentration and pH of the mobile phase may be represented three-dimensionally if sufficient data are available to construct a closely spaced network. In Figs. 6–8 the k' values of chelerithrine, sanguinarine and glaucine are plotted for various concentrations and pH values of the mobile phase. The data points become the intersections of a net, forming a three-dimensional surface. In consequence, during the optimization process, both the concentration of the

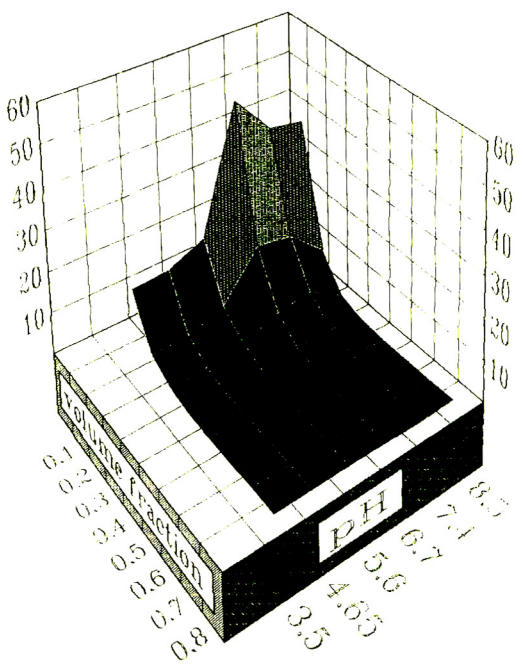

Fig. 6. Combined effects of pH and methanol concentration in the mobile phase on the chromatographic behaviour of chelerithrine. See text for discussion.

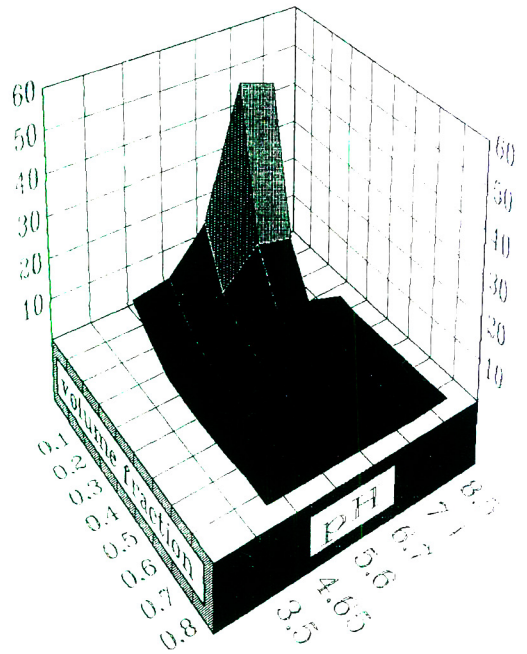

Fig. 7. Combined effects of pH and methanol concentration in the mobile phase on the chromatographic behaviour of sanguinarine. See text for discussion.

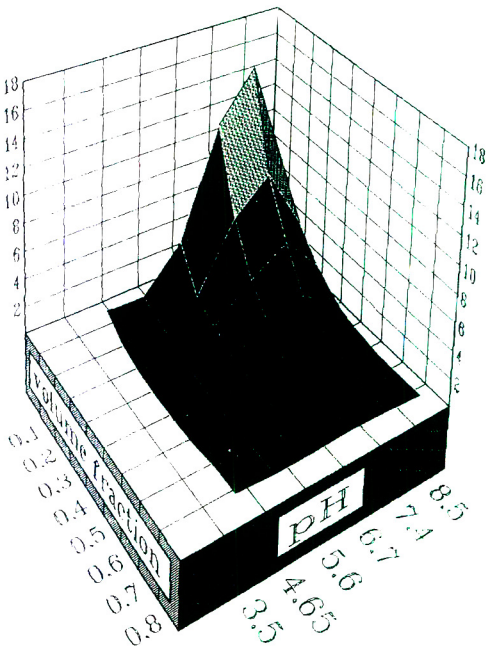

Fig. 8. Combined effects of pH and methanol concentration in the mobile phase on the chromatographic behaviour of glaucine. See text for discussion.

organic solvent and the pH of the mobile phase should be carefully established.

All data collected so far for a mobile phase composed of methanol and buffer, alkaloids as solutes and unmodified silica gel as the stationary phase are similar to the general behaviour of k' in Figs. 6–8. At low pH (<4.5), k' for the alkaloids is essentially independent on the concentration of methanol and at a high concentration of methanol ($\varphi > 0.5$) k' in practice is independent of both pH and concentration of methanol. Such plots are useful in predicting of the conditions for the chromatography and preconcentration of alkaloids from crude aqueous extracts.

The applicability of the investigated chromatographic system to the separation of some quaternary alkaloids, obtained from *Chelidonium maius* L. roots, is demonstrated in Fig. 9. The resolution between chelirubine–sanguinarine and chelilutine–chelerithrine is even better than in a normal-phase system [24]. One of the disadvantage of the present chromatographic system is the low column efficiency. It is well known that in ion exchange the kinetic processes are slow, especially when a mobile phase rich in water is used. For the column used in this work, the efficiency was measured for real samples of berberine and chelerithrine. The number of theoretical plates depends strongly on the concentration of methanol and for 25×0.4 cm I.D. column packed with 10-μm particles of silica gel it is about 2500 for a 50% methanol concentration [25]. It should be kept in mind that the proposed chromatographic system will be used for the preliminary separation and preconcentration of alkaloids present in crude plant extracts.

4. Conclusions

This study has demonstrated that the chromatographic system described can be successfully applied to the analytical chromatography or

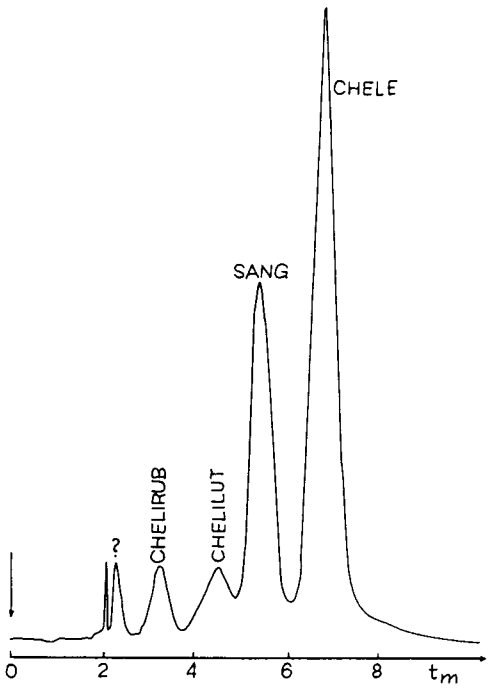

Fig. 9. Chromatogram of some quaternary alkaloids obtained from *Chelidonium majus* L. Stationary phase, LiChrosob Si 60, $d_p = 10$ μm; mobile phase, methanol–water–phosphate buffer (40:40:20, v/v/v); pH of the mobile phase, 6.9. Peaks: 1 = unknown; 2 = chelirubine; 3 = chelilutine; 4 = sanguinarine; 5 = chelerithrine.

preconcentration of alkaloids. These enriched and cleaner samples can subsequently be rechromatographed using normal- or reversed-phase chromatography.

The concentration of methanol and pH or a combination of these parameters can be used to adjust the order and degree of retention of alkaloids. The described system is simple and cheap and the alkaloids are chromatographed as salts so they are more stable than in normal-phase systems, where they are chromatographed as free bases.

References

[1] J. Jane, *J. Chromatogr.*, 111 (1975) 227.
[2] B.B. Wheals, *J. Chromatogr.*, 187 (1980) 65.
[3] B.A. Bidlingmeyer, J.K. Del Rios and J. Korpi, *Anal. Chem.*, 54 (1982) 442.
[4] H. Richardson and B.A. Bidlingmeyer, *J. Pharm. Sci.*, 73 (1984) 1480.
[5] H. Lingeman, H.A. van Munster, J.H. Beynen, W.J.M. Underberg and A. Hulshoff, *J. Chromatogr.*, 352 (1986) 261.
[6] R.M. Smith and J.O. Rabuor, *J. Chromatogr.*, 464 (1989) 117.
[7] J. Adamovics and S. Unger, *J. Liq. Chromatogr.*, 9 (1986) 141.
[8] K.M. Patel and J.T. Sparrow, *J. Chromatogr.*, 150 (1978) 542.
[9] H. Kaizuka and K. Takahashi, *J. Chromatogr.*, 258 (1983) 135.
[10] W.J. Th. Brugman, S. Heemstra and J.C. Kraak, *Chromatographia*, 15 (1982) 282.
[11] J. Crommen, *J. Chromatogr.*, 186 (1979) 705.
[12] H. Svendsen and T. Greibokk, *J. Chromatogr.*, 212 (1981) 153.
[13] R.A. Wall, *J. Chromatogr.*, 194 (1980) 353.
[14] W. Gołkiewicz, J. Kuczyński and L. Jusiak, *Chem. Anal. (Warsaw)*, 36 (1991) 67.
[15] W. Gołkiewicz, J. Kuczyński and L. Jusiak, *Chem. Anal. (Warsaw)*, 36 (1991) 209.
[16] S.H. Hansen, *J. Chromatogr.*, 209 (1981) 203.
[17] S.H. Hansen and P. Helboe, *J. Chromatogr.*, 285 (1984) 53.
[18] G.B. Cox and R.W. Stout, *J. Chromatogr.*, 384 (1987) 315.
[19] R. Verpoorte and A.B. Svendsen (Editors), *Chromatography of Alkaloids, Part B*, Elsevier, Amsterdam, 1984.
[20] N. el Tayer, H. van de Waterbeemd and B. Testa, *J. Chromatogr.*, 320 (1985) 293.
[21] R. Eksteen, J.C. Kraak and P. Linssen, *J. Chromatogr.*, 148 (1978) 413.
[22] C.J.C.M. Laurent, H.A.H. Billiet and L. de Galan, *Chromatographia*, 17 (1983) 394.
[23] B.L. Karger, J.N. Le Page and N. Tanaka, in Cs. Horvath (Editor), *High Performance Liquid Chromatography, Advances and Perspectives*, Vol. 1, Academic Press, New York, 1980, pp. 137–139.
[24] W. Gołkiewicz, M. Gadzikowska, J. Kuczyński and L. Jusiak, *J. Planar Chromatogr.*, 6 (1993) 382.
[25] W. Gołkiewicz and M. Gadzikowska, *Chem. Anal. (Warsaw)*, in press.

ELSEVIER

Journal of Chromatography A, 686 (1994) 93–100

JOURNAL OF CHROMATOGRAPHY A

Direct chromatographic resolution of four optical isomers of diltiazem hydrochloride on a Chiralcel OF column

Kazuhiro Ishii*, Kenjirou Minato, Noriyuki Nishimura, Takaaki Miyamoto, Tadashi Sato

Analytical Chemistry Research Laboratory, Tanabe Seiyaku Co., Ltd., 16–89, Kashima 3-chome, Yodogawa-ku, Osaka, Japan

First received 28 June 1994; revised manuscript received 26 July 1994

Abstract

Diltiazem hydrochloride is a calcium channel blocker which is administered as a single enantiomer. The direct resolution of four optical isomers of diltiazem hydrochloride was studied on both normal- and reversed-phase chiral HPLC columns. Four optical isomers of diltiazem hydrochloride were completely resolved on a Chiralcel OF column within 30 min. This chiral resolution was applied to determine three optical impurities that might be present in diltiazem hydrochloride bulk drug and its tablets. The determination of three optical impurities in the diltiazem hydrochloride bulk drug and those in tablets was successfully achieved at levels down to 0.05% by the area percentage method.

1. Introduction

HPLC for the determination of the optical purity of chiral substances is now a well developed technique. The past 15 years have given rise to a profusion of new developments such as chiral stationary phases (CSPs), derivatizing reagents and chiral mobile phase additives, all of which have proved effective in achieving chiral separations.

Four major approaches involving the separation of optical isomers by HPLC are (1) direct separation on a CSP [1–3], (2) derivatization with an achiral reagent and separation on a CSP [4,5], (3) direct separation on an achiral stationary phase with the use of a chiral mobile phase additive [6,7] and (4) derivatization with a chiral reagent and separation of the resulting diastereomers using an achiral support [8–10].

Diltiazem hydrochloride, *d*-3-acetoxy-*cis*-2,3-dihydro-5-[2-(dimethylamino)ethyl]-2-(*p*-methoxyphenyl)-1,5-benzothiazepine-4-(5*H*)-one hydrochloride, is a calcium channel blocker widely used in the treatment of angina pectoris, hypertension and supraventricular tachyarrythmias [11,12]. Diltiazem hydrochloride has asymmetric carbons at positions 2 and 3. Two isomers, *cis* and *trans*, exist, depending on the relative positions of the substituents at these positions. Each isomer also has optical isomers, the *d*- and *l*-forms. Diltiazem hydrochloride is the *d-cis*-(2*S*,3*S*)-isomer.

The efficacy of the *d-cis*- and *l-cis*-diltiazem hydrochloride was investigated. It was found that only *d-cis*-diltiazem hydrochloride had a coronary vasodilating effect. That is, the coronary

* Corresponding author.

0021-9673/94/$07.00
SSDI 0021-9673(94)00704-7

vasodilating effect of *dl-cis*-diltiazem hydrochloride was further dependent on the absolute configuration of position 2 and position 3, and only *d-cis*-diltiazem hydrochloride was active [13]. On the other hand, it was found that the stimulating effect for electroencephalography of *l-cis*-diltiazem hydrochloride was twice as strong as that of *d-cis*-diltiazem hydrochloride [14]. Therefore, it is very important for ensuring efficacy and safety to determine the optical impurity in diltiazem hydrochloride bulk drug and its tablets.

Enantiomeric resolution of diltiazem hydrochloride was first achieved by the formation of diastereomeric derivatives with a chiral reagent and subsequent separation by HPLC [9,10]. Recently, the direct chiral resolution of enantiomers of diltiazem hydrochloride has been reported using a normal-phase chiral HPLC column (Chiralcel OC) [15] and a reversed-phase chiral HPLC column (ovomucoid-conjugated column) [16]. However, the direct resolution of the four optical isomers of diltiazem hydrochloride has not been reported.

A number of cellulose-based HPLC chiral stationary phases and an ovomucoid-conjugated column, Ultron ES-OVM, have been developed, and are now commercially available. The resolution of the four optical isomers of diltiazem hydrochloride was examined on four cellulose tris(phenylcarbamate) derivatives having as substituents on the phenyl groups none, 4-CH_3, 3,5-$(CH_3)_2$ and 4-Cl and on an ovomucoid-conjugated column.

This paper describes a method for the simultaneous determination of three optical impurities in diltiazem hydrochloride bulk drug and its tablets on a Chiralcel OF column.

2. Experimental

2.1. Apparatus

The HPLC equipment consisted of a Shimadzu (Kyoto, Japan) LC-9A pump equipped with Rheodyne Model 7125 injector with a 20-μl loop and a Shimadzu SPD-6A variable-wavelength UV detector. The detector output was monitored using a Shimadzu Chromatopac C-R5A.

Chiralcel OC, OG, OD and OF columns (250 × 4.6 mm I.D.; 10 μm particle size) used were purchased from Daicel (Tokyo, Japan), and the ovomucoid-conjugated silica gel column, Ultron ES-OVM (150 × 4.6 mm I.D.; 5 μm particle size), was purchased from Shinwa Kako (Kyoto, Japan).

2.2. Chemicals and materials

Diltiazem hydrochloride, *dl-cis*-diltiazem and *dl-trans*-diltiazem were synthesized by Tanabe Seiyaku (Osaka, Japan) [17–19]. HPLC-grade hexane, *n*-propanol, 2-propanol, acetonitrile, methanol and ethanol were obtained from Katayama (Tokyo, Japan). All other chemicals were of analytical-reagent grade or higher quality.

2.3. Chromatographic conditions

Chiralcel column

Samples were dissolved in ethanol to 1 mg/ml and the injection volume was 2–10 μl. The column temperature was maintained in the range 10–40°C using water-jacket thermostatic control. Hexane–2-propanol or –*n*-propanol containing 0–1% (v/v) diethylamine was used as the eluent at a flow-rate of 1.0 ml/min, and UV detection was carried out at 254 nm.

Ultron ES-OVM column

Samples were dissolved in ethanol to 1 mg/ml and the injection volume was 2–10 μl. The column temperature was maintained in the range 10–40°C using water-jacket thermostatic control. The mobile phases consisted of phosphate buffers at different pHs and ionic strengths with ethanol as the organic modifier, and the flow-rate was 1.0 ml/min. UV detection was carried out at 254 nm.

2.4. Sample preparation

Twenty Herbesser tablets were powdered. An amount equivalent to 50 mg of diltiazem hydro-

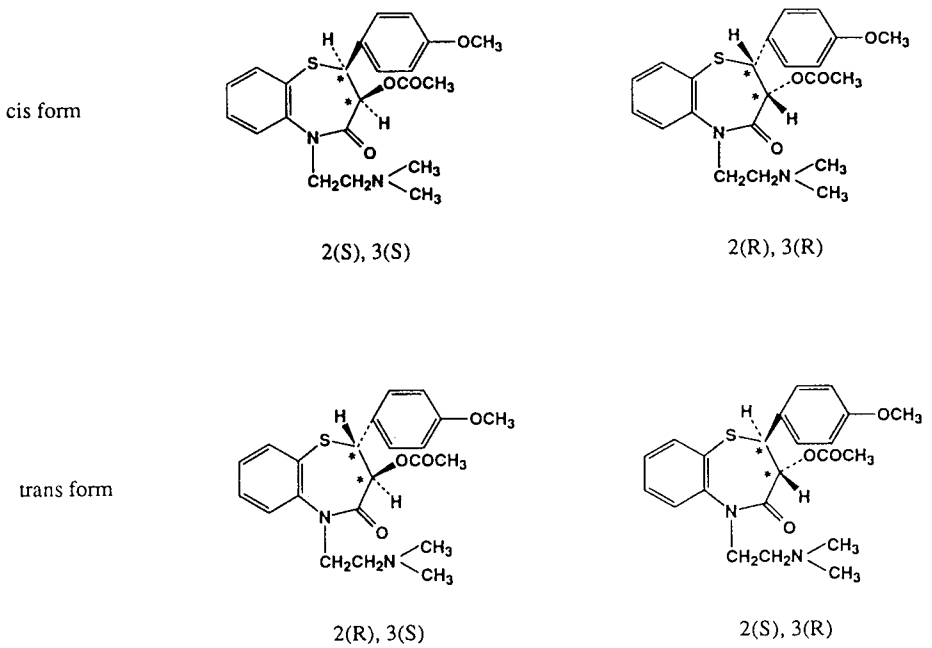

Fig. 1. Stereochemical structures of diltiazem.

chloride was weighed into a 100-ml volumetric flask, and 50 ml of ethanol were added. The flask was shaken for 15 min, ethanol was added to volume and the mixture was filtered. The filtrate was used as the sample solution (1 mg/ml of diltiazem hydrochloride) for injection into the HPLC system.

3. Results and discussion

The resolution of the four optical isomers of diltiazem hydrochloride shown in Fig. 1 was investigated by normal- and reversed-phase chiral HPLC using derivatized cellulose packings and an ovomucoid-conjugated column.

3.1. Normal-phase chiral HPLC

Different types of derivatized cellulose packings were investigated for the enantiomer separation of *cis*- and *trans*-diltiazem hydrochloride. The Chiralcel materials used (Fig. 2) are phenylcarbamate derivatives which are adsorbed on silica gel. Cellulose-based phases have mobile phase restrictions because the cellulose is soluble in certain solvents. Hexane with 2-propanol is generally used as the mobile phase and diethylamine is added (<1.0%) for basic compounds. Therefore, the enantiomer separation of *cis*- and *trans*-diltiazem hydrochloride was examined using as the mobile phase hexane–2-propanol containing diethylamine.

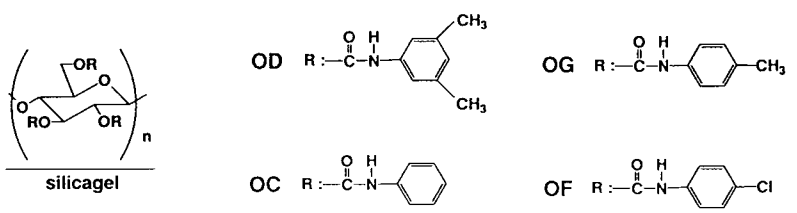

Fig. 2. Structures of Chiralcel packings.

Table 1
Effect of chiral stationary phase on separation of enantiomers of *cis*- and *trans*-diltiazem hydrochloride

Column (Chiralcel)	*dl-cis*-Diltiazem				*dl-trans*-Diltiazem			
	k'_1	k'_2	α	R_s	k'_1	k'_2	α	R_s
OC	5.34	9.05	1.69	1.76	5.25	(no separation)		
OG	3.13	4.43	1.42	2.49	2.75	3.17	1.15	0.99
OD	1.69	1.86	1.10	0.70	1.62	(no separation)		
OF	2.62	5.46	2.08	3.29	1.81	3.34	1.84	2.40

HPLC conditions: mobile phase, hexane–2-propanol (1:1, v/v) containing 1% (v/v) diethylamine; temperature, 30°C; flow-rate, 1 ml/min; detection, UV at 254 nm (0.32 AUFS). k'_1 = Capacity factor of first-eluting enantiomer; k'_2 = capacity factor of second-eluting enantiomer.

Table 1 summarizes the capacity factors (k'), separation factors (α) and resolutions (R_s) for the enantiomer separation of *cis*- and *trans*-diltiazem hydrochloride. These data show that the Chiralcel OF column gave the best resolution. In general, the separation of the enantiomers of *cis*-diltiazem hydrochloride was better than the separation of those of *trans*-diltiazem hydrochloride. In particular, the four optical isomers of diltiazem hydrochloride were completely resolved on the Chiralcel OF column (Fig. 3). In all instances, the *l*-isomers eluted first.

Okamoto *et al.* [20] showed the importance of hydrogen bonding between the carbamate group of the stationary phase and the solute for chiral recognition. As diltiazem hydrochloride has an ester group, such hydrogen bonding is likely to occur. This interaction might play an important role in chiral recognition. In addition, Okamoto *et al.* [20] also pointed out the participation of $\pi-\pi$ interactions of phenyl groups on the stationary phase with aromatic groups of the solute. The 2-phenyl ring of diltiazem hydrochloride could be involved in $\pi-\pi$ interactions. From the result, the interaction of *trans*-diltiazem with the chiral stationary phase, hydrogen bonding and $\pi-\pi$ interactions, etc., are assumed to be weaker than those for *cis*-diltiazem hydrochloride owing to steric hindrance. With cellulose trisphenylcarbamate derivatives, the substituent on the phenyl groups had a great influence on their optical resolving power. The substituent

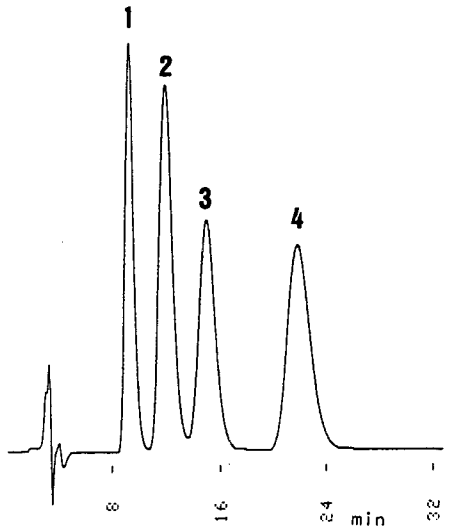

Fig. 3. Direct chromatographic separation of four optical isomers of diltiazem on Chiralcel OF. Peaks: 1 = *l-trans*-diltiazem; 2 = *l-cis*-diltiazem; 3 = *d-trans*-diltiazem; 4 = *d-cis*-diltiazem. Mobile phase: hexane–2-propanol (1:1, v/v) containing 0.1% (v/v) diethylamine; temperature, 30°C; flow-rate, 1 ml/min; detection, UV at 254 nm; sample loading, 10 μg.

appeared to change the ability of the carbamate moiety to undergo hydrogen bond formation [20].

Further analytical method development was investigated using the Chiralcel OF column. The effect of diethylamine was investigated in the concentration range 0–1.0%. Diethylamine concentration had little effect on retention. The resolution was constant and optimum with 0.05–0.5% of diethylamine. The values of α were 2.10–2.12 for *dl-cis* diltiazem hydrochloride and 1.95–1.97 for *dl-trans* diltiazem hydrochloride with 0.05–0.5% diethylamine. In order to prevent the detrimental effect of the basic mobile phase on the stationary phase, as ester groups are present in the packing material, only 0.1% (v/v) diethylamine was used in subsequent work.

Concentrations of 40–60% of 2-propanol in the mobile phase were investigated (Table 2), in the presence of 0.1% of diethylamine as a tailing-suppressing agent. An increase in 2-propanol concentration resulted in a corresponding decrease in retention. The resolution was im-

Table 2
Effect of 2-propanol concentration on k', α and R_s

Concentration of 2-propanol (%, v/v)	*dl-cis*-Diltiazem				*dl-trans*-Diltiazem			
	k'_1	k'_2	α	R_s	k'_1	k'_2	α	R_s
40	3.30	6.96	2.11	3.69	2.27	4.42	1.95	3.21
45	2.98	6.29	2.11	3.58	2.11	4.00	1.90	3.02
50	2.62	5.49	2.10	3.47	1.80	3.54	1.97	3.05
55	2.52	5.27	2.09	3.24	1.76	3.29	1.87	2.63
60	2.34	4.87	2.08	3.13	1.64	3.03	1.85	2.51

HPLC conditions: mobile phase, hexane–2-propanol containing 0.1% (v/v) diethylamine; temperature, 30°C; flow-rate, 1 ml/min; detection, UV at 254 nm (0.32 AUFS). k'_1 = Capacity factor of first-eluting enantiomer; k'_2 = capacity factor of second-eluting enantiomer.

proved with a decrease in 2-propanol concentration. The effect of the structure of the polar modifier was investigated using mobile phases of hexane with 2-propanol or *n*-propanol. *n*-Propanol decreased k', but the effect on α and R_s was not significant. Considering the enantiomeric separation, mutual selectivity and retention of *cis*- and *trans*-diltiazem hydrochloride, 50% of 2-propanol was selected as a polar modifier.

The chromatography was evaluated at temperatures from 20 to 40°C. The retention was lengthened when the column temperature was decreased. However, the effect on resolution was not significant.

3.2. Reversed-phase chiral HPLC

The enantiomer separation of *cis*- and *trans*-diltiazem hydrochloride was investigated on an Ulton ES-OVM column by changing mobile phase conditions such as modifier, pH, buffer concentration and temperature.

The effect of mobile phase was studied in the pH range 3.0–6.0 while maintaining a 20 m*M* phosphate buffer concentration in a buffer–ethanol (9:1, v/v) composition. The results are shown in Fig. 4 and indicate that resolution of the enantiomers of *cis*- and *trans*-diltiazem hydrochloride increased with increasing pH. *d-cis*-Diltiazem hydrochloride was retained strongly by the Ultron ES-OVM column at pH 6. Baseline separation between the enantiomers of *cis*-diltiazem hydrochloride was achieved throughout the pH range 4–6. However, the resolution of diastereomeric *l-cis*-diltiazem hydrochloride and *d-trans*-diltiazem hydrochloride was poor, with partial overlapping when the four optical isomers were chromatographed together.

The separation of the four optical isomers of diltiazem was investigated by changing the modifier (to acetonitrile or methanol), buffer concentration and temperature of column. The resolution of the enantiomers of *trans*-diltiazem hydrochloride was poorer using acetonitrile as the modifier. The resolution of diastereomeric *l-cis*-diltiazem hydrochloride and *d-trans*-diltiazem hydrochloride was poor with either

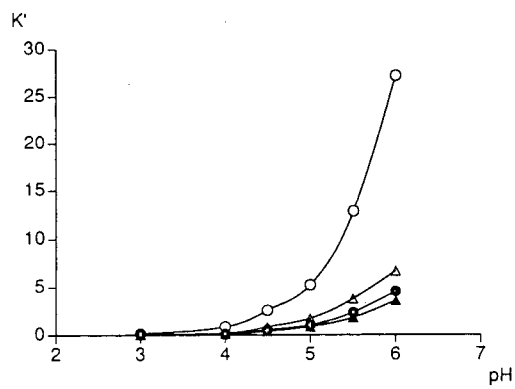

Fig. 4. Effect of pH on resolution of enantiomers of *cis*- and *trans*-diltiazem: ○ = *d-cis*-diltiazem; ● = *l-cis*-diltiazem; △ = *d-trans*-diltiazem; ▲ = *l-trans*-diltiazem. Column, ES-OVM; temperature, ambient; mobile phase, 20 m*M* phosphate buffer–ethanol (9:1); flow-rate, 1 ml/min; detection, UV at 254 nm; ambient. Sample loading, 2 μg.

methanol or ethanol as the modifier. As expected, the resolution was slightly improved by changing the ionic strength and column temperature. However, these effects were not very large and not important for chiral recognition.

The simultaneous resolution of four optical isomers of diltiazem hydrochloride was not achieved on the Ultron ES-OVM column. In general, the separation of the enantiomers of *cis*-diltiazem hydrochloride was better than that of the enantiomers of *trans*-diltiazem hydrochloride as on the Chiralcel column. In all instances the *l*-isomers eluted first as on the Chiralcel column.

3.3. Determination of three optical isomers in diltiazem hydrochloride

From the above evaluations, the optimum chromatographic conditions for the determination of three optical isomers in diltiazem hydrochloride using Chiralcel OF were defined as follows: column, Chiralcel OF; temperature, 30°C; mobile phase , hexane–2-propanol (1:1, v/v) containing 0.1% (v/v) diethylamine; and flow-rate, 1.0 ml/min. Typically, UV detection at 254 nm and a sample loading of 10 μg were used.

This chiral separation method was applied to the determination of optical impurity in the diltiazem hydrochloride product at low levels.

The method was examined for precision, accuracy, linearity and limit of detection under the above conditions. The precision of the method was evaluated by performing six replicate injections of a solution of *d-cis*-diltiazem hydrochloride containing ca. 1% of *l-cis*-, *d-trans*- and *l-trans*-diltiazem hydrochloride. The mean results were 0.95, 0.81 and 0.82% for *l-cis*-, *d-trans*- and *l-trans*-diltiazem hydrochloride, respectively, and the relative standard deviation was not more than 0.2%. The method was sufficiently precise.

The linearity and accuracy of the method were evaluated by recovery tests. The linearity and accuracy of method were determined by analysing spiked solutions containing 0.05, 0.1, 0.3, 0.5, 1.0 and 2.0% of *l-cis*-, *d-trans*- and *l-trans*-diltiazem hydrochloride in the presence of diltiazem hydrochloride. The method exhibited good linearity over the range tested, following

Table 3
Relationship between theoretical and found percentages

Optical impurity	Theoretical (%)	Found (%)	Difference (%)
l-cis-Diltiazem	0.05	0.07	+0.02
	0.10	0.12	+0.02
	0.30	0.31	+0.01
	0.49	0.48	−0.01
	0.96	0.99	+0.03
	1.85	1.86	+0.01
l-trans-Diltiazem	0.05	0.06	+0.01
	0.10	0.11	+0.01
	0.30	0.27	−0.03
	0.49	0.42	−0.07
	0.96	0.82	−0.14
	1.85	1.58	−0.28
d-trans-Diltiazem	0.10	0.10	0
	0.30	0.27	−0.03
	0.49	0.42	−0.07
	0.96	0.84	−0.12
	1.85	1.60	−0.26

HPLC conditions as in Fig. 3.

the linear equations $y = 0.9989x + 0.0148$ for *l-cis*-diltiazem hydrochloride, $y = 0.8593x + 0.0047$ for *d-trans*-diltiazem hydrochloride and $y = 0.8408x + 0.0153$ for *l-trans*-diltiazem hydrochloride, where y = observed response and x = theoretical response. The correlation coefficient was 1.00 for the three optical isomers. Therefore, the method was considered to be linear in the examined range of concentrations. The relationship between the theoretical and found percentages of each optical isomer is shown in Table 3. Good accuracy was obtained. The limit of quantification was determined to be about 0.05% for the three optical impurities in the presence of diltiazem hydrochloride, and the limit of detection was about 0.01% (1 ng) (signal-to-noise ratio = 4). Typical chromatograms of diltiazem hydrochloride spiked with ca. 0.05 and 0.1% of the three optical isomers are shown in Fig. 5.

The determination of optical impurities in diltiazem hydrochloride by the peak area percentage method showed acceptable precision, accuracy, linearity and detection limit.

Ten samples of diltiazem hydrochloride bulk drug and its tablets manufactured in Tanabe were analysed by this method. The results confirmed that the levels of optical impurities in diltiazem hydrochloride and tablets were below the detection limit (0.01%). The optical purity was excellent.

Finally, this method was compared with the methods reported previously. Enantiomer of diltiazem hydrochloride was first resolved by an indirect diastereomeric method using a chiral reagent followed by separation on a non-chiral column [9,10]. The indirect methods have several disadvantages, e.g., the cost and steady supply of the chiral reagent and the direct influence of

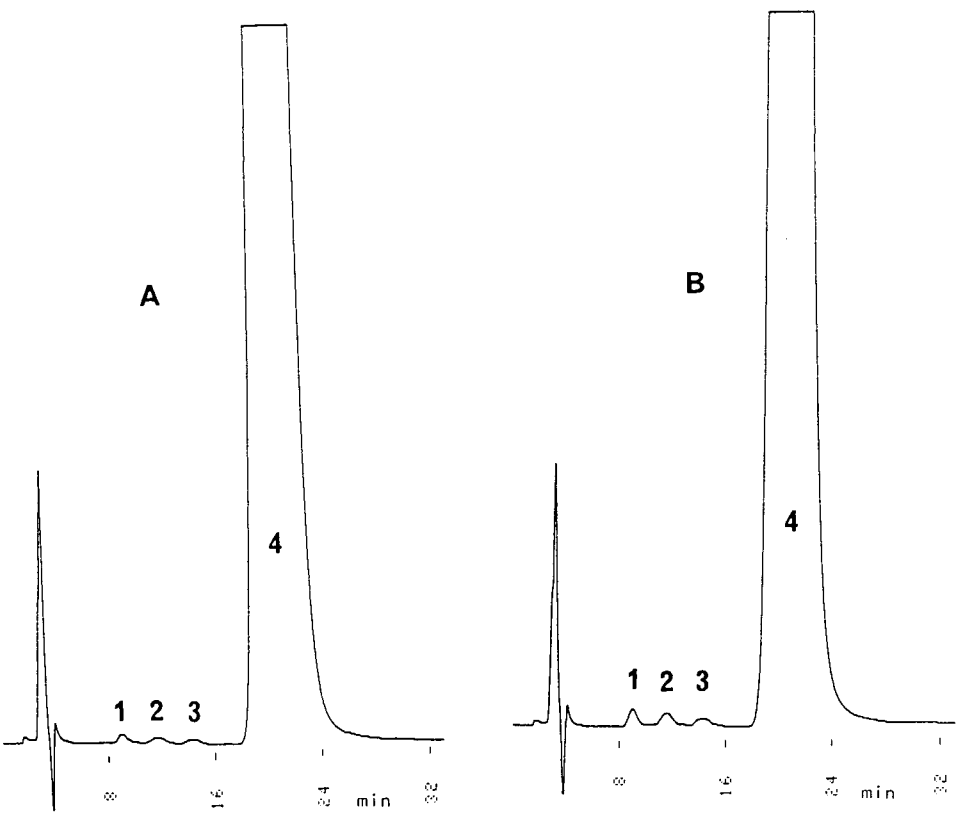

Fig. 5. Typical chromatograms of diltiazem spiked with (A) ca. 0.05 and (B) 0.1% of three optical isomers. Peaks: 1 = *l-trans*-diltiazem; 2 = *l-cis*-diltiazem; 3 = *d-trans*-diltiazem; 4 = *d-cis*-diltiazem. HPLC conditions as in Fig. 3.

the optical purity of the reagent on the analytical value. A method for the direct determination of the optical purity of diltiazem hydrochloride using an ES-OVM column has been reported [16]. However, the simultaneous determination of the three optical impurities in diltiazem hydrochloride was not achieved by the direct method on an ES-OVM column. The present method permitted the simultaneous determination of the three optical impurities in diltiazem hydrochloride bulk drug and those in tablets at levels dowm to ca. 0.05% by the area percentage method. Therefore, this method has advantages over our previous methods with regard to separation, sensitivity and ease of use.

4. Conclusions

Four optical isomers of diltiazem hydrochloride were successfully separated on a Chiralcel OF column in the normal-phase HPLC mode. The simultaneous determination of three optical impurities in diltiazem hydrochloride bulk drug and its tablets was successfully achieved at levels down to 0.05% by the area percentage method. The present method offers advantages over the reported methods, viz., a derivatization method and a direct method on an ES-OVM column, with regard to separation, sensitivity and ease of use. This method can be used for the investigation of the optical impurity profile of diltiazem hydrochloride in quality control and for the optimization of the optical resolution in the synthetic procedure, because the absolute configuration of optical impurities in diltiazem hydrochloride can be assigned by comparison with a reference sample. The method is also applicable to stereo-selective pharmacokinetic studies of diltiazem hydrochloride.

References

[1] F.A. Maris, R.J.M. Vervoot and H. Hindriks, *J. Chromatogr.*, 547 (1991) 45.
[2] J.R. Kern, *J. Chromatogr.*, 543 (1991) 355.
[3] I. Marle, A. Karlsson and C. Petterson, *J. Chromatogr.*, 604 (1992) 185.
[4] N. Oi and H. Kitahara, *J. Liq. Chromatogr.*, 9 (1986) 511.
[5] W.H. Pirkle and T.C. Pochapsky, *J. Chromatogr.*, 434 (1986) 233.
[6] C. Pettersson and M. Joseffsson, *Chromatographia*, 21 (1986) 321.
[7] M. Prevot, M. Tod, J. Chalom, P. Nicolas and O. Petitjean, *J. Chromatogr.*, 605 (1992) 33.
[8] T. Kinoshita, Y. Kasahara and N. Nimura, *J. Chromatogr.*, 210 (1981) 77.
[9] R. Shimizu, K. Ishii, N. Tsumagari, M. Tanigawa and M. Matsumoto, *J. Chromatogr.*, 253 (1982) 101.
[10] R. Shimizu, T. Kakimoto, K. Ishii, Y. Fujimoto, H. Nishi and N. Tsumagari, *J. Chromatogr.*, 357 (1986) 119.
[11] M. Chaffman and R.N. Brodgen, *Drugs*, 29 (1985) 387.
[12] M.T. Buckley, S.M. Grant, K.L. Goa, D. McTavish and E.M. Sorkin, *Drugs*, 39 (1990) 757.
[13] T. Nagao, M. Sato, H. Nakajima and A. Kiyomoto, *Jpn. J. Pharmacol.*, 22 (1972) 1.
[14] T. Nagao, M. Sato, Y. Iwasawa, T. Takada, R. Ishida, H. Nakajima and A. Kiyomoto, *Jpn. J. Pharmacol.*, 22 (1972) 467.
[15] K. Ishii, K. Banno, T. Miyamoto and T. Kakimoto, *J. Chromatogr.*, 564 (1991) 338.
[16] H. Nishi, N. Fujimura, H. Yamaguchi and T. Fukuyama, *J. Chromatogr.*, 633 (1993) 89.
[17] H. Kugita, H. Inoue, M. Ikezaki and S. Takeo, *Chem. Pharm. Bull.*, 18 (1970) 2028.
[18] H. Kugita, H. Inoue, M. Ikezaki, M. Konda and S. Takeo, *Chem. Pharm. Bull.*, 18 (1970) 2284.
[19] H. Kugita, H. Inoue, M. Ikezaki, M. Konda and S. Takeo, *Chem. Pharm. Bull.*, 19 (1971) 595.
[20] Y. Okamoto, M. Kawashima and K. Hatada, *J. Chromatogr.*, 363 (1986) 173.

ELSEVIER

Journal of Chromatography A, 686 (1994) 101–108

JOURNAL OF CHROMATOGRAPHY A

Adsorption effects on retention behaviour of hydrocarbons in gas–liquid and gas–solid chromatography with the use of modified alumina coated with diphenyl phthalate as column packings

Sadaaki Moriguchi*, Kunishige Naito, Shinsuke Takei

Department of Materials Science, Faculty of Engineering, Ibaraki University, Hitachi, Ibaraki 316, Japan

First received 25 May 1994; revised manuscript received 9 August 1994

Abstract

Adsorption effects on the retention of hydrocarbons were investigated in gas–liquid–solid chromatography using modified alumina beads, preheated at 1150 and 1200°C, coated with diphenyl phthalate as column packings. At a column temperature above the melting point of diphenyl phthalate, the same method as used in a previous study could be applied for interpreting the solute retention behaviour. At a column temperature below the melting point of the stationary phase, the retention mechanism could be successfully understood by considering that some adsorption equilibria took part in solute retention on the basis of the distribution of diphenyl phthalate in a solid form on the modified alumina surface.

1. Introduction

A jump in log(retention volume) near the melting point of a stationary phase has been observed when the former was plotted against the reciprocal of the absolute column temperature. This phenomenon is caused by the phase transition of the stationary phase between the liquid and solid forms. Gas–liquid and gas–solid chromatography can be performed at column temperatures above and below the melting point, respectively, and in the transition range of the column temperature gas–liquid–solid chromatography can be conducted [1–3].

We previously studied the dependence of the retention volume of hydrocarbons on column temperature using the modified alumina coated with polyethylene glycol 6000 (PEG 6000) as column packing. It was found that no jump in log(retention volume) of a given solute took place at low stationary phase loadings when modified alumina with a low adsorption capacity was coated with PEG 6000 and even at high stationary phase loadings when modified alumina with a high adsorption capacity was used as a solid support. We drew the important conclusion that the thickness of a triple layer was at least required for a polar stationary phase to exhibit the same properties as those of a bulk liquid [4].

In this study, the retention volume of various solutes was examined as a function of stationary phase loading using modified alumina preheated

* Corresponding author.

0021-9673/94/$07.00
SSDI 0021-9673(94)00754-3

at 1150 or 1200°C and coated with diphenyl phthalate. In addition, we examined the retention behaviour of each solute at a column temperature below the melting point of diphenyl phthalate.

2. Experimental

Modified alumina beads were prepared by preheating activated alumina beads, Neobead MS·C (60–80 mesh) (Mizusawa Industrial Chemicals, Tokyo, Japan), at 1150 and 1200°C for 3 h. Diphenyl phthalate (m.p. 73°C) was used as a stationary phase without further purification. Some C_6–C_7 saturated and unsaturated hydrocarbons were used as organic solutes. A 10-g amount of the modified alumina was added to 25 cm^3 of dichloromethane solution containing the required amount of diphenyl phthalate. Diphenyl phthalate was thoroughly deposited on the modified alumina beads by evaporating the dichloromethane gradually with continuous stirring. The column packings so prepared were packed into a stainless-steel column (100 × 0.3 cm I.D.) after drying at 120°C for 2 h.

A Hitachi Model 023 gas chromatograph equipped with a thermal conductivity detector was used in conjunction with a Hitachi Model QPD 33 recorder for gas chromatography. Gas chromatographic measurements and the determination of the specific surface area of the modified alumina coated with diphenyl phthalate were carried out as described previously [5].

3. Results and discussion

The net retention volume of each solute, V_R', was measured as a function of column temperature between 104 and 46°C, which included the melting point of diphenyl phthalate. Fig. 1 shows an experimental plot of log V_{NL} ($V_{NL} = V_R'/W_L$) against $1/T$ for *n*-hexane using the modified alumina preheated at 1150°C as solid support, where W_L is the mass of diphenyl phthalate packed in the column and T (K) is the column temperature. Log V_{NL} increased linearly with

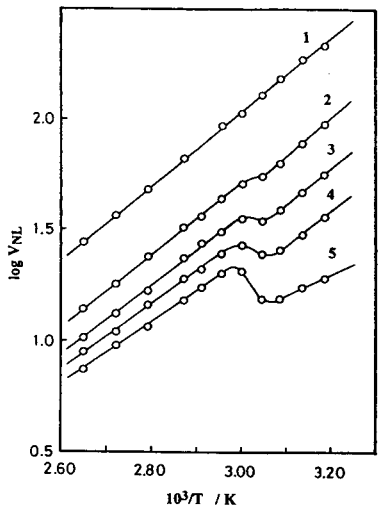

Fig. 1. Graph of log V_{NL} against $1/T$. Solid support, modified alumina preheated at 1150°C; stationary phase, diphenyl phthalate with the following loadings: 1 = 5%; 2 = 10%; 3 = 15%; 4 = 20%; 5 = 25%. Solute, *n*-hexane.

increase in $1/T$. With increase in stationary phase loading, a jump in log V_{NL} occurred more sharply near a column temperature of 60°C. This temperature is almost the same regardless of the stationary phase loading but is slightly lower than the melting point of diphenyl phthalate. This phenomenon is usually referred to as the phase transition of the stationary phase used, fusion or solidification. Hence the occurrence of this phenomenon is evidence that a liquid layer with the same properties as those of the bulk phase of the stationary phase is formed on the solid support. According to this idea, it is clear that no bulk liquid layer is formed on the modified alumina at a stationary phase loading of 5%, because a plot of log V_{NL} against $1/T$ showed no jump in the former parameter. At stationary phase loadings above 10%, diphenyl phthalate is present in the liquid form on the modified alumina at column temperatures above ca. 60°C and in the solid form at lower column temperatures. Similar results were obtained for the other solutes.

Fig. 2 shows plots of reduced retention volume, V_{NR} ($V_{NR} = V_R'/W_S$), against stationary phase loading, X_L ($X_L = W_L/W_S$), for *n*-heptane

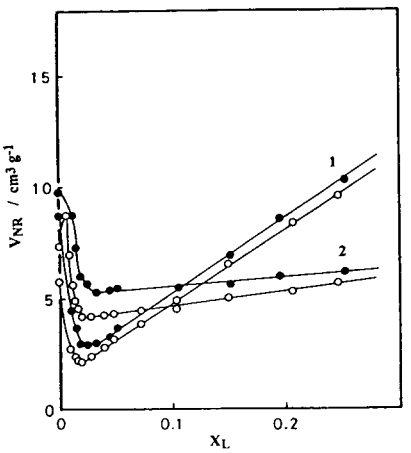

Fig. 2. Variation of V_{NR} with X_L at a column temperature of 85°C. Solid supports, modified alumina preheated at (●) 1150 and (○) 1200°C; stationary phase, diphenyl phthalate. Solutes: 1 = cyclohexene; 2 = *n*-heptane.

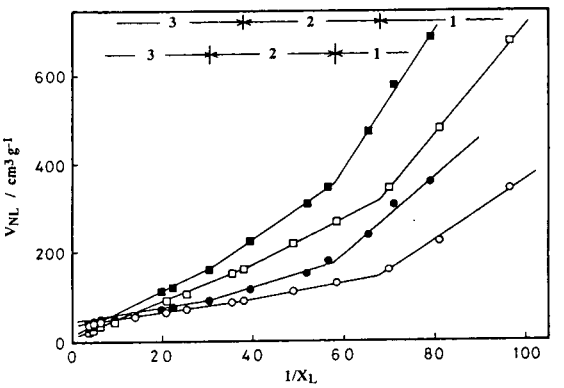

Fig. 3. Variation of V_{NL} with $1/X_L$ at a column temperature of 85°C. Solid supports, modified alumina preheated at (●, ■) 1150 and (○, □) 1200°C. Stationary phase, diphenyl phthalate. Solutes: ○, ● = cyclohexene; □, ■ = *n*-heptane.

and cyclohexene when the modified alumina preheated at 1150 and 1200°C was coated with various amounts of diphenyl phthalate, where W_S is the mass of bare solid support in the column. For both hydrocarbon solutes, V_{NR} rapidly decreased to a minimum and then increased linearly with increasing X_L. The rapid decrease in V_{NR} with X_L indicates that deactivation of the modified alumina surface occurred owing to gradual occupation of active sites for adsorption with diphenyl phthalate molecules. During this deactivation, the modified alumina surface was completely covered with a monolayer of diphenyl phthalate. A further increase in X_L results in the formation of a bulk liquid layer of diphenyl phthalate on the deactivated surface of the modified alumina. The linear increase in V_{NR} with X_L in this range of X_L can thus be caused by a dominant contribution of solution partitioning into a liquid layer of diphenyl phthalate. The value of V_{NR} for each solute is always smaller when using the modified alumina preheated at 1200°C (specific surface area 26.7 m^2 g^{-1}) than when using the modified alumina preheated at 1150°C (specific surface area 32.8 m^2 g^{-1}). This result indicates that interfacial adsorption equilibria still contribute significantly to solute retention in this instance.

Fig. 3 shows plots of V_{NL} against $1/X_L$ for the same solutes as in Fig. 2. The plot of V_{NL} against $1/X_L$ for each solute can be well approximated with a straight line in each of three $1/X_L$ ranges. Two stationary phase loadings, X_{L1} and X_{L0}, were calculated as fixed values regardless of the nature of the solutes at the intersection of two adjacent straight lines (Table 1).

Both X_{L1} and X_{L0} determined on the modified alumina preheated at 1200°C are smaller than the corresponding stationary phase loadings determined on the modified alumina preheated at 1150°C. We thought that these stationary phase loadings are meaningful where the solid support surface was completely covered with a monolayer of stationary phase used. The occupying area of a molecule of diphenyl phthalate (0.54 nm^2), calculated from X_{L0} and the BET surface area of liquid-free modified alumina, is in good agreement with the cross-sectional area of the same molecule (0.53 nm^2) calculated from the density [6] and the molecular mass of diphenyl phthalate according to Emmett and Brunauer's equation [7]. This result supports the above idea that the modified alumina surface is first covered with a monolayer of diphenyl phthalate. Thus, X_{L0} corresponds to a stationary phase loading where the modified alumina surface is completely covered with a monolayer of diphenyl phthalate. According to a previous model for solid surfaces [8] in which the modified alumina sur-

Table 1
Liquid phase loadings at two intersection points between two adjacent straight lines in Fig. 3

Solute	W_{L1}/W_S (%, w/w)		W_{L0}/W_S (%, w/w)	
	A	B	A	B
n-Hexane	1.76	1.42	3.14	2.78
2-Methylpentane	1.79	1.42	3.09	2.96
1-Hexene	1.77	1.38	3.11	2.69
2-Hexene	1.81	1.40	3.05	2.96
Cyclohexane	1.72	1.43	2.95	2.64
Cyclohexene	1.82	1.41	3.13	2.33
n-Heptane	1.77	1.45	3.02	2.52

(A) Modified alumina preheated at 1150°C; (B) modified alumina preheated at 1200°C. Column temperature, 85°C.

face includes two subsurfaces with high and low adsorption capacities, X_{L1} corresponds to a stationary phase loading where the subsurface with a high adsorption capacity (subsurface 1) is completely covered with a monolayer of diphenyl phthalate.

In the range of stationary phase loadings below X_{L1} (region 1), subsurface 1 is considered to be partly covered with a monolayer of diphenyl phthalate. Hence the modified alumina surface includes an uncoated part of subsurface 1, bare surface of subsurface 2 (subsurface with low adsorption capacity) and surface of a monolayer of diphenyl phthalate. We assumed that a monolayer of diphenyl phthalate had such a dense structure that no solute molecule can penetrate or dissolve in the monolayer. Taking account of the concurrent contribution of adsorption equilibria on these three subsurfaces to solute retention, the following equation can be written:

$$V_{NL} = -(K_1 - K_A)(s_L N_{Av}/M_L) + K_S\sigma_{S0}/X_L \quad (1)$$

where K_1 and K_A are distribution constants for adsorption on subsurface 1 and a monolayer of diphenyl phthalate, respectively, and K_S is an apparent distribution constant for adsorption on the solid surface of modified alumina. $K_S\sigma_{S0}$ is equal to the net retention volume at $X_L = 0$ and $K_S\sigma_{S0} = K_1S_1 + K_2S_2$, where K_2 is the distribution constant for adsorption on subsurface 2. S_1 and S_2 are the specific surface areas of subsurfaces 1 and 2, respectively, and $\sigma_{S0} = S_1 + S_2$, s_L is the occupying area of a diphenyl phthalate molecule, M_L is the molecular mass of diphenyl phthalate, N_{Av} is Avogadro's number and σ_{S0} is the specific surface area of liquid-free modified alumina.

In the range of stationary phase loadings between X_{L1} and X_{L0} (region 2), subsurface 2 is considered to be gradually covered with a monolayer of diphenyl phthalate after subsurface 1 is completely covered. In this instance, the modified alumina surface consists of the bare surface of subsurface 2 and the surface of a monolayer of diphenyl phthalate. Adsorption equilibria on these two subsurfaces contribute to solute retention. We assumed that K_A is the same for both adsorption equilibria on the surface of the monolayer formed on subsurfaces 1 and 2. Then the retention volume of a solute in this region can be written in the following form:

$$V_{NL} = -(K_2 - K_A)(s_L N_{Av}/M_L) + K_2\sigma_{S0}/X_L \quad (2)$$

In the range of stationary phase loadings above X_{L0} (region 3), the deactivated surface of modified alumina (bare surface of a monolayer of diphenyl phthalate) is considered to be further covered with a bulk liquid-like layer. In this instance, solution partitioning into a bulk liquid-like layer becomes more important, and adsorption equilibria on the deactivated surface of modified alumina and the surface of a bulk liquid-like layer become less significant with respect to solute retention. Considering that such

Table 2
Distribution coefficients for adsorption, K_S (cm), K_1 (cm) and K_2 (cm)

Solute	$K_S \times 10^5$		$K_1 \times 10^5$		$K_2 \times 10^5$	
	A	B	A	B	A	B
n-Hexane	2.43	2.44	3.40	3.62	1.19	1.09
2-Methylpentane	2.01	2.05	2.74	3.06	1.07	0.888
1-Hexene	3.38	4.06	5.07	6.62	1.23	1.10
2-Hexene	3.23	3.98	4.79	6.50	1.25	1.08
Cyclohexane	2.27	2.08	3.25	3.10	1.03	0.911
Cyclohexene	3.32	3.76	5.01	6.18	1.16	0.981
n-Heptane	6.15	6.24	8.73	9.33	2.85	2.68

(A) Modified alumina preheated at 1150°C; (B) modified alumina preheated at 1200°C. Column temperature, 85°C.

sorption equilibria take part concurrently in solute retention, the retention volume of a solute can be expressed as follows:

$$V_{NL} = K'_{exp} + [K_A \sigma_{S0} - K'_{exp} X_{L0}]/X_L \quad (3)$$

where $K'_{exp} = K'_L - \alpha(K_A - K'_S)$ and α is a proportionality constant relating $X_L - X_{L0}$ to the surface area of the deactivated surface covered with a bulk liquid-like layer.

Table 2 gives values of K_S, K_1 and K_2 calculated from retention data observed at a column temperature of 85°C.

As assumed previously, K_1 is always larger than K_2 for each solute. The apparent adsorption constant, K_S, of each solute is almost the same for both modified aluminas used as solid supports. Subsurface 1 of modified alumina preheated at 1200°C has a larger K_1 value than that preheated at 1150°C, whereas subsurface 2 of modified alumina preheated at 1200°C, has a smaller K_2 value than that preheated at 1150°C. Table 3 shows very similar values of K_A for each solute calculated separately in three regions. Similar values of K_A are also obtained regardless of preheating temperature of modified alumina. This result means that the surface properties of modified alumina can be shielded with a monolayer of diphenyl phthalate.

Fig. 4 shows a plot of V_{NR} vs. X_L for each solute at a column temperature of 46°C, at which diphenyl phthalate loaded on modified alumina

Table 3
Distribution coefficients for adsorption, K_A (cm)

Solute	$K_A \times 10^5$					
	Region 1		Region 2		Region 3	
	A	B	A	B	A	B
n-Hexane	0.796	0.891	0.895	0.895	0.909	0.891
2-Methylpentane	0.702	0.748	0.739	0.760	0.758	0.750
1-Hexene	0.776	0.693	0.894	0.882	0.915	0.882
2-Hexene	0.920	0.881	0.971	0.972	0.996	0.958
Cyclohexane	0.857	1.01	1.01	0.997	1.03	0.998
Cyclohexene	1.16	1.08	1.18	1.15	1.19	1.17
n-Heptane	1.91	2.13	2.10	2.02	2.16	2.04

(A) Modified alumina preheated at 1150°C; (B) modified alumina preheated at 1200°C. Column temperature, 85°C.

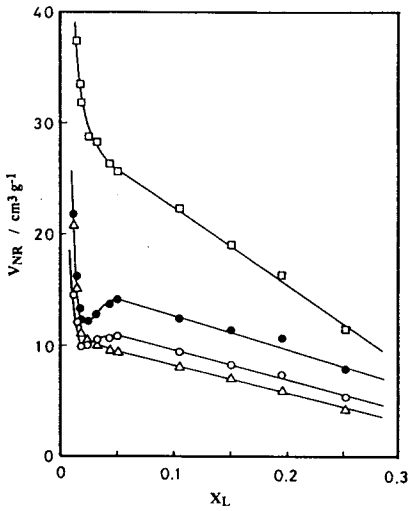

Fig. 4. Variation of V_{NR} with X_L at a column temperature of 46°C. Solid support, modified alumina preheated at 1150°C; stationary phase, diphenyl phthalate. Solutes: ○ = cyclohexane; ● = cyclohexene; △ = 1-hexene; □ = *n*-heptane.

is thought to exist in the solid form. With increasing X_L, V_{NR} of cyclohexane and cyclohexene rapidly decreased to a minimum, then increased to a maximum and finally decreased linearly with a further increase in X_L beyond 5%. For *n*-heptane and 1-hexene, V_{NR} suddenly decreased and then decreased linearly with increasing X_L. Such different profiles of the V_{NR} vs. X_L curves are probably related to different solubilities of diphenyl phthalate in the adsorbed layer of each solute: diphenyl phthalate can be easily dissolved in such a layer of cyclic solutes but only slightly in a layer of linear solutes. This phenomenon is observed only when a thin, solidified bulk liquid layer of diphenyl phthalate is formed on a monolayer in a small amount compared with the amount of the solute injected. Fig. 5 shows the dependence of the specific surface area of liquid-coated modified alumina, A_S, on X_L.

The profile of A_S vs. X_L for liquid-coated modified alumina preheated at 1150°C is similar to that of the V_{NR} vs. X_L plots for *n*-heptane and 1-hexene. Fig. 6 shows a plot of V_{NR} vs. A_S. In the range of X_L above 5%, a straight line was

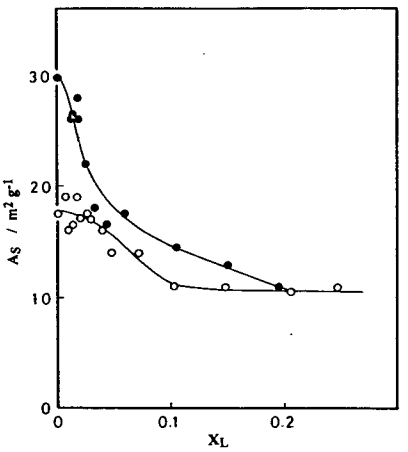

Fig. 5. Variation of A_S with X_L. Solid supports, modified alumina preheated at (●) 1150 and (○) 1200°C. Stationary phase, diphenyl phthalate.

drawn on the V_{NR} vs. A_S diagram. We thought that the decrease in V_{NR} in this region was caused by that of A_S. The previous method was applied to analyse the retention data in this instance, taking account of the contribution of adsorption equilibria on the solid surface of the modified alumina and the organic surface of diphenyl phthalate in the solid form.

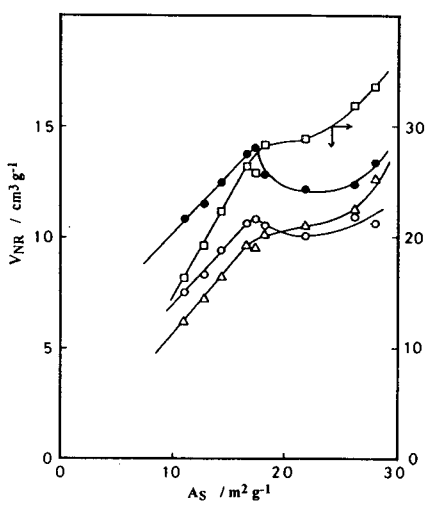

Fig. 6. Graph of V_{NR} against A_S. Solid support, modified alumina pre-heated at 1150°C; stationary phase, diphenyl phthalate. Solutes: ○ = cyclohexane; ● = cyclohexene; △ = 1-hexene; □ = *n*-heptane. Column temperature, 46°C.

In regions 1 and 2, the same retention mechanism as used previously could be applied to interpret the dependence of the retention volume of each solute on stationary phase loading. Hence Eqs. 1 and 2 were valid for the experimental data observed in these two regions. In region 3, the diphenyl phthalate loaded is present in a solid form on modified alumina surface, so we considered that two adsorption equilibria on the bare surface of a monolayer and the surface of the solidified bulk liquid layer of the stationary phase took part in solute retention. The reduced retention volume, V_{NR}, can be written as follows:

$$V_{NR} = K_A[\sigma_{S0} - \alpha(X_L - X_{L0})] + K'_S\alpha(X_L - X_{L0}) \quad (4)$$

where K'_S is a distribution constant for adsorption on the surface of the solidified bulk liquid layer of diphenyl phthalate. Eq. 4 can be expressed as

$$V_{NR} = -K''_{exp}X_L + K_A\sigma_{S0} + K''_{exp}X_{L0} \quad (5)$$

where $K''_{exp} = \alpha\ (K_A - K'_S)$. Dividing both sides of the above equation by X_L, the following equation is obtained:

$$V_{NL} = -K''_{exp} + [K_A\sigma_{S0} + K''_{exp}X_{L0}]/X_L \quad (6)$$

Eq. 5 indicates that a plot of V_{NR} against X_L gives a linear graph with a slope of $-K''_{exp}$ and an intercept of $K_A\sigma_{S0} + K''_{exp}X_{L0}$. This equation can be fitted to a linear part of a V_{NR} vs. X_L plot shown in Fig. 4.

Calculated distribution constants for adsorption, K_S, K_1, K_2 and K_A, are given in Tables 4 and 5. Table 4 shows that K_1 is always larger than K_2 for each solute. In this instance, similar values were obtained for K_S, K_1 and K_2 for each solute, regardless of the preheating temperature of the modified alumina used. This result means that both modified alumina supports show very similar surface properties for the adsorption of hydrocarbons under this condition. In Table 5, almost the same values of K_A are calculated separately in each of three regions regardless of the preheating temperature of the modified alumina.

Plotting logarithms of K_1, K_2 and K_A against $1/T$ gave linear graphs for each solute. Fig. 7 shows such linear graphs for *n*-heptane. Hence, it is reasonable to consider that a monolayer of diphenyl phthalate has a rigid structure like as solid crystals, so that no solute molecule can penetrate into the monolayer. It is surprising that the heterogeneous characteristics of the solid surface of modified alumina could be converted into deactivated, homogeneous characteristics by covering it with a thin layer such as a monolayer of diphenyl phthalate.

We conclude that reasonable results were obtained through the above analysis of the experimental data on the basis of a previous model for the solid surface of modified alumina and the distribution of the stationary phase on

Table 4
Distribution coefficients for adsorption, K_S (cm), K_1 (cm) and K_2 (cm)

Solute	$K_S \times 10^5$		$K_1 \times 10^5$		$K_2 \times 10^5$	
	A	B	A	B	A	B
n-Hexane	10.2	11.6	15.0	17.6	4.22	4.55
2-Methylpentane	8.39	9.33	12.2	14.1	3.50	3.69
1-Hexene	15.1	18.3	23.2	30.0	4.66	4.64
2-Hexene	15.0	17.8	23.1	29.0	4.69	4.84
Cyclohexane	8.73	8.84	12.6	13.4	3.68	3.47
Cyclohexene	15.5	17.2	24.2	28.5	4.26	4.06
n-Heptane	36.3	34.4	54.6	52.5	13.1	13.3

(A) Modified alumina preheated at 1150°C; (B) modified alumina preheated at 1200°C. Column temperature, 46°C.

Table 5
Distribution coefficients for adsorption, K_A (cm)

Solute	$K_A \times 10^5$					
	Region 1		Region 2		Region 3	
	A	B	A	B	A	B
n-Hexane	3.43	3.14	3.55	3.30	3.56	3.30
2-Methylpentane	2.84	2.59	2.88	2.70	2.83	2.69
1-Hexene	3.07	2.89	3.53	3.30	3.55	3.31
2-Hexene	3.49	3.37	3.88	3.62	3.89	3.58
Cyclohexane	3.28	3.38	3.63	3.54	4.01	3.64
Cyclohexene	3.92	3.78	4.45	4.27	5.20	4.51
n-Heptane	8.95	9.86	9.78	9.33	9.63	9.34

(A) Modified alumina preheated at 1150°C; (B) modified alumina preheated at 1200°C. Column temperature, 46°C.

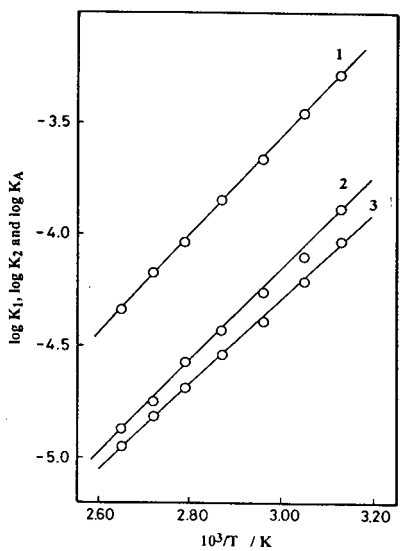

Fig. 7. Graphs of (1) log K_1, (2) log K_2 and (3) log K_A against $1/T$. Solute, *n*-heptane; solid support, modified alumina preheated at 1200°C; stationary phase, diphenyl phthalate.

modified alumina under the conditions where diphenyl phthalate was present in either the liquid or solid form. Our results show that a mixed retention mechanism is very useful for interpreting the dependence of retention data on stationary phase loading in gas–liquid and gas–solid chromatography.

References

[1] R. Annino and P.F. McCrea, *Anal. Chem.*, 42 (1970) 1486.
[2] J. Serpinet, *J. Chromatogr.*, 77 (1973) 289.
[3] J.-M. Braun and J.E. Guillet, *Macromolecules*, 9 (1976) 617.
[4] S. Moriguchi and S. Takei, *J. Chromatogr.*, 350 (1985) 15.
[5] K. Naito, H. Ogawa, S. Moriguchi and S. Takei, *J. Chromatogr.*, 299 (1984) 73.
[6] *Yukikagaku Handobukku*, Gihodoshuppan, Tokyo, 1984, p. 1871.
[7] P.H. Emmett and S. Brunauer, *J. Am. Chem. Soc.*, 59 (1937) 1553.
[8] K. Naito and S. Takei, *J. Chromatogr.*, 190 (1980) 21.

ELSEVIER

Journal of Chromatography A, 686 (1994) 109–119

JOURNAL OF CHROMATOGRAPHY A

N-, O- and P-selective on-column atomic emission detection in capillary gas chromatography

Stig Pedersen-Bjergaard*, Tyge Greibrokk

Department of Chemistry, University of Oslo, P.O. Box 1033 Blindern, 0315 Oslo, Norway

First received 3 May 1994; revised manuscript received 2 August 1994

Abstract

A 350-kHz He plasma sustained on-column was evaluated for N-, O- and P-selective atomic emission detection in capillary gas chromatography. As the plasma caused peak tailing when sustained in 2.0 ml/min of carrier gas, 15 ml/min of auxiliary helium was added to the discharge. For N- and O-selective detection, CH_4 mixed with O_2 or N_2, respectively, were used as plasma dopant. Even with this extensive plasma doping, non-specific responses arose from eluting hydrocarbons due to temporary changes in the background level of atomic N and O. Without background correction, element-to-carbon selectivities for N and O were limited to 100:1 and 40:1, respectively. For both elements, detection limits at the 50 pg/s level and linearities of $5 \cdot 10^2$ were obtained. P-selective detection was carried out with H_2–CH_4 as plasma dopant, and provided a 39 pg/s detection limit for P. The phosphorus-to-carbon selectivity was 2300:1 and the linearity was $2 \cdot 10^2$. With background correction, both selectivities and detection limits are expected to improve significantly.

1. Introduction

Even though the first papers combining gas chromatography (GC) and atomic emission spectroscopy (AES) were published in 1965 [1,2], the development and applications of this promising technique were until recently restricted to a relatively small number of research laboratories. In 1989, however, the first completely automated atomic emission detector for capillary GC became commercially available [3]. This new accessibility combined with the great versatility of GC–AES suggests that atomic emission detectors may replace a range of universal and element-selective GC detectors within the near future.

In both commercial and non-commercial atomic emission detector systems, the plasma is sustained inside a 1–6 mm I.D. silica discharge tube placed in continuation of the capillary GC column. In order to stabilize the plasma within this tube, typically 50–150 ml/min of make-up gas (helium) are added. Recently, however, two publications [4,5] demonstrated on-column atomic emission detection where a 350-kHz plasma was sustained inside the end of the GC capillary column (0.32 mm I.D.). Owing to the small volume of the detector cell, introduction of make-up gas was unnecessary, and the plasma was sustained in only 2 ml/min of GC carrier gas (helium). Because dilution of the GC effluent was avoided, detection limits were improved significantly and the consumption of high-purity helium was reduced. In addition, no ferrules

* Corresponding author.

0021-9673/94/$07.00
SSDI 0021-9673(94)00723-3

were used to connect the GC column and the plasma tube as the plasma was sustained inside the column. This eliminated air leaks at the inlet of the discharge region which are commonly observed with GC–AES systems. The 350-kHz on-column plasma was combined with a single 0.2-m focal length low-resolution monochromator, which resulted in a sensitive and inexpensive GC–AES system for C-, H-, S-, F-, Cl-, Br- and I-selective detection.

This system was utilized in the present work for the first study of on-column N-, O- and P-selective atomic emission detection in capillary GC. Optimization of the plasma conditions and wavelength selection were emphasized in order to maximize both the signal-to-noise ratios and elemental selectivities and to suppress interactions between analyte constituents and the GC capillary containing the discharge. The aim of the work was to evaluate the on-column plasma in a simple, inexpensive GC–AES system. For this reason, more complicated technical solutions, such as real-time spectral background correction or extensive purification of the GC carrier gas, were not included.

2. Experimental

2.1. Equipment

GC was carried out with a Model 4200 gas chromatograph from Carlo Erba (Milan, Italy) equipped with a capillary split/splitless injection port and a 20 m × 0.32 mm I.D. HP-1 (0.17 μm) fused-silica GC column from Hewlett-Packard (Avondale, PA, USA). Helium at 2.0 ml/min (41 cm/s) was used as the carrier gas.

The on-column detector cell which was placed in the flame ionization detection (FID) block on the top of the gas chromatograph was the same as used in two recent studies [4,5] (Fig. 1). A 5 cm length of stationary phase and polyimide coating was burned off the end of the GC column. The last 2 cm of this uncoated capillary (0.38 mm O.D. × 0.32 mm I.D.) serving as the plasma tube was placed inside a 2-cm piece of silica tube (1/8 in. O.D. × 0.5 mm I.D.) for

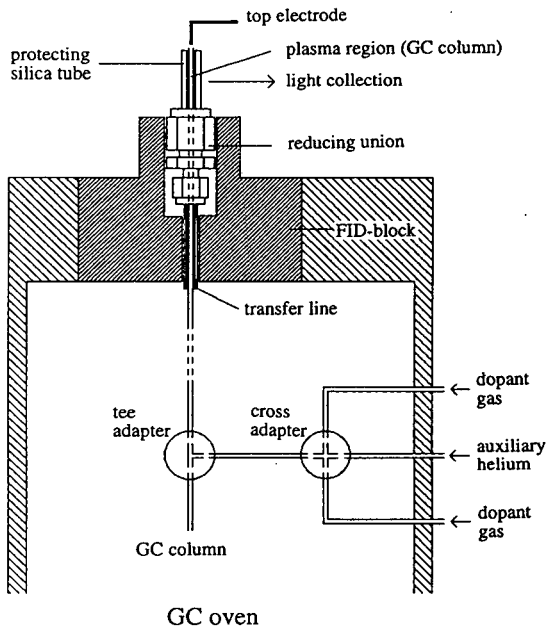

Fig. 1. Detector cell and gas flow system.

mechanical protection. The protecting silica tube was fitted into the top of a 1/16–1/8 in.-reducing union from Swagelok (Solon, OH, USA) by a 1/8-in. (1 in. = 2.54 cm) graphitized vespel ferrule. The GC column was extended through this reducing union and through a 4.5-cm piece of 1/16-in. steel tubing (transfer line) to the GC oven. The reducing union and the transfer line were mounted in the heated FID block of the gas chromatograph in order to prevent condensation of high-boiling analytes. A 350-kHz plasma was generated inside the GC column between a 1 mm diameter steel wire at the outlet (top electrode) and the grounded FID block by an HPG-2 radiofrequency power supply from ENI Power Systems (Rochester, NY, USA).

The introduction of dopant gases was modified compared with the previous papers reporting on-column atomic emission detection [4,5]. In this work, the dopants were introduced close to the outlet of the GC column. In addition, a third inlet was established at this point for introduction of auxiliary helium. The pressure drop across two 1.4 m × 20 μm I.D. fused-silica capillaries was utilized to restrict the flow of dopant

gases, whereas the auxiliary helium was introduced through a 1.4 m × 100 μm I.D. restrictor. All three capillaries were connected to a ZX1C 1/16-in. cross (0.25 mm bore) from Valco (Houston, TX, USA) with Valco FS1-.4 high-temperature polyimide adapters for fused silica. This cross, which was placed inside the GC oven (Fig. 1), served to mix the dopant gases and the auxiliary helium. These were subsequently guided by a 10-cm piece of 0.32 mm I.D. fused-silica capillary to a ZT1C 1/16-in. Valco tee (0.25 mm bore) placed in-line with the capillary GC column 40–70 cm from the outlet. This tee, which also was fitted with Valco FS1-.4 high-temperature polyimide adapters, served to mix the dopants and auxiliary helium with the GC carrier gas.

The optical part of the system has been described in detail elsewhere [4–9]. The plasma was viewed side-on through the wall of the uncoated fused-silica GC column and the protecting silica tube. Atomic emission was measured in the 600–1000-nm region by a Model H-20 IR monochromator from Instruments SA (Metuchen, NJ, USA) equipped with either 50- or 500-μm entrance and exit slits. The optical resolution was 0.4 nm with 50-μm slits. A long-pass filter with a 595-nm cut-off from Melles Griot (Irvine, CA, USA) was used to reject second and third-order radiation, and a pair of achromatic lenses ($f = 58$ mm, 12.7 mm diameter) from Newport (Fountain Valley, CA, USA) were used to image the emission on the monochromator. Light-to-current conversion was performed by an R2658 photomultiplier tube from Hamamatsu (Shizuoka-ken, Japan). This was operated at 1050 V with a Hamamatsu C665 d.c. power supply. Signals from the photomultiplier tube were collected by a Model 428 current amplifier from Keithly Instruments (Cleveland, OH, USA), and recorded on an SR 6335 strip-chart recorder from Graphtec (Yokohama, Japan).

2.2. Gases

Helium (99.9999%) from Hydro (Oslo, Norway) was used both as the GC carrier gas and as the auxiliary plasma gas. This was passed through an OMI-1 indicating purifier from Supelco (Bellefonte, PA, USA) placed in-line between the pressurized cylinder and the gas chromatograph. Traces of 99.998% oxygen, 99.9997% hydrogen, 99.99% nitrogen or 99.95% methane (all from AGA, Oslo, Norway) were added as dopant gases to the on-column plasma.

2.3. Chemicals

For the optimization and performance studies, the following model compounds of analytical-reagent grade were used unless stated otherwise: nitrobenzene (N, O), triethyl phosphate (P), *n*-tetradecane (C), 1-fluoronaphthalene (F), 1,2-dichlorobenzene (Cl) and 1,1,2,2-tetrabromoethane (Br).

2.4. Calculation of elemental selectivities, detection limits and dynamic ranges

The $X_{element}$-to-$Y_{element}$ selectivity was defined as the ratio of the peak response per gram of element X to the peak response per gram of element Y. In cases where the response for Y was negative or bipolar, the total span of the vertical excursion was used. The detection limit for element X was defined as the amount of X required to produce a peak twice the height of the peak-to-peak noise, divided by the full width at half-height of the peak in seconds. The peak-to-peak noise measurement was taken over a time period of 30 s. The dynamic range for element X was defined as the range of sample concentration over which the response factor for X (area per unit mass) varied by less than 10%.

3. Results and discussion

In two recent papers [4,5], a 350-kHz He plasma sustained inside the end of the capillary GC column (0.32 mm I.D.) was utilized for C-, H-, S-, F-, Cl-, Br- and I-selective atomic emission detection. Owing to the small volume of the detector cell, the plasma was maintained in only 2 ml/min of GC carrier gas (helium) without

dilution of the effluent by make-up gas. This resulted in significantly improved detection limits and reduced consumption of high-purity helium. The on-column plasma was combined with a 0.2-m focal length low-resolution monochromator in order to build an inexpensive single-channel GC–AES system. In the present work, this simple technology was evaluated for N-, O- and P-selective atomic emission detection. Optimization of both plasma conditions and wavelength selection were emphasized in order to maximize the performance and to understand both the advantages and limitations of the concept.

3.1. Technical aspects of dopant gas introduction

In the first two papers concerned with on-column atomic emission detection [4,5], GC was accomplished using helium as the carrier gas premixed with traces of O_2 and H_2. The latter served as dopant gases for the plasma in order to suppress non-specific responses and to eliminate distortion of chromatographic peaks in the discharge. However, two problems were inherently connected with this premixing of GC carrier gas and dopant gases: (a) the system required a relatively long period for stabilization following any changes regarding the dopant gases, and (b) polar stationary phases and sample constituents could be degraded owing to the presence of O_2 in the GC column. In this work, both problems were eliminated by introducing the dopant gases close to the outlet of the GC column through two 20 μm I.D. fused-silica restrictors. In addition, a third inlet was established at this point for introduction of auxiliary helium, whereby the flow of plasma gas could be varied independently of the GC carrier gas. The dopants and the auxiliary helium were introduced by a tee placed in the GC column 40–70 cm from the plasma region at the outlet (Fig. 1). With this piece of GC column behind the mixing point, old plasma cells could be replaced several times without disconnecting the tee union. Thus, replacement was easily performed within 5 min by cutting off the used uncoated end of the GC column followed by burning off a new 5-cm length of polyimide coating and stationary phase in a lighter flame. Careful inspection of the uncoated region was carried out in order to ensure that no stationary phase remained in the uncoated end of the GC column.

In this work, a piece of the HP-1 column (containing stationary phase) was used between the tee for gas introduction and the plasma. This was done because the HP-1 capillary was easily available by cutting 40–70 cm off the main column. As the capillary was short compared with the main column, it was found not to cause any problems regarding separation and detection. Alternatively, a well deactivated fused-silica capillary with the same dimensions can be used. This, however, was not tested in this work.

3.2. Atmospheric contamination of the plasma

Several publications have demonstrated that nitrogen and oxygen are among the most difficult elements to determine succesfully by GC–AES owing to the practical problems of excluding air from the plasma [6,10–20]. Air leaks in the GC–AES system and atmospheric impurities in the plasma gases contribute to elevated background levels of atomic nitrogen and oxygen in the discharge. For both elements, this results in deterioration of the signal-to-noise ratios and in temporary baseline fluctuations (non-specific responses) during elution of hydrocarbons.

In this work, plasma contamination was reduced by utilizing high-purity helium (99.9999%), which was passed through a purifier tube to decrease further the levels of oxygen and moisture. In addition, ferrules used in the system were frequently checked for leaks or replaced, and connections involving steel tubing were welded. However, air leaks inside the components of the gas chromatograph (e.g., split/splitless injection port, regulators and gauges) and back-diffusion of air into the discharge were not considered owing to the technological problems of their elimination.

3.3. Nitrogen-selective detection

Initial experiments with N-selective detection utilizing the on-column plasma sustained in pure

helium suffered from a low nitrogen-to-carbon selectivity (ca. 20:1) and from tailing or splitting of chromatographic peaks within the discharge. In order to suppress these problems, the plasma composition was optimized by the introduction of dopant gases. From earlier studies, either O_2 [10–12,15,16] or $H_2 + O_2$ [13,14] have been used as plasma dopants for N-selective detection. With the on-column plasma, however, superior results were obtained with a mixture of CH_4 and O_2. CH_4 served to suppress peak tailing and enhanced the nitrogen-to-carbon selectivity by a factor of 5. O_2 was added as a co-dopant in order to avoid deposition of carbon formed from CH_4 and from eluting components. The levels of CH_4 and O_2 were controlled by the intensities of the 656.3-nm H line and the 777.2-nm O line, both relative to the 706.5-nm He line. The optimum values corresponded to $I_H/I_{He} \approx 5$ and $I_O/I_{He} \approx 1$, providing a total concentration of plasma dopants below 1%. Above these levels the signal-to-noise ratios decreased significantly whereas the peak shapes and the nitrogen-to-carbon selectivity were not further improved. With optimum levels of CH_4 and O_2, non-specific responses from hydrocarbons were negative. If the concentration of O_2 in the plasma was increased, however, they changed polarity. Unfortunately, negative and positive interferences were not balanced at moderate O_2 levels, but a dipolar response occurred.

In addition to the plasma composition, signal-to-noise ratios and elemental selectivities were also affected by the intensity and the background characteristics of the emission line used. As background correction was not applied in the present system, the near-infrared portion of the spectrum was considered to be most convenient owing to the low abundance of interfering molecular emission. Within this region, 746.8 nm was found to be superior for N-selective detection. Besides providing lower signal-to-noise ratios and nitrogen-to-carbon selectivities, most of the other strong N-emission lines in the near-infrared region suffered from spectral interferences caused by adjacent emission lines for C, Cl or Br when the low-resolution monochromator was used. For this reason, N-selective detection was carried out at 746.8 nm.

The excitation conditions of the discharge not only were determined by the chemical composition of the plasma, but also were affected by the power level supplied by the plasma generator. With the present system, the applied power was varied between 10 and 20 W. Below 10 W the plasma became unstable and above 25–30 W the GC column melted. As expected, both the signals and signal-to-noise ratios for N increased when the applied power was increased (Fig. 2). A similar relationship has previously been observed for on-column detection of carbon, hydrogen, sulfur and the halogens [4,5]. As the nitrogen-to-carbon selectivity and chromatographic peak shapes did not deteriorate when the applied power was increased, 20 W was selected as the operating level in order to maximize both the detector sensitivity and signal-to-noise ratios. At this power level, the wall of the fused-silica GC column was only slightly affected by the plasma after 1 week of continuous operation. Hence plasma capillaries were used for 4–7 days before replacement.

In two recent papers reporting on-column atomic emission detection [4,5], the plasma was sustained in the GC carrier gas only. With this configuration, the flow of helium provided for the discharge could not be varied independently of the GC carrier gas flow. In the present work, however, this was possible as an inlet for auxiliary helium was established close to the on-column plasma (Fig. 1). This enabled the conditions for the chromatography and the plasma to be optimized separately. A flow-rate of the GC carrier gas of 2.0 ml/min was selected, which

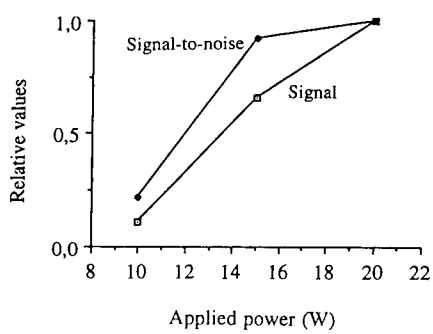

Fig. 2. Effect of applied power on signals and signal-to-noise ratios for N-selective detection.

Table 1
Effect of auxiliary helium on on-column nitrogen-selective detection

Auxiliary He flow-rate (ml/min)	Signal	Signal-to-noise ratio	Nitrogen-to-carbon selectivity	$t_{0.1w}$ [b] (s)
0	1.00[a]	1.00[a]	32:1	4.4
15	0.27	1.86	100:1	4.4

[a] Value defined as 1.00.
[b] Peak width at one tenth of peak maximum.

was a compromise between speed of analysis and chromatographic resolution. Initial work demonstrated almost no peak tailing in the N mode when the plasma was sustained in the GC carrier gas only. However, both the signal-to-noise ratios and the nitrogen-to-carbon selectivity were improved when 15 ml/min of auxiliary helium were added to the on-column plasma (Table 1). In addition, auxiliary helium was found to suppress the release of background nitrogen during the elution of fluorinated compounds. These effects probably arose since the analyte residence time was shortened, and as analyte interactions involving the wall of the plasma capillary were suppressed by the auxiliary helium. Therefore, even though the signals decreased and the operating costs increased, auxiliary helium was used throughout this work for N-selective detection.

When the on-column detector was operated at 746.8 nm with plasma conditions optimized for N-selective detection, a 50 pg/s detection limit of N and a $5 \cdot 10^2$ linearity were obtained (Table 2). With "conventional operation" of the 350-kHz plasma utilizing the same optical system and with the plasma sustained inside a 1 mm I.D. discharge tube in 60 ml/min of helium, a 1 ng/s detection limit of N was obtained. Hence on-column detection improved the signal-to-noise ratios by a factor of approximately 20, even without extensive special precautions to exclude air from the plasma. The on-column detection limit of N was among the lowest reported in the literature [10–16,21], and was significantly lower than those obtained using other GC–AES systems without extensive plasma gas purification [10–12].

Even though the nitrogen-to-carbon selectivity was only 100:1, the present system possessed considerable practical utility since non-specific responses were negative. For the determination of N-containing compounds in complicated matrices, however, a higher nitrogen-to-carbon selectivity is required. Because this value was not enhanced by further plasma doping, either extensive purification of the plasma gas (reduction of the nitrogen background level) or real-time spectral background correction has to be ap-

Table 2
System performance characteristics[a] for N-selective detection compared with literature values

Parameter	This work: on-column r.f. plasma	Microwave plasma [12]	Commercial instrument (HP) [21]
Wavelength	746.8 nm	746.8 nm	174.2 nm
Dopant gas	O_2–CH_4	O_2	O_2–H_2
N detection limit	50 pg/s	4000 pg/s	50 pg/s
Nitrogen-to-carbon selectivity	100:1	–	2000:1
Linearity	$5 \cdot 10^2$	$1 \cdot 10^3$	$2 \cdot 10^4$

[a] All results were obtained with a monochromator equipped with 500-μm slits.

plied. Further purification of the plasma gas may improve both the nitrogen-to-carbon selectivity and signal-to-noise ratios. However, as discussed above, this is technologically difficult because atmospheric contamination probably occurs at several points both in the gas chromatograph and in the small detector cell. With real-time spectral background correction, however, carbon interferences may be subtracted from the N signal by monitoring the N and C channels simultaneously. Even though both the complexity and the cost of the system will be increased, real-time spectral background correction probably is the best choice in order to realize the full advantage of the high-sensitivity performance provided by on-column N-selective atomic emission detection.

3.4. Oxygen-selective detection

O-selective detection with the on-column plasma sustained in pure helium was of no practical value owing both to large non-specific responses from hydrocarbons (oxygen-to-carbon selectivity $\approx$ 10:1) and to extensive tailing of chromatographic peaks. As the first step to improve the system performance, the composition of the plasma was optimized. From the literature, H_2 [18,19], N_2 [10,11,17], CH_4 [6] and N_2–CH_4 [13,14] have been used as plasma dopants for O-selective detection. Among these, N_2–CH_4 was found to be superior with the on-column plasma. CH_4 served to suppress peak tailing and enhanced the oxygen-to-carbon selectivity by a factor of 4. N_2 was added as co-dopant to the on-column plasma in order to eliminate deposition of carbon formed from CH_4 and from eluting components. The amounts of CH_4 and N_2 were controlled by the intensities of the 653.3-nm H line and the 868.0-nm N line, both relative to the 706.5-nm He line. The optimum levels corresponded to $I_H/I_{He} \approx 3$ and $I_N/I_{He} \approx 1$, providing a total concentration of plasma dopants below 1%. Further plasma doping reduced the signal-to-noise ratios without any improvement of the oxygen-to-carbon selectivity.

In contrast to nitrogen, only a few intense emission lines are available for atomic oxygen in the near-infrared region of the spectrum. Among these, 777.2 nm provided the best results regarding both the oxygen-to-carbon selectivity and signal-to-noise ratios. For this reason, 777.2 nm was used throughout this work for O-selective detection.

The signals and signal-to-noise ratios for O increased in a similar way to those observed for N when the power supplied by the plasma generator was increased from 10 to 20 W. Because the peak shapes and the oxygen-to-carbon selectivity were unaffected by the power level, O-selective detection was carried out at the upper limit of the potential working range (20 W) in order to maximize both the signals and signal-to-noise ratios.

Similarity between O and N was also observed regarding the effect of introducing auxiliary helium. With 2.0 ml/min of GC carrier gas, the peak shapes, signal-to-noise ratios and oxygen-to-carbon selectivity were improved when 15 ml/min of auxiliary helium was added to the plasma (Table 3). In addition, auxiliary helium served to suppress serious interferences caused by the release of background oxygen during the elution of fluorinated or chlorinated compounds [22]. Consequently, auxiliary helium was added to the

Table 3
Effect of auxiliary helium on on-column oxygen-selective detection

Auxiliary He flow-rate (ml/min)	Signal	Signal-to-noise ratio	Oxygen-to-carbon selectivity	$t_{0.1w}$ [b] (s)
0	1.00[a]	1.00[a]	26:1	6.8
15	0.21	3.16	40:1	4.8

[a] Value defined as 1.00.
[b] Peak width at one tenth of peak maximum.

on-column plasma throughout this work also for O-selective detection.

When the present system was operated at 777.2 nm with plasma conditions optimized for O-selective detection, a 51 pg/s detection limit of O and a $5 \cdot 10^2$ linearity were obtained (Table 4). Also, the detection limit of O was improved by a factor of ca. 20 when the 350-kHz plasma was sustained on-column. The on-column detection limit of O was among the lowest reported in the literature [6,10–14,17–21], even though no extensive precautions were considered to exclude air from the plasma. As for N, the practical applicability of the system for O-selective detection was higher than predicted by the low selectivity reported relative to carbon (40:1) because non-specific responses were negative. For some applications, however, a higher oxygen-to-carbon selectivity is required. As this value was not further improved by plasma doping, the most convenient solution to suppress non-specific responses is through real-time spectral background correction.

3.5. Phosphorus-selective detection

Besides N and O, P is among the most difficult non-metallic elements to determine by GC–AES owing to the formation of non-volatile compounds with O_2 that adhere to the silica discharge tube. This results in tailing of chromatographic peaks and in degradation of the linearity for the phosphorus response [14]. The high affinity of P towards hot silica surfaces was also evidenced in this work. Initial attempts at P-selective detection with the on-column plasma sustained in pure helium suffered from extensive peak tailing and from poor repeatability and linearity. As a first step to improve the system performance, optimization of the plasma composition was carried out. From earlier studies, either H_2 [13,14,23,24] or N_2 [25] have been used as plasma dopants for P-selective detection. With the on-column plasma, however, H_2–CH_4 was found to be superior. H_2 served to reduce peak tailing and CH_4 enhanced the phosphorus-to-carbon selectivity by a factor of 2–3. The levels of H_2 and CH_4 were controlled by the intensities of the 656.3-nm H line and the 940.5-nm C line, both relative to the 706.5-nm He line. Even with relatively high levels of H_2 and CH_4 in the plasma ($I_H/I_{He} \approx 8$ and $I_C/I_{He} \approx 0.02$), peak tailing was observed in the P chromatograms. This was eliminated, however, and the linearity for the phosphorus response was improved when 15 ml/min of auxiliary helium was added to the on-column plasma (Table 5). In addition, both the signal-to-noise ratios and the phosphorus-to-carbon selectivity were enhanced. Consequently, auxiliary helium was used throughout this work also for P-selective detection.

Among the most intense emission lines for phosphorus in the near-infrared region of the spectrum, 979.7 nm was found to provide the highest phosphorus-to-carbon selectivity and signal-to-noise ratios. Unfortunately, the adjacent 979.3-nm Br line caused a positive spectral interference from brominated compounds owing to the low resolving power of the mono-

Table 4
System performance characteristics[a] for O-selective detection compared with literature values

Parameter	This work: on-column r.f. plasma	Microwave plasma [12]	Commercial instrument (HP) [21]
Wavelength	777.2 nm	777.2 nm	777.2 nm
Dopant gas	N_2–CH_4	–	H_2–N_2–CH_4
O detection limit	51 pg/s	3000 pg/s	120 pg/s
Oxygen-to-carbon selectivity	40:1	80:1	1000:1
Linearity	$5 \cdot 10^2$	$1 \cdot 10^3$	$5 \cdot 10^3$

[a] All results were obtained with a monochromator equipped with 500-μm slits.

Table 5
Effect of auxiliary helium on on-column phosphorus-selective detection

Auxiliary He flow-rate (ml/min)	Signal	Signal-to-noise ratio	Phosphorus-to-carbon selectivity	$t_{0.1w}$ [b] (s)
0	1.00[a]	1.00[a]	818:1	17.6
15	0.38	1.41	2313:1	6.4

[a] Value defined as 1.00.
[b] Peak width at one tenth of peak maximum.

chromator used. With 500-μm slits, the phosphorus-to-bromine selectivity was limited to 10:1. This value was improved by a factor of 2 when the slit widths were reduced from 500 to 50 μm. Although the 979.7-nm line was used in this work, the detection wavelength may be changed to the 975.0-nm P line in order to suppress interferences caused by brominated compounds.

As for N and O, the signals and signal-to-noise ratios increased when the power level supplied by the plasma generator was increased from 10 to 20 W, whereas the selectivity relative to carbon and chromatographic peak shapes remained unaffected. Therefore, 20 W was selected as the operating level also for P-selective detection.

With the on-column detector optimized for P-selective detection, a 39 pg/s detection limit of P was obtained (Table 6). This value was high compared with the 1.5–3 pg/s limits reported utilizing either the 177.5-nm line [13,14,21] or the 253.6-nm line [23,25]. This difference probably arose because the phosphorus emission lines in the ultraviolet region of the spectrum have better signal-to-background characteristics than those in the near-infrared portion. The $2 \cdot 10^2$ linearity of the on-column detector was relatively low compared with most other elements detected on-column [4,5]. However, linearity problems for P-selective detection are general in GC–AES, and may occur even in conventional atomic emission detectors utilizing both high flow-rates of make-up gas and water-cooled discharge tubes [13,14]. The 2300:1 phosphorus-to-carbon selectivity obtained with the present single-channel spectrometer was acceptable for most practical applications. As mentioned above, however, care must be taken when utilizing the 979.7-nm P line owing to the possibility of cross-over interferences from brominated compounds.

3.6. Text mixture

In Fig. 3, C-, N-, O- and P-selective chromatograms from four subsequent injections of a multi-element test mixture are shown. Comparison of the C-selective chromatogram with the

Table 6
System performance characteristics[a] for P-selective detection compared with literature values

Parameter	This work: on-column r.f. plasma	Microwave plasma [12]	Commercial instrument (HP) [21]
Wavelength	979.7 nm	253.6 nm	177.5 nm
Dopant gas	H_2–CH_4	H_2	H_2
P detection limit	39 pg/s	3 pg/s	1 pg/s
Phosphorus-to-carbon selectivity	2300:1	10600:1	5000:1
Linearity	$2 \cdot 10^2$	$5 \cdot 10^2$	$1 \cdot 10^3$

[a] All results were obtained with a monochromator equipped with 500-μm slits.

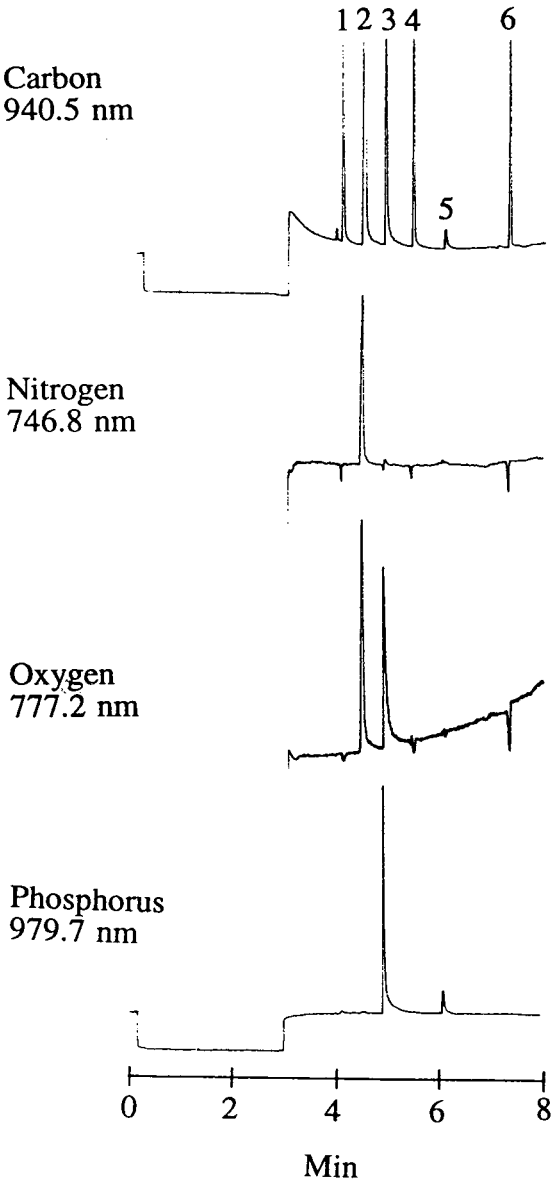

Fig. 3. C-, N-, O- and P-selective chromatograms for a test mixture. Peaks: 1 = 1,2-dichlorobenzene; 2 = nitrobenzene; 3 = triethyl phosphate; 4 = 1-fluoronaphthalene; 5 = 1,1,2,2-tetrabromoethane; 6 = *n*-tetradecane.

traces for N, O and P confirms the absence of peak tailing in the on-column plasma. In addition, the chromatograms support the practical utility of the present single-channel high-sensitivity system for on-column atomic emission detection, even though some of the selectivity values obtained for N and O remained low even after optimization of the experimental conditions. The practical utility of the system was further supported by preliminary experiments indicating that elemental response factors for N, O and P varied by less than 25%. Hence the on-column detector was probably relatively insensitive to positional variations of the atoms within eluting analyte molecules.

Acknowledgements

Dr. Milton L. Lee and Dr. Paul B. Farnsworth at Brigham Young University, UT, USA, are acknowledged for their help in the initial stages of this study.

References

[1] A.J. McCormack, S.C. Tong and W.D, Cooke, *Anal. Chem.*, 37 (1965) 1470.
[2] C.A. Bache and D.J. Lisk, *Anal. Chem.*, 37 (1965) 1477.
[3] R. Baum, *Chem. Eng. News*, (1989) 37.
[4] S. Pedersen-Bjergaard and T. Greibrokk, *Anal. Chem.*, 65 (1993) 1998.
[5] S. Pedersen-Bjergaard and T. Greibrokk, *J. Microcol. Sep.*, 6 (1994) 11.
[6] S. Pedersen-Bjergaard and T. Greibrokk, *J. High. Resolut. Chromatogr.*, 15 (1992) 677.
[7] R.J. Skelton, P.B. Farnsworth, K.E. Markides and M.L. Lee, *J. High. Resolut. Chromatogr.*, 11 (1988) 75.
[8] R.J. Skelton, H.-C.K. Chang, P.B. Farnsworth, K.E. Markides and M.L. Lee, *Anal. Chem.*, 61 (1989) 2292.
[9] R.J. Skelton, K.E. Markides, M.L. Lee and P.B. Farnsworth, *Appl. Spectrosc.*, 44 (1990) 853.
[10] J.P.J. van Dalen, P.A. de Lezenne Coulander and L. de Galan, *Anal. Chim. Acta*, 94 (1977) 1.
[11] K.S. Brenner, *J. Chromatogr.*, 167 (1978) 365.
[12] O. Qing-Yu, W. Guo-Chuen, Z. Ke-Wei and Y. Wei-Lu, *Spectrochim. Acta, Part B*, 38 (1983) 419.
[13] B.D. Quimby and J.J. Sullivan, *Anal. Chem.*, 62 (1990) 1027.
[14] J.J. Sullivan and B.D. Quimby, in P.C. Uden (Editor) *Element-Specific Chromatographic Detection by Atomic Emission Spectroscopy*, American Chemical Society, Washington DC, 1992, Ch. 4.
[15] M. Wu, M.L. Lee and P.B. Farnsworth, *J. Anal. At. Spectrom.*, 7 (1992) 197.

[16] W. Braun, N.C. Petterson, A.M. Bass and M.J. Kurylo, *J. Chromatogr.*, 55 (1971) 237.
[17] Z. Ke-Wei, O. Qing-Yu, W. Guo-Chuen and Y. Wei-Lu, *Spectrochim. Acta, Part B*, 40 (1985) 349.
[18] K.J. Slatkavitz, P.C. Uden and R.M. Barnes, *J. Chromatogr.*, 355 (1986) 117.
[19] C. Bradley and J.W. Carnahan, *Anal. Chem.*, 60 (1988) 858.
[20] S.R. Goode and L.K. Kimbrough, *J. Anal. At. Spectrom.*, 3 (1988) 915.
[21] *HP 5921A Atomic Emission Detector—Specification Guide*, Hewlett-Packard, Avondale, PA, 1989.
[22] W.R. McLean, D.L. Stanton and G.E. Penketh, *Analyst*, 98 (1973) 432.
[23] S.A. Estes, P.C. Uden and R.M. Barnes, *Anal. Chem.*, 53 (1981) 1829.
[24] R. Gross, B. Platzer, E. Leitner, A. Schalk, H. Sinabell, H. Zach and G. Knapp, *Spectrochim. Acta, Part B*, 47 (1992) 95.
[25] B. Rivière, J.-M. Mermet and D. Deruaz, *J. Anal. At. Spectrom.*, 2 (1987) 705.

ELSEVIER

Journal of Chromatography A, 686 (1994) 121–128

JOURNAL OF CHROMATOGRAPHY A

Isoelectric focusing of histones in extremely alkaline immobilized pH gradients: comparison with capillary electrophoresis

Alessandra Bossi[a], Cecilia Gelfi[b], Antonia Orsi[a], Pier Giorgio Righetti[a,*]

[a]*Chair of Biochemistry, Faculty of Pharmacy and Department of Biomedical Sciences and Technologies, University of Milan, Via Celoria 2, 20133 Milan, Italy*

[b]*Istituto Tecnologie Biomediche Avanzate, CNR, Via Ampère 56, Milan, Italy*

First received 9 June 1994; revised manuscript received 29 July 1994

Abstract

Various classes of calf thymus histones (fractions II-AS, VI-S, VII-S and VIII-S) were separated to the steady state in an extremely alkaline immobilized pH gradient, covering non-linearly the pH 10–12 interval. Successful separations were obtained in 5%T, 4%C polyacrylamide matrices, reswollen in 8 *M* urea, 1.5% Tween 20, 1.5% Nonidet P-40 and 0.5% Ampholine pH 9–11. Additionally, in order to quench the very high conductivity of the gel region on the cathodic side, the reswelling solution contained a 0–10% (anode to cathode) sorbitol gradient. The best focusing was obtained by running the gel at 17°C, instead of the customary 10°C. All major histone components had p*I* values between pH 11 and 12 and only minor components (possibly acetylated and phosphorylated forms) focused below pH 11. By summing up all bands in Arg- and Lys-rich fractions, eight to ten major components and at least twelve minor zones are clearly resolved. In contrast, capillary zone electrophoresis (in a coated capillary, 7 *M* urea, 50 m*M* Tris–acetate buffer, pH 8.0) can only resolve six major fractions and two minor, broad zones.

1. Introduction

Histones are extremely alkaline proteins, unusually rich in lysine (Lys) and arginine (Arg), which act as counter ions to the high negative charge of nucleic acids and have thus a major role in the organization of chromatin structure. In the nuclei of all eukaryotic cells DNA is packed basically in the same way: two each of histones H2A, H2B, H3 and H4 form the fundamental chromatin subunit, the nucleosome, whereas histone H1 is associated with the chromosomal linker region. Four of these five histone classes each consist of several variants, differing to some extention their amino acid sequence [1,2]. The rest arises from various post-translational modifications which affect principally the charge, in the case of acetylation, phosphorylation, ADP-ribosylation, or the mass, in the case of ubiquination, of the parent histone molecule.

There are three basic electrophoretic methods for histone fractionation. The first is electrophoresis in acetic acid–urea gels, according to Panyim and Chalkley [3], which separates molecules, to a large extent, on the basis of charge. The second technique is electrophoresis in Tri-

* Corresponding author.

0021-9673/94/$07.00
SSDI 0021-9673(94)00714-4

ton–acetic acid–urea (TAU) gels for separating the various subtypes of H2A, H2B and H3 and their modified forms [4–6]. The third is electrophoresis in sodium dodecyl sulphate (SDS) gels, which separates principally on the basis of mass and, in a few instances, also on the basis of different extents of phosphorylation [7]. As an additional variant, capillary zone electrophoresis (CZE) has been successfully applied to histone typing. CZE is performed in a free phase, in an uncoated capillary, in 110 m*M* phosphate buffer (pH 2.0) containing 0.03% (w/v) hydroxypropylmethyl (HPM)-cellulose [8]. By CZE, rat liver core histones were separated into five major and four minor peaks.

Ideally, isoelectric focusing (IEF), owing to its very high resolving power, could be well suited for histone analysis, provided that a strongly alkaline pH gradient can be established [9]. Indeed, there are only a few reports on IEF of histones in soluble, carrier ampholyte buffers. In one, the following subfractions have been isolated and reported to have p*I* 10.5 10.5 (H1), 10.5 (H2A), 11.0 (H2B) and 11.0 (H3) [10]. Similar data have also been obtained by Kopelovich et al. [11]. In reality, conventional IEF of histones to steady-state conditions seems to be an impossible proposition, owing to the well known fact that [especially in two-dimensional (2-D) maps] it is almost impossible to obtain stable pH gradients above pH 8 [12]. In fact, for most alkaline proteins, one had to resort to non-equilibrium pH gradient electrophoresis [13]. Moreover, in one of the few instances in which such 2-D separations were tried, it was reported that histones gave pronounced artefacts resulting from their interaction with another group of nuclear proteins, the so called "high mobility group" (HMG) non-histone proteins [14].

With the advent of immobilized pH gradients (IPG) [12], owing to the possibility of extending the fractionation interval to pH 10 and above, focusing of histones seemed a more realistic proposition. In fact, early attempts were disastrous. Righetti et al. [15] reported in 1983 that IPG matrices interacted strongly with at least two classes of proteins, histones and the histone-like, HMG-chromatin proteins, forming insoluble complexes. By preparing soluble strings of "carboxyl-surface" homopolymers of p*K* 3.6 and 4.6 Immobilines, sparse along the neutral polyacrylamide coil (5%T, 0%C linear polymers containing 10 m*M* total Immobilines), it was shown that these would complex by ionic interaction with HGMs and precipitate out of solution [15]. Later, when novel Immobiline compounds with a very high p*K* could be synthesized, it was shown to be possible to create stable pH gradients in the pH 10–11 interval, where a number of very alkaline proteins (e.g., lysozyme, cytochrome *c*) [16] and enzymes (e.g., elastase) [17] could be successfully fractionated. However, even in this last case, focusing of histones was not feasible [16].

Based on their amino acid composition, theoretical p*I* calculations predict that most histones should have p*I* values in the pH 11–12 range, and even higher. At such high pH values, Righetti et al. [15] had shown that interaction between histones and the Immobiline matrix should cease (see Fig. 5 in ref. [15]). Thus, in principle, focusing of histones should be feasible provided that one can create such extremely alkaline pH gradients. In this work, we modelled IPG intervals in the pH 10–12 range and achieved some unique separations of histones under true steady-state conditions. To our knowledge, this has not been reported previously.

2. Experimental

2.1. Materials

All IPG experiments were performed in an LKB 2117 Multiphor II horizontal electrophoresis system together with an LKB 2297 Macrodrive 5 power supply and Multitemp II thermostat. IPG gel casting was carried out by using an LKB 2117-903 2-D gradient and Immobiline gel kit. Acrylamide, N,N′-methylenebisacrylamide (Bis), N,N,N′,N′-tetramethylethylenediamine (TEMED), Repel-Silane, Gel Bond PAG film, agarose and Ampholine (pH 9–11) were pur-

chased from Pharmacia–LKB Biotechnology (Uppsala, Sweden). The ten acrylamido buffer kit (p*I* Select) was purchased from Fluka (Buchs, Switzerland). Cytochrome *c* protein standard, the histone preparations II-AS, VI-S (Arg rich, slightly Lys rich), VII-S (slightly Lys rich) and VIII-S (Arg rich, subgroup F), all from calf thymus, and the two classes of detergent used (Tween 20 and Nonidet P-40) were obtained from Sigma (St. Louis, MO, USA) and sorbitol from Merck (Darmstadt, Germany).

2.2. Analytical IPGs

The technique has been described in detail previously [12]. Briefly, an IPG pH 10–12 interval was calculated and optimized with the computer program of Giaffreda et al. [18] (available from Hoefer Scientific, San Francisco, CA, USA). It was immobilized on to a 5%T, 4%C polyacrylamide matrix, typically having a size of 10×11 cm with a 0.5 mm thickness, bound to a polyester foil (Gel Bond PAG). After casting and polymerization, the gels were extensively washed in distilled water, dried and then reconstituted to their original mass by reswelling in a cassette in the presence of different amounts of additives. The optimum reswelling cocktail, able to maintain histones in solution, was found to be 8 *M* urea–1.5% Tween 20–1.5% Nonidet P-40–0.5% Ampholine covering a 2 pH unit interval (pH 9–11) and a 0–10% (anode to cathode) sorbitol gradient. In addition, all gels were run under light paraffin oil, so as to prevent CO_2 adsorption [19]. Protein samples (generally 1–2 mg/ml) were usually loaded (in a 30–50-μl volume) in plastic troughs at the anodic gel side, after a brief prefocusing step (1 h) at low voltage gradients (500 V). Analytical IPGs were run at 10 and 17°C, 1300 V, for a maximum of 4 h. Staining was effected with Coomassie Blue R-250 in 10% acetic acid–30% ethanol in the presence of 0.1% copper sulphate [20].

2.2. Capillary zone electrophoresis

CZE was performed on a Waters Quanta 4000E Ion Analyzer, equipped with Millennium software. The fused-silica capillary was purchased form Polymicro Technologies (Phoenix, AZ, USA) and coated with a covalently bound layer composed of the novel, highly hydrolysis-resistant, highly hydrophilic monomer N-acryloylaminoethoxyethanol (AAEE) (6%T at 0%C) [21] so as to completely suppress electroendosmosis and prevent histone binding to the wall. A mixture of all available histones (II-AS, VI-S, VII-S and VIII-S), at a concentration of 5 mg/ml, was dissolved in 110 m*M* phosphate buffer (pH 2.0) in the presence of 0.03% HPM-cellulose. The capillary (37 cm × 100 μm I.D.) was equilibrated in 50 m*M* Tris–acetate buffer (pH 8.0) in 7 *M* urea. Sample injection was for 8 s at 15 kV and the run was at 15 kV, 95 μA, 25°C, in the cathodic direction. Detection was at 214 nm.

3. Results

Knowing a priori that histones should have p*I* values in the pH 11–12 range, and perhaps even higher, attempts were made to create an extremely alkaline range, encompassing the pH 10–12 interval, with the IPG technique. In principle, such a gradient should not perform well, owing to the strong electrosmotic flow created by the net positive charge of the matrix, forcing a strong solvent flow directed towards the anodic gel extremity. The best gradient we could achieve with existing Immobiline buffers is shown in Fig. 1. The recipe was 10.8 m*M* of p*K* 10.3 with 7.5 m*M* of p*K* 4.6 Immobilines at the acidic extremity and just 10 m*M* of p*K* >13 quaternary base at the cathodic gel end. It should be noted that in fact this gradient has a marked sigmoidal profile. This is due to the paucity of Immobiline buffers in this pH region and because, in the cathodic chamber, the p*K* >13 Immobiline has to act simultaneously as a buffering and titrant ion. By chemical laws, such a gradient could never be linear [22]. Note additionally that the quaternary Immobiline (denoted p*K* >13 species) is used as a free ion to drive the pH in the gel matrix up to 12 (presumably it dictates alone the pH course in the

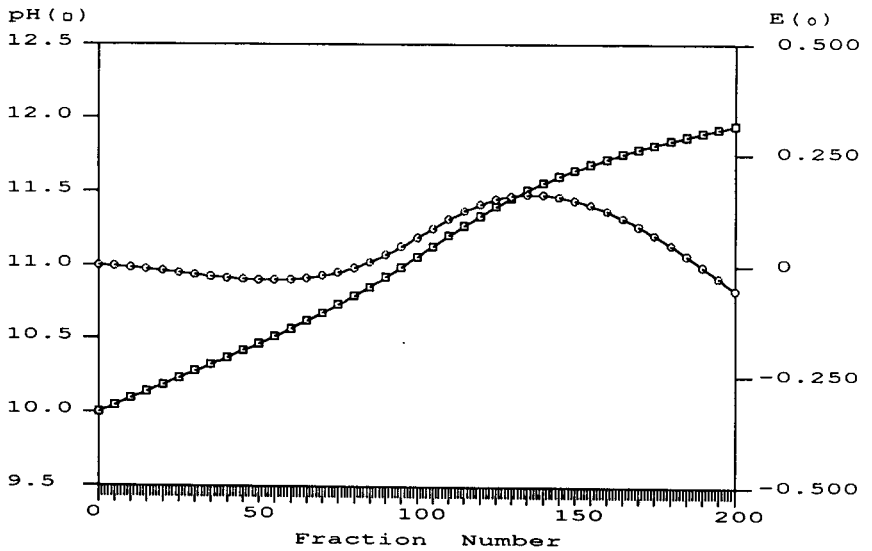

Fig. 1. Profile of a pH 10–12 immobilized gradient. □ = pH gradient; ○ = deviation from linearity. The average buffering power of the gradient is 8 mequiv./l · pH. The gradient was calculated and optimized with the program of Giaffreda et al. [18].

pH 11–12 interval). As it cannot violate the law of electroneutrality, it will then have as a counter ion the free OH^- groups generated by dissociation of water. Note in fact that, in order to reach pH 12, precisely 10 m*M* of p*K* >13 Immobiline are needed, which will be matched by 10 mmol of free OH^- which have to be present in the bulk solvent, by definition, at pH 12.

Fig. 2A shows the separation, in the pH 10–12 IPG gradient outlined above, of two different histone families, the VIII-S (tracks 1–3) and II-AS (tracks 4–6) groups. The separation was performed in 7 *M* urea–1.5% Nonidet P-40–0.5% Ampholine pH 9–11 at 10°C. Although still not optimum, this separation is nevertheless unique in that it displays five major histone bands, focused in a steady-state position in the upper gel region (pH 11–12 interval), i.e., precisely where histones are supposed to band. Moreover, the spectrum of components seems to reflect the amino acid composition of these proteins, since samples 1–3 (VIII-S, Arg-rich) have a much heavier band distribution in the more alkaline positions than samples 4–6 (II-AS, a mixed population of Arg- and Lys-rich), which are more abundant in the lower p*I* positions. It is also clear that fraction VIII-S must contain some components with p*I* 12 and higher, as some bands (see track 3) are seen to reach the cathodic gel extremity and collect just under the electrodic compartment. Fig. 2A in fact does not do justice to the high quality of the separation. Although not visible here, a number of minor components are also sharply focused in the pH 10–11 interval, which appears here as an empty region. Fig. 2B shows an expansion of this region, developed about 20 times more (combined product of time and lens opening). A large number of minor components (more than a dozen, sharply focused bands) are now seen focusing in this region (perhaps representing acetylated and phosphorylated forms). At the bottom of the photograph (ca. pH 10) is seen the imprint of the sample application surface well, of rectangular profile, showing that indeed there is almost no protein precipitation at the sample port.

We further tried a number of experimental modifications in order to improve the pattern of Fig. 2A and B. The final set-up employed consisted in reswelling the gels in 8 *M* urea, 1.5% Nonidet P-40, 1.5% Tween 20 and 0.5% Ampholine (pH 9–11 range) against a 0–10% (anode to cathode) gradient of sorbitol and

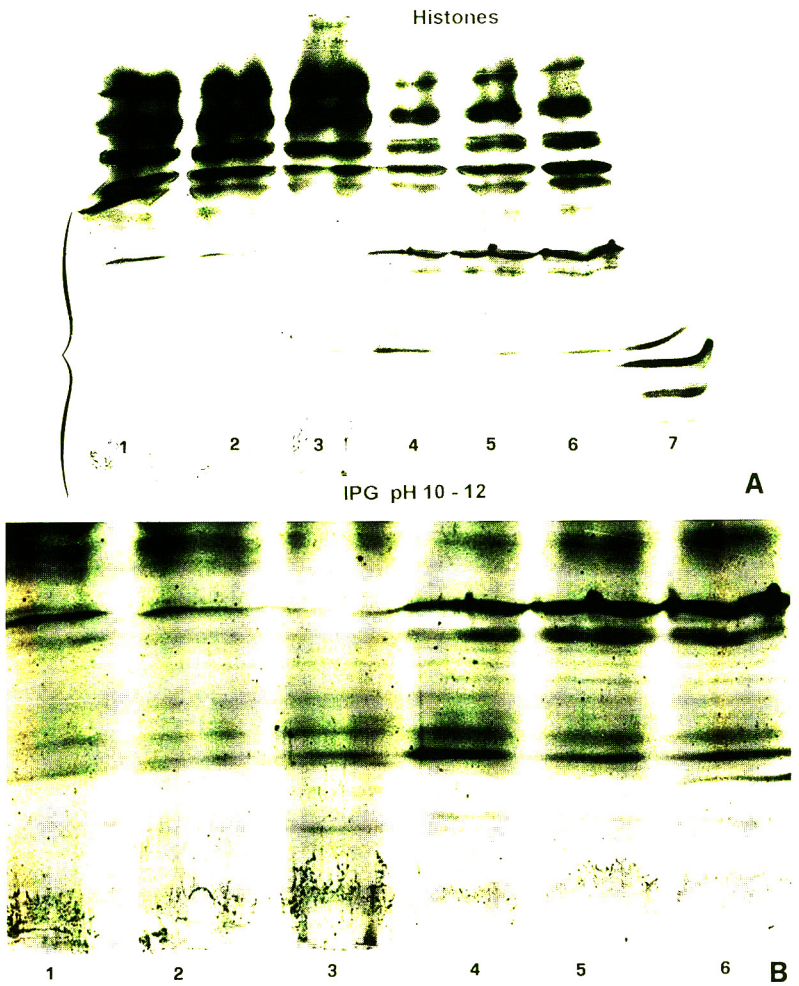

Fig. 2. Focusing of histones in the pH 10–12 interval of Fig. 1. (A) gel 5%T, 4%C polyacrylamide matrix, containing a 10–12 IPG, reswollen in 7 *M* urea, 1.5% Nonidet P-40 and 0.5% Ampholine pH 9–11. The gel was run at 10°C under a layer of light paraffin oil at 500 V for the first hour, followed by increasing voltage gradients, after sample penetration, up to 1300 V for a total of 4 h. The samples (2 mg/ml; 50 μl seeded) were loaded in plastic wells at the anodic gel surface. Staining with Coomassie Brilliant Blue R-250 in Cu^{2+}. Tracks 1–3 = VIII-S histones; 4–6 = II-AS histones; 7 = cytochrome *c* (the main upper band has a p*I* of 10.6). (B) Expansion of the bracketted gel region in (A), developed with a twentyfold increase in exposure (time × lens opening). Note the fine spectrum of sharp bands (more than a dozen) focusing in the pH 10–11 region.

running the gels at 17°C instead of the customary 10°C. The results are shown in Fig. 3, which we believe is the first true equilibrium focusing of histones to be reported. With the markedly improved performance of this gradient, we can now see at least ten major histone fractions (combined among all the different populations) truly focusing in the pH 11–12 range. Moreover, the banding pattern clearly follows the inherent amino acid composition of each fraction: 1 = VII-S, Lys-rich, 3 = mixed-population of Arg- and Lys-rich and 4 = VIII-S, Arg-rich. Although not visible here, the lower gel portion (pH 10–11 interval) again shows the large number of minor components visible in the over-exposed photograph in Fig. 2B.

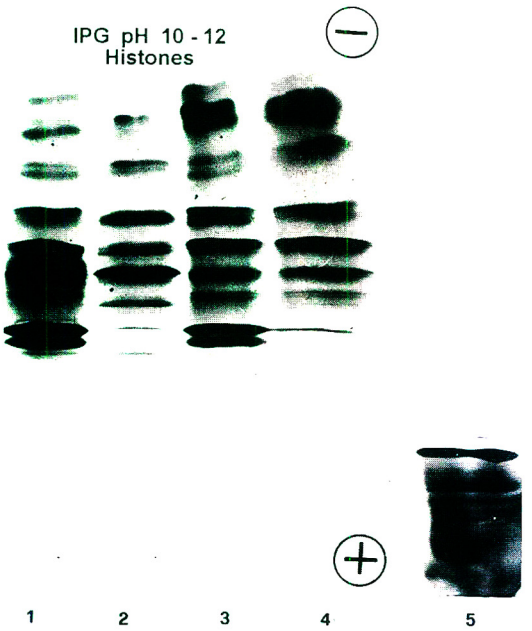

Fig. 3. Focusing of histones in the pH 10–12 interval of Fig. 1. All conditions as in Fig. 2, except that the gel was reswollen in 8 *M* urea–1.5% Nonidet P-40–1.5% Tween 20–0.5% Ampholine pH 9–11 and a 0–10% (anode to cathode) gradient of sorbitol and run at 17°C instead of 10°C as in Fig. 2. Histone samples: 1 = VII-S; 2 = VI-S; 3 = II-AS; 4 = VIII-S. The p*I* 10.6 marker (cytochrome *c*) is in track 5.

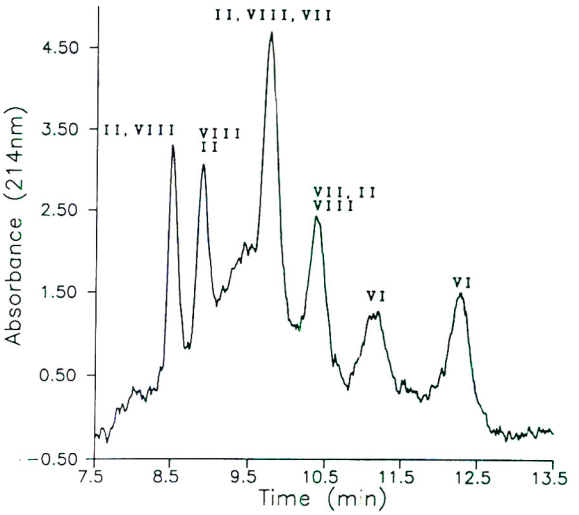

Fig. 4. CZE of histones obtained with a Waters Quanta 4000E Ion Analyzer. Capillary, 37 cm × 100 μm I.D., coated with a layer of poly(AAEE); running buffer, 50 m*M* Tris–acetate (pH 8.0) in 7 *M* urea; sample, mixture of all histone fractions (5 mg/ml) dissolved in 110 m*M* phosphate buffer (pH 2.0) and 0.03% HMP-cellulose; injection, 8 s at 15 kV; run, 15 kV, 95 μA, 25°C; detection at 214 nm.

As we became aware, during this work, of the data of Lindner et al. [8] on the CZE of histones, we tried to compare histone patterns under the two different electrokinetic protocols. Fig. 4 shows the CZE profile of a mixture of all histone samples, run at pH 8.0 (7 *M* urea) in a coated capillary. Six major fractions are resolved, identified by running separately the four different histone standards. Note that here the transit times should follow the p*I* spectrum, the early-eluting peaks representing the p*I* 12 species and the slow-migrating bands the p*I* 11 fractions.

4. Discussion

It might be asked how well our histone p*I* data are correlated with the literature in the field. Owing to recent progress in nucleic acid research, an exponentially growing number of protein sequences are being published, derived from gene sequences. We have taken, at random, a number of histone sequences published in the period 1987–89 and calculated the resulting p*I* value with the help of our IPG program [18] (modified not to account for the ionic product of water and without any correction for activity coefficients of ions). For example, for mouse (*Mus musculus*) Liu et al. [23] have reported a 125 amino acid (AA) sequence for histone H2B, resulting in an M_r of 13 765 and a calculated p*I* of 11.45. In the same species, for histone H1.0, a 193 AA sequence has been published, resulting in an M_r of 20 715 and a p*I* of 11.95 [24]. In a third report, mouse histone H1.1 was given an AA sequence of 211, resulting in an M_r of 21 135 and a p*I* of 11.84 [25]. In muscovy duck, histone H2A was assigned an AA sequence of 128, resulting in an M_r of 13 825 and a p*I* of 11.98 [26], while histone H2B had a sequence of 125 AA, resulting in an M_r of 13 765 and a p*I* of 11.37 [26]. In *Tetrahymena pyriformis*, Histone H1 had a sequence of 165 AA, an M_r of 17 943 and a p*I* of 11.33 [27]. In *Caenorhabditis elegans*,

histone H1.1 was assigned a sequence of 207 AA, an M_r of 21 263 and a p*I* of 11.80 [28]. In *Homo sapiens*, histone H2A.X was given a sequence of 142 AA, with a corresponding M_r of 15 013 and a p*I* of 11.97 [29]. The present data on p*I* values of all classes of histones fall nicely in all these literature ranges. However, they do not agree with the data of Valkonen and Piha [30], who reported, in conventional IEF, p*I* values ranging from 9 (histone H_1) to 10.5 (histone H_4).

It might be asked what effects the various additives have on the true p*I* values of histones. We have on purpose avoided giving precise p*I*s, as pH measurements in such extremely alkaline gradients are besieged by severe problems. We have reported, however, that 8 *M* urea increases the p*K* values of both acidic and alkaline Immobilines by as much as 1 pH unit [12]. It is nevertheless to be expected that also the p*K* values of acidic and basic groups of proteins will shift to a similar extent so that, on a relative scale, the p*I* positions will be very much the same as predicted by the theoretical curve in Fig. 1. The other additives should not have, per se, much effect on the IPG interval reported here. We have already described that detergents do not modify the p*K* values of Immobilines [12]; in addition, the Ampholines used focus only in the lower IPG interval (pH 10–11), as also visible from their refractive lines, once focused. Additionally (and also in order to answer to one referee's comment), it would have been useful to compare gel slab focusing with capillary IEF and not with capillary zone electrophoresis. The problem is that there does not seem to be, at present, an easy way to perform IPGs in capillaries, owing to difficulties in pumping in such minute gradient volumes, amplified also by major difficulties in avoiding interference from silanols at such extremely alkaline pH values.

Focusing with IPGs at pH extremes (both acidic and alkaline) requires respect of basic laws in physics. In early attempts made in 1985 by one of us (P.G.R., on a summer sabbatical in Tucson, AZ, in M. Bier's laboratory), the mildly forbidden pH 3–4 region was explored, in an attempt to focus dansylated amino acids [31]. We had severe experimental problems, as we overlooked the fact that, at pH 3, the gel has to bear a 1 m*M* net negative charge, which results in electroendosmotic (EEO) flow of positive charges (with their hydration water) to the cathode and on complete anode dehydration (with severe risks of sparks and gel burning). In those days, EEO was not in the limelight as it is today, owing to the advent of the CZE technique. As a result of these experiments, we had to include, in our IPG computer modelling, the contribution of the dissociation products of water to conductivity and buffering capacity (which can be neglected in the pH 4–10 range) [32]. If things were so difficult at pH 3–4, then they should be impossible in the pH 10–12 range where, at the cathodic gel extreme, the gel should bear a 10 m*M* net positive charge and the EEO flux should be ten times higher. The fact is that the combination of 8 *M* urea and a sorbitol gradient acts as a very efficient conductivity quencher, markedly reducing the anode-directed water transport. Quenching of conductivity is also necessary in order to sharpen the highest p*I* components. It is in fact seen in Fig. 2A that the higher p*I* species are diffuse, as opposed to the sharper lower p*I* components. The pattern in Fig. 2A resembles an elution profile in chromatography, where late-eluting peaks are more diffuse. The mechanism here is different, however: the voltage gradient at the pH 12 extreme is 100 times less than at the pH 10 gel end, as it follows the 100-fold difference in conductivity between the two gel extremes. We tried to even out this huge difference by the combined action of two additives: the small amount of carrier ampholytes, which focus only in the pH 10–11 interval, increasing the conductivity in this region, and the sorbitol gradient, which quenches the conductivity in the pH 11–12 interval. This seems to be a successful strategy, as shown in Fig. 3, a truly amazing achievement for any focusing system.

Acknowledgements

This work was supported in part by grants from the Radius Project in Biotechnology (ESA,

Paris), by Progetto Strategico Tecnologie Chimiche Innovative (CNR, Comitato Chimica) and P.F. Biotecnologia e Biostrumentazione (CNR, Rome).

References

[1] M.K. Urban, S.G. Franklin and A. Zweidler, *Biochemistry*, 18 (1979) 3952–3960.
[2] R.D. Cole, *Anal. Biochem.*, 136 (1984) 24–30.
[3] S. Panyim and R. Chalkley, *Arch. Biochem. Biophys.*, 130 (1969) 337–43.
[4] C.R. Alfageme, A. Zweidler, A. Mahowald and L.H. Cohen, *J. Biol. Chem.*, 249 (1974) 3729–3734.
[5] L.H. Cohen, K.M. Newrock and A. Zweidler, *Science*, 190 (1975) 994–996.
[6] A. Zweidler, *Methods Cell Biol.*, 17 (1978) 223–233.
[7] M. Blumenfeld, *Biochem. Genet.*, 17 (1979) 163–169.
[8] H. Lindner, W. Helliger, A. Dirschlmayer, M. Jaquemar and B. Puschendorf, *Biochem. J.*, 283 (1992) 467–471.
[9] P.G. Righetti, *Isoelectric Focusing: Theory, Methodology and Applications*, Elsevier, Amsterdam, 1983.
[10] G.E. Dobretsov, T.A. Borschevskaya, V.A. Petrov and F.V. Saevsky, *Biofizika*, 17 (1972) 749–755.
[11] L. Kopelovich, G. Wolfe and L. Pfeffer, *Proc. Soc. Exp. Biol. Med.*, 151 (1976) 400–406.
[12] Righetti, P.G., *Immobilized pH Gradients: Theory and Methodology*, Elsevier, Amsterdam, 1990, pp. 207–210.
[13] P.Z. O'Farrell, H.M. Goodman and P.H. O'Farrell, *Cell*, 12 (1977) 1133–1142.
[14] L. Wen, R.K. Tweten, P.J. Isackson, J.J. Iandolo and G.R. Reeck, *Anal. Biochem.*, 132 (1983) 294–304.
[15] P.G. Righetti, M. Delpech, F. Moisand, J. Kruh and D. Labie, *Electrophoresis*, 4 (1983) 393–398.
[16] C. Gelfi, M.L. Bossi, B. Bjellqvist and P.G. Righetti, *J. Biochem. Biophys. Methods*, 15 (1987) 41–48.
[17] P.K. Sinha and P.G. Righetti, *J. Biochem. Biophys. Methods*, 15 (1987) 199–206.
[18] E. Giaffreda, C. Tonani and P.G. Righetti, *J. Chromatogr.*, 630 (1993) 313–327.
[19] K. Altland and A. Banzhoff, *Electrophoresis*, 7 (1986) 529–553.
[20] P.G. Righetti and J.W. Drysdale, *J. Chromatogr.*, 98 (1974) 271–321.
[21] M. Chiari, C. Micheletti, M. Nesi, M. Fazio and P.G. Righetti, *Electrophoresis*, 15 (1994) 177–186.
[22] E. Gianazza, G. Dossi, F. Celentano and P.G. Righetti, *J. Biochem. Biophys. Methods*, 8 (1983) 109–133.
[23] T.J. Liu, L. Liu and W.F. Marzluff, *Nucleic Acid Res.*, 15 (1987) 3023–3039.
[24] A. Alonso, B. Breuer, H. Bouterfa and D. Doenecke, *EMBO J.*, 7 (1988) 3003–3008.
[25] G. Cheng, A. Nandi, S. Clerk and A.I. Skoultchi, *Proc. Natl. Acad. Sci. U.S.A.*, 86 (1989) 7002–7006.
[26] R. Toenjes, K. Munk and D. Doenecke, *J. Mol. Evol.*, 28 (1989) 200–211.
[27] T. Hayashi, H. Hayashi and K. Iwai, *J. Biochem.*, 102 (1987) 369–376.
[28] J.R. Vanfleteren, S.M. Van Bun and J.J. Van Beeumen, *Biochem. J.*, 255 (1988) 647–652.
[29] C. Mannironi, W.M. Bonner and C.L. Hatch, *Nucleic Acid Res.*, 17 (1989) 9113–9126.
[30] K.H. Valkonen and R.S. Piha, *Anal. Biochem.*, 104 (1980) 499–505.
[31] A. Bianchi-Bosisio, P.G. Righetti, N.B. Egen and M. Bier, *Electrophoresis*, 7 (1986) 128–133.
[32] R.A. Mosher, M. Bier and P.G. Righetti, *Electrophoresis*, 7 (1986) 59–66.

ELSEVIER

Journal of Chromatography A, 686 (1994) 129–142

JOURNAL OF CHROMATOGRAPHY A

Separation and characterization of tetracycline antibiotics by capillary electrophoresis

Marina F.M. Tavares, Victoria L. McGuffin*

Department of Chemistry, Michigan State University, East Lansing, MI 48824, USA

First received 5 October 1993; revised manuscript received 28 June 1994

Abstract

The electrophoretic behavior of the antibiotics tetracycline, chlortetracycline, demeclocycline, oxytetracycline, doxycycline, methacycline and minocycline has been characterized by capillary electrophoresis in phosphate buffer solutions in the pH range 4–11. A complete set of acid–base equilibrium constants and electrophoretic mobilities was determined and, subsequently, was used in a computer-assisted optimization program to assess the separation of the tetracyclines. Under the predicted optimum conditions (pH 7.5, 18.2 m*M* ionic strength, 4.3 m*M* buffer concentration, and constant current of 20 μA), the separation was performed satisfactorily and all tetracyclines were readily identified. Moreover, the common impurities in tetracycline resulting from dehydration and epimerization reactions were discriminated under the same conditions. The determination of tetracycline, doxycycline and minocycline was performed in commercially available pharmaceutical formulations. During the dissolution of the contents of hard-filled capsules, a minimum recovery of 95% of the active ingredient was obtained. A calibration curve of peak height versus concentration gave a slope of $6.15 \cdot 10^{-4}$ cm M^{-1}, intercept of $-1.18 \cdot 10^{-5}$ cm, and coefficient of determination equal to 0.9989. The analysis using UV-absorbance detection at 260 nm provided a detection limit of $1 \cdot 10^{-5}$ *M* at a signal-to-noise ratio of approximately 3, with a linear range of two orders of magnitude.

1. Introduction

Tetracyclines are a group of clinically important natural products and semi-synthetic derivatives, characterized by a broad-spectrum activity against pathogenic microorganisms [1,2]. In addition to their extensive therapeutical use, these drugs have found application in the preservation of harvested fruits and vegetables, extermination of insect pests, and as an animal feed supplement [3–5].

All members of the group possess closely related chemical structures, derived from a common hydronaphthacene nucleus containing four fused rings [1,5], as shown schematically in Fig. 1. The presence of multiple functional groups with acid–base properties confers an amphoteric character to the tetracyclines, most of which exhibit an isoelectric point between 4 and 6. The same structural features contribute to their high solubility in polar organic solvents and water, which is enhanced at low pH. These compounds undergo complex formation and precipitation reactions with a variety of metallic cations, among which the complexes with calcium, mag-

* Corresponding author.

0021-9673/94/$07.00
SSDI 0021-9673(94)00668-7

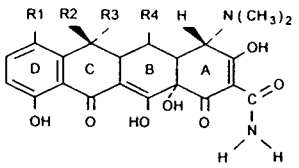

NAME	SYMBOL	R1	R2	R3	R4
TETRACYCLINE	TC	H	OH	CH_3	H
CHLORTETRACYCLINE	CTC	Cl	OH	CH_3	H
DEMECLOCYCLINE	DMCC	Cl	OH	H	H
OXYTETRACYCLINE	OTC	H	OH	CH_3	OH
DOXYCYCLINE	DOC	H	H	CH_3	OH
METHACYCLINE	MTC	H	$=CH_2$		OH
MINOCYCLINE	MNC	$N(CH_3)_2$	H	H	H

Fig. 1. Chemical structures of common tetracycline antibiotics.

nesium, and aluminum have been particularly well characterized [5].

Commercially available tetracycline and tetracycline derivatives may contain significant amounts of degradation products [6–8]. These contaminants are often isomers with only minor structural differences from the original precursor. The most important contaminants in tetracycline are the products of epimerization, dehydration and combined epimerization–dehydration reactions, as shown schematically in Fig. 2. Epianhydrotetracycline has been implicated in several toxic manifestations, such as renal dysfunction, caused by ingestion of degraded tetracycline products [1].

The analytical methodology applied to tetracyclines has supported microbiological production, synthetic and pharmacological studies and clinical applications. Several techniques have been employed [2,5,9], including microbiological assays [5], spectrophotometry [10–12], phosphorimetry [13], chemiluminescence [14], as well as chromatographic and flow injection methods [15]. Many of these methods do not provide a

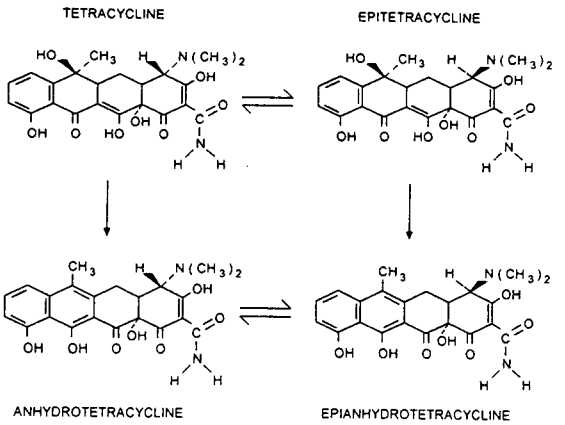

Fig. 2. Decomposition of tetracycline by epimerization and dehydration pathways.

precise and accurate means to determine the tetracycline content in the presence of known degradation products. In particular, the microbiological methods lack specificity, since the total drug activity is estimated without correlation to the chemical structure. Also, metabolites and degradation products with no antimicrobial activity cannot be determined by these methods. Among the chromatographic techniques, thin-layer, paper and column chromatography followed by UV spectrometric assay have been used extensively [16–22]. However, these methods have proven to be laborious, often require extensive sample pretreatment, and generally exhibit poor sensitivity and precision. Gas chromatographic methods, although rapid and specific, require derivatization of the polar functional groups under carefully controlled conditions. Consequently, their application is limited to antibiotics that are thermally stable after derivatization. Liquid chromatography, especially the reversed-phase and ion-exchange modes, has become the method of choice for tetracyclines in recent years [6–8,23–30]. Some of these procedures, however, use mobile phases of relatively low pH at which the tetracyclines are known to epimerize. Other methods employ mobile phases containing high salt concentration which, in combination with the low pH, can be deleterious to the column stability. Moreover, because of the structural similarities of the tetra-

cyclines and their potential contaminants, complete resolution is not usually achieved.

The physicochemical properties of tetracyclines, particularly their ionic nature, multiple ionization sites, and water solubility, make them suitable for electrophoretic analysis. Capillary electrophoresis (CE) has gained increased acceptance for the analysis of pharmaceuticals [9,31–34], as a result of relevant features such as high efficiency, high speed, full automation and compatibility with a variety of detection schemes. Based on the preliminary studies of antibiotics by Yeo et al. [34], we have explored the use of CE as a promising alternative to the available analytical methodologies for tetracyclines. A computer-assisted optimization program developed in previous work [35] was used to assess the separation of seven naturally occurring and synthetically produced tetracyclines, as well as their decomposition products. Based on this program, an optimized analytical method was developed and applied to the quantitation of tetracyclines in commercially available pharmaceutical drugs.

2. Experimental

2.1. Capillary electrophoresis system

The system consisted of a regulated high-voltage d.c. power supply (Model EH50R0.19XM6; Glassman High Voltage, Whitehouse Station, NJ, USA), operated under constant-current conditions. The power supply was connected via platinum rod electrodes to two small reservoirs containing the solution under investigation. Fused-silica capillary tubing (Polymicro Technologies, Phoenix, AZ, USA), with dimensions of 111.9 cm total length × 75 μm I.D. × 375 μm O.D., was immersed at each end in the solution reservoirs. The capillary surface was conditioned prior to use by rinsing with 1 *M* sodium hydroxide for 10 min, followed by rinsing with the solution under investigation, preferably overnight but at least for a 2-h period. During operation, the capillary was maintained at 25.0°C by means of a thermostatically controlled water bath (Model RTE 9B; Neslab Instruments, Portsmouth, NH, USA). Injection was performed hydrodynamically by maintaining a 2-cm difference in height between the liquid levels at the inlet and outlet reservoirs during a 1-min period. Detection was performed by means of an on-column UV-absorbance spectrophotometer (Model UVIDEC 100-V; Jasco, Tokyo, Japan), at a fixed wavelength of 260 nm. A detection window of 0.5 cm length was created by removing the polyimide coating from the capillary at a distance of 43.4 cm. The electroosmotic flow velocity was determined by the resistance-monitoring method [36].

2.2. Reagents

The phosphate buffer solutions were prepared from reagent-grade chemicals and deionized distilled water. In order to control both the buffer concentration and ionic strength, the solutions were formulated to contain sodium chloride in addition to the sodium salts of phosphoric acid. For any given pH, the total concentration of sodium was maintained constant and the ratio of sodium from each source, sodium chloride and buffer salts, was equal to unity. For determination of the acid–base equilibrium constants and electrophoretic mobilities, the buffer was varied from pH 4 to 11 with a total sodium concentration of 10 m*M*. For the separation of tetracycline standards and samples, the solutions were buffered at pH 7.5 with a total sodium concentration of 15 m*M*.

The antibiotics tetracycline (TC), chlortetracycline (CTC), demeclocycline (DMCC), oxytetracycline (OTC), doxycycline (DOC), methacycline (MTC) and minocycline (MNC) were obtained as reagent-grade standards (Sigma, St. Louis, MO, USA). Stock aqueous solutions of individual tetracycline standards as well as mixtures containing different combinations of the standards were prepared at a nominal concentration of 5 m*M* in pH 7.5 phosphate buffer solution. For the calibration curve, a 1 m*M* standard solution of tetracycline was diluted consecutively to 0.5, 0.1, 0.05 and 0.01 m*M* with the same buffer solution and was analyzed imme-

diately to prevent losses by adsorption on the glassware [37].

Pharmaceutical formulations of tetracycline (250 mg), doxycycline (50 mg) and minocycline (100 mg) were obtained as hard-filled capsules from Warner-Chilcott Labs. (Warner-Lambert, Morris Plains, NJ, USA). An appropriate mass of the drug was dissolved in pH 7.5 phosphate buffer to make a solution of 25 m*M* nominal concentration. The undissolved filler and binder materials were removed by centrifugation. An aliquot of the supernatant solution was then diluted to 5 m*M* concentration with pH 7.5 phosphate buffer solution and analyzed immediately.

In order to study the decomposition of tetracycline, a 25 m*M* solution was prepared by complete dissolution of an appropriate weight of the standard in hydrochloric acid at pH 2. This sample was heated at 70°C for 1 h, cooled in an ice bath, and then diluted to 5 m*M* concentration with pH 7.5 phosphate buffer solution. The sample was analyzed by reversed-phase liquid chromatography according to the method of Mack and Ashworth [7] in order to confirm the formation of the epi-, anhydro- and epianhydro-decomposition products of tetracycline.

2.3. Data processing

All data processing and numerical calculations were performed on a 80-386 microprocessor-based computer in a spreadsheet format (Microsoft Excel, version 4.0; Microsoft, Redmond, WA, USA). The optimization program developed in previous work [35] was written in the Forth-based programming language Asyst (version 2.1; Keithley Asyst, Rochester, NY, USA) to be executed on a 80-286 microprocessor-based computer.

3. Results and discussion

3.1. Characterization of the electrophoretic behavior of tetracyclines

In order to characterize the electrophoretic behavior of tetracyclines, knowledge of the acid–base equilibrium constants and electrophoretic mobilities of the individual species is required. The equilibrium constants (K_a) of very few tetracyclines have been reported in the literature [5]. After an initial misassignment [38] the attribution of pK_a values to specific functional groups in the molecule was reevaluated [39] and is now generally accepted. The most acidic group of tetracycline, with a typical pK_a value of approximately 3.3, is the hydroxyl group of the tricarbonyl system in ring A (Fig. 1). The second equilibrium constant, with a pK_a value of approximately 7.6, corresponds to the dicarbonyl system between rings B and C. The third constant, with a pK_a value of approximately 9.7, is assigned to the dimethylamine functionality in ring A. The highest equilibrium constant, with a pK_a of 10.7, was recently attributed to the phenolic group in ring D [39].

The electrophoretic determination of these constants is based on experimental measurements of effective mobility as a function of pH [35]. In CE, the effective mobility (μ_{eff}) of a solute (i) comprised of several species (j) in dynamic acid–base equilibrium, is related to the migration time of the substance (t_i) from the injector to the detector position (L_{det}) according to:

$$\mu_{eff,i} = \sum (\alpha_j \mu_j) = \frac{L_{tot} L_{det}}{V t_i} - \mu_{osm} \quad (1)$$

where L_{tot} is the total capillary length, V is the voltage, μ_{osm} is the electroosmotic mobility, μ_j is the electrophoretic mobility and α_j is the distribution function of species j. The distribution functions are related to the pH and to the acid–base equilibrium constants or pK_a values of the solutes under consideration [40]. Experimental values of the effective mobility, determined over a broad pH range, can be analyzed by a numerical regression procedure where the equilibrium constants and electrophoretic mobilities serve as adjustable parameters [35]. The best values for these parameters are then determined by the least-squares method. Table 1 presents the constants determined by the above procedure for seven members of the tetracycline group. All constants in Table 1 have been corrected to the

Table 1
Acid–base equilibrium constants and electrophoretic mobilities of tetracyclines at 25°C, corrected to the conditions of zero ionic strength

Solute	Equilibrium constant[a]					Electrophoretic mobility[a] ($\times 10^5$ cm^2 V^{-1} s^{-1})					
	$pK_{(+2,+1)}$	$pK_{(+1,0)}$	$pK_{(0,-1)}$	$pK_{(-1,-2)}$	$pK_{(-2,-3)}$	$\mu_{(+2)}$	$\mu_{(+1)}$	$\mu_{(0)}$	$\mu_{(-1)}$	$\mu_{(-2)}$	$\mu_{(-3)}$
TC	–	3.46	7.39	9.59	12.1	–	15.4	1.30	−15.2	−33.6	−64.7
CTC	–	3.60	7.52	9.88	10.4	–	19.5	−1.75	−19.1	−30.5	−43.8
DMCC	–	3.64	6.81	9.43	12.1	–	14.4	−0.04	−13.3	−36.8	−44.6
OTC	–	3.57	7.49	9.44	10.5	–	16.4	−0.60	−15.8	−34.7	−42.3
DOC	–	3.56	7.48	9.36	12.1	–	13.3	0.41	−12.5	−35.9	−57.7
MTC	–	3.56	7.29	9.46	12.0	–	14.3	0.02	−14.2	−34.4	−66.1
MNC	4.22[b]	4.22[b]	6.86	9.32	11.9	32.5	–	3.62	−7.75	−31.5	−53.7

[a] Subscripts denote charge of the species.
[b] Average pK_a corresponding to protonation of the amine groups in rings A and D (Fig. 1).

condition of zero ionic strength [41], and are in good agreement with values previously reported in the literature [39].

A graph of the effective mobility versus pH is a valuable tool for the preliminary assessment of a separation, because it can indicate regions of pH where the solute mobilities differ and the separation is likely to be achieved. The effective mobility curves displayed in Fig. 3A–C correspond to selected mixtures of tetracyclines containing four, five, and seven components, respectively. It is evident that the electrophoretic behavior of the tetracyclines is quite similar throughout the entire pH range and the separation appears to be very difficult. Consequently, a systematic procedure to determine the optimum separation conditions is highly desirable.

3.2. Optimization of the electrophoretic separation of tetracyclines

The separation of the tetracyclines was approached by means of a computer-assisted optimization routine developed in previous work [35]. In this approach, the quality of the separation is assessed by means of a response function developed originally for chromatographic separations [42], designated the chromatographic resolution statistic (CRS):

$$\mathrm{CRS} = \left\{ \sum_{i=1}^{n-1} \left[\frac{(R_{i,i+1} - R_{\mathrm{opt}})^2}{(R_{i,i+1} - R_{\mathrm{min}})^2 R_{i,i+1}} \right] + \sum_{i=1}^{n-1} \frac{R_{i,i+1}^2}{(n-1)R_{\mathrm{avg}}^2} \right\} \cdot \frac{t_f}{n} \quad (2)$$

where $R_{i,i+1}$ is the resolution between pairs of adjacent solute zones, R_{avg} is the average resolution of all solute pairs, R_{opt} is the optimum desired resolution, R_{min} is the minimum acceptable resolution, t_f is the migration time of the last solute, and n is the number of solutes in the sample. The chromatographic resolution statistic considers the resolution of all solutes in the sample, rather than solely the least-resolved pair, and incorporates three important aspects of the separation. The first term in Eq. 2, named the resolution term, evaluates the resolution between all adjacent solute zones in comparison to the defined values for optimum and minimum resolution. The resolution term decreases as $R_{i,i+1}$ approaches R_{opt} and reaches the minimum value of zero when $R_{i,i+1}$ is exactly equal to R_{opt}. Any further increase in resolution offers no additional improvement in the quality of the separation, hence the resolution term is maintained at a constant value close to zero. The resolution term increases rapidly as $R_{i,i+1}$ approaches R_{min} and becomes undefined when $R_{i,i+1}$ is exactly equal to R_{min}. The second term

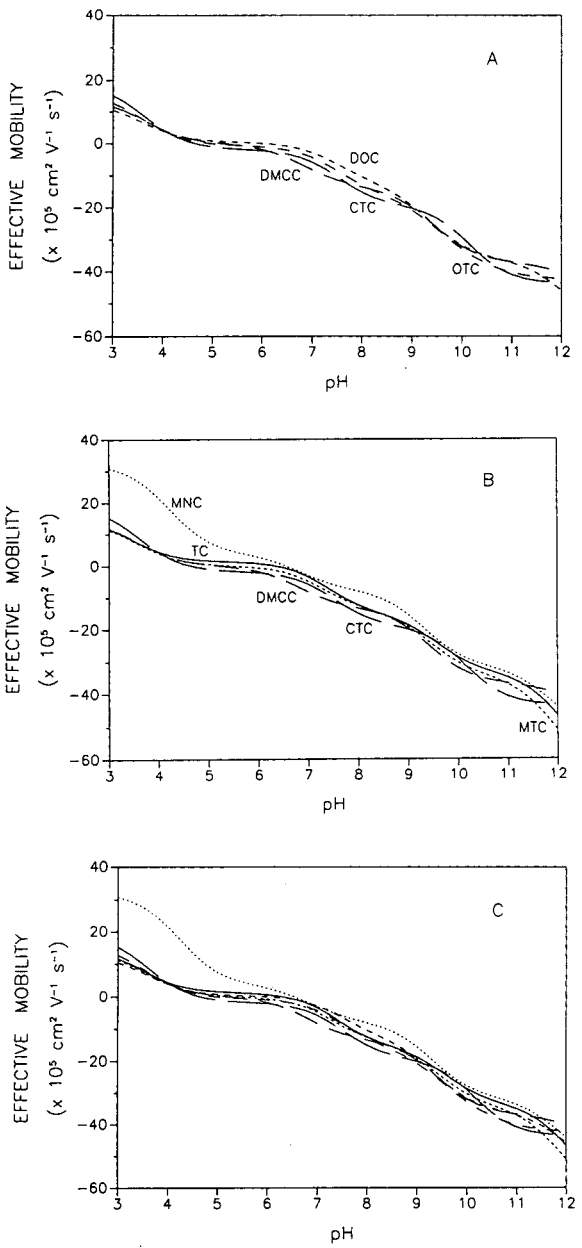

Fig. 3. Effective mobility curves as a function of pH for selected four- (A), five- (B) and seven- (C) component mixtures of tetracyclines at 25°C, corrected to the conditions of zero ionic strength.

of Eq. 2, named the distribution term, considers the relative spacing of the solute zones. The distribution term approaches a minimum value of unity when the resolution of each solute pair is equal to the average resolution, which is the case when all zones are uniformly spaced. The final multiplier term in Eq. 2 takes into consideration the analysis time and the complexity of the sample.

The resolution between adjacent solute zones is defined as the difference between their mean migration time (t) divided by their average temporal base width (w):

$$R_{i,i+1} = \frac{2(t_{i+1} - t_i)}{w_i + w_{i+1}} \tag{3}$$

The migration time of each zone to the detector position is determined by the net rate of zone migration (v_i), which is a vectorial summation of the electrophoretic (v_{ep}) and electroosmotic (v_{osm}) velocities:

$$t_i = \frac{L_{det}}{v_i} = \frac{L_{det}}{v_{ep} + v_{osm}} = \frac{L_{det} L_{tot}}{(\mu_{ep} + \mu_{osm})V} \tag{4}$$

According to Eq. 4, the prediction of migration time requires knowledge of the electrophoretic and electroosmotic mobilities. Hence, the computer program is structured on theoretical models for these migration processes that are applicable under a variety of operational conditions. The electrophoretic migration subroutine is based on classical equilibrium calculations [35] and requires as input the acid–base equilibrium constants and electrophoretic mobilities of the tetracyclines (Table 1). The electroosmotic migration may be determined from experimental measurements or, if not available, from a theoretical model. In this model [36], a mathematical function that relates the zeta potential to the pH and sodium concentration of the buffer solution is utilized to calculate the electroosmotic mobility.

The base width of a normally distributed zone is proportional to the standard deviation of the temporal distribution (τ):

$$w_i = 4\tau \tag{5}$$

where τ is expressed in time units, and is related

to the standard deviation of the spatial distribution (σ) by means of the zone velocity:

$$\tau = \frac{\sigma}{v_i} \quad (6)$$

The variance of the spatial distribution (σ^2) arises from several dispersive phenomena that occur during the migration of the solute zone. If these processes are independent, then the variances are statistically additive [43]:

$$\sigma^2 = \sum \sigma_n^2 \quad (7)$$

where σ_n^2 represents the individual contributions to the total variance. Among the dispersive mechanisms, the contributions to the zone variance resulting from longitudinal diffusion as well as finite injection and detection volumes are considered in the optimization program.

An overall expression for resolution in Eq. 3 can be derived by combining appropriately Eqs. 4–7. The resolution of each solute pair is then used to determine the overall quality of the separation by means of the CRS function in Eq. 2. In order to implement these calculations, input values for parameters related to the buffer composition (pH, ionic strength and concentration), capillary dimensions (diameter and length), and instrumental parameters (applied voltage or current) must be specified. By methodically varying these parameters and evaluating the overall quality of the separation by means of the CRS function, the computer program can be used to predict the experimental conditions required for optimal separation of the solutes.

The optimization of the tetracycline separation was simulated using instrumental parameters and capillary dimensions that are representative of the experimental system (see above). In the search for the optimum conditions, the current was varied from 5.00 to 22.50 μA with increments of 0.25 μA, the pH from 4.0 to 11.0 with 0.1 increments, the ionic strength from 5.00 to 22.50 m*M* with 0.25 m*M* increments, and the buffer concentration from 0.50 to 11.00 m*M* with 0.15 m*M* increments. The surface maps and corresponding contour plots presented in Figs. 4 and 5 allow for visual inspection of the CRS response function within the defined range of parameters. Although there are several local minima of the CRS function, the most promising region occurs between pH 7 and 8. Within this region, the CRS function decreases rapidly as the current approaches 20 μA (Figs. 4A and 5A). The function behaves similarly as the buffer concentration approaches 4 m*M* (Figs. 4B and 5B). In contrast, the ionic strength surface map is composed of several very sharp minima in the region between 15 and 20 m*M*, which indicates that this variable must be controlled carefully.

The computer program predicts the correct elution order for all tetracyclines, and provides a reasonable estimate of migration time and peak width, as demonstrated in Table 2. The agreement between predicted and experimental values for migration time and peak width is typically 1.7 and 23%, respectively.

3.3. Analytical determination of tetracyclines

The experimental separation of the seven tetracyclines was performed in the vicinity of the optimal conditions, as shown in Fig. 6C. Because of similarities in the equilibrium constants and mobilities of the tetracyclines, complete separation is not possible under the predicted optimum conditions. However, qualitative analysis may be performed since all tetracyclines may be identified unequivocally in the mixture. Quantitative analysis is possible for selected mixtures containing four and five tetracyclines (Fig. 6A and B, respectively), as suggested by visual inspection of the effective mobility curves (Fig. 3A and B, respectively). This analysis represents an improvement over the available methodology for tetracyclines, since there is a substantial gain in efficiency (ca. $3 \cdot 10^4$ theoretical plates) and reduction in analysis time (< 6 min). Reversed-phase liquid chromatographic methods, which are among the most commonly employed methods for tetracyclines, provide efficiencies on the order of $3 \cdot 10^3$ plates and analysis times as long as 30 min for typical mixtures [2].

A common concern during the manufacture and storage of tetracycline antibiotics is the control of impurities. Tetracyclines can degrade

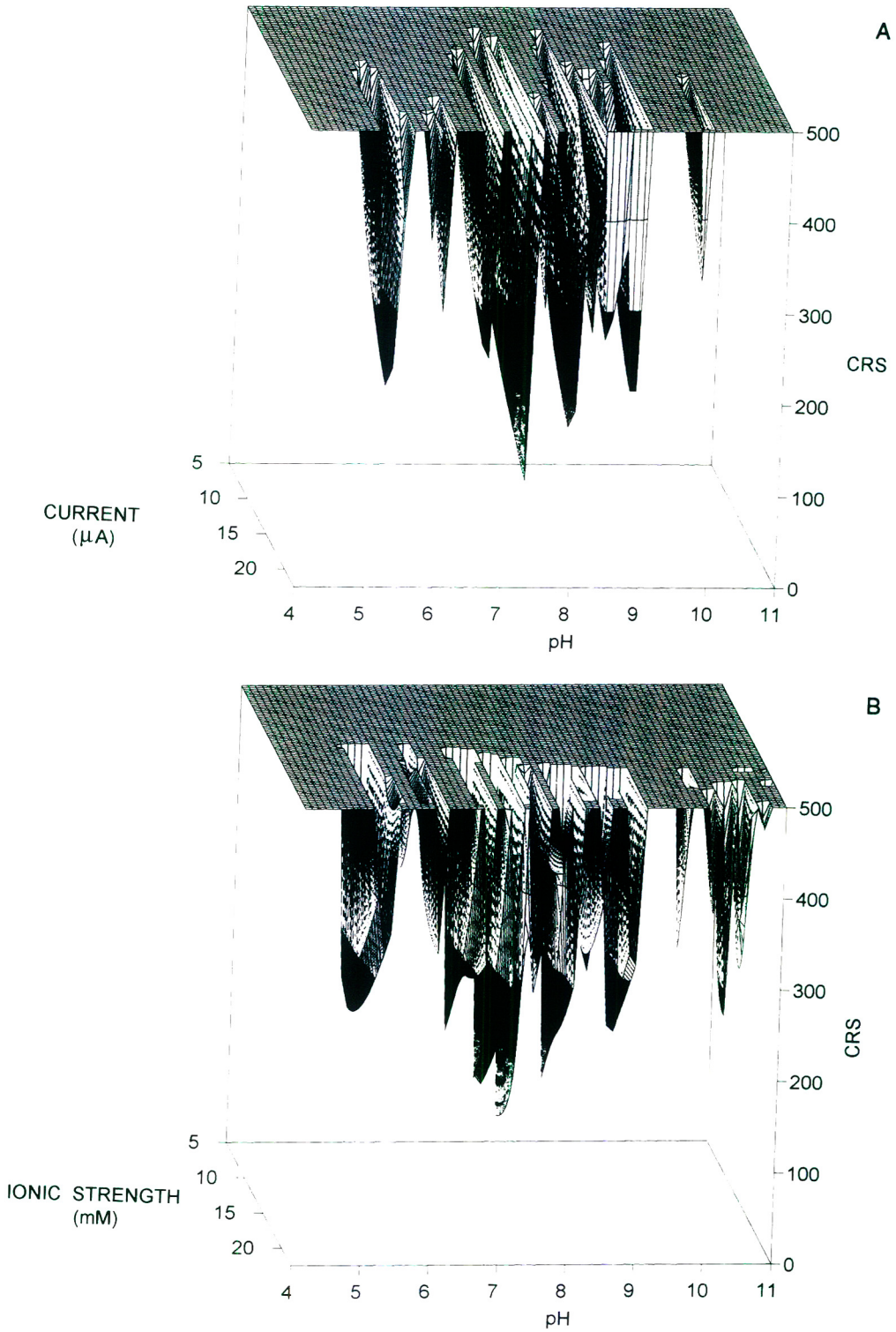
A
500
400
300
CRS
200
100
0
5
10
15
20
CURRENT
(μA)
4
5
6
7
8
9
10
11
pH
B
500
400
300
CRS
200
100
0
5
10
15
20
IONIC STRENGTH
(mM)
4
5
6
7
8
9
10
11
pH

Fig. 4.

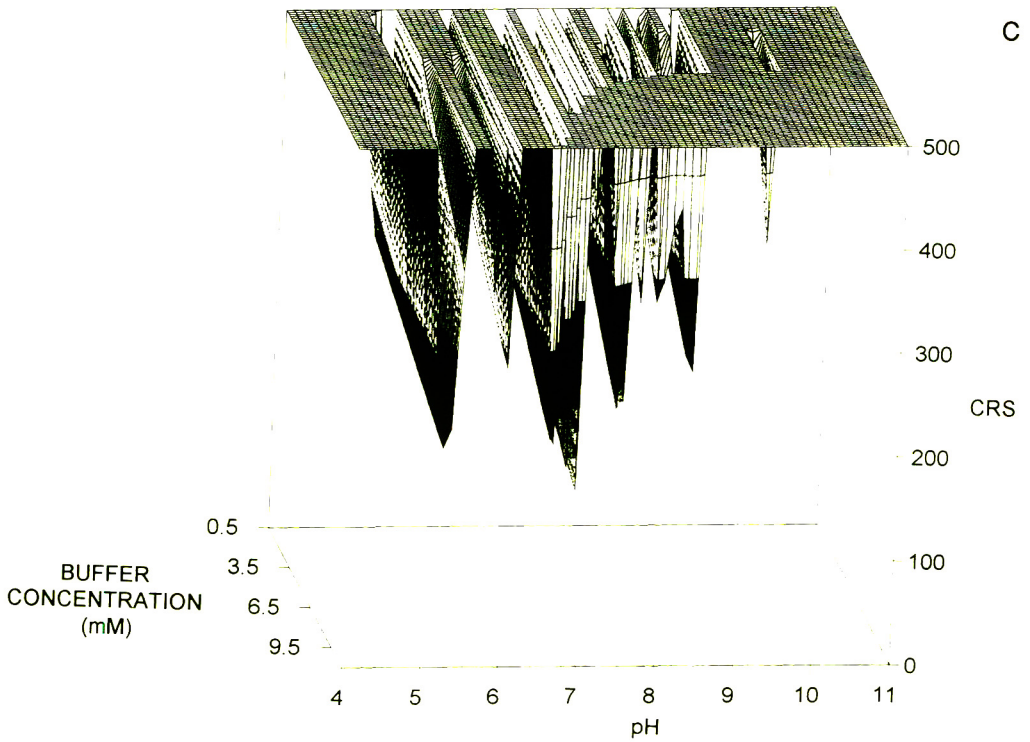

Fig. 4. Surface maps representing the separation of tetracyclines by CE. (A) CRS as a function of pH and applied current with constant ionic strength of 18 m*M* and buffer concentration of 4.5 m*M*. (B) CRS as a function of pH and ionic strength with constant buffer concentration of 4.5 m*M* and current of 20 μA. (C) CRS as a function of pH and buffer concentration with constant ionic strength of 18 m*M* and current of 20 μA.

through at least four different mechanisms, epimerization, dehydration, hydrolysis and oxidation, where the former two are the most important processes [5]. The epimerization of the dimethylamine group in ring A of tetracycline produces the inactive and non-toxic epitetracycline (Fig. 2). The dehydration followed by aromatization of ring C produces anhydrotetracycline, which is also inactive and nontoxic. Both epimerization of anhydrotetracycline and dehydration of epitetracycline lead to the formation of the inactive, but rather toxic epianhydrotetracycline. The kinetics of the epimerization and dehydration reactions have been extensively studied [5,44,45], indicating that these processes can be accelerated at very low pH and under high-temperature conditions. In Fig. 7A and B, the electropherogram of a tetracycline standard is displayed together with a sample that was previously decomposed by heating under acidic conditions. Although primary standards were not available, the decomposition products may be tentatively identified based on the observed changes in electrophoretic mobility. The dehydration reaction decreases the molecular mass and produces a more planar structure, both of which result in an increase in the electrophoretic mobility of anhydrotetracycline relative to that of tetracycline. The epimerization reaction changes the structural features only slightly, resulting in a small decrease in the mobility of the epimers relative to those of tetracycline and anhydrotetracycline. Because the decomposition products are well resolved from the principal component, this method can be used to identify and quantitate tetracycline and its impurities in commercially available pharmaceutical formulations, as demonstrated in Fig. 7C.

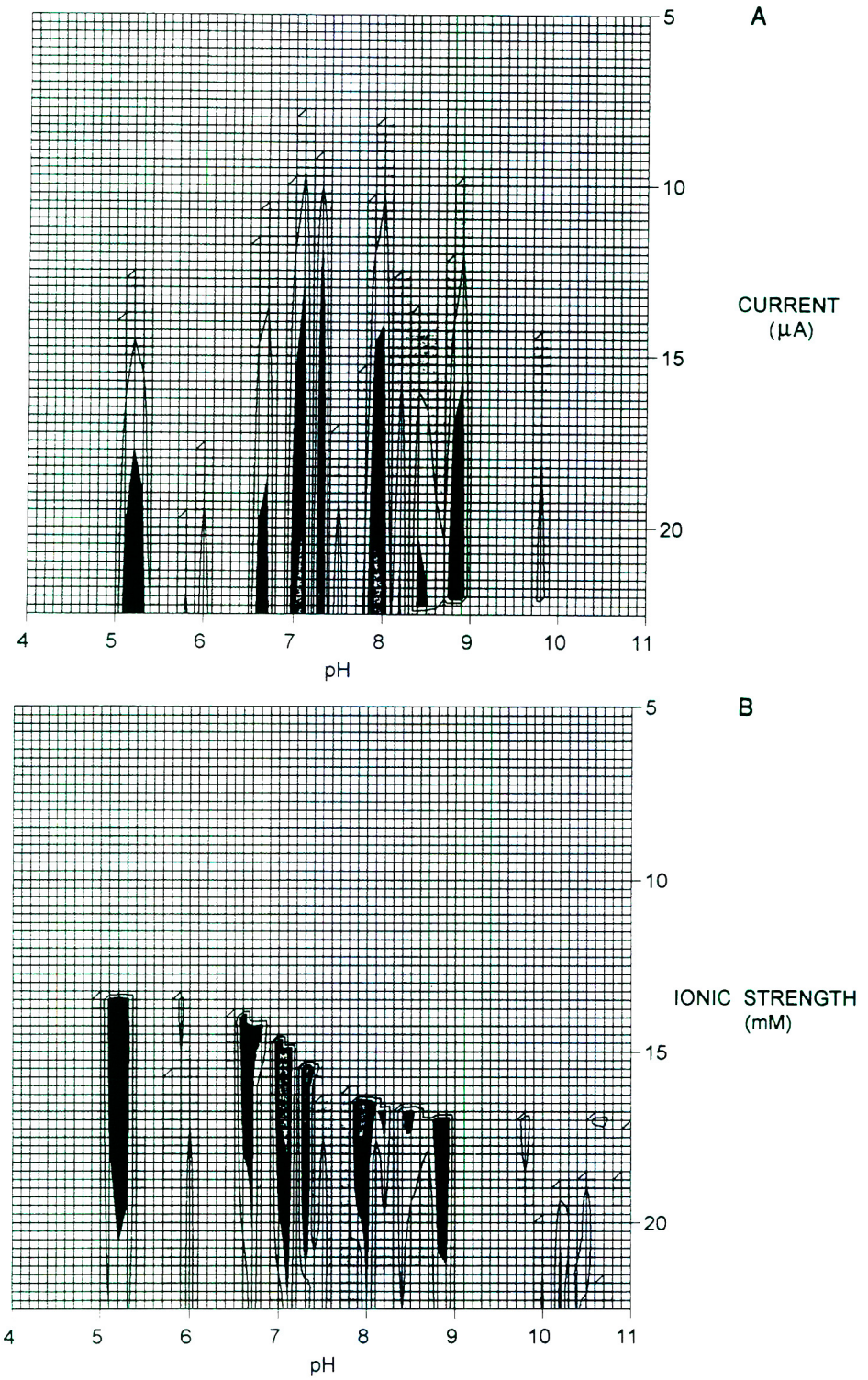
A
5
10
15
20
CURRENT
(μA)
4
5
6
7
8
9
10
11
pH
B
5
10
15
20
IONIC STRENGTH
(mM)
4
5
6
7
8
9
10
11
pH

Fig. 5.

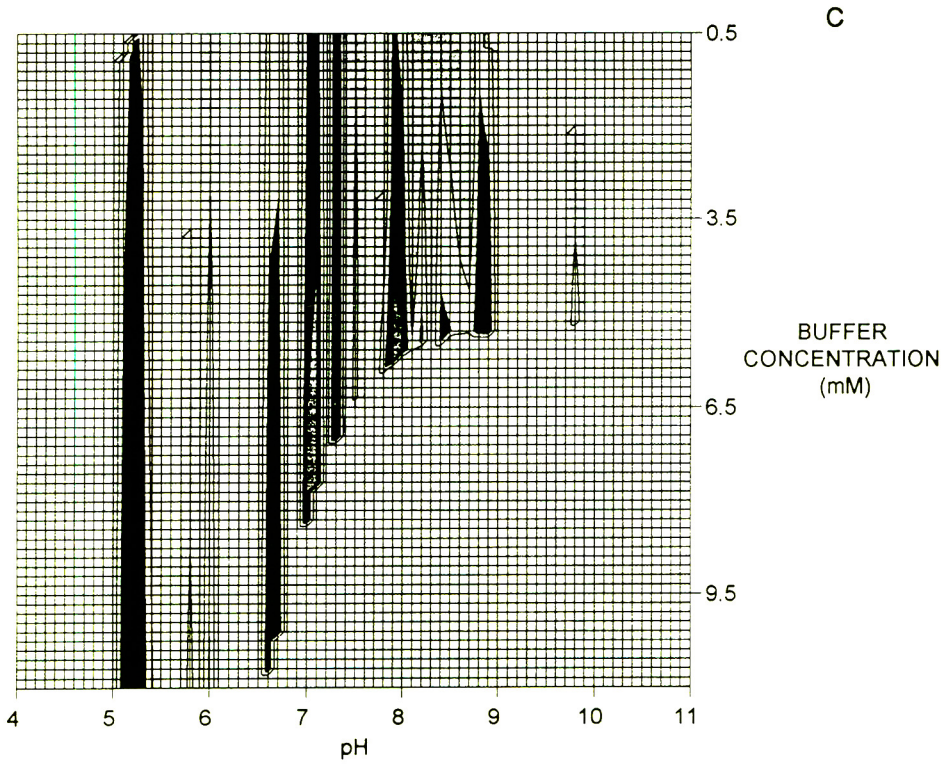

Fig. 5. Contour maps representing the separation of tetracyclines by CE. (A) CRS as a function of pH and applied current with constant ionic strength of 18 m*M* and buffer concentration of 4.5 m*M*. (B) CRS as a function of pH and ionic strength with constant buffer concentration of 4.5 m*M* and current of 20 μA. (C) CRS as a function of pH and buffer concentration with constant ionic strength of 18 m*M* and current of 20 μA.

Table 2
Comparison of experimentally (Exp) determined migration time and base width of tetracyclines with computer-simulated (Calc) values in the vicinity of the optimum conditions (pH 7.5, ionic strength 18.2 m*M*, buffer concentration 4.3 m*M* and constant-current conditions of 20 μA)

Solute	Migration time (min)			Width (min)		
	Exp	Calc[a]	Error (%)[b]	Exp	Calc[c]	Error (%)[b]
MNC	5.05	5.03	0.4	0.085	0.098	− 15
DOC	5.16	5.14	0.4	0.068	0.100	− 47
TC	5.25	5.24	0.2	0.081	0.102	− 26
OTC	5.41	5.30	2.0	0.081	0.104	− 29
MTC	5.48	5.32	2.9	0.085	0.104	− 22
CTC	5.59	5.46	2.3	0.115	0.107	+ 7.0
DMCC	5.71	5.49	3.9	0.123	0.108	+ 12

[a] Calculated from Eq. 1 with an experimentally determined electroosmotic mobility of $6.40 \cdot 10^{-4}$ cm^2 V^{-1} s^{-1}.
[b] Error (%) = 100(Exp − Calc)/Exp.
[c] Calculated from Eqs. 5–7 with theoretical contributions to spatial variance of $5.34 \cdot 10^{-3}$ to $5.80 \cdot 10^{-3}$ cm^2 for diffusion, $1.78 \cdot 10^{-2}$ cm^2 for injection and $2.08 \cdot 10^{-2}$ cm^2 for detection [35].

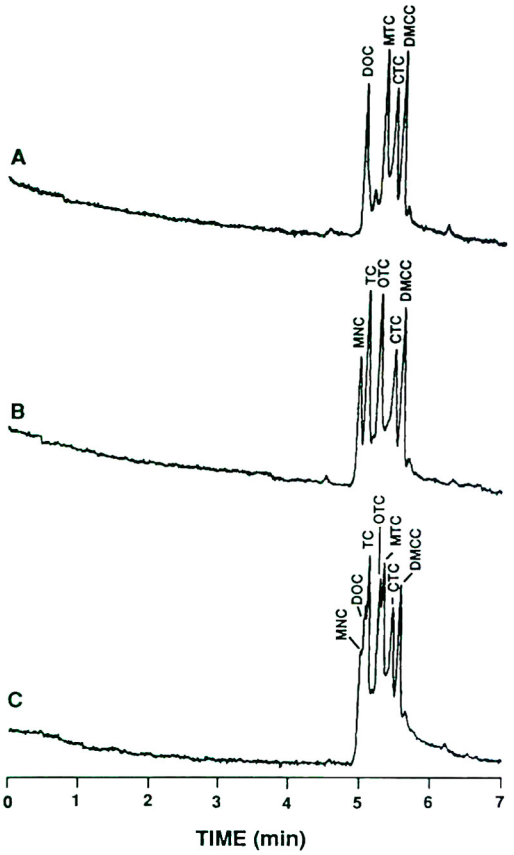

Fig. 6. Separation of selected four- (A), five- (B) and seven- (C) component mixtures of tetracyclines by CE in the vicinity of the optimum conditions identified from Figs. 4 and 5. Experimental conditions: pH 7.5 phosphate buffer, buffer concentration 4.3 m*M*, total sodium concentration 15 m*M*, ionic strength 18.2 m*M* and applied current of 20 μA.

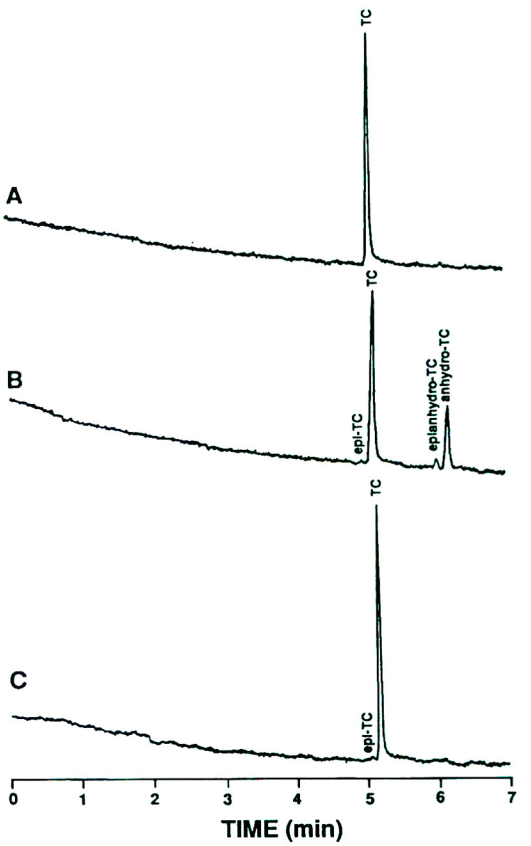

Fig. 7. Electrophoretic separation of tetracycline and its decomposition products under the optimized experimental conditions given in Fig. 6. (A) Tetracycline standard. (B) Tetracycline standard previously treated with pH 2 hydrochloric acid at 70°C for 1 h. (C) Tetracycline pharmaceutical formulation as hard-filled capsules.

In the analysis of tetracycline in hard-filled capsules, a minimum recovery of 95% of the active ingredient was obtained. A calibration curve of peak height versus concentration gave a slope of $6.15 \cdot 10^{-4}$ cm M^{-1}, intercept of $-1.18 \cdot 10^{-5}$ cm, and coefficient of determination equal to 0.9989. The detection limit was $1 \cdot 10^{-5}$ *M* at a signal-to-noise ratio of approximately 3 [46], with a linear range of two orders of magnitude. In addition to tetracycline, other commercially available pharmaceutical formulations were examined, such as doxycycline and minocycline, with comparable analytical figures of merit.

Among the tetracyclines characterized in this work, chlortetracycline presented the most unusual electrophoretic behavior, as illustrated in Fig. 8. The chlortetracycline standard exhibits a marked asymmetry in the direction of a contaminant, which possesses a migration time coincident with that of tetracycline. Chlortetracycline is known to decompose to form tetracycline under relatively mild conditions [47–49]. The results presented herein suggest that this decomposition may be enhanced by application of an electric field. Consequently, electrophoretic techniques may not be suitable to monitor

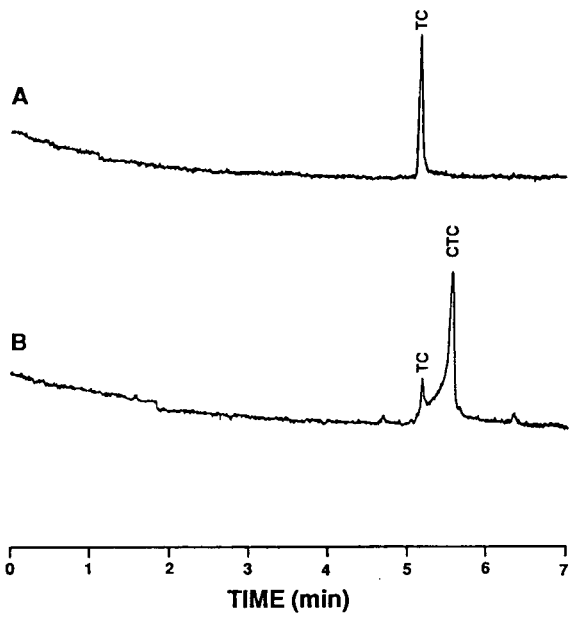

Fig. 8. Electrophoretic behavior of chlortetracycline under the optimized experimental conditions given in Fig. 6. (A) Tetracycline standard. (B) Chlortetracycline standard.

chlortetracycline in pharmaceutical formulations. It is noteworthy that the decomposition of chlortetracycline had a deleterious effect upon the separation shown in Fig. 6C. In the absence of this zone asymmetry, resolution is significantly improved and qualitative and quantitative analysis of the tetracyclines is more accurately achieved (Fig. 9).

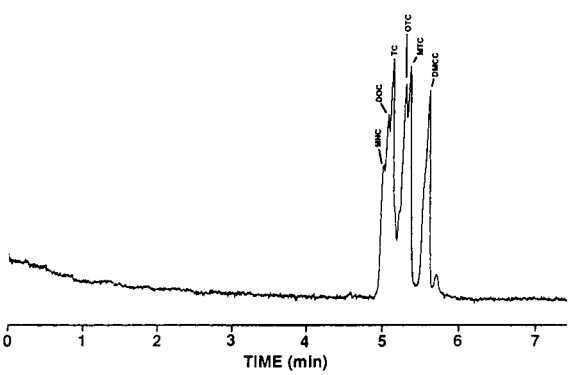

Fig. 9. Electrophoretic separation of tetracyclines in the absence of chlortetracycline under the optimized experimental conditions given in Fig. 6.

4. Conclusions

In this work, CE was characterized as a resourceful analytical method for tetracycline, its natural and synthetic analogues, as well as common impurities arising during manufacture or from decomposition during storage. The electrophoretic behavior of seven members of the group was thoroughly studied in the pH range 4–11, and a complete set of acid–base equilibrium constants and electrophoretic mobilities was derived. These constants were used as input to a computer program, which established the optimal conditions for the separation. The analysis of tetracyclines in pharmaceutical formulations was satisfactorily achieved under the predicted optimum conditions.

Acknowledgements

This research was supported by the US Department of Energy, Office of Basic Energy Sciences, Division of Chemical Sciences, under contract number DE-FG02-89ER14056. Additional support was provided by the Dow Chemical Co. and Eli Lilly Co. The authors acknowledge Dr. Gerald Larson (Michigan State University) for the pharmaceutical samples. M.F.M.T. gratefully acknowledges a fellowship from the Conselho Nacional de Desenvolvimento Científico e Tecnológico (CNPq) of Brazil.

References

[1] H.P. Lambert and F.W. O'Grady, *Antibiotic and Chemotherapy*, Churchill Livingstone, London, 6th ed., 1992.

[2] A. Aszalos, *Modern Analysis of Antibiotics, Drugs and the Pharmaceutical Sciences*, Vol. 27, Marcel Dekker, New York, 1986.

[3] A.P. De Leenheer and H.J.C.F. Nelis, *J. Pharm. Sci.*, 68 (1979) 999–1002.

[4] J.P. Sharma, E.G. Perkins and R.F. Bevill, *J. Chromatogr.*, 134 (1977) 441–450.

[5] L.A. Mitscher, *The Chemistry of the Tetracycline Antibiotics (Medicinal Research Series*, Vol. 9), Marcel Dekker, New York, 1978.

[6] J. Hermansson and M. Andersson, *J. Pharm. Sci.*, 71 (1982) 222–229.
[7] G.D. Mack and R.B. Ashworth, *J. Chromatogr. Sci.*, 16 (1978) 93–101.
[8] K. Tsuji and J.H. Robertson, *J. Pharm. Sci.*, 65 (1976) 400–404.
[9] R.K. Gilpin and L.A. Pachla, *Anal. Chem.*, 65 (1993) 117R–132R.
[10] H. Ping-Kay and F. Wai-Kwong, *Analyst*, 116 (1991) 751–752.
[11] K.M. Emara, H.F. Askal and G.A. Salèh, *Talanta*, 38 (1991) 1219–1221.
[12] U. Saha, A.K. Sen, T.K. Das and S.K. Bhowal, *Talanta*, 37 (1990) 1193–1196.
[13] J.X. Duggan, *J. Liq. Chromatogr.*, 14 (1991) 2499–2525.
[14] A.B. Syropoulos and A.C. Calokerinos, *Anal. Chim. Acta*, 255 (1991) 403–411.
[15] A.A. Alwarthan, S.A. Al-Tamrah and S.M. Sultan, *Analyst*, 116 (1991) 183–186.
[16] W. Naidong, S. Hua, E. Roets and J. Hoogmartens, *J. Planar Chromatogr.-Mod. TLC*, 5 (1992) 92–98.
[17] W. Naidong, C. Hauglustaine, E. Roets and J. Hoogmartens, *J. Planar Chromatogr.-Mod. TLC*, 4 (1991) 63–68.
[18] W. Naidong, S. Hua, K. Verresen, E. Roets and J. Hoogmartens, *J. Pharm. Biomed. Anal.*, 9 (1991) 717–723.
[19] K.J. Kovács-Hadady, *J. Planar Chromatogr.-Mod. TLC*, 4 (1991) 456–459.
[20] W. Naidong, S. Geelen, E. Roets and J. Hoogmartens, *J. Pharm. Biomed. Anal.*, 8 (1990) 891–898.
[21] W. Naidong, T. Cachet, E. Roets and J. Hoogmartens, *J. Planar Chromatogr.-Mod. TLC*, 2 (1989) 424–429.
[22] J.S. Kang and S.J. Ebel, *J. Planar Chromatogr.-Mod. TLC*, 2 (1989) 434–437.
[23] N.H. Khan, P. Wera, E. Roets and J. Hoogmartens, *J. Liq. Chromatogr.* 13 (1990) 1351–1374.
[24] W. Naidong, E. Roets and J. Hoogmartens, *J. Pharm. Biomed. Anal.*, 7 (1989) 1691–1703.
[25] A. Aszalos, C. Haneke, M.J. Hayden and J. Crawford, *Chromatographia*, 15 (1982) 367–373.
[26] J.H. Knox and J. Jurand, *J. Chromatogr.*, 186 (1979) 763–782.
[27] A.P. De Leenheer and H.J.C.F. Nelis, *J. Chromatogr.*, 140 (1977) 293–299.
[28] J.H. Knox and J. Jurand, *J. Chromatogr.*, 110 (1975) 103–115.
[29] E.R. White, M.A. Carrol, J.E. Zarembo and A.D. Bender, *J. Antibiot.*, 28 (1975) 205–214.
[30] A.G. Butterfield, D.W. Hughes, N.J. Pound and W.L. Wilson, *Antimicrob. Ag. Chemother.*, 4 (1973) 11–15.
[31] P.D. Grossman and J.C. Colburn (Editors), *Capillary Electrophoresis —Theory and Practice*, Academic Press, San Diego, CA, 1992.
[32] M.T. Ackermans, J.L. Beckers, F.M. Everaerts and I.G.J.A. Seelen, *J. Chromatogr.*, 590 (1992) 341–353.
[33] M. Lookabaugh, M. Biswas and I.S. Krull, *J. Chromatogr.*, 549 (1991) 357–366.
[34] S.K. Yeo, H.K. Lee and S.F.Y. Li, *J. Chromatogr.*, 585 (1991) 133.
[35] M.F.M. Tavares and V.L. McGuffin, *Anal. Chem.*, in press.
[36] M.F.M. Tavares and V.L. McGuffin, *Anal. Chem.*, in press.
[37] A.E. Ciarlone, B.W. Fry and D.M. Ziemer, *Microchem. J.*, 42 (1990) 250–255.
[38] L.J. Leeson, J.E. Krueger and R.A. Nash, *Tetrahedron Lett.*, 18 (1963) 1155–1160.
[39] N.E. Rigler, S.P. Bag, D.E. Leyden, J.L. Sudmeier and C.N. Reilley, *Anal. Chem.*, 37 (1965) 872–875.
[40] J.N. Butler, *Ionic Equilibrium —A Mathematical Approach*, Addison-Wesley, Reading, MA, 1964.
[41] R.A. Robinson and R.H. Stokes, *Electrolyte Solutions —The Measurement and Interpretation of Conductance, Chemical Potential and Diffusion in Solutions of Simple Electrolytes*, Butterworths, London, 1959.
[42] T.D. Schlabach and J.L. Excoffier, *J. Chromatogr.*, 439 (1988) 173–184.
[43] J.C. Giddings, *Unified Separation Science*, Wiley-Interscience, New York, 1991.
[44] K.D. Schlecht and C.W. Frank, *J. Pharm. Sci.*, 64 (1975) 352–354.
[45] B.A. Hoener, T.D. Sokoloski, L.A. Mitscher and L. Malspeis, *J. Pharm. Sci.*, 63 (1974) 1901–1904.
[46] P.A. St. John, W.J. McCarthy and J.D. Winefordner, *Anal. Chem.*, 39 (1967) 1495–1497.
[47] W. Naidong, E. Roets, R. Busson and J. Hoogmartens, *J. Pharm. Biomed. Anal.*, 8 (1990) 881–889.
[48] M. Sokolic, B. Filipovic and M. Pokorny, *J. Chromatogr.*, 509 (1990) 189–193.
[49] W. Naidong, E. Roets and J. Hoogmartens, *Chromatographia*, 30 (1990) 105–109.

ELSEVIER

Journal of Chromatography A, 686 (1994) 143–148

JOURNAL OF CHROMATOGRAPHY A

Routine determination of anions by capillary electrophoresis and ion chromatography

R. Stahl

Nuclear Research Center Karlsruhe, Institut für Heisse Chemie, P.O. Box 3640, D-76021 Karlsruhe, Germany

First received 10 May 1994; revised manuscript received 8 August 1994

Abstract

Non-suppressed ion chromatography and capillary electrophoresis are used in routine analysis for the identification and determination of anions such as fluoride, formate, chloride, carbonate, bromide and nitrate in aqueous soil leachates and process solutions. Practical aspects of the analysis of samples that contain unknown components using these two orthogonal methods are discussed. The detection limits are found to be about 0.2 μg/ml for chromatography and about 2 μg/ml for electrophoresis. Both methods show linear calibration functions in the concentration ranges 1–50 and 5–50 μg/ml, respectively.

1. Introduction

Ion chromatography (IC) is an excellent method for the simultaneous determination of several inorganic anions in simple matrices such as drinking water and rainwater [1,2]. In complex sample matrices such as process solutions containing unknown components, waste water or soil leachates, one has to make sure that no co-eluting peaks appear. One possibility is to apply a coupled ion chromatograph with two chromatographic systems interconnected via an automatic column-switching valve [3]. On the other hand, capillary electrophoresis (CE) has recently been demonstrated to be a useful technique for the separation of different ions [4,5]. According to Jones and Jandik [6], who separated 30 anions, CE seems to be a very successful method for the determination of unknown components in solutions. In this paper, applications of CE and IC for the identification and determination of anions in routine analysis are discussed.

2. Experimental

2.1. Equipment and chemicals

The instrumental equipment used and the operating conditions for IC and CE are listed in Table 1. The IC analyses are performed under two different conditions using (a) phthalic acid (PA) [7] and (b) *p*-hydroxybenzoic acid (PHBA) as eluent. All eluents are filtered through a 0.45-μm membrane filter before use.

As most inorganic ions have a low or no absorbance in the high-energy UV region, a higher sensitivity in CE is attained with indirect detection. According to the results of Buchberger and Haddad [8], the carrier electrolyte (pH 8.2) is prepared from sodium chromate

0021-9673/94/$07.00
SSDI 0021-9673(94)00746-2

Table 1
Conditions for CE and IC

Method	Parameter	Conditions
CE	Instrumentation	Lauerlabs automated capillary electrophoresis system (Bischoff, Leonberg, Germany)
	Capillary	120 cm effective length × 75 μm I.D., uncoated (Scientific Glass Engineering, Weilerstadt, Germany)
	Temperature	30°C
	Buffer	5 m*M* chromate–0.2 m*M* TTAB, adjusted to pH 8.2 with 5 m*M* H_2SO_4
	Injection	25 mbar, 0.1 min
	Voltage	−30 kV
	Detection	275 nm, Lambda 1000 (Bischoff)
	Data acquisition	PC and Hyperdata software
IC	Instrumentation	Solvent degasser (ERC Alteglofsheim, Germany) Isocratic pump (Bischoff) Ion chromatograph including injection valve (100 μl) and conductivity detector (30°C) (Metrohm)
	Eluent 1	4 m*M* phthalic acid (pH 4.4) adjusted with Tris [7]
	Column 1	Vydac 302IC, flow-rate 2.5 ml/min, pressure 5.5 MPa
	Eluent 2	1.5 m*M* *p*-hydroxybenzoic acid (pH 8.4) adjusted with NaOH, stored under nitrogen
	Column 2	Alltech Anion R (100 mm × 4.1 mm I.D.), flow-rate 1.5 ml/min, pressure 6.4 MPa
	Data acquisition	PC and PE–Nelson software

tetrahydrate. As electroosmotic flow (EOF) modifier, a solution of tetradecyltrimethylammonium bromide (TTAB) is used after passing it through a solumn filled with a strong anion-exchange resin. Before each series of analyses, the carrier electrolyte is freshly prepared by mixing sodium chromate and TTAB solution; the pH is adjusted with sulfuric acid. The data acquisition of the electropherograms is started with a delay time of 8 min after the application of high voltage.

Standard solutions (1000 μg/ml) of all the investigated anions are prepared from the corresponding dried sodium salts. Before injection, suitable concentrations are obtained by dilution with distilled water. For the characterization of the methods, the concentration interval from 1 to 50 μg/ml is subdivided into eleven equidistant calibration points.

2.2. Sample preparation

Sample preparation is simple. All samples are filtered through a 0.45-μm membrane filter before use. Soil extracts are diluted 1:10 with eluent, if necessary, and process samples are diluted 1:5 with buffer solution.

3. Results and discussion

3.1. Process solution

Difluoromonochloromonobromomethane (CF_2BrCl; Halone), used in fire extinguishers, has been proved to cause severe damage in the atmosphere [9,10]. Therefore, it has to be replaced and disposed of by law in Germany [11]. One method that is being investigated is the chemical decomposition of Halone in solution [12]. The chromatogram of such a solution shows distinct signals for F^-, Cl^-, Br^- and $HCOO^-$ (Fig. 1). The emergence of a system peak is caused by the pH of the sample, which is not identical with the pH of the eluent. Identification of the anions is done by using standard chro-

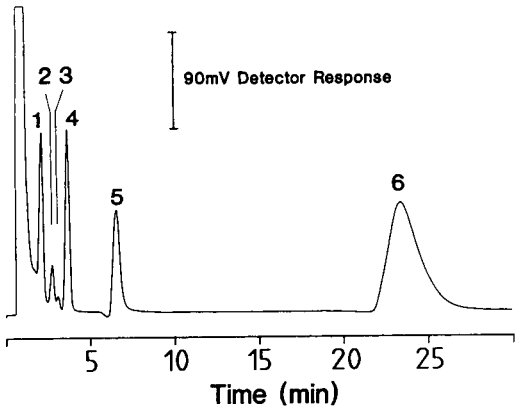

Fig. 1. Separation of a process solution. Conditions: 1.5 m*M* PHBA (pH 8.8); Alltech Anion R column; flow-rate = 1.5 ml/min. Peaks: 1 = fluoride; 2 = formate; 3 = carbonate; 4 = chloride; 5 = bromide; 6 = system peak.

matograms (Fig. 2) and spiking. The corresponding electropherogram (Fig. 3) is consistent with that of the standard mixture (Fig. 4). In both electropherograms the signals of the anions exhibit the same retention times, thus confirming the results.

3.2. Soil extracts

Two independent samples of soil extracts were investigated. The chromatograms of both samples are very similar and show, in addition to the sulfate and chloride signals, a third peak just

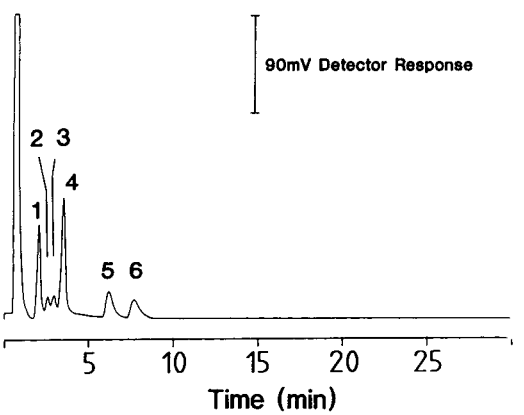

Fig. 2. Separation of a standard mixture. Conditions as in Fig. 1. Peaks: 1 = fluoride; 2 = formate; 3 = traces of carbonate; 4 = chloride; 5 = bromide; 6 = nitrate (5 μg/ml each).

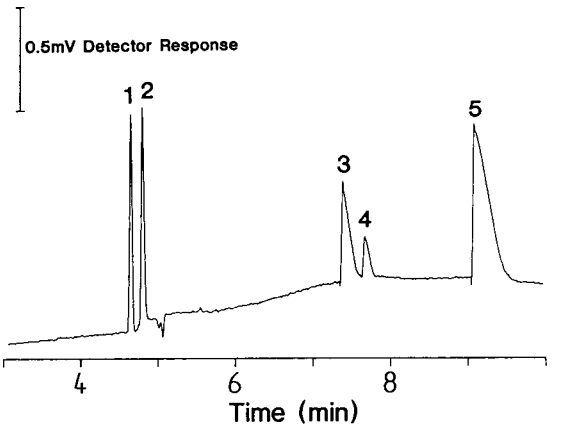

Fig. 3. Electropherogram of a process solution. Conditions: 5 m*M* chromate–0.2 m*M* TTAB (pH 8.2); −30 kV. Peaks: 1 = bromide; 2 = chloride; 3 = fluoride; 4 = formate; 5 = carbonate.

before the chloride signal when PA is used as the eluent. When PHBA is used instead, more signals appear in the same region. By using standard anion mixtures these peaks are identified in sample 1 to be (1) $HCOO^-$, (2) CO_3^{2-}, (3) Cl^- and (4) NO_3^- (Fig. 5). In sample 2 F^- is additionally identified (Fig. 6). Owing to the overlapping system peak, the quantification of sulfate is difficult. Again, the identification of the anions is confirmed by the results of CE without any problems (Figs. 7 and 8).

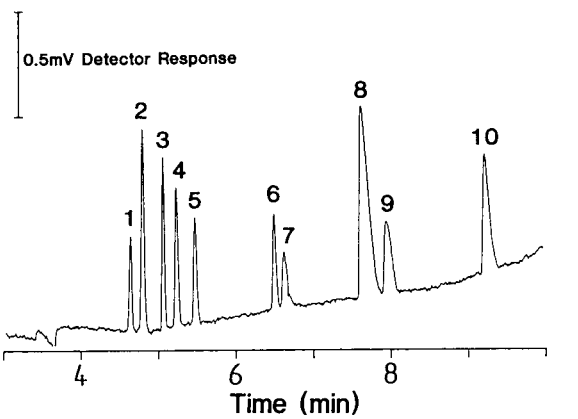

Fig. 4. Electropherogram of a standard mixture. Conditions as in Fig. 3. Peaks: 1 = bromide; 2 = chloride; 3 = sulfate; 4 = nitrite; 5 = nitrate; 6 = chlorate; 7 = perchlorate; 8 = fluoride; 9 = formate; 10 = carbonate (30 μg/ml each).

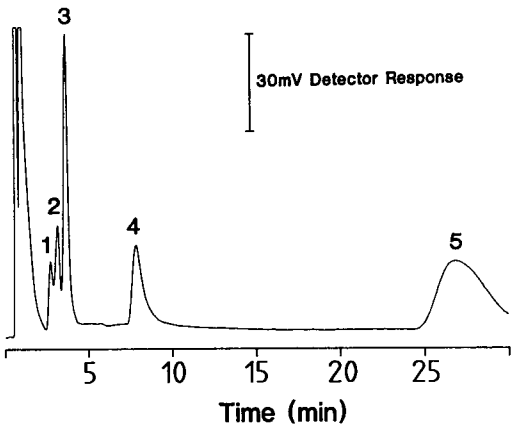

Fig. 5. Separation of extract of soil No. 1. Conditions as in Fig. 1. Peaks: 1 = formate; 2 = carbonate; 3 = chloride; 4 = nitrate; 5 = sulfate and system peak.

3.3. General aspects

The calibration graphs are obtained by injecting standard solutions. Each point of the calibration graph corresponds to the mean value obtained from six independent measurements. The resulting calibration functions show that the methods give a linear response. The corresponding parameters for the quality check are listed in Tables 2 and 3. From the standard deviation of the measurement of the lowest concentration, the detection limits are calculated

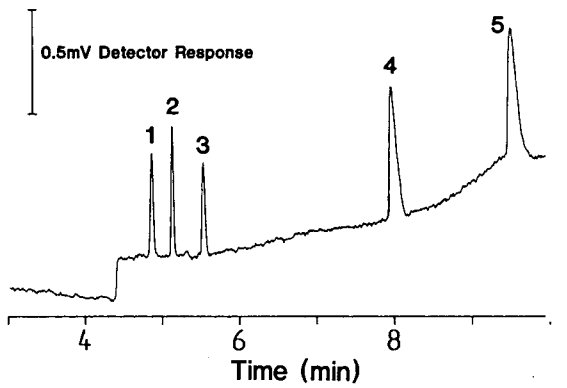

Fig. 7. Electropherogram of soil extract No. 1. Conditions as in Fig. 3. Peaks: 1 = chloride; 2 = sulfate; 3 = nitrate; 4 = formate; 5 = carbonate.

[13]. Under the given conditions the detection limit in CE is about ten times higher than that in IC. Increasing the injection time in CE only partially improves the detection limit, because the resolution of the fluoride and formate signals decreases significantly. With increasing age of the chromate buffer the retention times are steadily reduced. For that reason, in automated systems the integration parameters have to be chosen carefully.

Determination of the fluoride ion is not possible. The peak areas show a definite tendency towards higher values with increasing buffer age.

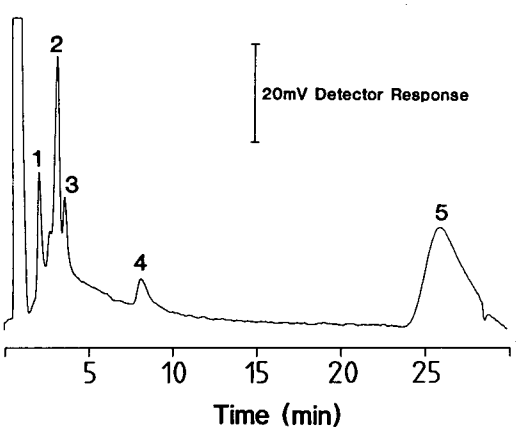

Fig. 6. Separation of extract of soil No. 2. Conditions as in Fig. 1. Peaks: 1 = Fluoride; 2 = carbonate (shoulder = formate); 3 = chloride; 4 = nitrate; 5 = sulfate and system peak.

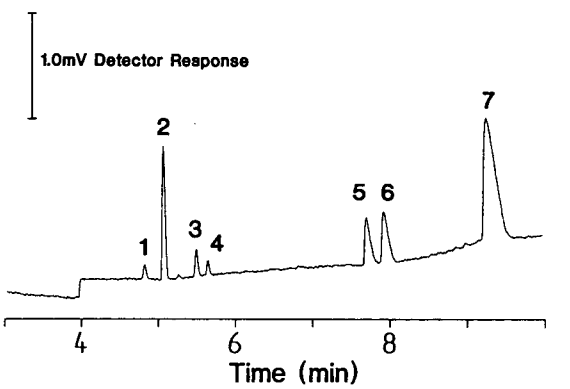

Fig. 8. Electropherogram of soil extract No. 2. Conditions as in Fig. 3. Peaks: 1 = chloride; 2 = sulfate; 3 = fluoride; 3 = nitrate; 4 = unknown; 5 = fluoride; 6 = formate; 7 = carbonate.

Table 2
Ion chromatography with PHBA: calibration parameters

Anion	Retention time (min)	Sensitivity (mV s ml/μg)	Blank (μg/ml)	S.D. (mV s)	Detection limit[a] (μg/ml)
F^-	2.3	301	−0.2	63	0.1
$HCOO^-$	2.9	112	−0.5	54	0.1
Cl^-	3.8	403	−0.1	73	0.2
Br^-	6.6	184	−0.6	36	0.2

[a] Detection limit = $3\sigma_{(1\ \mu g/ml)}$/sensitivity.

Table 3
Capillary electrophoresis: calibration parameters

Anion	Retention time (min)	Sensitivity (mV s ml/μg)	Blank (μg/ml)	S.D. (mV s)	Detection limit[a] (μg/ml)
Br^-	5.0	31	−0.3	19	1.7
Cl^-	5.2	75	−0.3	33	1.1
SO_4^{2-}	5.5	56	−0.3	30	1.0
NO_2^-	5.7	56	−0.2	47	1.1
NO_3^-	5.9	44	−0.3	32	1.4
ClO_3^-	7.0	38	0.9	47	2.4
ClO_4^-	7.2	31	0.9	48	4.3
F^-	7.7	–	–	–	–
$HCOO^-$	8.7	93	0.6	101	1.6
CO_3^{2-}	9.2	–	–	–	–

[a] Detection limit = $3\sigma_{(5\ \mu g/ml)}$/sensitivity.

This is confirmed by statistical tests (Wallis, Neuman, Cox–Stuart, Mann) [14].

The most important feature of CE is the distinct separation of the signals. Consequently, the quantification step is easier than in IC. Comparative analyses are reported in Tables 4 and 5. The scattering of the results and the confidence limits of the calibration have been taken into account [14]. In general, the results are comparable in accuracy and precision. Stan-

Table 4
Concentrations (μg/ml) of fluoride, chloride, sulfate, nitrate and formate in aqueous soil extracts (confidence level 90%)

Sample No.	Method	F^-	Cl^-	NO_3^-	$HCOO^-$	SO_4^{2-}
1	CE	–	8.4 ± 0.9	13.6 ± 1.4	10.2 ± 1.2	11.9 ± 0.6
	IC (PA)	–	9.8 ± 0.3	14.0 ± 2.6	–	12.3 ± 1.4
	IC (PHBA)	–	9.8 ± 0.2	13.4 ± 0.5	7.8 ± 0.4	–[a]
2	CE	–[b]	2.6 ± 0.5	8.2 ± 1.0	6.7 ± 1.6	29.9 ± 0.5
	IC (PA)	–	3.1 ± 0.2	7.0 ± 1.9	–	26.9 ± 2.0
	IC (PHBA)	4.9 ± 0.2	2.5 ± 0.2	7.9 ± 0.5	6.9 ± 0.4	–[a]

[a] Overlapping of system peak.
[b] Only qualitative.

Table 5
Concentrations (μg/ml) of fluoride, formate, chloride and bromide in a process solution (confidence level 90%)

Method	F^-	Cl^-	Br^-	$HCOO^-$
CE	–[a]	8.9 ± 0.5	20.9 ± 0.7	8.8 ± 1.2
IC (PHBA)	8.2 ± 0.2	8.1 ± 0.2	18.9 ± 0.4	6.1 ± 0.4

[a] Only qualitative.

dard additions to the analysed samples indicate that for these samples there are no substantial matrix interferences.

In routine operation it is important to use the chromate buffer freshly prepared just before each series of analyses. After not more than 15 injections the buffer must be replaced by a fresh solution. A 5-min capillary purge is performed prior to all injections to remove remaining constituents of the last sample from the capillary. The purge is accomplished by a pressure of 2 bar applied to the buffer vial. To check the validity of the calibration, three standards are analysed once before and after the measurement of the unknown samples. Each sample is measured three times.

4. Conclusions

The use of capillary electrophoresis combined with existing chromatographic methodology has been demonstrated to be an excellent analytical tool to confirm the identity and purity of ion chromatographic peaks. Especially with complex sample matrices CE is capable of separating simultaneously many more components than IC. Therefore, CE is an efficient technique for screening analysis. Studies on the determination of fluoride and other anions are in progress.

Acknowledgements

The cooperation and assistance of J. Scherwitzl, R. Durst and S. Fetzner is greatly appreciated.

References

[1] B. Rössner and G. Schwedt, *Fresenius' Z. Anal. Chem.*, 320 (1985) 566.
[2] F. Wagner, P. Valenta and H.W. Nürnberg, *Fresenius' Z. Anal. Chem.*, 320 (1985) 470.
[3] W.R. Jones, A.L. Heckenberg and P. Jandik, *J. Chromatogr.*, 366 (1986) 225.
[4] W. Beck, *Nachr. Chem. Tech. Lab.*, 41 (1993) M1.
[5] S.F.Y. Li, *Capillary Electrophoresis*, Elsevier, Amsterdam, New York, 1992.
[6] W.R. Jones and P. Jandik, *J. Chromatogr.*, 546 (1991) 445.
[7] R. Stahl, *Chromatographia*, 37 (1993) 300.
[8] W. Buchberger and P.R. Haddad, *J. Chromatogr.*, 608 (1992) 59.
[9] F.S. Rowland and D.G. Aldrich, *Environ. Conserv.*, 15 (1988) 101.
[10] G. Fellenberg, *Chemie der Umweltbelastung*, Teubner, Stuttgart, 1990, p. 99.
[11] *Bundesgesetzblatt*, Verordnung 662, 6 May 1991.
[12] U. Bauder, Nuclear Research Centre Karlsruhe, personal communication, 1993.
[13] R.A. Cochrane and D.E. Hillman, *J. Chromatogr.*, 241 (1982) 392.
[14] S. Ebel, *Statistik (Würzburger Skripten zur Analytik*, Reihe 1), Bayrische Julius-Maximilians Universität, Würzburg, 1992.

ELSEVIER

Journal of Chromatography A, 686 (1994) 149–154

JOURNAL OF CHROMATOGRAPHY A

Short communication

Pyrrolidides as derivatives for the determination of the fatty acids of triacylglycerols by gas chromatography

W. Vetter*, W. Walther

Pharma Division, Preclinical Research, F. Hoffmann-La Roche, Ltd., CH-4002 Basle, Switzerland

First received 5 July 1994; revised manuscript received 18 August 1994

Abstract

Triacylglycerols can be converted quantitatively into the pyrrolidides of their constituent fatty acids. On the basis of this reaction, an easy and highly accurate gas chromatographic method for the determination of the fatty acids from triacylglycerols has been developed.

1. Introduction

Pyrrolidides have been recognized as useful derivatives of fatty acids for characterization by gas chromatography–mass spectrometry (GC–MS) [1–4]. We have recently worked out a convenient one-step procedure for the conversion of free fatty acids into their pyrrolidides [5]. This procedure consists in the treatment of the fatty acids with a mixture of trimethylsilylimidazole (TMSI) and pyrrolidine for several hours at room temperature, whereby quantitative derivatization results. No workup, except dilution with ethyl acetate, is necessary before GC analysis because all reagents and side-products (imidazole, TMSI, TMS-pyrrolidine and TMS-OH) are sufficiently volatile to be easily separated from the pyrrolidides of the common fatty acids by GC.

The ease of preparation and the thermodynamic stability of the pyrrolidides {$\Delta\Delta H$ of the reaction $CH_3COOCH_3 + HN(CH_2)_4 \rightarrow CH_3CON(CH_2)_4 + CH_3OH$ is calculated to be -1 ± 5 kJ mol^{-1} [6]} suggest that they might be useful not only for structure analysis by GC–MS, but also for the quantitative analysis of mixtures of fatty acids by GC.

Fats and oils are the most common source of mixtures of fatty acids. We introduce here a facile one-step method for the conversion of triacylglycerols into the pyrrolidides of their constituent fatty acids. In close analogy to the method described above for the free acids [5], triacylglycerols are reacted with a mixture of pyrrolidine and imidazole for a few hours at 60°C. After dilution with an inert solvent, the reaction mixture can be used directly for GC analysis.

2. Experimental

2.1. Sample preparation

The triacylglycerol (1 mg) is dissolved in a solution of 20 μl of pyrrolidine and 20 mg of

* Corresponding author.

0021-9673/94/$07.00
SSDI 0021-9673(94)00797-7

imidazole and left at 60°C overnight to ensure quantitative reaction (shortening the reaction time by increasing the temperature is not recommended, because of a progressively intense yellow coloration of the reaction mixture above 60°C). The reaction mixture is diluted with 1 ml of ethyl acetate. Using the on-column injection technique, 1 μl of this solution is injected into the gas chromatograph.

2.2. Instrumentation

A Carlo Erba Vega 6000 gas chromatograph equipped with a flame-ionisation detector and an on-column injector was employed.

2.3. Gas chromatography

Two fused-silica columns, coated with different stationary phases were used: column A, 23 m × 0.32 mm I.D., coated with SE-30 [poly(dimethylsiloxane) gum, cross-linked] with film thickness 0.25 μm (laboratory made) and column B, 15 m × 0.25 mm I.D., coated with Stabilwax (Crossbond Carbowax-PEG) with film thickness 0.25 μm (Restek, Bellefonte, PA, USA). The carrier gas was hydrogen at a linear velocity of 50 cm s^{-1}. The injection port temperature was ca. 30°C and the detector temperature was 250°C for column A and 350°C for column B.

3. Results and discussion

Fig. 1 shows the results of a kinetic study on the conversion of glycerol trioleate into oleic acid pyrrolidide using the proposed reagent. For comparison, some other reagent mixtures are also shown, including a 1:1 (v/v) mixture of pyrrolidine and trimethylsilylimidazole used previously for the conversion of fatty acids into pyrrolidides [5]. Comparison of the reaction rates of the different imidazole-containing mixtures in Fig. 1 indicates that imidazole functions as a catalyst, presumably by the formation of a hydrogen bond to the carbonyl group of the ester, facilitating the nucleophilic attack of the

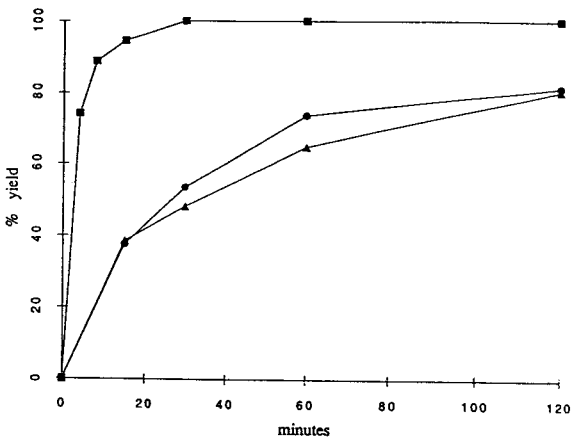

Fig. 1. Kinetics of the reaction of triolein with excess neat pyrrolidine at 60°C, catalysed in various ways. □ = Pyrrolidine–imidazole (1:1, w/w); ● = pyrrolidine–imidazole (1:0.1, w/w); ▲ = pyrrolidine–trimethylsilylimidazole (1:1, w/w).

pyrrolidine. The intermediacy of an imidazolide is excluded because methyl stearate remains essentially unchanged in the presence of a large excess of imidazole in dimethylformamide at 60°C.

The series of chromatograms in Fig. 2 show the progressing conversion of glycerol trioleate into the pyrrolidide of oleic acid, passing through the intermediate diacylglycerols and the monoacylglycerols. (To facilitate the GC analysis, the samples were trimethylsilylated before injection into the gas chromatograph.) The series of chromatograms shows that the conversion of the fat becomes complete after about 40 min under the conditions given in the caption of Fig. 2.

The GC retention times of the pyrrolidides are expected to be longer than those of the methyl esters owing to three additional carbon atoms and the higher polarity of the amide group. This difference in retention times was quantified by determining the Kovats retention indices of both derivatives of selected fatty acids on a column with a poly(dimethylsiloxane) coating (column A). Table 1 shows the result of this analysis. As can be seen, the difference between the Kovats retention index of the pyrrolidides and the methyl esters is ca. 600 units in all three cases:

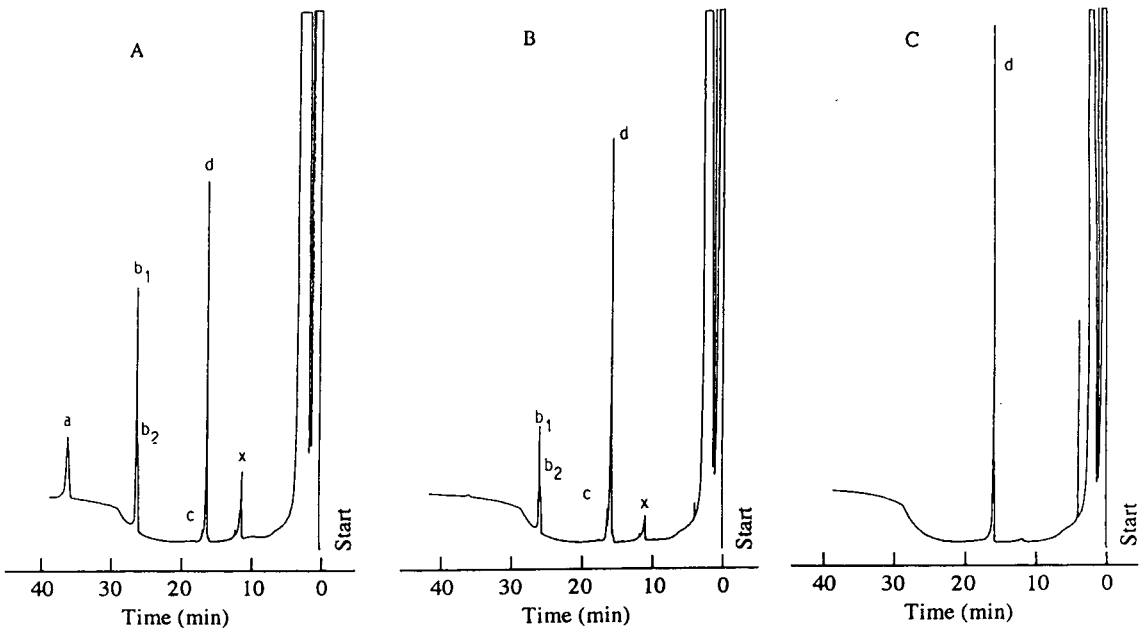

Fig. 2. Progress of the reaction of triolein with pyrrolidine–imidazole (1:1, w/w) at 60°C, (A) after 5 min, (B) after 10 min and (C) after 30 min. The mixture was diluted with bis(trimethylsilyl)trifluoroacetamide before injection into the gas chromatograph for better separation of the intermediates. Peaks: a = trioleine; b_1 = 1,3-dioleyl-2-TMS-glycerol; b_2 = 1,2-dioleyl-3-TMS-glycerol; c = 1,2-di-TMS-3-oleylglycerol; d = oleyl pyrrolidide; x = contaminant. GC temperature programme: column A, from 50 to 200°C at 25°C min^{-1}, 200 to 330°C at 5°C min^{-1}, held at 330°C for 10 min.

ca. 300 for the additional CH_2 groups and ca. 300 for the increased polarity.

We used silicon-based columns for the determination of the pyrrolidides. Carbowax columns, which are sometimes used for the separation of closely related methyl esters, were employed in an experiment designed to demonstrate a similar separating efficiency for methyl esters and pyrrolidides (Fig. 3). Owing to the lower volatility of the pyrrolidides, the bleeding of the column is more significant than it is for the corresponding methyl esters. Columns with increased thermal stability would be desirable for the pyrrolidides.

Table 1
Kovats retention indices of the pyrrolidides and the methyl esters of three selected fatty acids on SE-30 stationary phase

Acid	Pyrrolidide	Methyl ester
Palmitic acid	2520	1920
γ-Linolenic acid	2650	2050
Tetracosanoic acid	3350	2730

In order to assess this procedure with regard to its use for the determination of the fatty acids in fats and oils, we prepared first an equimolar mixture of methyl esters of fatty acids from C_{12} to C_{24} (because they are available from many fatty acids in highly pure form) and then a mixture of triglycerides from C_{12} to C_{20}. To achieve the highest possible accuracy, all esters were checked for homologues and other impurities by GC and capillary supercritical fluid chromatography (SFC), and the masses in the mixture were corrected where necessary. The mixtures were analysed by GC after conversion of the esters into the pyrrolidides as described under Experimental section. The results are reported as response factors (*RF* values) in relation to that of stearoylpyrrolidide whose *RF* was set to 1.000 (Table 2, column 3).

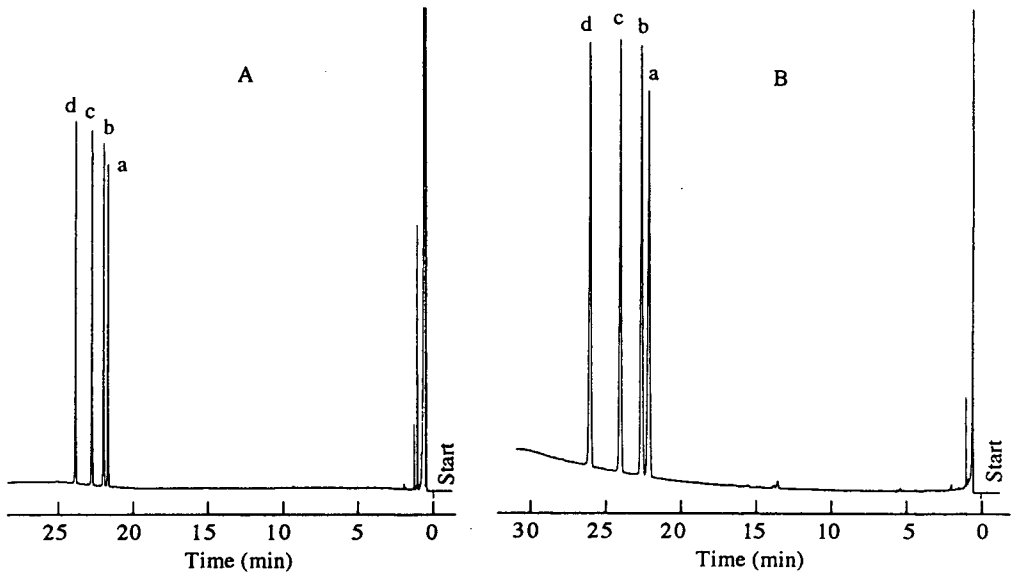

Fig. 3. Comparison of the separation of (A) the methyl esters and (B) the pyrrolidides of four C_{18} fatty acids on a Carbowax stationary phase. Peaks: a = stearic; b = oleic; c = linoleic; d = linolenic acid. GC temperature programme: column B, 50 to 190°C at 25°C min^{-1}, 190 to 250°C at 2°C min^{-1}, held at 250°C for 10 min.

For the methyl esters of the common saturated and unsaturated fatty acids it has been established in careful studies [7,8] that experimental relative response factors can be calculated by the following equation:

$$RF_{(n)} = \frac{M_n}{EC_n} \cdot \frac{EC_s}{M_s} \quad (1)$$

where M = molecular mass of methyl esters (n) and methyl stearate (s) and EC = mass of all "effective carbons", i.e. those in $-CH_2-$, $=CH-$ or $-CH_3$ groups (the degree of saturation is not relevant).

Taking the same approach, it should also be possible to calculate the relative RF values of pyrrolidides, provided the values of the effective carbons in the pyrrolidine ring are properly taken into account. From studies of secondary

Table 2
Determination of pyrrolidides produced from a mixture of fatty acid methyl esters

Compound	RF (calc.)[a]	RF (found)[b]	S.D. (%)[c]	S.D. (%)[d]
C_{12}	1.072	1.070	±0.1	±0.1
C_{14}	1.042	1.037	<±0.1	<±0.1
C_{16}	1.019	1.019	<±0.1	<±0.1
C_{18}	1.000	1.000		
C_{20}	0.985	0.982	<±0.1	±0.3
C_{22}	0.972	0.973	<±0.1	±0.3
C_{24}	0.961	0.962	±0.5	±0.3

[a] RF values calculated with Eq. 1.
[b] RF values found, mean of six samples, each analysed six times.
[c] Standard deviation of the mean of column 3.
[d] Average standard deviation of six GC injections from each sample.

amines, it is known that carbon atoms in the α-position must only be taken at half of their mass, i.e., 6 instead of 12 each [9]. Assuming that pyrrolidides behave in the same fashion as secondary amines and using Eq. 1, the values in column 2 in Table 2 are obtained.

Columns 3–5 in Table 2 show the results for the pyrrolidides obtained from the mixture of methyl esters. The average peak areas of the various pyrrolidides taken from six samples, each analysed six times, normalized with respect to that of stearic acid are given in column 3. They represent the *RF* values based on 1.000 for stearic acid. The standard deviations of the means are given in column 4. The standard deviations obtained for six parallel GC injections of one reaction mixture, representing the GC error, are given in the last column. It is seen that both errors are very satisfactory and, except for one at 0.5%, all are $\leq 0.3\%$. Comparing columns 2 and 3 it is seen that the experimental and the calculated values all agree very well also. The difference in the worst case is 0.5%.

The results for the pyrrolidides produced from the mixture of triglycerides are presented in Table 3. The experimental values in column 3 represent eight samples, each analysed twice by GC. The standard deviations (last column) are those of the overall error, consisting of derivatization and GC analysis. Comparing the results with those of Table 2 shows that they are of comparable quality. The higher deviation of the average values from the theoretical values for certain acids, e.g., palmitic acid, may be due to an impurity present in the sample in question, which raises the *RF* value found.

On the basis of these results, we are confident that the pyrrolidide method can be developed into a method for the analysis of fats and oils which is equally as accurate but much easier than all present methods using methyl esters.

The reagent mixture used in this analysis, pyrrolidine and imidazole, is of course not suitable to convert free fatty acids into pyrrolidides. If free fatty acids have to be dealt with, trimethylsilylimidazole has to be added to the reagents in order to convert the acids into trimethylsilyl esters for consecutive attack by pyrrolidine [5]. Longer reaction times are then required, as shown in Fig. 1. The same measure has to be taken if water is present in the oil to ensure that saponification of the triglyceride does not impair the results.

4. Conclusions

Fats and oils are quantitatively converted into the pyrrolidides of the constituent fatty acids under mild conditions using a mixture of pyrrolidine and imidazole. The diluted reaction mixture can be applied without further workup to the gas chromatograph for quantitative analysis. The accuracy and reproducibility of the results are comparable to those of the methods using methyl esters [8]. The whole procedure is considerably simpler and thus more easily amenable to automatic handling than any of the

Table 3
Determination of pyrrolidides produced from a mixture of fatty acid triacylglycerols

Compound	*RF* (calc.)[a]	*RF* (found)[b]	S.D. (%)[c]
C_{12}	1.072	1.066	±0.3
C_{14}	1.042	1.050	±0.3
C_{16}	1.019	1.028	±0.2
C_{18}	1.000	1.000	
C_{20}	0.985	0.988	±0.1

[a] *RF* values, calculated with Eq. 1.
[b] Average of eight samples, each analysed twice.
[c] Overall standard deviation of all sixteen analyses.

conventional schemes using methyl esters. Problems may arise when Carbowax columns are necessary for the separation of unsaturated fatty acids above C_{18}, because of the insufficient thermal stability of these columns at the required temperatures.

Acknowledgements

We are indebted to Mr. S. Masur, Mr. P. Samirant and in particular to Mrs. E. Kirscher and Mrs. G. Leder for their careful experimental work, Mr. G. Oesterhelt for GC–MS results and Dr. J. Schildknecht for thermochemical calculations.

References

[1] W. Vetter, M. Vecchi and W. Walther, *Helv. Chim. Acta*, 54 (1971) 1599.
[2] B.A. Andersson and R.T. Holman, *Lipids*, 9 (1974) 185.
[3] B.A. Andersson, *Prog. Chem. Fats Lipids*, 16 (1978) 279.
[4] W.W. Christie, *Gas Chromatography and Lipids*, Oily Press, Ayr, 1988, p. 166.
[5] W. Vetter and W. Walther, *J. Chromatogr.*, 513 (1990) 405.
[6] J.B. Pedley, R.D. Naylor and S.P. Kirby, *Thermochemical Data of Organic Compounds*, Chapman and Hall, London, 1986.
[7] R.G. Ackman and J.C. Sipos, *J. Am. Oil Chem. Soc.*, 41 (1964) 377.
[8] J.D. Craske and C.D. Bannon, *J. Am. Oil Chem. Soc.*, 64 (1987) 1413.
[9] R.G. Ackman, *J. Gas Chromatogr.* 6 (1968) 497.

ELSEVIER

Journal of Chromatography A, 686 (1994) 155–157

JOURNAL OF CHROMATOGRAPHY A

Short communication

Chromatographic tank designed to obtain highly reproducible high-performance thin-layer chromatograms of gangliosides and neutral glycosphingolipids☆

G.A. Nores*, R.K. Mizutamari[1], D.M. Kremer[1]

Departamento de Química Biológica, Facultad de Ciencias Químicas, Universidad Nacional de Córdoba and CIQUIBIC, CONICET, 5016 Córdoba, Argentina

First received 22 February 1994; revised manuscript received 3 May 1994

Abstract

Although high-performance thin-layer chromatography (HPTLC) is one of the most useful methods in glycosphingolipid studies, there are some difficulties with the reproducibility of the chromatographic patterns. When mixtures of solvents with different vapour pressures are used as the mobile phase, saturation of the tank is a critical point for obtaining reproducible chromatograms. A chromatographic tank designed to give optimal saturation conditions, resulting in highly reproducible chromatograms, is described.

Glycosphingolipids (GSLs) are amphiphatic molecules with a hydrophobic moiety formed by an N-acylated long-chain amino alcohol (ceramide) and a hydrophilic moiety of one to several sugars. They are membrane components with the oligosaccharide protruding into the extracellular space. Their oligosaccharide variability and topographic distribution make them potential key molecules in the interactions of the cells. They have been involved in several important cellular processes such as cell recognition, growth regulation, development and oncogenesis [1,2].

Ion-exchange and normal-phase liquid chromatography are the most common methods used for analytical studies of GSLs. Since high-performance silica gel became available, high-performance thin-layer chromatography (HPTLC) has become a powerful analytical tool in the GSL field [3]. However, the major difficulty with HPTLC is the low reproducibility of the chromatographic pattern obtained after different runs. In our experience, in order to obtain a reproducible pattern, the critical point is the saturation of the chromatographic tank. When mixtures of solvents having different vapour pressures are used, if the tank is not saturated the ascending solvent mixture becomes enriched in the less volatile solvent.

For the separation of GSLs, mixtures of chloroform, methanol and water are used and as the ascending solvent mixture will be enriched in

* Corresponding author.

☆ In memoriam of Dr. Ranwel Caputto, deceased 19 April 1994.

[1] Recipients of scholarships from the Consejo de Investigaciones Científicas y Técnicas de la Provincia de Córdoba (CONICOR).

0021-9673/94/$07.00
SSDI 0021-9673(94)00645-8

water, it will become more polar, affecting the migration of the GSLs. Although saturation of the tank can be obtained within 3–4 h, when the tank is opened in order to put the plate in, saturation is lost to a variable extent. One way to solve this problem is to put the plate inside the tank, not contacting the solvent; only after saturation is obtained should the plate be permitted to touch the solvent mixture. Under these conditions we were able to obtain reproducible chromatograms. However, the long time required for saturation of the tank constitutes an obvious disadvantage.

Here, we describe a tank into which a small fan is introduced, thus reducing the saturation time to ca. 3 min instead of the usual 3–4 h. Fig. 1 shows a diagram of this chromatographic tank. The lid, which contains the small fan, must be kept tightly closed by using a silicone-rubber seal. The solvent mixture and the plate are put simultaneously into the tank.

There are several possible ways to keep the plate out of contact with the solvent. We found it practical and easy to hang it up using a small clamp and a string. The fan is turned on for 3 min and then the plate is lowered until it touches the solvent. Using this system, we were able to obtain perfect reproducibility of the chromatograms in a minimum of time. Several runs with GSLs (gangliosides and neutrals) were carried out using the same batch of solvent mixture. The slowest and fastest migrating chromatograms of the series are shown in Fig. 2; it can be seen that the general aspects of the patterns are similar and the variability of the R_F values is very small: in every case, the relative standard deviation of the R_F value found for different GSLs was of the order of 3–4% of the media.

Although we have not described the tank previously, we have already used it to study very complex GSL patterns such as insect GSLs [4] and antibodies to GSL [5,6]. In addition, the tank has been successfully applied to the HPTLC analysis of other compounds such as amino acids (urine and plasma samples), nucleotides and phospholipids.

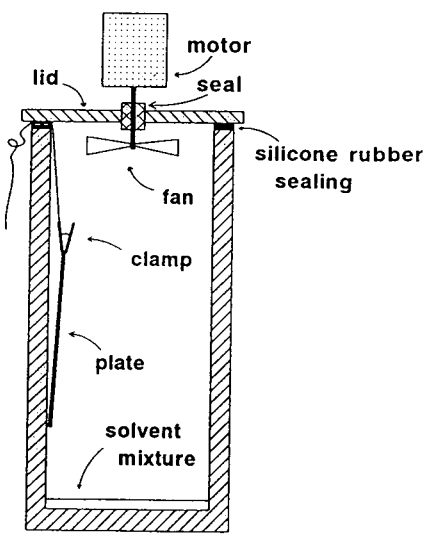

Fig. 1. Cross-section of the chromatographic tank.

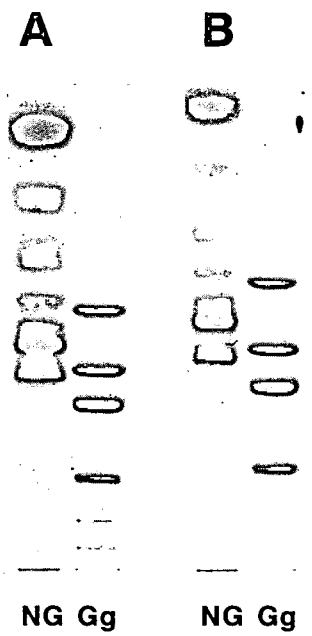

Fig. 2. Chromatograms of gangliosides (Gg) and neutral glycosphingolipids (NG). Human meconium neutral glycosphingolipids and an artificial mixture of gangliosides (total human brain gangliosides plus GM2 and GM_3) were separated on HPTLC plates (Merck, Darmstadt, Germany) using chloroform–methanol–0.2% aqueous $CaCl_2$ (60:37:8) and stained with orcinol reagent. The chromatograms are (A) the slowest and (B) the fastest migrating ones from a series of runs made in the course of 1 week.

Acknowledgements

This work was supported by grants from CONICOR, CONICET and SeCyT (UNC), Argentina. The authors thank B.L. Caputto and H.J. Maccioni for critical reading of the manuscript.

References

[1] J.N. Kanfer and S. Hakomori, *Sphingolipid Biochemistry*, Plenum Press, New York, 1983.
[2] S. Hakomori, *J. Biol. Chem.*, 265 (1990) 18713.
[3] S.K. Kundu, *Methods Enzymol.*, 72 (1981) 185.
[4] F. Helling, R.D. Dennis, B. Weske, G.A. Nores, J. Peter-Katalanic, U. Dabrowsky, H. Egge and H. Wiegandt, *Eur. J. Biochem.*, 200 (1991) 409.
[5] G.A. Nores, R.D. Dennis, F. Helling and H. Wiegandt, *J. Biochem.*, 110 (1991) 1.
[6] R.K. Mizutamari, H. Wiegandt and G.A. Nores, *J. Neuroimmunol.*, 50 (1994) 215.

ELSEVIER

Journal of Chromatography A, 686 (1994) 158–163

JOURNAL OF CHROMATOGRAPHY A

Short communication

Bidirectional isotachophoresis II. Fifteen electrolyte systems covering the pH range 3.5–10

Takeshi Hirokawa

Applied Physics and Chemistry, Faculty of Engineering, Hiroshima University, Kagamiyama 1, Higashi-Hiroshima 724, Japan

First received 11 May 1994; revised manuscript received 26 July 1994

Abstract

Fifteen electrolyte systems useful for bidirectional isotachophoresis were proposed covering the pH range 3.5–10. The pH dependence on the R_E values of the terminating zones was simulated for all the electrolyte systems proposed, together with the isotachophoretic velocities. A 10 m*M* HCl solution was the anionic leading electrolyte and a 10 m*M* KOH solution the cationic one, of which the pH was adjusted by adding ten kinds of pH buffers. The present simulation might be conveniently used to select an appropriate bidirectional electrolyte system for the samples of interest.

1. Introduction

In our previous paper [1], it was demonstrated that an isotachophoretic (ITP) stacking configuration could be formed in a separation tube both for anions and cations of a sample, when the anolyte was a leading electrolyte for anions and the catholyte was one for cations and the sample was injected to the interface in a separation tube. Obviously, such a bidirectional electrolyte system is useful for the simultaneous analysis of anions and cations in a sample when a dual-detector system is available. Even when such detection system is not available, the electrolyte system can be conveniently used for successive analysis of anions and cations.

The pH difference between the anolyte and the catholyte of the bidirectional electrolyte system is not arbitrary, because the pH-buffering ions in each electrolyte simultaneously play the role of terminating ions, and the suitability of the buffers as terminator depends on the pH of the leading electrolyte used in combination.

In this paper, fifteen electrolyte systems suitable for bidirectional ITP were proposed covering the pH range of 3.5–10. The pH dependence of the R_E values of the terminators was simulated for convenient selection of the operational system (R_E is one of the qualitative indices of ITP [2]). The ITP velocities were also simulated to show the difference of the migration time of cationic and anionic zones.

2. Theoretical

2.1. Operational electrolyte system for bidirectional ITP

Fig. 1 shows a typical bidirectional electrolyte system. The anolyte is a HCl solution buffered by adding β-alanine to pH 3.6 [abbreviated as

0021-9673/94/$07.00
SSDI 0021-9673(94)00706-3

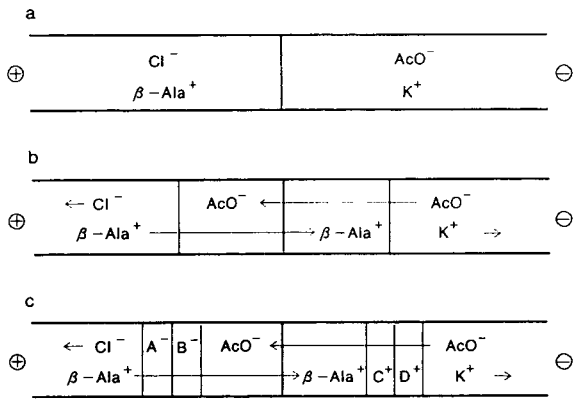

Fig. 1. Schematic diagrams of capillary bidirectional ITP. The anolyte (an anionic leading electrolyte) is a HCl solution buffered by β-alanine and the catholyte (a cationic leading electrolyte) is a KOH solution buffered by acetic acid (electrolyte system a in Table 1). A^-, B^-, C^+ and D^+ are sample components. (a) Before migration, (b) blank run, (c) steady state of sample components.

HCl/β-Ala (pH 3.6)]. The catholyte is a KOH solution buffered by adding acetic acid to pH 4.8 [abbreviated as KOH/acetic acid (pH 4.8)]. After electrophoretic migration started, as shown in Fig. 1b, acetic acid buffer can be a suitable terminator for anions, and β-alanine plays the role of a terminator for cations. When a sample mixture is injected, as shown in Fig. 1c, the anionic and cationic components migrate isotachophoretically toward electrodes. As is obvious from Fig. 1b, the constituents of two terminating zones developed are the same (acetic acid and β-alanine), but the concentrations and the pH values were different from each other [1].

2.2. Restriction in the selection of bidirectional electrolyte system

Several leading electrolytes for cationic analysis and anionic analysis have been proposed [2–4]. The pH of the solution ranges from 3 to 10. As discussed previously [1], these leading electrolytes cannot be combined arbitrarily. That is, the pH difference between the anolyte and the catholyte should be approximately in the range defined as follows:

$$0.5 \leq pH_C - pH_A \leq 1.5 \quad (1)$$

where pH_C and pH_A are the pH values of the catholyte and the anolyte, respectively. Consequently, the pH of the catholyte should be appropriately higher than that of the anolyte. In the derivation of Eq. 1, it was assumed that the anolyte and the catholyte of the bidirectional electrolyte system have the maximum buffering ability, that is the pH value of each electrolyte solution is equal to the pK_a of the pH-buffering counter ion used.

When the difference $pH_C - pH_A$ is too small or too large, the effective mobility of the terminators might become inappropriately large or small. Fig. 2a shows a typical bidirectional elec-

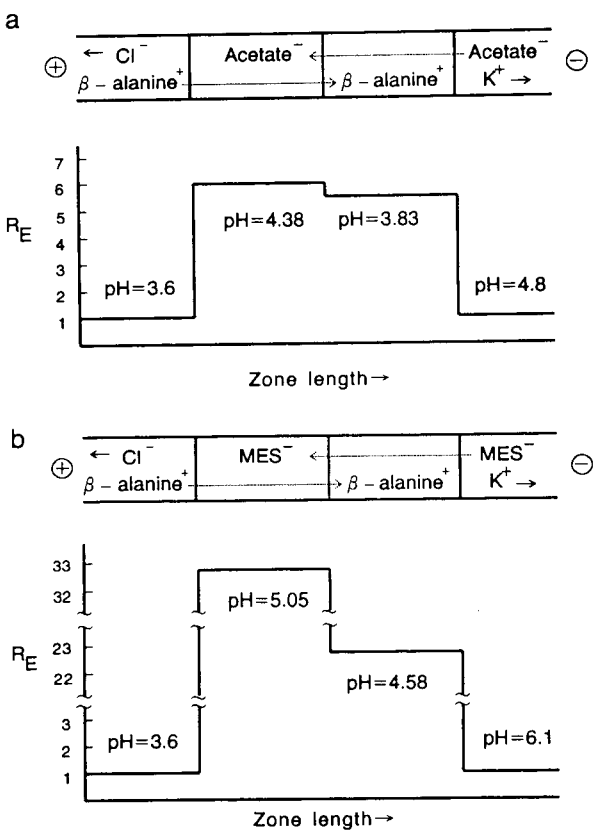

Fig. 2. Simulated R_E profile of bidirectional ITP. (a) HCl/β-alanine (pH_C 3.6)–KOH/acetic acid (pH_A 4.8) system, (b) HCl/β-alanine (pH_C 3.6)–KOH/MES (pH_A 6.1). The leading anion was 10 m*M* Cl^- and the leading cation was 10 m*M* K^+.

trolyte systems of HCl/β-alanine (pH_C 3.6)–KOH/acetic acid (pH_A 4.8). Obviously, this electrolyte system fulfills Eq. 1. According to our simulation, the effective mobility and R_E value of terminating acetate ion were $12.5 \cdot 10^{-5}$ cm^2 V^{-1} s^{-1} and 5.99, respectively, at the steady state. These values for the other terminator β-alanine were $12.5 \cdot 10^{-5}$ cm^2 V^{-1} s^{-1} and 5.73, respectively. Simulated effective mobility suggested acetic acid and β-alanine are suitable as the terminators. The effective mobility simulated for the leading ion ($\bar{m}_L$) was $74.7 \cdot 10^{-5}$ cm^2 V^{-1} s^{-1} for Cl^- and $71.4 \cdot 10^{-5}$ cm^2 V^{-1} s^{-1} for K^+.

On the other hand, if a leading electrolyte KOH/MES(pH_A 6.1) is combined with that of HCl/β-alanine (pH_C 3.6), this system does not fulfill Eq. 1. In such case, as shown in Fig. 2b, R_E values of MES and β-alanine become too large or effective mobilities become too small according to our simulation. The effective mobility and R_E value of terminating MES ion were $1.95 \cdot 10^{-5}$ cm^2 V^{-1} s^{-1} and 38.3, and those of β-alanine were $3.15 \cdot 10^{-5}$ cm^2 V^{-1} s^{-1} and 22.7, respectively. These values suggest that the electrolyte system shown in Fig. 2b is practically of no analytical use.

For the above bidirectional simulation of the steady state of bidirectional ITP, a simulation program for isotachophoretic separation (SIPS) program was used [2] on a personal computer Model PC-9801RA2 (NEC, Tokyo, Japan). It should be noted that the simulation of bidirectional ITP separation can be carried out as the combination of independent simulations for anions and cations, because there is no essential difference between the steady state of bidirectional ITP and that of unidirectional ITP. Simulational procedures and the examples were detailed in the Refs. [4] and [2], respectively.

2.3. Fifteen electrolyte systems for bidirectional ITP

Taking into account the limitation on the pH difference described by Eq. 1, fifteen kinds of electrolyte systems were proposed as shown in Table 1. Eight kinds of anionic buffers and nine kinds of cationic buffers were used to cover the

Table 1
Electrolyte systems for bidirectional ITP

Anolyte: 10 m*M* HCl + buffer				Catholyte: 10 m*M* KOH + buffer			
Cationic buffer	m_0^* ($\times 10^{-5}$/cm V^{-1} s^{-1})	pK_a	pH range	Anionic buffer	m_0 ($\times 10^{-5}$/cm V^{-1} s^{-1})	pK_a	pH range
(a) β-Alanine	36.7	3.552	3.0–4.2	Ac	42.4	4.756	4.2–5.6
(b) ε-AMC	28.8	4.373	3.6–5.2	Ac			4.2–5.6
(c) β-Alanine	36.7	3.552	3.0–4.2	SUC	33.0	4.207	4.8–6.2
					60.9	5.637	
(d) ε-AMC	28.8	4.373	3.6–5.2	SUC			4.6–6.0
(e) Creatinine	37.2	4.828	4.4–5.4	MES	28.0	6.095	5.4–6.6
(f) Histidine	29.6	6.040	5.2–6.6	MES			5.4–6.6
(g) Histidine			5.6–6.8	MOPS	24.4	7.15	6.6–7.8
(h) Imidazole	52.0	7.150	6.4–7.6	GlyGly	31.5	8.400	7.8–9.0
(i) Tris	29.5	8.076	7.2–8.6	GlyGly			7.8–9.0
(j) Tris			7.4–8.6	Histidine	28.8	9.342	8.8–10.2
(k) Ammediol	32.0	8.780	8.0–9.4	Histidine			8.8–10.0
(l) Ammediol			8.0–9.4	Valine	28.4	9.710	9.2–10.4
(m) Ammediol			8.2–9.4	β-Alanine	30.8	10.24	9.6–10.6
(n) Ethanolamine	44.3	9.498	8.8–10.2	β-Alanine			9.6–10.8
(o) Ethanolamine			8.8–10.0	Proline	29.0	10.64	10.0–11.2

Ac = Acetic acid; ε-AMC = ε-aminocaproic acid; SUC = succinic acid; MES = N-morpholinoethanesulfonic acid; MOPS = 3-morpholinopropanesulfonic acid; GlyGly = glycylglycine; Tris = tris(hydroxymethyl)aminomethane.

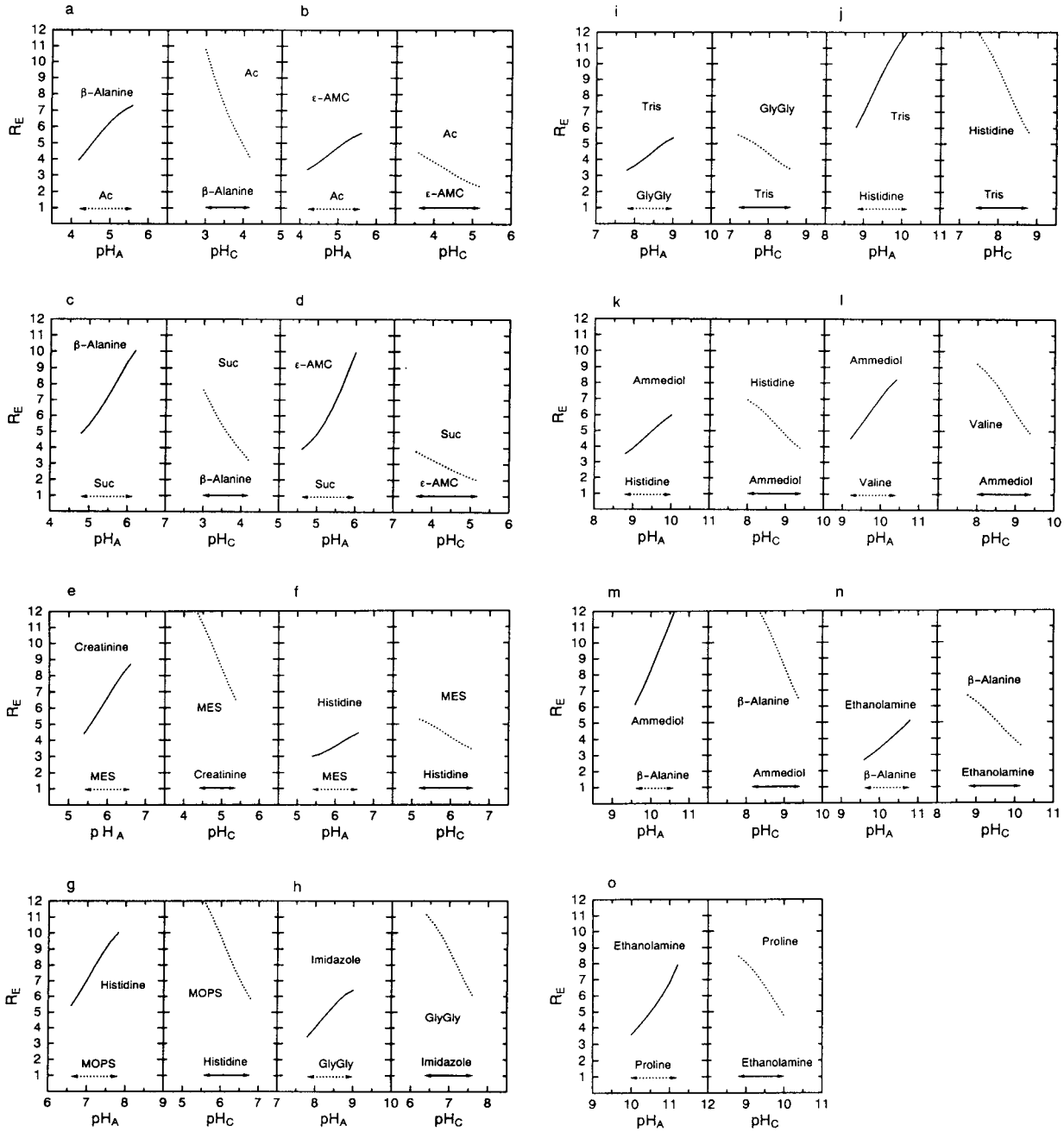

Fig. 3. pH dependence on R_E values of the terminators for bidirectional electrolyte systems listed in Table 1. Solid curves = terminating cations; broken curves = terminating anions. (a) HCl/β-alanine–KOH/acetic acid system, (b) HCl/ε-AMC–KOH/acetic acid system, (c) HCl/β-alanine–KOH/succinic acid system, (d) HCl/ε-AMC–KOH/succinic acid system, (e) HCl/creatinine–KOH/MES system, (f) HCl/histidine–KOH/MES system, (g) HCl/histidine–KOH/MOPS system, (h) HCl/imidazole–KOH/glycylglycine system, (i) HCl/Tris–KOH/glycylglycine system, (j) HCl/Tris–KOH/histidine system, (k) HCl/ammediol–KOH/histidine system, (l) HCl/ammediol–KOH/valine system, (m) HCl/ammediol–KOH/β-alanine system, (n) HCl/ethanolamine–KOH/β-alanine system, (o) HCl/ethanolamine–KOH/proline system.

pH range 3.5–10. The leading anion was 10 m*M* Cl^- and the leading cation was 10 m*M* K^+. The mobilities and pK_a values of the buffers at 25°C used for simulation were also listed in Table 1.

3. Results and discussion

Using bidirectional electrolyte systems shown in Table 1, the R_E values of the anionic and cationic terminators were simulated and the pH dependence profiles were shown in Fig. 3a–o, where a–o corresponds to electrolyte systems a–o in Table 1. The pH values of the leading electrolyte was varied in the range $pK_a \pm 0.5$ keeping $R_E < 12$ (effective mobility $> 1.95 \cdot 10^{-5}$ $cm^2\ V^{-1}\ s^{-1}$).

In Fig. 3a, for example, the left solid curve shows the R_E values of the cationic terminator (β-alanine), where the pH of the cationic leading electrolyte (pH of anolyte, pH_A) is varied in the range 4.2–5.6 by adding acetic acid to 10 m*M* KOH. The right broken curve in Fig. 3a shows the R_E values of the anionic terminator (acetic acid), where the pH of the anionic leading electrolyte (pH of catholyte, pH_C) is varied in the pH range 3.0–4.2 by adding β-alanine to 10 m*M* HCl. By using Fig. 3, one can select bidirectional ITP electrolyte system suitable for the sample components of interest. The method is detailed in Refs. [2]–[4].

Table 2 summarizes the ITP velocities simulated for bidirectional electrolyte systems listed in Table 1, when the inner diameter of the separation tubes was 0.5 mm and the migration current was 100 μA. The velocities of anions were shown with negative signs. The tabulated velocities (v) can be used to estimate the values with different inner diameters (d mm) and currents (I) on the assumption of no temperature change in the separation tube:

$$v\ (\text{cm/min}) = \text{tabulated velocity} \cdot (0.25/d^2) \cdot I/100 \qquad (2)$$

Obviously from Table 2, the ITP velocities of the electrolyte systems proposed were approximately the same with each other (2 cm/min) both for anions and cations. Therefore, the length of the separation tube can be adjusted to coincide the starting time of the anionic sample

Table 2
ITP velocities for the bidirectional electrolyte systems

System[a]	pH_A	Anionic velocity (cm/min)	pH_C	Cationic velocity (cm/min)
a	3.6	−2.04	4.8	2.04
b	4.4	−2.33	4.8	2.04
c	3.6	−2.04	5.6	1.92
d	4.4	−2.33	5.6	1.92
e	4.8	−2.17	6.0	2.35
f	6.0	−2.34	6.0	2.35
g	6.0	−2.34	7.2	2.44
h	7.2	−1.93	8.4	2.27
i	8.0	−2.35	8.4	2.27
j	8.0	−2.35	9.4	2.32
k	8.8	−2.29	9.4	2.32
l	8.8	−2.29	9.8	2.32
m	8.8	−2.29	10.2	2.23
n	9.4	−2.04	10.2	2.23
o	9.4	−2.04	10.6	2.18

Anolyte: 10 m*M* HCl + buffer; catholyte: 10 m*M* KOH + buffer.
[a] Bidirectional electrolyte systems listed in Table 1.

zones and cationic ones, or to delay the detection.

To detect both cations and anions by using the single detector system without switching, the zones should be driven to the detector by a suitable hydrostatic flow. An electroosmotic flow in a fused-silica capillary tube may be useful for the purpose because it is an ideal plug flow. However, since the electroosmotic flow is generally not so high compared with the ITP velocity, an additional pressure-driven flow is necessary.

In conclusion, ITP can be bidirectional as capillary zone electrophoresis by using an appropriate bidirectional electrolyte system, which consists of a leading electrolyte for anions (anolyte) and that for cations (catholyte). The fifteen electrolyte systems in Table 1 will be useful to achieve bidirectional ITP.

References

[1] T. Hirokawa, K. Watanabe, Y. Yokota and Y. Kiso, *J. Chromatogr.*, 633 (1993) 251.

[2] T. Hirokawa, M. Nishino, N. Aoki, Y. Kiso, Y. Sawamoto, T. Yagi and J. Akiyama, *J. Chromatogr.*, 271 (1983) D1.

[3] F.M. Everaerts, J.L. Beckers and Th.P.E.M. Verheggen, *Isotachophoresis —Theory, Instrumentation and Applications*, Elsevier, Amsterdam, Oxford, New York, 1976, pp. 283–301.

[4] P. Boček, M. Deml, P. Gebauer and V. Dolnik, in B.J. Radola (Editor), *Analytical Isotachophoresis*, VCH, Basle, Cambridge, New York, 1988.

Bioaffinity Chromatography

Second, Completely Revised Edition

By **J. Turková**

Journal of Chromatography Library Volume 55

Bioaffinity chromatography is now the preferred choice for the purification, determination or removal of many biologically active substances. The book includes information on biologically active substances with their affinants, solid supports and methods of coupling, summarized in tables covering classical, high-performance liquid and large-scale bioaffinity chromatography.

Optimization of the preparation and the use of highly active and stable biospecific adsorbents is discussed in several chapters. Following a chapter dealing with the choice of affinity ligands, affinity-sorbent bonding is described in detail. Other chapters give information on solid supports, the most common coupling procedures and a general discussion of sorption and elution. Several applications of bioaffinity chromatography are described, e.g. quantitative evaluation of biospecific complexes and many applications in medicine and in the biotechnology industry.

Contents:

© 1993 818 pages Hardbound
Price: Dfl. 495.00 (US$ 282.75)
ISBN 0-444-89030-0

ORDER INFORMATION

ELSEVIER SCIENCE B.V.
P.O. Box 330
1000 AH Amsterdam
The Netherlands
Fax: (+31-20) 5862 845
For USA and Canada
P.O. Box 945
Madison Square Station
New York, NY 10159-0945
Fax: (212) 633 3680

US$ prices are valid only for the USA & Canada and are subject to exchange rate fluctuations; in all other countries the Dutch guilder price (Dfl.) is definitive. Customers in the European Union should add the appropriate VAT rate applicable in their country to the price(s). Books are sent postfree if prepaid.

ELSEVIER SCIENCE

Send your article on floppy disk!

All articles may now be submitted on computer disk, with the eventual aim of reducing production times and improving the reliability of proofs still further. Please follow the guidelines below.

With revision, your disk plus one final, printed and exactly matching version (as a printout) should be submitted together to the editor. **It is important that the file on disk to be processed and the printout are identical.** Both will then be forwarded by the editor to Elsevier.

The accepted article will be regarded as final and the files will be processed as such. Proofs are for checking typesetting/editing: only printer's errors may be corrected. No changes in, or additions to the edited manuscript will be accepted.

Illustrations should be provided in the usual manner and, if possible, on a **separate** floppy disk as well.

Please follow the general instructions on style/arrangement and, in particular, the reference style of this journal as given in the "Guide for Authors".

The preferred storage medium is a 5¼ or 3½ inch disk in MS-DOS or Macintosh format, although other systems are also welcome.

Please label the disk with your name, the software & hardware used and the name of the file to be processed.

For further information on the preparation of compuscripts please contact:

Elsevier Science B.V.
Journal of Chromatography A
P.O. Box 330
1000 AH Amsterdam, The Netherlands
Phone: (+31-20) 5862 793 Fax: (+31-20) 5862459

ELSEVIER SCIENCE

PUBLICATION SCHEDULE FOR THE 1995 SUBSCRIPTION

Journal of Chromatography A and *Journal of Chromatography B: Biomedical Applications*

MONTH	O 1994	N 1994	D 1994	
Journal of Chromatography A	683/1 683/2 684/1	684/2 685/1 685/2 686/1	686/2 687/1 687/2 688/1 + 2	The publication schedule for further issues will be published later.
Bibliography Section				
Journal of Chromatography B: Biomedical Applications				

INFORMATION FOR AUTHORS

(Detailed *Instructions to Authors* were published in *J. Chromatogr. A*, Vol. 657, pp. 463–469. A free reprint can be obtained by application to the publisher, Elsevier Science B.V., P.O. Box 330, 1000 AH Amsterdam, Netherlands.)

Types of Contributions. The following types of papers are published: Regular research papers (full-length papers), Review articles, Short Communications and Discussions. Short Communications are usually descriptions of short investigations, or they can report minor technical improvements of previously published procedures; they reflect the same quality of research as full-length papers, but should preferably not exceed five printed pages. Discussions (one or two pages) should explain, amplify, correct or otherwise comment substantively upon an article recently published in the journal. For Review articles, see inside front cover under Submission of Papers.

Submission. Every paper must be accompanied by a letter from the senior author, stating that he/she is submitting the paper for publication in the *Journal of Chromatography A* or *B*.

Manuscripts. Manuscripts should be typed in **double spacing** on consecutively numbered pages of uniform size. The manuscript should be preceded by a sheet of manuscript paper carrying the title of the paper and the name and full postal address of the person to whom the proofs are to be sent. As a rule, papers should be divided into sections, headed by a caption (*e.g.*, Abstract, Introduction, Experimental, Results, Discussion, etc.). All illustrations, photographs, tables, etc., should be on separate sheets.

Abstract. All articles should have an abstract of 50–100 words which clearly and briefly indicates what is new, different and significant. No references should be given.

Introduction. Every paper must have a concise introduction mentioning what has been done before on the topic described, and stating clearly what is new in the paper now submitted.

Experimental conditions should preferably be given on a *separate* sheet, headed "Conditions". These conditions will, if appropriate, be printed in a block, directly following the heading "Experimental".

Illustrations. The figures should be submitted in a form suitable for reproduction, drawn in Indian ink on drawing or tracing paper. Each illustration should have a caption, all the *captions* being typed (with double spacing) together on a *separate sheet*. If structures are given in the text, the original drawings should be provided. Coloured illustrations are reproduced at the author's expense, the cost being determined by the number of pages and by the number of colours needed. The written permission of the author and publisher must be obtained for the use of any figure already published. Its source must be indicated in the legend.

References. References should be numbered in the order in which they are cited in the text, and listed in numerical sequence on a separate sheet at the end of the article. Please check a recent issue for the layout of the reference list. Abbreviations for the titles of journals should follow the system used by *Chemical Abstracts*. Articles not yet published should be given as "in press" (journal should be specified), "submitted for publication" (journal should be specified), "in preparation" or "personal communication".

Vols. 1–651 of the *Journal of Chromatography*; *Journal of Chromatography, Biomedical Applications* and *Journal of Chromatography, Symposium Volumes* should be cited as *J. Chromatogr.* From Vol. 652 on, *Journal of Chromatography A* (incl. Symposium Volumes) should be cited as *J. Chromatogr. A* and *Journal of Chromatography B: Biomedical Applications* as *J. Chromatogr. B*.

Dispatch. Before sending the manuscript to the Editor please check that the envelope contains four copies of the paper complete with references, captions and figures. One of the sets of figures must be the originals suitable for direct reproduction. Please also ensure that permission to publish has been obtained from your institute.

Proofs. One set of proofs will be sent to the author to be carefully checked for printer's errors. Corrections must be restricted to instances in which the proof is at variance with the manuscript.

Reprints. Fifty reprints will be supplied free of charge. Additional reprints can be ordered by the authors. An order form containing price quotations will be sent to the authors together with the proofs of their article.

Fundamentals of Adsorption

Proceedings of the Fourth International Conference, Kyoto, Japan, 17–22 May 1992

Edited by **M. Suzuki**

Studies in Surface Science and Catalysis Volume 80

Fundamentals of Adsorption contains 2 plenary lectures and 96 selected papers from the IVth International Conference, Kyoto, May, 1992. The topics cover a wide range of studies from fundamentals to applications: characterization of porous adsorbents, molecular simulation, adsorption isotherms, diffusion in adsorbents, breakthrough detection, chromatography, pressure swing operation, etc. Model studies on adsorption, surface characterization, microporosimetry, molecular simulations of equilibrium and diffusion, computer simulation of adsorption beds, and many theoretical studies are also included. Special attention is given to: bulk gas separation and purification, solvent recovery, bioproduct separation, environmental pollution control, methane storage, adsorption cooling and resources recovery.

© 1993 818 pages Hardbound
Price: Dfl. 575.00 (US$ 328.50)
ISBN 0-444-98658-8
Co-edition with and distributed in Japan by Kodansha Scientific Ltd.

ELSEVIER SCIENCE

ORDER INFORMATION

ELSEVIER SCIENCE B.V.
P.O. Box 330
1000 AH Amsterdam
The Netherlands
Fax: (+31-20) 5862 845
For USA and Canada
P.O. Box 945
Madison Square Station
New York, NY 10159-0945
Fax: (212) 633 3680

US$ prices are valid only for the USA & Canada and are subject to exchange rate fluctuations; in all other countries the Dutch guilder price (Dfl.) is definitive. Customers in the European Union should add the appropriate VAT rate applicable in their country to the price(s). Books are sent postfree if prepaid.